TOR VERGATA
UNIVERSITÀ DEGLI STUDI DI ROMA

PhD in Civil Engineering

Environmental Engineering Section

XXXVI Cycle

Development of tools for the application of soil gas radon deficit technique to identify and quantify LNAPL in the subsurface

Alessandra Cecconi

A.Y. 2022/2023

Tutor: Prof. Ing. Renato Baciocchi

Co-Tutor: Prof. Ing. Iason Verginelli

Coordinator: Prof. Tullia Iori

CONTENTS

PREFACE

The occurrence of light non-aqueous phase liquids (LNAPL) in the subsurface is a significant issue at hydrocarbon-contaminated sites (US EPA, 1995). LNAPL primarily originates from releases of fuels and oils, and its wide range of components is among the most frequently encountered organic contaminants in the subsurface environment (CL:AIRE, 2014). The assessment of petroleum-contaminated sites has progressed over time, improving efficiency in terms of time and cost (Sweeney and Ririe, 2017). However, it is still common that the evaluation of the presence and distribution of LNAPL at these sites relies on traditional methods like the collection of soil cores for laboratory analysis, and the installation of groundwater monitoring wells to observe the apparent thickness of the floating free product (US EPA, 2004). However, these methodologies are often insufficient to provide exhaustive information for a comprehensive site assessment and the planning and monitoring of effective remediation activities (ITRC, 2018, 2019). To overcome such technological and economic barriers, several technologies have been introduced and tested in the field over the last few decades. These include Electrical Resistivity Tomography (ERT), Ground-Penetrating Radar (GPR), Laser-Induced Fluorescence (LIF) and the Optical Imaging Profiler (OIP) (Bertolla et al., 2014; McCall et al., 2018; Shao et al., 2019; Teramoto et al., 2019; García-Rincón et al., 2020; Lu et al., 2021; Meng et al., 2022; Mineo, 2023). Many of these methods, although promising, require further investigation to ensure their efficiency in the field, as the achievement of reliable results is often conditioned by the site characteristics (ITRC, 2019; Mineo, 2023). Among the available alternatives, the use of tracer techniques is another way to characterize and monitor LNAPL and assess the efficacy of in-situ remediation technologies implemented for LNAPL source zone remediation (Rao et al., 2000). The use of ^{222}Radon (Rn), a natural partitioning tracer that selectively partitions into the NAPL, has been explored in recent years within this context. Rn is a naturally occurring radioactive gas, resulting from the decay of ^{226}Radium, as an intermediate step in the radioactive decay chain of ^{238}Uranium (Ball et al., 1991). A portion of the Rn atoms produced in soil grains and rocks is released from the solid matrix into the pore space (Nazaroff et al., 1989). Within the pore volume, Rn partitions among the different phases in the subsurface, being consequently present in the soil as sorbed to the soil grains, dissolved in water and dispersed in the soil gas, reaching a site-

specific equilibrium concentration (Nazaroff, 1992). The presence of LNAPL in the subsurface causes Rn to preferentially partition into this additional phase, resulting in a change in the equilibrium concentration value that would be observed compared to that in the absence of contamination (ITRC, 2000). Indeed, different works have shown that Rn activities in soil gas or water in areas containing LNAPL are lower than those obtained from adjacent areas without LNAPL (background Rn value). Therefore, this method has the potential to identify and possibly quantify LNAPL in the subsurface by monitoring Rn in soil gas (Schubert et al., 2001; García-González et al., 2008; Yoon et al., 2013; Barbosa et al., 2014; Cohen et al., 2016; De Simone et al., 2017; Castelluccio et al., 2018; De Miguel et al., 2018, 2020; Mattia et al., 2020; Barrio-Parra et al., 2021; Briganti et al., 2024) or water (Hunkeler et al., 1997; Fan et al., 2007; Schubert et al., 2007a, 2007c; Galhardi and Bonotto, 2012; Yoon et al., 2013; Ponsin et al., 2015; Briganti et al., 2020, 2024) and determining the Rn deficit between the two zones. Several configurations were tested for the applications of the method through Rn measurements in soil gas. The most prevalent configuration involves using temporary soil gas probes to take soil gas samples at a depth of about 0.8 m to 1 m. Rn concentrations are then derived from those samples using portable field instrumentation. Although the results obtained are often qualitatively positive, some limitations have been identified and several aspects still need to be investigated for an effective implementation of the method. Difficulties encountered are associated with the heterogeneity of the soil's lithostratigraphy (Schubert, 2015; Cohen et al., 2016), as variations in radium concentration due, for example, to differences in lithostratigraphic units among rock types, or the soil water content, can result in differences in Rn production (Nazaroff, 1992). These complexities have not yet been fully addressed or overcome and may still be considered an open topic. Another aspect related to subsoil characteristics is the potential impact of the distance between soil gas probes and the LNAPL source zone on the performance of the Rn deficit technique in the unsaturated zone (Cohen et al., 2019). Indeed, the applicability of the Rn deficit method may be limited in cases where there is a reduced Rn characteristic diffusion length, depending on the soil properties. Although some authors have previously mentioned this mechanism (e.g., De Miguel et al., 2020; Höhener and Surbeck, 2004), it was not thoroughly investigated.

The objective of this thesis is to improve the comprehension of the dynamics governing the transport of Rn in soil gas, especially in the presence of LNAPL in the

subsurface and under less explored conditions, such as the occurrence of local advective phenomena. Furthermore, the research aims to provide theoretical and practical tools for the application of the soil gas Rn deficit technique for the assessment of LNAPL occurrence in the subsurface.

To achieve these objectives, the initial effort consisted of a theoretical analysis focused on advancing the overall understanding of soil gas Rn diffusive transport in the subsoil (Chapter 3) (Cecconi et al., 2022). A 3-layer, one-dimensional steady-state analytical model was developed to investigate the variations of Rn in the gas profile within the subsurface in the presence of LNAPL. This first modeling effort concentrated on assessing the influence of specific site parameters (such as soil type, volumetric NAPL content, water table depth, and the vertical distance of the soil gas probe from the NAPL source) on the profiles of subsurface soil gas Rn concentrations and deficits, thus impacting the interpretation of field results. A second model was later developed to improve the understanding of Rn behavior in less traditional contexts, considering the presence of advective phenomena in the subsurface (Chapter 4). Although diffusion is typically the primary transport mechanism for gases, local advective phenomena cannot always be excluded, especially in specific scenarios such as water table fluctuations or the occurrence of methanogenesis (US EPA, 2015). The combination of diffusion and advection can have varied effects on Rn activity both in background areas and LNAPL impacted zones, depending on the nature of the advective flux. If left unaddressed, these effects can introduce additional confounding factors into the interpretation of Rn data to assess NAPL contamination (Cecconi et al., 2023b). In both these modeling works it has been shown, as also reported in literature, that the distance between the point where soil gas Rn is measured and the LANPL source area is a crucial factor for the effective application of the technique. However, the common application of the method involves the use of temporary soil gas probes, which typically only allow for superficial Rn measurements (less than 1 m). Therefore, the use of soil gas probes to apply the Rn deficit technique for estimating LNAPL would only be effectively applicable if the probes are installed in proximity to the source zone. To address this issue, we have developed an alternative Rn measurement protocol for the application of the Rn deficit technique (Chapter 5) (Cecconi et al., 2023a). In this approach, soil gas Rn can be monitored in the headspace of groundwater monitoring wells that are typically screened in the portion affected by the presence of LNAPL. To verify the method's performance, some

tests were conducted at two sites with known diesel or gasoline contamination, using portable instrumentation. The preliminary tests confirmed the method's applicability for determining the presence of residual phase in the unsaturated zone, with results consistent with those obtained with other lines of evidence. However, the interpretation of the Rn data still revealed some uncertainties, due to heterogeneities in the subsurface and to temporal variability of Rn emissions. To address the daily variability of soil gas Rn concentrations, an alternative sampling mode was tested (Chapter 6). Soil gas Rn measurements were still performed in groundwater monitoring wells but using passive Rn analyzers. The devices were installed in the headspace of the wells for a few days to provide Rn activity data representative of the point under investigation. This approach potentially improves the performance of the method and overcomes some of the limitations encountered, by allowing Rn measurements to be performed at a depth close to the NAPL source zone and also ensuring that detected Rn deficits are independent of daily Rn variations.

CHAPTER 1

1 LIGHT NON-AQUEOUS PHASE LIQUIDS

Environmental pollution is a major challenge in the 21st century, affecting the balance of ecosystems and profoundly impacting society. Pollution can be defined as an undesirable alteration in the physical, chemical, or biological characteristics of air, water, or soil (NRC, 1966). Among these impacts, soil contamination is primarily caused by human activities, including industrial practices, the use of chemicals in agriculture, and improper disposal of waste (Panagos et al., 2013). Of particular concern in this context is petroleum hydrocarbons contamination, due to their high toxicity and persistence as pollutants that pose a threat to all forms of life on Earth (Negi et al., 2021; Vandana et al., 2022). Oil exploration, transportation, storage, and refining in the petroleum industry at various facilities (such as fuel manufacturing plants, refineries, industrial facilities, gas stations, airports, military bases, and smaller-scale storage at residential properties) whether unintentional or due to human activities, are the main contributors to hydrocarbon pollution (CL:AIRE, 2002; Osin et al., 2017). Petroleum is a complex mixture of organic compounds. It is composed primarily of hydrocarbons, mostly aliphatic (C1-50), monoaromatic (BTEX), and polyaromatic hydrocarbons, with some heteroatomic components such as nitrogen, oxygen, and sulfur, and trace amounts of metals (King, 1988; Henry, 1998). The specific compounds found in petroleum can vary, but more than 500 different compounds have been identified (Fingas, 2022). Among these, hydrocarbons exhibit different properties based on the number of carbon atoms in their chain or the type of chemical bonds that link them (Greenshields and Rossini, 2002). However, organic compounds commonly found in petroleum products have low solubility in water due to their non-polar nature (CL:AIRE, 2014), resulting in the occurrence of a physical interface between these compounds and water (CL:AIRE, 2017). Therefore, spills of petroleum products in the subsurface can easily lead to the formation of Light Non-Aqueous Phase Liquids (LNAPL), which is a separate phase that is immiscible with water and characterized by densities lower than that of water (US EPA, 1995). Consequently, LNAPL typically consists of a complex mixture of mostly hydrocarbon organic chemicals with a wide range of physical, chemical, and toxicological properties that can affect their environmental fate and risk (US EPA, 1995). LNAPL is of particular interest in environmental studies and is one of the most prevalent organic forms of pollution in the subsurface environment due to the widespread use of fuels and oils such as gasoline, diesel, and heating oils in various industries (CL:AIRE, 2014; Ossai et al., 2020). The historical impact of accidental releases and inadequate

disposal practices further increases the prevalence of LNAPL contamination and adds complexity to the challenge of managing the environmental risks associated with this product (US EPA, 1995). In fact, the immiscibility of LNAPL with water and their distinct behaviors in subsurface systems pose challenges related to groundwater quality. To address this issue, the development of effective management and remediation strategies necessitates an understanding of LNAPL transport, fate, and distribution mechanisms (Alden et al., 2024; CL:AIRE, 2014).

1.1 LNAPL MOBILITY LIMITS IN THE SUBSURFACE

Following the spill of petroleum products and during their movement through porous media, various processes can transform its constituent components, resulting in physical and chemical redistribution across the mineral, aqueous, and gaseous phases of the soil, based on their specific partition coefficients (Corapcioglu and Baehr, 1987; Parker, 1989). The equilibrium concentration of an organic compound in water at a specific temperature and pressure defines its solubility, thus revealing the contaminant's mobility in the liquid phase of both unsaturated and saturated zones. The maximum dissolved concentration in water, or effective solubility, of each compound of the spilled product is a function of its pure compound solubility and the mole fraction of the chemical in the organic phase (O'Reilly et al., 2001), as reported in Eq. 1.1:

$$S_{e,i} = S_i \cdot X_i \qquad \text{Eq. 1.1}$$

where $S_{e,i}$ (mg L^{-1}) represents the effective solubility of the i-th compound in the mixture, S_i (mg L^{-1}) the solubility of the pure compound, and X_i (-) represents its mole fraction. At equilibrium conditions, Henry's law describes the partitioning of a compound between the gas phase and the aqueous phase, providing an estimate of a contaminant's tendency to volatilize. The concentration of each component in the gaseous phase can then be derived from the following relationship:

$$C_{g,i} = H_i \cdot C_{w,i} \qquad \text{Eq. 1.2}$$

where $C_{g,i}$ and $C_{w,i}$ (mg L^{-1}) respectively refer to the concentration of the i-th component in the gaseous and aqueous phases, while H (-) denotes Henry's dimensionless constant. Note that when the maximum dissolved concentration in water is reached, $C_{w,i}$ corresponds to $S_{e,i.}$ The direct volatilization of the individual chemical compounds constituting the petroleum product can be described by Raoult's law, which defines the variation in a compound's vapor pressure p_i (Pa) in relation to its mole fraction X_i (-) and to the vapor pressure of the pure compound p_i^0 (Pa).

$$p_i = X_i \cdot p_i^0 \qquad \text{Eq. 1.3}$$

Organic compounds also tend to partially adsorb to the organic carbon of the soil (Li and Gupta, 1994). The organic carbon partition coefficient K_{oc} (L kg^{-1}) reflects the tendency of a compound to partition between the soil organic fraction and water. The

concentration of the i-th component as sorbed phase $C_{s,i}$ (mg kg^{-1}) also accounts for the organic carbon fraction of the soil foc (-), and can be written as follows (ASTM E 1739-95; ASTM PS 104-98):

$$C_{s,i} = K_{oc,i} \cdot f_{oc} \cdot C_{w,i} \quad \text{Eq. 1.4}$$

When the various constituent compounds of the released petroleum product reach their maximum adsorption, volatilization, or solubility value under equilibrium conditions, the saturation concentration of the soil is reached, and they generally form a separate phase. For a pure chemical, the saturation concentration (C_{sat}) can be calculated as follows (ASTM E 1739-95; ASTM PS 104-98):

$$C_{sat} = K_{sw} \cdot S \quad \text{Eq. 1.5}$$

With K_{sw} (L kg^{-1}) the soil-water partition coefficient that can be written as (ASTM, 2000):

$$K_{sw} = \frac{K_{oc} \cdot f_{oc} \cdot \rho_s + \theta_w + H \cdot \theta_g}{\rho_s} \quad \text{Eq. 1.6}$$

With ρ_s (kg m^{-3}) the soil density, θ_w (-) the volumetric water content, and θ_g (-) the volumetric gas content of the soil.

For mixtures of chemicals that are partially soluble in water, like petroleum products, the concentration at which the mixture will be present in the soil's phases is a function of its composition (Brost and De Vaull, 2000). The soil saturation limit for the mixture can be described with (Johnson et al., 1992):

$$\sum_{i=1}^{N} \frac{C_{sat} \cdot X_i \cdot \rho_s}{S_i(\theta_w + K_{oc,i} \cdot f_{oc} \cdot \rho_s + H_i \cdot \theta_g)} = 1 \quad \text{Eq. 1.7}$$

When the saturation concentration is exceeded, the soil can be considered as a four-phase system so that the contaminants can exist in aqueous, vapor, adsorbed, and separated phases. The last one can occur as an immobile phase due to capillarity and the effect of surface tension of the particles, but as the concentration increases, the contaminant may no longer be mechanically retained by the soil, bringing to the presence of mobile, separate phase in the subsoil (ITRC, 2018). While immobile LNAPL (residual phase) exists as isolated pools of fluid trapped in the soil pores (Figure 1.1), the additional presence of mobile LNAPL (LNAPL body) can be conceptualized as a continuous, connected body of liquid in the porous media that is

able to move under applied pressure gradients (Figure 1.2) (ITRC, 2009). Changing conditions, such as varying water table levels, can cause LNAPL to move between the state of being mobile and immobile (Johnston and Trefry, 2010).

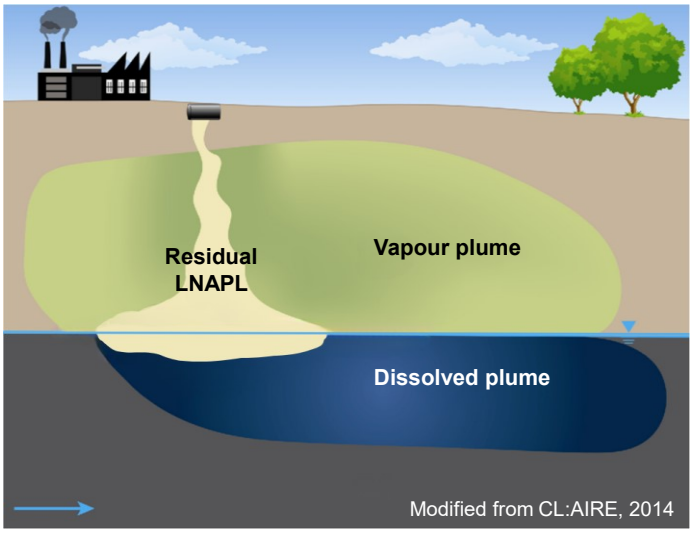

Figure 1.1. Conceptualization of a LNAPL spill creating residual, immobile LNAPL in the subsurface (CL:AIRE, 2014).

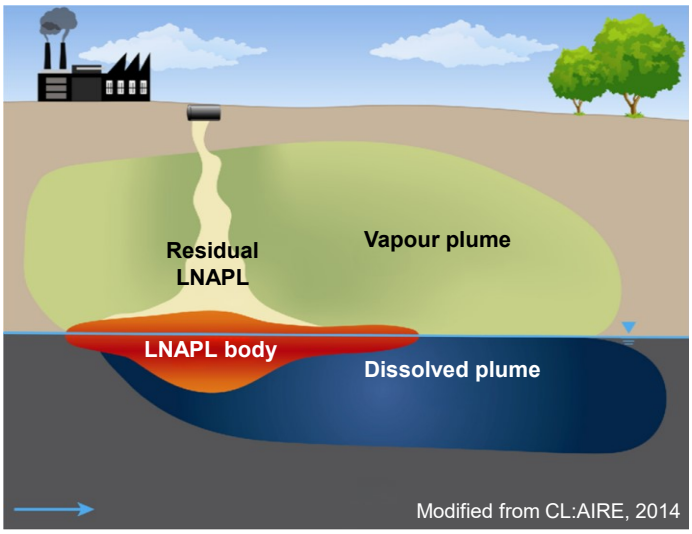

Figure 1.2. Conceptualization of a LNAPL spill creating both residual LNAPL and free, mobile phase (LNAPL body) in the subsurface (CL:AIRE, 2014).

The term residual concentration C_{res} (mg kg^{-1}) can then be defined as the concentration below which the NAPL, if present, will not migrate due to gravity, and can be specified as (Brost and De Vaull, 2000):

$$C_{res} = \frac{\theta_{r,N} \cdot \rho_N}{\rho_s} \cdot 10^6 \text{ mg kg}^{-1} \quad \text{Eq. 1.8}$$

With $\theta_{r,N}$ (-) the residual non-aqueous phase volume fraction, defined as in Eq. 1.9, ρ_N (g cm^{-3}) the density of LNAPL and $S_{r,N}$ (-) the fraction of residual LNAPL filled void.

$$\theta_{r,N} = S_{r,N} \cdot \theta_t \quad \text{Eq. 1.9}$$

Brost and De Vaull (2000) provide data to define conservative C_{res} values that can screen sites for NAPL mobility. Table 1.1 presents a comparison between calculated C_{sat}, soil values, and measured C_{res}, soil values for specific chemicals and hydrocarbon mixtures.

Table 1.1 Residual NAPL concentration and soil saturation limit (Brost and De Vaull, 2000)

Compound/mixture	**$S_{r,N}$ (-)**	**C_{res} (mg kg^{-1})**	**C_{sat} (mg kg^{-1})**	**ρ_N (g cm^{-3})**
Benzene	0.24	53 000	444	0.88
o-Xylene	0.01	2000	143	0.88
Gasoline	0.02 – 0.6	3400 – 80 000	106	0.78
Diesel	0.04 – 0.2	7700 – 34 000	18	0.94
Fuel oil	0.08 – 0.2	17 000 – 50 000	18	0.94
Mineral oil	0.1 – 0.5	20 000 – 150 000	3	0.81

1.2 LNAPL TRANSPORT

To describe the behavior and distribution of LNAPL in the subsurface, it is assumed that LNAPL coexists with water and interstitial air within soil pores. The Vertical Equilibrium Model (VEQ) replaces the pancake model, which historically depicted LNAPL as floating above groundwater in a stratified way (Farr et al., 1990; Lenhard and Parker, 1990). According to the VEQ model, the movement and distribution of LNAPL are primarily governed by the force of gravity, the characteristics of the LNAPL (e.g., viscosity, density, and surface tension), and capillary pressure (Farr et al., 1990; Lenhard and Parker, 1990). Capillary pressure can be defined as the pressure difference created at the interface between two non-miscible fluids in contact with each other (Hillel, 1982), such as LNAPL/water, air/LNAPL, and air/water. After a spill, the product tends to move vertically and fill soil pores that were previously filled with air or water (ITRC, 2018). But for the LNAPL to enter the soil pores, and continue to migrate, it must overcome the capillary resistance or entry/displacement pressure of the soil porosities, displacing the water and gases within a pore space in the vadose zone or saturated area (Mercer and Cohen, 1990; API, 2007). Figure 1.3 shows an example of LNAPL held in pore space by the surrounding water. The curvature of the interface at point A indicates that the pressure in the LNAPL side of the interface (p_N) is greater than the pressure immediately adjacent in the water phase (p_w) (CL:AIRE, 2014). In the shown example, the entry pressure for the non-wetting fluid (LNAPL) to enter a wetting fluid (typically water), is given by:

$$p_N - p_w = \frac{2 \cdot \sigma \cdot \cos(\alpha_c)}{r} \qquad \text{Eq. 1.10}$$

With p_N (kg m^{-1} s^{-2}) NAPL pressure, p_w (kg m^{-1} s^{-2}) the water pressure, σ (kg s^{-2}) the interface tension α_c (°) the contact angle at the interface between the two fluids, and r (m) the pore entry radius.

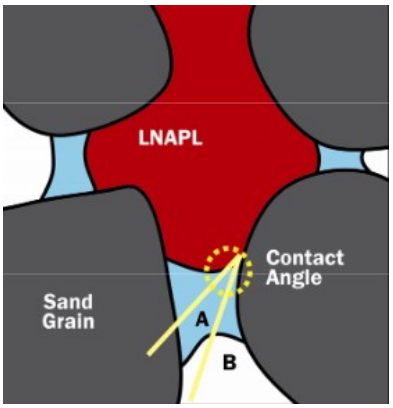

Figure 1.3. Schematic of non-wetting LNAPL and its contact angle with soil surfaces in the presence of water (CL:AIRE, 2014).

The resistance to LNAPL movement is greater in the saturated zone than in the vadose zone due to the entry pressure being higher for a water-saturated pore than for an air-occupied pore. As a result, LNAPL will migrate until it comes across a physical barrier, like low permeability strata, or it encounters the greater resistance to vertical migration when the product reaches the capillary fringe and the piezometric surface of the aquifer (CL:AIRE, 2014; ITRC, 2018; Boumaiza et al., 2022). However, for significant petroleum product releases, if LNAPL has sufficient pressure, once it reaches the capillary fringe, it will still penetrate deep into the aquifer, displacing water to a depth proportional to its driving force, while partially moving laterally along the upper boundary of the water-saturated zone. LNAPL will continue to vertically penetrate the saturated zone if the downward force due to the LNAPL head or the pressure due to LNAPL release exceeds the opposing forces due to the resistance of the soil matrix and the capillary forces (ITRC, 2018), and the product will continue to expand until the forces are balanced. Once this occurs, the mass can be considered stable, unless there are further releases or hydraulic changes in the subsurface (CL:AIRE, 2014). Typically, the system configuration will be that of a multiphase system in which the pores of the medium contain varying amounts of water, NAPL, and gas. In particular, the vadose zone becomes a three-fluid zone consisting of variable saturations of air, water, and LNAPL that together fully saturate the pore spaces. The presence of the gaseous phase decreases with depth, entering the capillary fringe, until the LNAPL penetration of the water table creates a two-fluid zone consisting of variable saturations of LNAPL and water (Figure 1.4) (Hamper and Seyedabbasi, 2023).

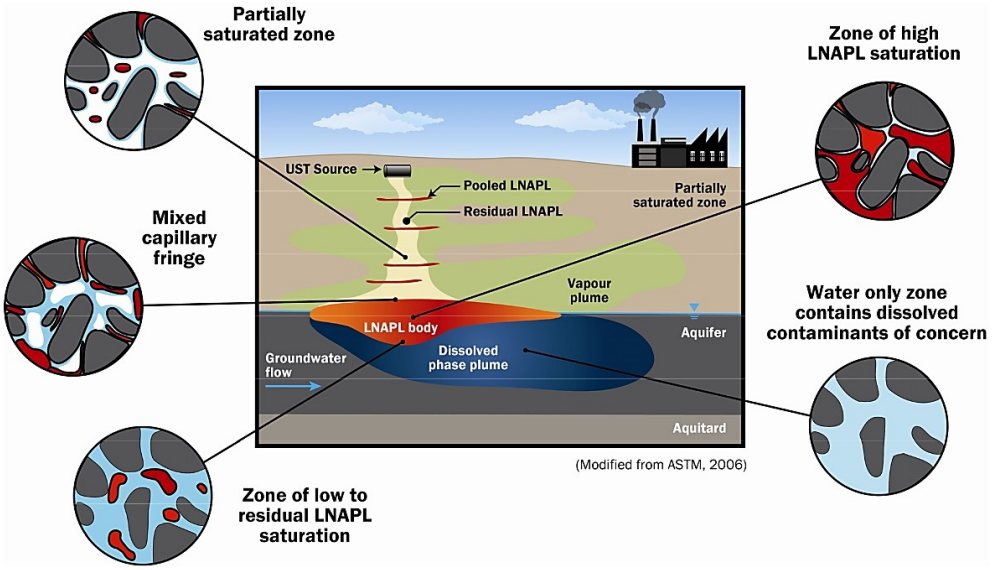

Figure 1.4. Variations in multi-phase system types are observed through a typical LNAPL body profile. Three-phase systems exist within the partially saturated zone and upper portions of the capillary fringe, while two-phase systems exist within the lower portions of the capillary fringe and saturated zone (CL:AIRE, 2014).

In a standard scenario of homogenous sandy soil and unconfined conditions, the vertical distribution of LNAPL saturation will usually follow a pattern referred to as a shark's fin (Frollini and Petitta, 2018), shown on a plot of percent LNAPL saturation versus depth. The area of highest saturation is typically found around the capillary fringe and extends simultaneously above and slightly below the water table. Saturation levels decrease both above and below this point (Farr et al., 1990; Lenhard and Parker, 1990). With complex conditions, LNAPL saturations deviate from the idealized shark fin description and vary significantly with depth due to the influence of soil heterogeneity and water table variability over time (Huntley and Beckett, 2002; Lenhard and García-Rincón, 2024). Changes in the water table due to seasonal variations or artificial pumping can affect the occurrence of LNAPL in both the aquifer and wells (Kemblowski and Chiang, 1990). Observed decreases in the thickness of LNAPL in an unconfined well within an aquifer with a fluctuating water table result from the distribution and redistribution of mobile LNAPL within the LNAPL body. For an unconfined and homogeneous aquifer, Cavelan et al. (2022) effectively illustrate the initial vertical equilibrium shark's fin distribution (Figure 1.5 i) and the changes that typically occur with changing water table level. As the water table lowers (Figure 1.5 ii), trapped LNAPL will drain, leading to an increase in LNAPL thickness in the well.

Instead, during the peak of the water table level (Figure 1.5 iv), LNAPL may become completely or partially trapped within the formation, resulting in either reduced or no thickness in the well. However, this ideal concept may not always apply because of the heterogeneity and water table location during the initial spill.

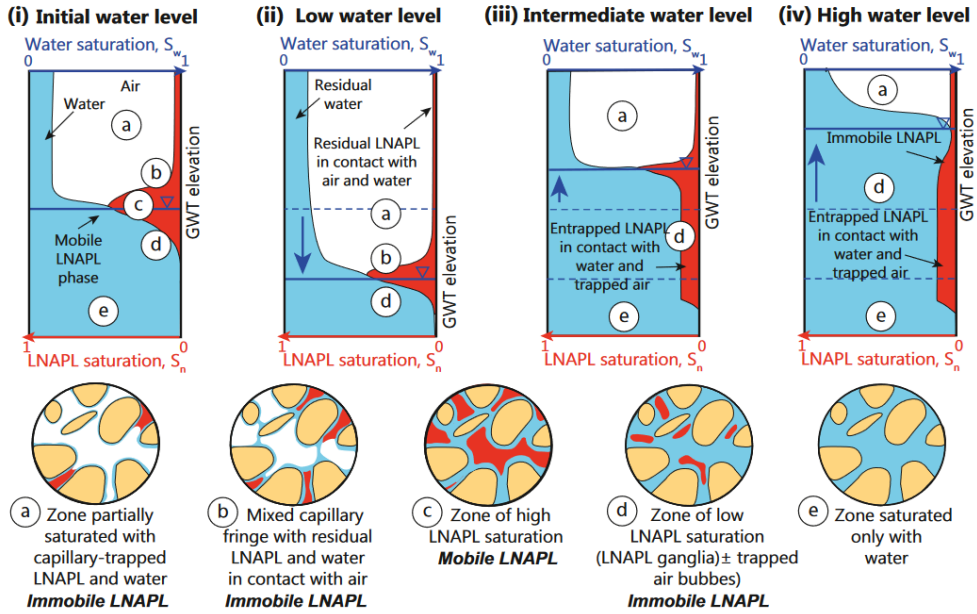

Figure 1.5. Variation in the multi-phase systems observed in the typical LNAPL body profile according to changes in water table levels (Cavelan et al., 2022).

Although capillary forces can retain NAPL in the pores and make it immobile, there still remains the possibility that its components might reach the aquifer through meteoric seepage, dissolve soluble constituents, and lead to a contaminated plume. Similarly, the most volatile components, particularly in the early stages of a spill, can pose a risk to human health by producing contaminated vapor plumes and, in some cases, potentially leading to vapor intrusion processes (US EPA, 2015; Verginelli, 2024). For these reasons, it is important to note that both mobile and immobile forms of LNAPL pose critical environmental issues, making them primary sources of long-term contamination.

1.3 LNAPL MASS REMOVAL

The acceptance of natural attenuation processes being important in hydrocarbon attenuation began in the early 1990s (Chapelle, 1999). The earliest models of mass balance in hydrocarbon source zones were inaccurate in assuming that mass removal of hydrocarbons only accounted for processes occurring in the aqueous phase without affecting the source zones of LNAPL (Garg et al., 2017). Over the past decade, a new scientific term, Natural Source Zone Depletion (NSZD), has emerged. NSZD refers to the collective naturally occurring processes that lead to a reduction of total LNAPL mass in the subsurface (ITRC, 2009). These processes include the transfer of chemical components to the aqueous and gaseous phases, aqueous phase biodegradation, and direct contact product biodegradation (Ng et al., 2014).

Physical processes involving the redistribution of LNAPL components in either the aqueous or gas phase gradually decrease the total mass of the contaminant in the subsurface. LNAPL usually contains volatile organic compounds (VOCs) that can vaporize during and after LNAPL migration in the subsurface, leading to the development of a vapor-phase plume in the partially saturated zone. This mass transfer depends on the vapor pressure of the single components and in a multi-component LNAPL this is approximated by Raoult's Law (Eq. 1.3). Additionally, soluble components are leached from LNAPL by groundwater flow or atmospheric precipitation, leading to the formation of a dissolved-phase plume (ITRC, 2009). The equilibrium dissolved-phase concentration (effective solubility) of the individual components may be again approximated by Raoult's Law (Eq. 1.1). Although this contribution may be significant, it is now recognized that NSZD mainly occurs through direct oil biodegradation, biodegradation of solubilized hydrocarbons at the oil/water interface, LNAPL volatilization and biodegradation in the vadose or smear zone, and only to a lesser extent, dissolution into groundwater and biodegradation in the saturated zone (Karimi Askarani et al., 2024). In particular, methanogenesis combined with the transport of gases such as methane, carbon dioxide, and volatile organic compounds through the vadose zone is accepted as the main mechanism of LNAPL-mass depletion (Garg et al., 2017). Naturally occurring microorganisms can degrade many of the compounds found in LNAPL by using them as a carbon substrate in microbially mediated redox reactions resulting in by-products such as carbon dioxide, methane, and water (Rivett and Thornton, 2008). In aerobic environmental conditions,

aerobic biodegradation (using oxygen as an electron acceptor) of most contaminants will occur preferentially, due to a greater energy yield relative to anaerobic processes (using other electron acceptors) such as denitrification, Fe/Mn reduction, or methanogenesis. Methanogenesis is a complex, multi-step process involving syntrophic interaction between two groups of organisms for the degradation of complex organic compounds (Garg et al., 2017): fermenters break down hydrocarbons in anaerobic LNAPL zones, resulting in the creation of dissolved hydrogen and/or acetate, which methanogens use to produce methane. This process is common in methanogenic ecosystems where anaerobic electron acceptors are rare or absent, but it can also occur in higher redox environments or in the presence of electron acceptors (Gieg et al., 2014). Anaerobic biodegradation may be slower than aerobic for many components but can account for most plume mass metabolized at LNAPL-release sites (CL:AIRE, 2014). At the Bemidji (US) site, where numerous NSZD studies have generated valuable field data to enhance the current understanding of the process, it has been shown that methanogenesis accounts for 85% of the contaminant degradation in both the vadose zone and the smear zone (Molins et al., 2010).

The gaseous expression of NSZD's conceptual model is illustrated in Figure 1.6 (Garg et al., 2017). Methanogenic organisms consume hydrocarbons in the saturated zone, capillary fringe, or lower unsaturated zone, where the majority of the LNAPL product is expected, generating CO_2 and CH_4, from a reaction similar to that shown in Eq. 1.11 for octane:

$$C_8H_{18} + 3.5\ H_2O \rightarrow 1.75\ CO_2(g) + 6.25\ CH_4(g) \qquad \text{Eq. 1.11}$$

CH_4 and CO_2 are transported upward into the vadose zone, along with smaller amounts of VOC, if volatilization processes are still occurring depending on LNAPL composition and the age of the spill. The upward transport of CH_4, and possibly VOC, is opposed to the downward transport of atmospheric oxygen. When methane and oxygen come together in the vadose zone, in the hydrocarbon oxidation zone, CO_2 is produced according to Eq. 1.12 (CRC CARE, 2018):

$$CH_4 + 2\ O_2 \rightarrow CO_2(g) + 2\ H_2O(g) \qquad \text{Eq. 1.12}$$

Ultimately, the primary outcome of the subsurface processes described is the release of CO_2 to the surface. When superficial LNAPL contamination occurs, as is often the

case in the initial stages of a spill, aerobic degradation processes are activated that limit the diffusion of oxygen to the underlying layers (CRC CARE, 2018). Consequently, undegraded methane may be present in the upper layers and be detectable as flux from the surface.

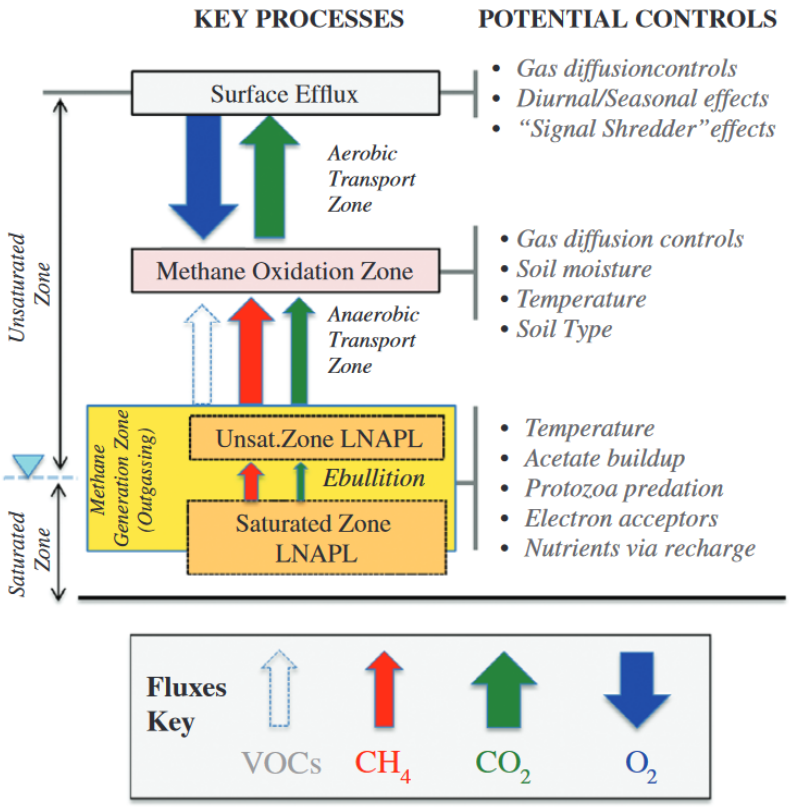

Figure 1.6. Conceptual model for the gaseous expression of natural source zone depletion processes, illustrating the main transport zones, gases involved, and potential control factors (Garg et al., 2017).

Figure 1.6 also provides a list of potential controls that could impact NSZD processes in each of the previously mentioned zones.

1.4 LNAPL DETECTION TECHNIQUES

There are two main drivers in the need for site characterization and LNAPL management: understanding the potential risks posed to receptors by current and possible future mobile LNAPL distributions, and comprehending LNAPL constraints on remediation selection, design, and operation (CL:AIRE, 2014). Site characterization is both an initial assessment process and an ongoing process that may remain essential throughout the remediation program for a site. For large and complex sites, it may be advantageous to use an approach that incorporates multiple lines of evidence and various integrated multi-disciplinary techniques to gather high-quality data that can serve as a foundation for the development of management plans (CL:AIRE, 2002). On smaller and less complex projects, the amount of investigation may be scaled down. For the identification of the presence of LNAPL, the determination of the extent of the contamination, its mobility, and the monitoring in terms of spatial evolution and concentration, there are several possible approaches. Some of the methods and technologies available are briefly described below.

1.4.1 Soil sampling

Soil characterization by soil sampling is one of the primary methods used to assess soil contamination and the relative contaminant concentrations (Figure 1.7). It typically involves the collection of soil samples at various depths and the laboratory analysis of the samples to determine chemical concentrations and composition, providing a direct quantitative estimate of the contamination (CL:AIRE, 2014). Analysis of soil samples can also be useful in assessing the distribution of LNAPL and evaluating the vertical variability and penetration depth of the product, valuable information for defining LNAPL behavior in the subsurface and understanding potential associated risks (ITRC, 2018). The selection of boring locations and depths should be based on available information regarding the hydrogeologic and contaminant conditions at the site. Ideally, the vertical investigation should continue to the zone of deepest LNAPL penetration (Mercer and Cohen, 1990). Field activities for conducting soil surveys may include contamination screening directly in the field, using instruments like portable photoionization detectors (PID), flame ionization detection (FID), or fluorescence analysis for headspace evaluation. Additionally, shaker tests, dye shaker tests, paint

filter tests, and paper towel tests serve as effective approaches to conveniently screen for LNAPL presence (CL:AIRE, 2014).

Figure 1.7. Collection of soil samples (© Earth Environmental & Geotechnical Ltd)

For LNAPL contamination, information on contaminant quantification with soil sample analysis is typically provided in terms of Total Petroleum Hydrocarbons (TPH). TPH includes volatile petroleum hydrocarbons, ranging from C6 to C10, and extractable petroleum hydrocarbons, from C10 to C28 (Kuppusamy et al., 2019). To approximate

the saturation of a multi-component complex LNAPL based on TPH data, the following equation can be used (Parker et al., 1996).

$$S_N = \frac{\rho_s \cdot TPH}{\rho_N \cdot \theta_t \cdot 10^6} \quad \text{Eq. 1.13}$$

Where S_N (-) represents the NAPL saturation of the pore space, ρ_s (g cm^{-3}) denotes the soil bulk density ρ_N (g cm^{-3}) stands for the NAPL density, θ_t (-) denotes the porosity, and TPH units are expressed in mg kg^{-1}.

Soil sampling and analysis can be useful for performing GC fingerprinting analysis of petroleum compounds in the soil (Yang et al., 2014). This method provides a profile and distribution of the chemical components found in the LNAPL, making it an effective tool for characterization, particularly in cases where multiple fuel types or sources are present or suspected. Furthermore, different types of fuel and oil exhibit distinctive GC fingerprints, which can be used to evaluate the extent of weathering and the combination of degradation processes that the LNAPL has undergone (CL:AIRE, 2014). Information upon petroleum hydrocarbon fingerprinting or weathering patterns, can also be used as an age dating and source identification technique (Christensen and Larsen, 1993). These techniques are employed in the field of environmental forensics to investigate contamination, an include other options like corrosion models for underground storage tanks, identifying the date when a chemical or additive became commercially available, biomarker analysis, stable isotope analysis and radiometric methods based on $^{228}Th/^{228}Ra$ ratios (Christensen and Larsen, 1993; Morrison, 2000, 2000; Oudijk, 2009; Lauer and Vengosh, 2016; Briganti et al., 2023).

The main advantages of the soil characterization by soil sampling relate to its ability to provide a quantitative estimate of contamination and its composition. On the other hand, cost is its main disadvantage because of the expenses associated with drilling, sampling, and quantitative analysis (Tsai et al., 2020). Furthermore, this technique may miss contaminants in locations where survey data are not available or contribute to new contamination pathways. It has also been noted that the small size of core samples may be insufficient to provide reliable average NAPL saturation (Mayer and Miller, 1992). When using soil TPH concentrations as an indicator of LNAPL presence, caution is advised by ITRC (2018) due to the potential impact of non-hydrocarbons such as soil organic matter and the analytical method chosen.

1.4.2 Monitoring wells

Groundwater monitoring wells are typically installed at sites contaminated or suspected of being contaminated with petroleum products. As well as groundwater sampling and analysis, wells can often be used to monitor for the possible presence of free LNAPL as a supernatant on top of the water in the well. Well screens in LNAPL monitoring wells should be long enough to ensure that the entire free LNAPL layer is within the screened interval during seasonal water table fluctuations and sand pucks should be coarser than the surrounding media to ensure movement of NAPL into the well (Mercer and Cohen, 1990). An interface meter can be employed to measure groundwater and LNAPL elevations, detecting the LNAPL-air and LNAPL-water interfaces within a well (CL:AIRE, 2014). Measurements of LNAPL height and thickness in monitoring wells can also be performed using hydrocarbon detection paste on a steel tape, that displays the top of floating hydrocarbons as a wet line and the top of water as a distinct color change, or a transparent bottom-loading bailer, that can be used to measure and sample LNAPL. LNAPL elevations measured in wells are generally assumed to represent the surface of the LNAPL in the surrounding formation (Mercer and Cohen, 1990). However, it should be noted that this assumption may not always be true. Although monitoring wells can help determine the presence or absence of LNAPL, they should not be the sole assessment tool. The absence of LNAPL in a monitoring well does not necessarily indicate the absence of LNAPL in the soil. The product may be present in concentrations that prevent it from moving freely in the subsurface, and therefore it may not enter the well screen as a supernatant product. It is equally important to be careful when monitoring the progress of remediation activities because if the measurable in-well LNAPL thickness becomes unmeasurable after remediation, it is not accurate to infer that there is no residual LNAPL in the surrounding subsurface. LNAPL could still be present in pores that are not continuous and at saturations lower than those required for lateral migration or mobilization into a monitoring well (ITRC, 2018). When the supernatant is visible in the well, its free phase thickness is often considered as an important factor. However, it is important to note that the thickness of measured LNAPL in wells (apparent thickness) differs from the actual thickness in the aquifer (Lenhard and Parker, 1990). The apparent thickness can be up to 2 to 10 times greater than the corresponding thickness of a formation saturated with LNAPL. This occurs because LNAPL perched above the water-saturated zone flows into the well and depresses the well water level.

In general, the difference between the two increases as the formation grain size decreases, the capillary fringe height increases, and the LNAPL density increases (Mercer and Cohen, 1990). Additionally, the influence of groundwater fluctuations on oil mobility and supernatant thickness is well recognized (Atteia et al., 2019), as previously described (Figure 1.8).

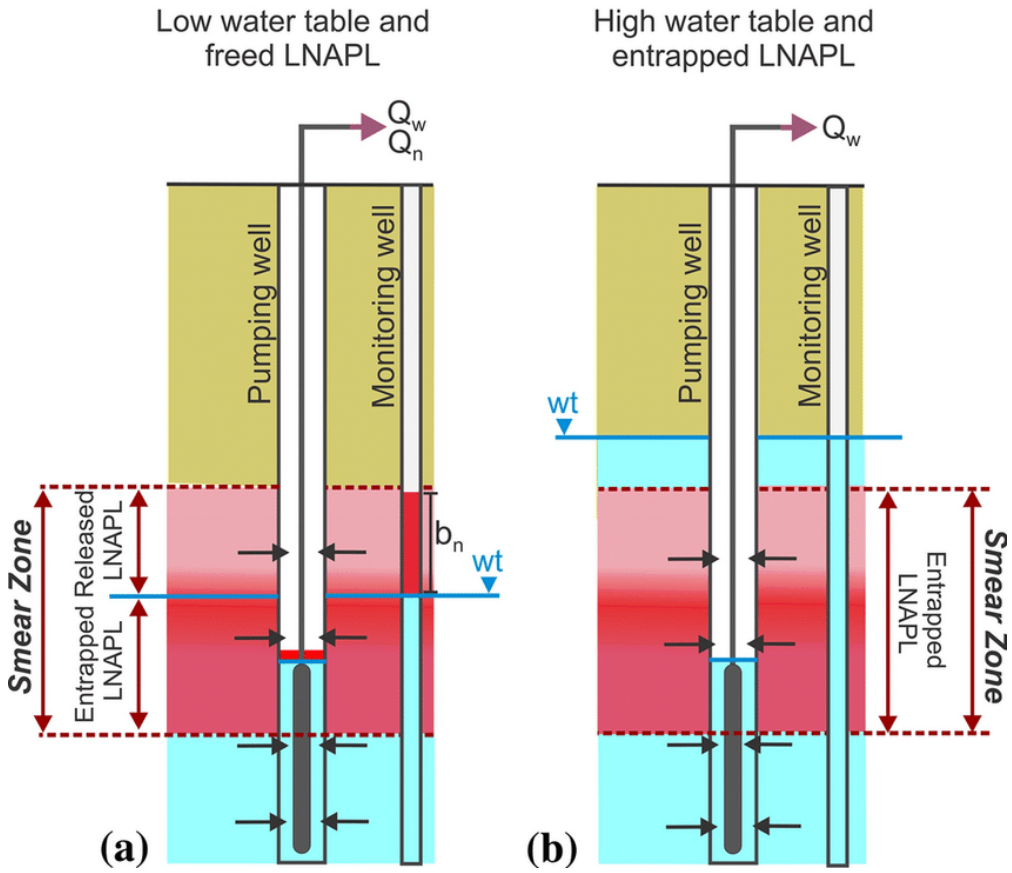

Figure 1.8. Mobilization of LNAPL in the subsurface and apparent thickness of LNAPL in wells as a function of groundwater table conditions (Teramoto et al., 2020)

Monitoring wells are also typically used to obtain groundwater samples for laboratory analysis of dissolved contaminant concentrations. Groundwater concentrations can support the determination of the presence of LNAPL, but they should not be considered absolute indicators. The concentrations of dissolved components can be affected by the variation in product compositions and degrees of weathering, making it impossible to identify a specific concentration in groundwater that indicates the presence of LNAPL. However, measurements of groundwater concentration closer to

the effective solubility indicate a higher likelihood of the presence of LNAPL (ITRC, 2018).

1.4.3 Direct push methods

In addition to traditional sampling methods, in-situ penetration tests have become a popular approach for site investigation (Tsai et al., 2020). Penetration tests usually involve the standard penetration test (SPT) and cone penetration test (CPT). These tests are conducted in boreholes using direct-push tools to deliver the sensor probes, sampling, and analytical devices to the desired depths. This method provides rapid results for site investigations, but it should be noted that the devices may not be suitable for all types of ground conditions, like gravel or highly consolidated soils (USDA, 2012). Furthermore, data is unreliable under unsaturated conditions, especially in clayey soils (USDA, 2012). Direct push investigation tools can be coupled with sensors to provide information on subsoil contamination. Specifically, for LNAPL, probes such as the Membrane Interface Probe (MIP), the Laser-induced fluorescence (LIF) and the Optical Image Profiler (OIP) (CL:AIRE, 2014; Mineo, 2023) are often used.

MIP is a tool that provides a semi-quantitative estimate of the distribution of VOC in unconsolidated formations (Figure 1.9). The MIP membrane is positioned in direct contact with the geological formation, allowing for the diffusion of subsurface VOC, which are collected in a carrier gas stream and subsequently detected using methods such as photoionization detector (PID) or flame ionization detector (FID) (ASTM, 2012). The method is able to quickly identify areas for further investigation by locating areas of high VOC concentrations and plumes but does not differentiate between contaminant phases. It is considered to provide screening level data that need to be supplemented with analytical information and should not be used as a replacement for traditional soil sampling and monitoring wells but instead be used as means to optimize a reduced number of boreholes and monitoring wells to achieve site characterization and long-term monitoring objectives (ITRC, 2019).

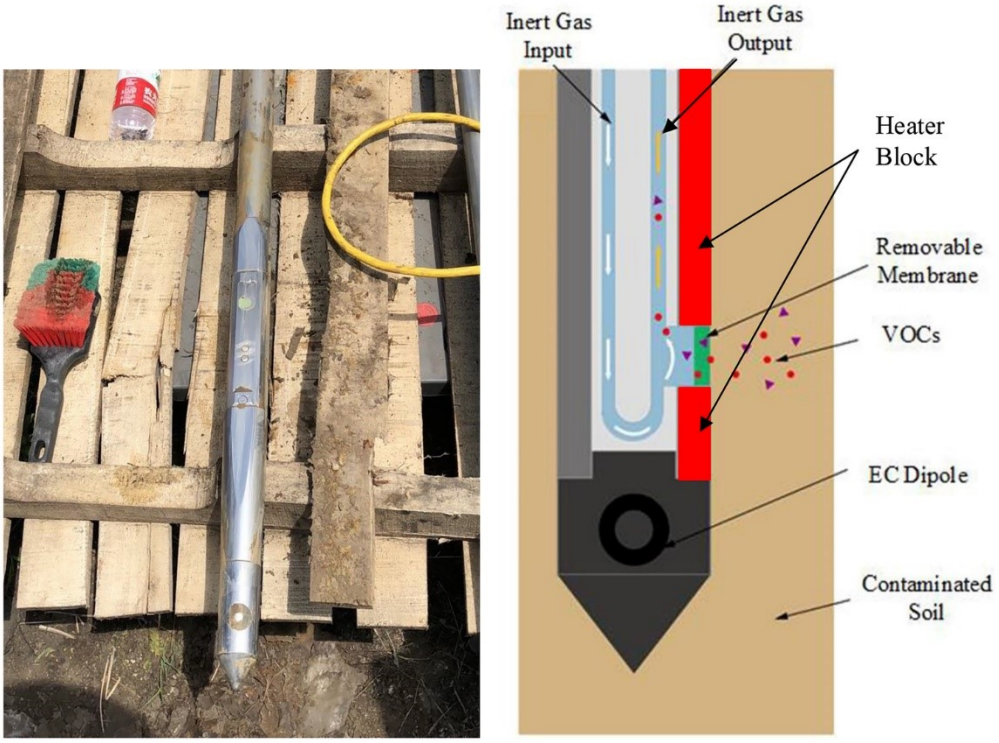

Figure 1.9. MIP probe (Wu et al., 2022)

LIF is an in-situ field screening technique used to detect LNAPL in real-time in the vadose zone, capillary fringe, and saturated subsurface soil. It provides detailed qualitative to semi-quantitative information about the distribution of subsurface contamination that fluoresces, such as petroleum products containing polycyclic aromatic hydrocarbons (Teramoto et al., 2019). Hydrocarbon mixtures produce overlapping spectra, making it impossible to identify individual species. However, they do provide some information about the relative concentrations and the type of LNAPL present (García-Rincón et al., 2020). To optimize detection capabilities for the unique chemistry of one class of NAPL, different LIF systems are required. The Ultra Violet Optical Screening Tool (UVOST®) and Rapid Optical Screening Tool (ROST®) LIF systems are two similar UV-laser-based systems optimized for detecting petroleum products, oils, and lubricants (ITRC, 2019).

The OIP provides photographic images of hydrocarbon fuel fluorescence in the subsurface, using a downhole ultraviolet light-emitting diode to induce fluorescence of fuel LNAPL. The photographic information provided by the OIP can enhance the understanding of LNAPL behavior in the subsurface, aiding in the interpretation of

lithology and formation characteristics (McCall et al., 2018). The ability of the OIP to detect contaminants is influenced by various physical and chemical factors. Confirmatory samples and analysis are necessary to assist with interpreting potential interferences, as false positive results can occur due to interferences such as mineral fluorescence (ITRC, 2019). ITRC (2019) recommends using UVOST® or OIP logging methods for a more accurate and efficient LNAPL assessment when using direct push technologies.

1.4.4 Surface geophysical methods

The investigation methods mentioned in the previous sections rely mainly on a grid of drilling and sampling approaches that provide a relatively limited temporal and spatial resolution, with in situ direct push techniques offering higher resolutions, while soil borings and monitoring well installation offer generally lower resolutions (Griffin and Watson, 2002). The use of nonintrusive methods is a valuable alternative, as is the case of geophysical techniques such as electrical resistivity tomography (ERT), ground-penetrating radar (GPR), and induced polarization (IP). The noninvasive geophysical methods mentioned above have been used for detecting NAPL in the shallow subsurface (Biosca et al., 2020). Geophysical methods measure contrasts in the physical properties of different materials and are used to infer or estimate parameters of interest in the subsurface over large areas. Surface geophysical tools are also indirect methods, so they require correlation or interpretation and can be subject to misinterpretation and for these reasons, are most powerful when used in combination with conventional measurements when they have the potential to reduce characterization and monitoring costs (ITRC, 2019). Electric Resistivity Tomography (ERT) is used to noninvasively determine the spatial variations (both laterally and with depth) of the electrical resistivity of the subsurface (Figure 1.10), which is a function of lithology (porosity, surface area), pore-fluid characteristics (for example, saline water, fresh water, NAPL), water content, and temperature (CL:AIRE, 2014). ERT has been proven to be a reliable survey method for high-resolution delineation of the spatial distribution of an oil plume (Arato et al., 2014; Mineo, 2023), but although a new release of electrically resistive NAPL that forms a continuous, sufficiently thick layer can be detected, ERT is highly unlikely to directly detect an aged NAPL release in the subsurface (ITRC, 2019).

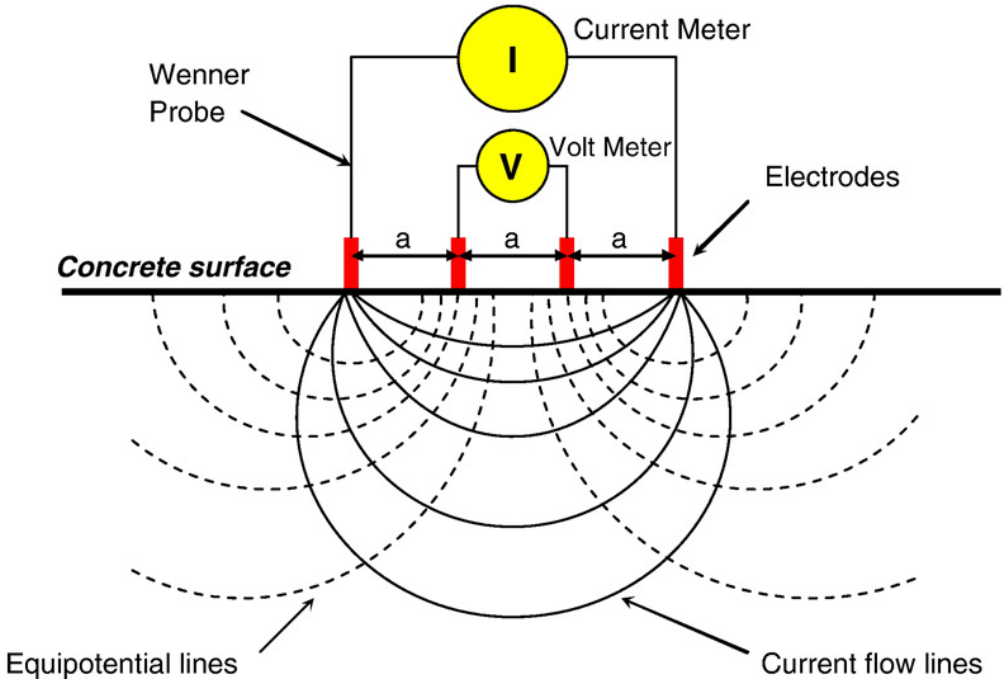

Figure 1.10. Scheme of electrical resistivity subsurface measurement (Robles et al., 2022)

Ground-penetrating radar (GPR) is a widely accepted tool for imaging and characterizing subsurface features, by reflecting high-frequency electromagnetic pulses or waves transmitted from a radar antenna (CL:AIRE, 2014). Its effectiveness depends strongly on site conditions, but it was proven to effectively survey the distribution of LNAPL in the subsurface, especially when there is a high percentage occupancy of pore space (US EPA, 2004). However, NAPL identification with GPR is typically limited to recent, shallow releases that exhibit little weathering of the NAPL via biodegradation (ITRC, 2019).

Induced polarization (IP) utilizes low-frequency polarization mechanisms in earth materials, measuring the ability of the soil to store electrical charges by measuring both the conductive and capacitive properties of the subsurface (Castelluccio et al., 2018). Some authors have identified a relationship between chargeability and organic pollutants. However, varied results have been achieved in field surveys of NAPL-contaminated ground (Johansson et al., 2015).

The interpretation of data obtained from geophysical methods can often be challenging and lead to unclear results, but the combination of different techniques can resolve potential ambiguities that may arise from the measurement of a single

geophysical parameter (Biosca et al., 2020). It should also be noted that geophysical approaches such as ERT and IP require the installation of electrodes on the ground surface and good ground contact. The inability to drill on the concrete surface of some contaminated sites limits the use of these geophysical methods.

1.4.5 Soil gas analysis

Investigative LNAPL identification methods can benefit from vadose zone soil gas surveys as a screening tool for locating potential contamination sources and planning the localization of monitoring wells (Mercer and Cohen, 1990; ITRC, 2018). Direct soil gas monitoring in the vadose zone can be a qualitative indicator of LNAPL impacts for volatile and semi-volatile hydrocarbons. Several chemical characteristics indicate whether a measurable vapor concentration can be detected. Ideally, the compounds detectable using soil gas analysis will partition significantly from water to soil gas, have sufficient vapor pressure to diffuse significantly upward in the vadose zone, be persistent, and also susceptible to detection and quantitation by affordable analytical techniques (Mercer and Cohen, 1990). Soil gas monitoring can be conducted using either permanent or temporary soil gas probes or flux chambers. These surveys use passive (sorbent collectors) or active (direct gas) sampling techniques to determine the spatial extent of VOC and, by inference, LNAPL at the water table or residual LNAPL in the partially saturated zone (CL:AIRE, 2014). Gas samples can be analyzed on site using portable equipment (Figure 1.11) or shipped to a laboratory. Field soil gas screening tools such as PID or FID detectors can be used along with visual observations of the soil core, as the borehole progresses, to verify the presence of contamination, and possibly LNAPL, in the borehole area (ITRC, 2019).

Figure 1.11. Active soil gas sampling using portable equipment (© ENVGUIDE)

Soil gas investigation can also be used to investigate NSZD rates and hydrocarbon degradation. This can be done by monitoring oxygen, carbon dioxide, methane, volatile organic compounds, and temperature in a vertical soil profile (ITRC, 2009; Kulkarni et al., 2022; Ririe and Sweeney, 2022). CO_2 respirometry can also assist in identifying potential sources of LNAPL by measuring CO_2 efflux in soil gas at ground level through a dynamic closed chamber, and differentiate between natural soil respiration CO_2 (Sihota et al., 2011). This can be done measuring background CO_2 flux associated with natural soil respiration, in a background location, or performing radiocarbon ^{14}C-CO_2 analysis (Karimi Askarani et al., 2024), to correct CO_2 efflux measures to be used for LNAPL assessment. Another feasible option is to use the passive flux trap method (Zimbron et al., 2014), which provide integral measurements of CO_2 efflux over the period of deployment . The traps consist of an upper and a lower solid phase sorbent that convert CO_2 into solid phase carbonates. The CO_2 mass accumulated in the bottom sorbent elements is used to calculate the soil CO_2 flux (McCoy et al., 2015).

It is important to note that soil gas analysis is considered qualitative or semi-quantitative and generally cannot quantify NAPL in the source zone, but has been successfully used as a screening technique at many contamination sites and often led to a more focused and cost-effective investigation of source areas (CL:AIRE, 2014). However, these methods can provide misleading results if subsurface conditions are not adequately understood, as the results can be affected by various factors, such as complex vapor transport pathways, and have limitations when dealing with sites containing non-volatile NAPL (ITRC, 2018).

1.4.6 Tracers

Different tracer-based methods have been developed and tested to determine their ability to estimate the location, amount, and distribution of NAPL contamination in laboratory and field conditions (CL:AIRE, 2014). Various types of tracers have been studied in this context, including interfacial tracers that accumulate at the interface between NAPL and water, biogeochemical tracers used to quantify abiotic and biotic reactivity, and partitioning tracers that selectively partition into the NAPL (Rao et al., 2000). In the latter approach, retardation factors for injected partitioning tracers, such as alcohols, are determined by measuring partitioning and nonreactive tracer concentrations in one or more monitoring wells (Annable et al., 1998). The migration of these tracers is then monitored at extraction wells. These data, together with each tracer's specific partitioning characteristics, dependent on the aquifer material and LNAPL (US EPA, 2005), can be used to locate and quantify NAPL contamination (Davis et al., 2002). These methods were primarily tested for Dense Non-Aqueous Phase Liquids (DNAPL), which are typically found in the deeper zones of the aquifer. It should be noted that this approach involves injecting chemicals as tracers, which can be costly and raise additional environmental concerns (Tsai et al., 2020). Alternatively, the use of ^{222}Radon, a natural partitioning tracer that selectively partitions into the NAPL, has been explored in recent years within this context (Mineo, 2023).

CHAPTER 2

2 RADON

Most of this chapter is taken from "Cecconi, A., Verginelli, I., Baciocchi, R., 2024. Assessing LNAPL in the subsurface using the soil gas Rn deficit technique: a literature overview of field studies. Manuscript submitted for publication."

Radon (Rn) is a chemically inert, colorless and odorless, noble gas. It is the heaviest known gas, with a density of 9.72 g L^{-1} at 0°C (i.e. 8 times higher than that of that of air). It is naturally found in the earth's crust and it is a radiogenic gas, produced by the radioactive decay process of ^{226}Ra, and is itself naturally radioactive, decaying directly into ^{218}Po (Stacks, 2015). Radioactive decay is the phenomenon of emission of energy in the form of ionizing radiation, like alpha particles, beta particles, and/or gamma rays. It occurs in unbalanced atoms called radionuclides, which decay into different atoms, known as decay products. This process continues until a stable state is reached, at which point the atom is no longer radioactive. The radionuclides that undergo multiple decays are known as series radionuclides, and the sequence of decay products they produce is called the decay chain. All decay products within the chain are radioactive, except for the final stable atom. Each radionuclide has a specific decay rate, measured in terms of its half-life, the time required for half of the radioactive atoms present to decay (Rösch, 2019)

Several isotopes of radon exist, depending on the referred decay chain. The naturally occurring isotopes that are found in greater quantities are (Gutiérrez Villanueva, 2008):

- ^{219}Rn, actinon, which belongs to the radioactive series of ^{235}U, is formed by the decay of ^{223}Ra and decays in ^{215}Po. It is characterized by a half-life of 3.92 seconds and is naturally present in very low amounts.
- ^{220}Rn, thoron, which belongs to the radioactive series of ^{232}Th, is formed by the decay of ^{224}Ra and decays in ^{216}Po. Thoron has a half-life of 55.6 seconds, but the isotope that produces it is instead quite abundant in nature.
- ^{222}Rn, radon, a more stable isotope, which belongs to the radioactive series of ^{238}U, is formed by the decay of ^{226}Ra and decays in ^{218}Po. It has the highest half-life of all isotopes, at 3.825 days, and is present in almost all mineral grains in the soils and rocks of the earth's crust.

This chapter discusses the behavior of the latter isotope, hereafter referred to as radon (Rn), which is the most studied and of interest in several fields due to its higher half-life and abundance in nature compared to the others.

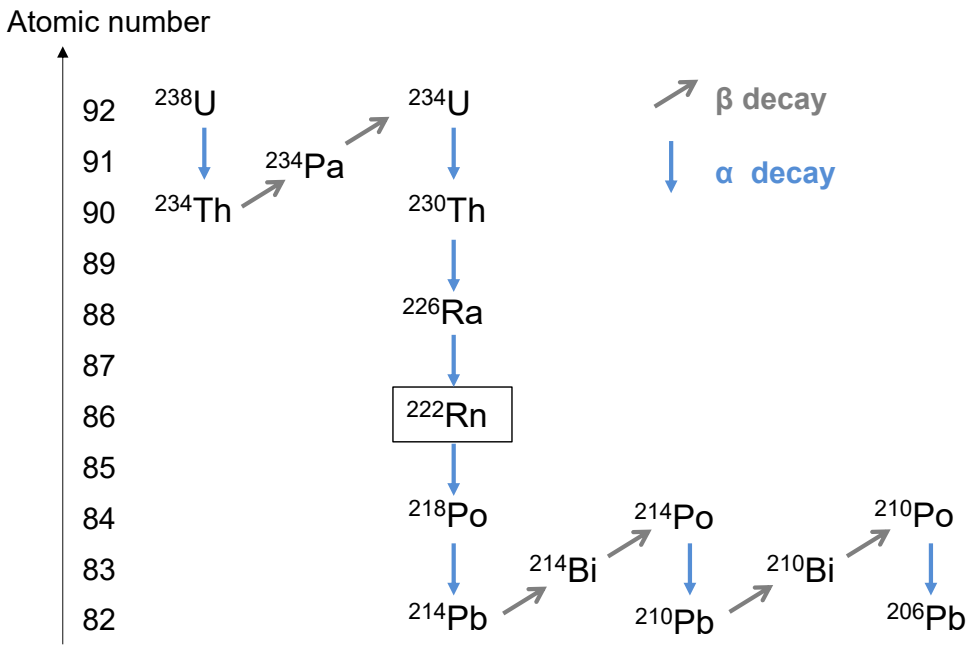

Figure 2.1. ^{238}Uranium decay series. Only main decays are shown. Gamma emitters are not indicated.

Rn is considered a health hazard since exposure to the gas over a long period increases the risk of developing lung cancer (NRC, 1999). Soil and rock are the primary sources of Rn exposure for people. The only other relevant sources are building materials (Nazaroff et al., 1989). During air inhalation, both Rn and its decay products can be inhaled. While Rn is normally expelled on exhalation due to its chemical properties, some of the decay products may remain in the respiratory system. These decay products emit alpha particles, which can affect the lung tissue and potentially cause the formation of cancer cells. Also, the presence of dissolved Rn in drinking water can cause an increased risk of cancer. However, the majority of the risk associated with Rn in water is due to inhalation of the fraction released into the air, rather than ingestion of the water itself (WHO, 2008).

2.1 RADON MIGRATION PROCESS AND ITS INFLUENCE FACTORS

The geological characteristics of a site, such as lithology, porosity and fluid contents, affect the Rn activity concentrations. The activity of a radioactive sample containing a radionuclide at a determined energetic level is the number of spontaneous disintegrations produced in a unit of time, indicating how fast the substance disintegrates with time (Gutiérrez Villanueva, 2008). Activity can be expressed in units of Becquerels (Bq), which corresponds to the number of atoms of any radioactive element required to produce one radioactive decay per second. The activity concentration of a given radionuclide can therefore be defined for unit of volume, expressed in Bq m^{-3}, or mass, expressed in Bq kg^{-1}. Typically, the ^{226}Ra content of soil and rocks is expressed as an activity concentration per unit mass, which is equivalent to the total production rate of ^{222}Rn in the soil (Nazaroff, 1992). For instance, a ^{226}Ra content of 1 Bq kg^{-1} is equivalent to a total ^{222}Rn production rate of 1 atom kg^{-1} s^{-1}. Since the activity concentration of a radioisotope A is related to the number of atoms N and its radioactive decay constant λ (with $A = N \cdot \lambda$), a total ^{222}Rn production rate of 1 atom kg^{-1} s^{-1} corresponds to $2.1 \cdot 10^{-6}$ Bq kg^{-1} s^{-1} (considering the radioactive decay constant λ for ^{222}Rn of $2.1 \cdot 10^{-6}$ s^{-1}).

The content of radium and uranium, Rn precursors, varies among different types of rocks. For instance, acid igneous rocks such as granites, some types of bituminous shale, and phosphatic rocks typically exhibit higher average uranium activity concentrations (Table 2.1).

Table 2.1. Typical Uranium activity concentrations in certain rock types (UNSCEAR, 1977)

Rock type	**^{238}U (Bq kg^{-1})**
Igneous - Acidic (e.g. granite)	59.2
Igneous - Intermediate (e.g. diorite)	22.9
Igneous - Mafic (e.g. basalt)	11.5
Igneous - Ultrabasic	0.4
Sedimentary - Limestone	27.7
Sedimentary - Carbonate	26.6
Sedimentary - Sandstones	18.5
Sedimentary - Shale	44.4

Being an inert gas with no tendency to form chemical bonds, Rn can move through porous materials such as soil even at significant distances from the point of generation. It can migrate in the subsurface by diffusion through the pores in the opposite direction to the concentration gradient, pressure-induced advection, and convective transport by another fluid. Then it can be released from the soil surface into the atmosphere or enter buildings through cracks, porous building materials, and other pathways (Nazaroff et al., 1989) if decay has not yet occurred. The different processes mentioned here, from generation to exhalation from the surface, are detailed below.

2.1.1 Emanation

When a ^{226}Ra atom decays into a Rn atom, it generates alpha particles that move in the opposite direction of the Rn atom, which continues to move in its direction until it transfers its energy to another material. This distance, called recoil range, is typically 20-70 nm in common solid materials, 100 nm in water, and 63 μm in air (Tanner, 1980). Depending on the point of Rn generation in the soil material, and to the geometry of the grains, therefore, three situations can occur: after having traveled a

short distance, the atom remains inside the same grain of soil; the atom passes through a pore and enters an adjacent grain; the atom is ejected from the grain, arriving in the interstitial space, and is later expelled by soil gases or water (Sakoda et al., 2011). The release of Rn into soil pores is primarily caused by the phenomenon of recoil. Emanation by diffusion can be disregarded due to the extremely low Rn diffusion coefficient in mineral matrices, which ranges from 10^{-31} to 10^{-69} m^2 s^{-1}, resulting in diffusion lengths between 10^{-7} and 10^{-26} µm (Nazaroff, 1992).

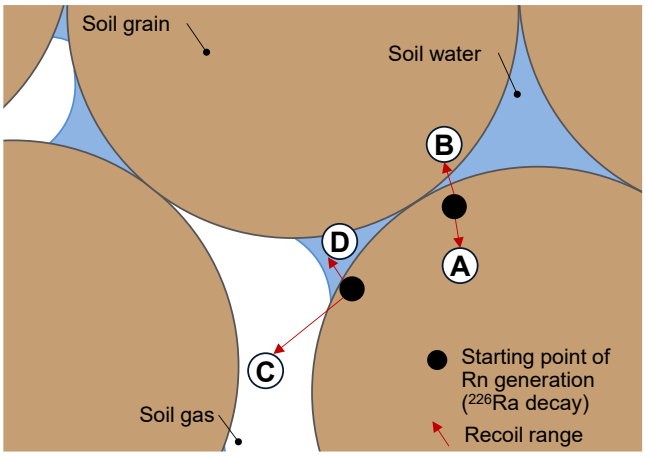

Figure 2.2. Scheme of Rn emanation phenomenon. Cases C and D represent the emanation phenomena. Cases A and B non-emanation. The black dots indicate the starting point of Rn generation, from 226Ra decay. The red arrows represent an indication of the recoil range, not in scale (after Sakoda et al. (2011)).

The emanation coefficient is a crucial parameter that characterizes the physical behavior of Rn in the context of emanation. It represents the fraction of Rn atoms that escape from mineral grains into the interstitial space. Various methods exist to determine its value, all based on measuring the maximum Rn concentration emanating from a sample in a closed space after achieving secular equilibrium, along with measuring radium in the same sample (Hassan et al., 2009).

Several factors can affect the emanation coefficient value. For instance, the distribution of ^{226}Ra is not homogeneous throughout the volume of the soil grain but rather is concentrated on its surface (Krishnaswami and Seidemann, 1988). Because smaller grains have a higher surface area to volume ratio, this results in larger amounts of radium and higher values of the emanation coefficient for finer grained soils. Furthermore, with smaller grains, Rn is more easily carried out of the grain itself in the recoil phenomenon (Sakoda et al., 2011). Additionally, as the water content

increases, there is an increase in emission due to the smaller recoil range of Rn in water compared to air, since this reduces the probability of a Rn atom to enter an adjacent grain by recoil and increases the probability of terminating its recoil in a pore that is at least partially saturated with water rather that in one that is dry (Nazaroff, 1992). It was also shown that with a high water content in the soil, close to saturation conditions, the emission coefficient remains almost constant (Nazaroff et al., 1989). It was observed that the emanation coefficient reaches a maximum value for water content of 5% for general soil type, for 1–2% for gravel and 10-15% for clay at 10–15% (Markkanen and Arvela, 1992).

It must be considered that there is a direct relationship between the Rn emanation coefficient in the soil and temperature. An increase in temperature causes a decrease in the physical adsorption of Rn onto grains. Consequently, the Rn diffusion coefficient increases, and its concentration in pore air increases as well (Stranden et al., 1984; Barrio-Parra et al., 2021). The emanation coefficient at different temperatures can be estimated using the following equation (Iskandar et al., 2004):

$$\varepsilon = \varepsilon_m + 0.0021 \cdot (T - T_m) \qquad \text{Eq. 2.1}$$

where ε_m (-) is the measured or known emanation coefficient, T_m (°C) is the soil temperature at the time of sampling, and ε (-) is the calculated emanation coefficient at temperature T (°C).

2.1.2 Partitioning in soil pores

In the case of uncontaminated soil, the distribution of Rn atoms in the soil can be classified into four states: bound within solid soil grains, sorbed onto the surface of soil grains, dissolved within water contained in the soil pores, and dispersed within the gas contained in the soil pores. As discussed in the previous section, the diffusion from the mineral matrix can be disregarded due to the low Rn diffusion coefficient in the solid phase. The exchange of Rn atoms among the remaining three states may be rapid relative to Rn's half-life (Nazaroff, 1992). Rn has moderate solubility in water, with a value of 230 $cm^3\ kg^{-1}$ at 20°C and 1 atm (NCRP, 1988). As a result, it can dissolve in subsoil pore water and be transported by groundwater in the saturated zone. However, Rn absorption in water is reversible, and its tendency to be desorbed, considering the value of the water/air partition coefficient, is quite high. At a temperature of 20°C the dimensionless partition coefficient of Rn between water and

air $k_{w/g}$ is in fact approximately 0.25. Therefore, the equilibrium Rn concentration in air is about four times that of Rn in water (Schubert et al., 2001). The dimensionless Henry's constant for Rn is a function of temperature T, following the relationship (Nazaroff, 1992; Perrier et al., 2009):

$$\mathrm{H(T)} = \frac{1}{(0.105 + 0.403 \cdot \mathrm{e}^{-0.0502 \cdot \mathrm{T}})} \qquad \text{Eq. 2.2}$$

Where T is expressed in °C. Note that the empirical relationship is consistent with experimental results, resulting in the coefficient values reported in Table 2.2 (Lee et al., 2010).

Table 2.2. Dimensionless Henry's constant values for Rn (Lee et al., 2010).

Temperature °C	Dimensionless Henry's constant
0	1.875 ± 0.155
10	2.365 ± 0.255
20	3.65 ± 0.27
30	5.27 ± 0.34

Rn interactions with the surfaces of soil grains may play a significant role in the emanation and transport processed in dry soils. However, sorption effects are likely to be smaller under typical soil moisture conditions in the environment (Schery et al., 1989). The partitioning of Rn between the water (or gas) and sorbed phases can be described by a linear sorption isotherm (Nazaroff, 1992).

2.1.3 Transport

On a long-term average basis, available evidence suggests that Rn transport from the soil into the atmosphere occurs predominantly by molecular diffusion (Nazaroff, 1992). Due to the higher Rn concentrations in soil gas compared to the atmosphere, Rn atoms diffuse through interstitial pores and migrate toward the soil surface. Fick's law describes the diffusive flux J_{diff} (Bq m^{-2} s^{-1}), directly proportional to the concentration gradient $\nabla \mathrm{Rn}$:

$$\mathrm{J_{diff}} = -\mathrm{D_e} \cdot \nabla \mathrm{Rn} \qquad \text{Eq. 2.3}$$

Where Rn (Bq m^{-3}) is the Rn activity concentration and D_e (m^2 s^{-1}) is Rn effective diffusion coefficient. The effective diffusion coefficient in the subsoil generally varies with the properties of the species being diffused, the pore structure, the types of fluids present in the pores, the degree of fluid saturation, the temperature, and the adsorption properties of the solid matrix. Various models can be utilized to estimate its value, depending on these parameters, as those of Penman, (1940a, 1940b), Marshall (1958), Millington and Quirk (1961) and Millington and Shearer (1971). The soil's water content significantly affects the effective diffusion coefficient of Rn in an inversely proportional manner, since Rn diffusion coefficient in water is about 4 orders of magnitude lower than that in air. Both values are shown below in Table 2.3. Note that when the soil is drier, Rn ability to migrate into the soil increases even though the rate of emanation decreases. Instead, when the water content increases, the rate of emanation also increases but the diffusivity and permeability of the soil are significantly reduced (Strong and Levins, 1982).

Table 2.3. Rn diffusion coefficients in air and water at 20°C.

Parameter	**Value**	**Reference**
Rn diffusion coefficient in air D_{mg}	$1.2 \cdot 10^{-5}$ m^2 s^{-1}	(Tanner, 1964)
Rn diffusion coefficient in water D_{mw}	$1.16 \cdot 10^{-9}$ m^2 s^{-1}	(Broecker and Peng, 1974)

It is also observed that the Rn diffusion coefficient decreases as the soil and sand grain size decrease, due to the decrease in porosity and increase in the bulk density (Chauhan et al., 2008).

It is important to note that advective transport can occur in the subsurface under the influence of pressure gradients, in addition to diffusive transport, which is typically considered predominant (Hillel, 1982; Scanlon et al., 2002). Darcy's Law describes the advective transport of a fluid through a porous medium when the flow is laminar and the resistance to flow is dominated by the viscosity of the fluid. In its differential form, Darcy's Law can be expressed as:

$$J_{adv} = -\frac{k_g}{\mu} \cdot \nabla p \qquad \text{Eq. 2.4}$$

Where J_{adv} ($m^3\ m^{-2}\ s^{-1}$) represents the volumetric advective flow, k_g (m^2) is the gas permeability of the soil; μ (kg $m^{-1}\ s^{-1}$) is the dynamic viscosity of the fluid and ∇p (kg $m^{-2}\ s^{-2}$) is the pressure gradient. Advection may be significant, particularly in the surface layer (approximately the first meter) of the soil due to barometric pressure gradients (Auer et al., 1996; Forde et al., 2019). At greater depths, advection is typically caused by pressure changes, such as faults and fractures, and the presence of gas carriers, such as CO_2 and CH_4 (Etiope and Lombardi, 1995; Čeliković et al., 2022). Local advection can also occur in conditions such as significant fluctuations of the groundwater table level (Qi et al., 2020; Man et al., 2021; Cavelan et al., 2022) and can be enhanced in soil materials with high permeability and fractures that create preferential paths in the soil gas (Cunningham and Williams, 1980; Scanlon et al., 2002). Chapter 4 presents a more detailed analysis of the impact of advection on Rn transport in soil gas.

2.1.4 Exhalation

Soil gas Rn is transported through the soil toward the surface and released into the atmosphere in a process known as exhalation. The exhalation rate is the number of Rn atoms released from a surface unit into the atmosphere can be expressed per unit time (Bq $m^{-2}\ s^{-1}$) or as a mass exhalation rate (Bq $kg^{-1}\ s^{-1}$). Rn exhalation rate J_{exh} (Bq $m^{-2}\ s^{-1}$) can be calculated as (Hassan et al., 2009):

$$J_{exh} = \rho_s \cdot \varepsilon \cdot C_{Ra} \cdot (\lambda \cdot D_e)^{\frac{1}{2}} \qquad \text{Eq. 2.5}$$

Where, ρ_s (kg m^{-3}) is the soil density, ε (-) is Rn emanation coefficient, C_{Ra} (Bq kg^{-1}) is the radium activity concentration in the soil, λ (s^{-1}) is the Rn decay constant and D_e ($m^2\ s^{-1}$) is Rn effective diffusion coefficient.

The process of exhalation is influenced by various factors. Some of these, such as soil water content, porosity, grain size, and temperature, have an influence on the Rn emanation and diffusion coefficient and, therefore, indirectly affect the exhalation rate (Hassan et al., 2009). On the other hand, other factors, such as the pressure difference between the ground surface and the soil, have a more direct impact on the exhalation phenomenon. A negative pressure difference occurs when the pressure at the ground surface is lower than the deep soil pressure. This leads to an increase in Rn concentration in the layers near the ground surface. Air, rich in Rn, is drawn upward from deeper layers (where the Rn concentration is higher than that near the

ground surface) to the upper layer, resulting in a smooth increase in the Rn exhalation rate. Conversely, a positive pressure difference occurs oppositely. Other external parameters that influence exhalation rate include wind (which is directly proportional) and rainfall (which is inversely proportional in the case of heavy rainfall) (Hassan et al., 2009; Čeliković et al., 2022). Daily variations in Rn flux are mainly attributed to soil temperature. It was observed that Rn flux is highest in the afternoon when temperature is highest and soil water content is lowest (Yang et al., 2014; Čeliković et al., 2022). High exhalation rates are typically found in seasons characterized by lower precipitation and low water content (Kitto, 2005; Zhuo et al., 2008; Hirao et al., 2010; López-Coto et al., 2013).

2.2 RADON MEASUREMENTS

The identification and estimation of Rn activity concentration in environmental matrices typically involves procedures that utilize its alpha emitter properties. The energy of alpha particles, emitted from Rn itself or its decay products, varies between 5.5 and 7.7 MeV (Stacks, 2015). Two main sampling approaches are generally used to detect Rn: passive mode, where Rn enters the instrument through natural diffusion, and active mode, where Rn is pumped into an Rn detecting device (Janik et al., 2014). Furthermore, three types of Rn sampling methods can be employed: instantaneous or grab sampling, continuous sampling, and integration techniques (Sumesh et al., 2024). Instantaneous techniques involve the collection of samples over a short period, such as 10 minutes, to be analyzed shortly thereafter, usually within 4 hours (George, 1990). For each sample, it provides a single activity concentration value, valid for the specific conditions at the time of the survey. It can be performed on-site using a portable instrument that allows for sampling and quick measurement of Rn activity concentration, or by taking samples in special containers to be later analyzed in specialized laboratories (Papastefanou, 2007). The detectors commonly used for this type of application are scintillation cells, ionization chambers, and semiconductor detectors. The signals are then converted into measurable pulses using appropriate processing electronics and algorithms. Measuring Rn or Rn progeny continuously involves simultaneous sampling and analysis, providing real-time results. This is particularly useful in situations where Rn activity concentrations can change significantly and rapidly. Measurement intervals typically range from 15 to 60 minutes, with useful results obtained after 2 to 3 hours of continuous sampling and counting. Continuous Rn and Rn progeny monitors offer real-time Rn activity concentration data and can measure other parameters such as temperature, pressure, or humidity. Additionally, they allow for the analysis of time trends in real-time recorded parameters. However, these instruments are expensive and complex, requiring trained personnel to operate (George, 1990). Integrating methods provide a single Rn activity concentration value that is representative of the average activity concentration over an observation period that can range from a few days to a year (Sukanya et al., 2022). Integrated measurement with passive instrumentation is usually the most commonly used.

Other criteria that differentiate them are the applicability of field measurements, portability, and cost. Various technologies can be used to measure Rn in the different configurations mentioned above. Some examples of this technology with further details are given below, classified according to the type of sampling.

2.2.1 Active mode

Active mode measurement methods, such as scintillation cells, ionization chambers, and semiconductor detectors, are typically utilized for field measurements or in situations where continuous measurement is required.

Scintillation cells, also known as Lucas cells (Lucas, 1957), are hermetically sealed containers that are filled with a sample containing the Rn gas, or the emanated Rn from water, to be analyzed. Rn gas can be collected inside the cell either using a pre-evacuated scintillation cell or by flow mode. A filter is typically included to prevent dust and Rn decay products from entering the cell and affecting the counting process (Sumesh et al., 2024). The internal coating of the scintillation cell is made of silver-activated zinc sulfide ZnS, which scintillates when alpha particles resulting from Rn decay strike it. Light photons are produced when alpha particles from Rn and its decay products interact with zinc sulfide in the cell (Sethy et al., 2014). The photons can then be counted using, for instance, a photomultiplier tube, and the resulting data, usually expressed in terms of Bq m^{-3}, is sent to a digital data logger.

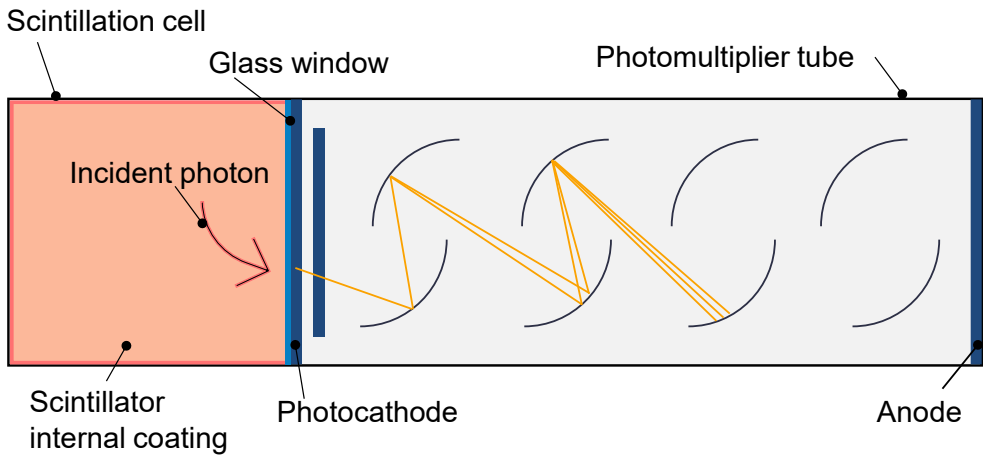

Figure 2.3. Schematic of a scintillation cell coupled with a photomultiplier tube.

Ionization chambers typically comprise cylindrical volumes with metal walls and two electrodes: one consisting of the walls themselves and the other of a central wire acting as an anode. An electrical field is established between the electrodes. Filtered air is either allowed to diffuse into the chamber or is pumped in. Electrons are produced by the ionization of sampled air by alpha particles of Rn and its decay products (Fortmann, 1993). Ions generated by Rn decay products are collected by the charged electret, and the charge decreases proportionally to the integrated Rn activity concentration over the exposure period. The measurement can be done either by measuring the total ionization in the chamber or by counting the pulses caused by individual alpha particles separately (Sukanya et al., 2022). These instruments are adequate for high-precision measurements but are usually complex and expensive (Nunes et al., 2023).

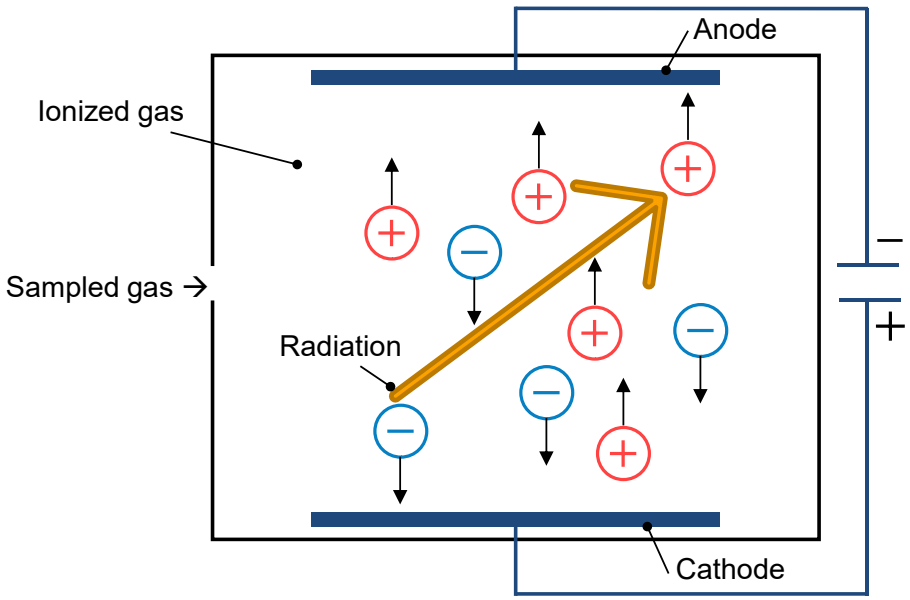

Figure 2.4. Schematic of an ionization chamber.

Semiconductor detectors use a semiconductor material (usually silicon) that is sensitive to the presence of charged particles, in particular transforming alpha radiation into an electrical signal. Charged particles passing through the device generate electron-lacuna pairs and are collected by the electrodes, creating ionization currents. The energy deposited in the detector material is directly converted to an electrical signal based on the electrostatic collection of Rn and its progeny. The gas is made to enter into the collection chamber either by passive diffusion or by active

methods like pumping through a filter paper. The main advantage of these detectors is their capacity to electronically discriminate the energy of each incident alpha particle (Sumesh et al., 2024).

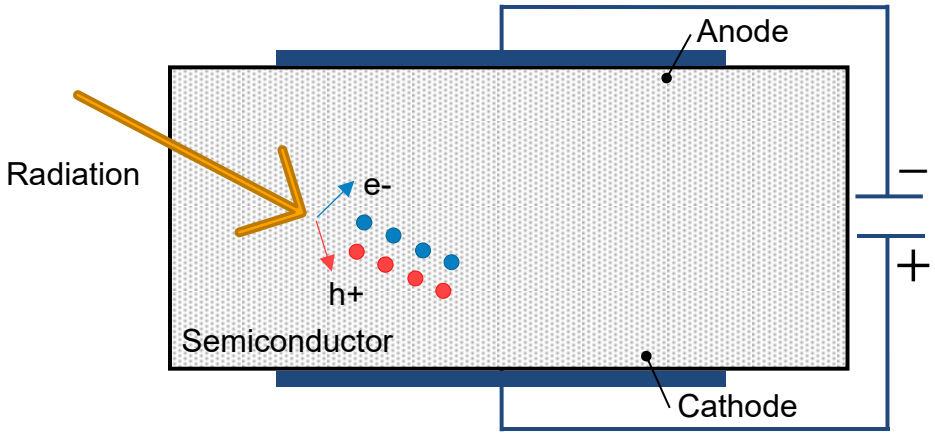

Figure 2.5. Schematic of a semiconductor detector.

2.2.2 Passive mode

Passive instrumentation is commonly used for integrated measurement. The commonly used devices are Solid State Nuclear Track Detectors (SSNTD), electrets ionization chambers, or activated carbon.

SSNTD relies on the use of materials that are sensitive to alpha radiation, which causes damage to the chemical bonds of the material itself, leaving traces known as tracks (Nikezic and Yu, 2004). These traces are distinguishable from the intrinsic irregularity and damage to the crystal structure and can be made visible under an optical microscope by chemically treating them with a basic solution (Miles and Sinnaeve, 1986). The traces can then be analyzed using optical or electronic techniques. SSNTDs are suitable for long-term measurements and provide a measure of the average Rn activity concentration during the exposure period (Nunes et al., 2023). Several sensitive materials are used for this purpose, such as LR-115 (cellulose nitrate), CR-39 (polyallydiglycol carbonate), and Makrofol (polycarbonate) (Gewali et al., 2021).

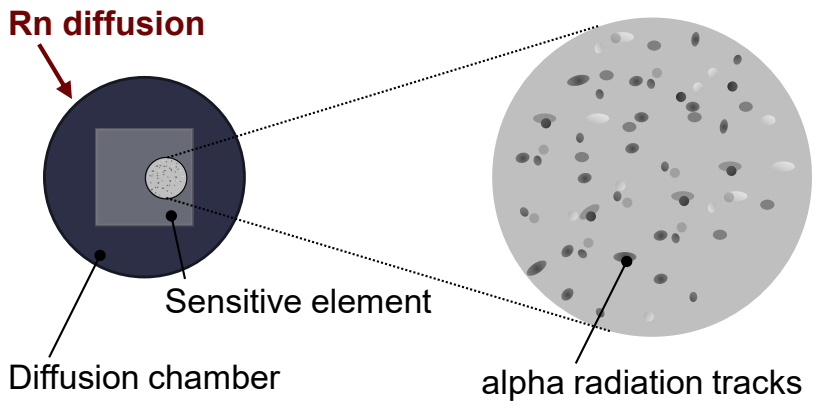

Figure 2.6. Schematic of a solid state nuclear track detector.

Electret ionization chambers are portable and passive integrating devices that consist of an electrically conducting chamber with an electret at the bottom and a filtered inlet at the top. The electret is usually a piece of polytetrafluoroethylene that has been electrically charged and processed to exhibit a stable charge. Rn passively diffuses in the chamber, and the alpha particles emitted by the decay process ionize the gas collected inside the chamber (Kotrappa et al., 1988). The surface charge of the electret produces an electrostatic field that collects ions generated by the ionization produced by Rn and its associated decay products inside the chamber, causing a drop in the surface voltage of the electret (Kotrappa et al., 1992). The charge reduction on the electret surface is measured by a specially designed electret voltage reader, and the result can be used as a time integrator of Rn exposure.

The method of activated carbon utilizes passive diffusion to collect Rn from the environment by adsorbing it onto activated charcoal, which has an affinity for many gases, including Rn (George, 1984). The collector, containing charcoal with adsorbed Rn and decay products, is sealed after exposure. Counting is typically performed at least 3 hours after exposure to ensure equilibrium between Rn and its progenitors (George, 1990). The measure can be performed employing two detection methods: gamma counting and liquid scintillation. Rn activity concentration can be determined by counting gamma rays emitted by Rn progeny during the decay process (ISO, 2019), using a standard gamma-ray spectrometer equipped with high-purity germanium HPGe or sodium iodide doped with thallium NaI (Tl) detectors (Sukanya et al., 2022). Liquid scintillation uses the high solubility of Rn in aromatic solvents such as toluene. To analyze charcoal exposed to Rn using this technology, it is mixed with

a liquid scintillation cocktail in which Rn readily dissolves (L'Annunziata, 2012). The alpha activity concentrations of Rn and its decay products are then measured by detecting the rate of photons emitted from the scintillation fluid using a liquid scintillation counter.

2.3 RADON AS A NATURAL TRACER FOR THE IDENTIFICATION OF LNAPL CONTAMINATION

In addition to its association with human health risks, Rn is also studied for its potential applications in the environmental field. Researchers are studying its behavior in the soil as a potential seismic precursor, and it is used in hydrological research to assess interactions between deep and surface waters due to its rapid dispersion in the air (Baskaran, 2016). Additionally, it is being studied as an environmental tracer due to its ubiquitous presence in nature, detectability, and inert behavior. Since radium is present in almost all minerals, Rn is constantly produced in every soil or aquifer matrix (Schubert, 2015). As an environmental tracer, it has the advantage of not creating additional environmental contamination, not altering the physical and chemical balance of the studied medium, and being suitable for large-scale and long-term studies (Quindos Poncela et al., 2013). Additionally, Rn has been shown to tend to preferentially partition into organic phases. For this reason, several authors suggested using Rn as an environmental tracer for the assessment of NAPL contamination (Schubert, 2015) in both the saturated (e.g., Hunkeler et al., 1997; Semprini et al., 2000; Fan et al., 2007; Schubert et al., 2007b; Yoon et al., 2013; Briganti et al., 2020, 2023) and vadose zone (e.g., Schubert et al., 2001; Höhener and Surbeck, 2004; Schubert et al., 2005; García-González et al., 2008; Barbosa et al., 2014; De Simone et al., 2015; Mateus and Pecequilo, 2015; Cohen et al., 2016; Castelluccio et al., 2018; Cohen et al., 2019; DeMiguel et al., 2020).

As described in the previous sections, Rn activity concentration in soil pores reaches equilibrium conditions due to continuous emanation and decay processes (Nazaroff, 1992). This equilibrium is regulated by the solid matrix of the soil, and it is disturbed in the presence of LNAPL (Semprini et al., 2000). Rn in soil pores will tend to partition into the NAPL, resulting in a decrease in concentration in both water and interstitial gases (Figure 2.7). Indeed, it has been shown (e.g., Semprini et al., 2000; Davis et al., 2002; Höhener and Surbeck, 2004; Schubert, 2015; Castelluccio et al., 2018; Briganti et al., 2020; Barrio-Parra et al., 2021) that in the NAPL-contaminated portions of the subsurface there is a local decrease of Rn, known as Rn deficit, in groundwater or soil gas compared to the background concentration in unaffected areas. Thus, the Rn-deficit technique (Semprini et al., 2000) can be used to predict the presence of NAPL in the subsurface. In this technique, Rn concentration in an uncontaminated

soil can be considered as the background value of the area: it is related to the radium activity concentration (from which Rn originates), the dimensionless emanation coefficient of Rn, soil porosity and soil density (Andrews and Wood, 1972). In the presence of NAPL Rn will partition in the soil pores between water, gas, and the NAPL phase (Schubert et al., 2001). Considering linear partitioning, it is possible to retrieve Rn concentration in soil gas or groundwater in the presence of NAPL.

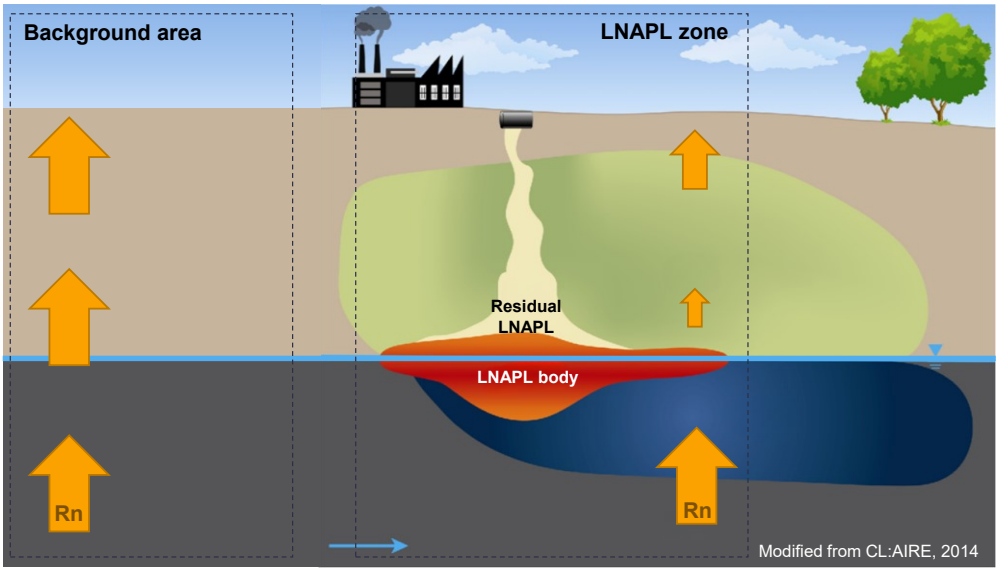

Figure 2.7. Schematic of Rn behavior in the subsurface, in the LNAPL zone (minor expected activity, on the right) and the background uncontaminated zone (major expected activity, on the left) (modified from CL:AIRE (2014)).

Additional information on the theory behind the technique and the configurations tested for its application is provided in the following paragraphs.

2.3.1 Radon deficit in equilibrium conditions

Under the assumption of equilibrium conditions, Rn activity concentration in the soil pores, in an uncontaminated (background) area Rn_0 (Bq m^{-3}), can be described as (Andrews and Wood, 1972):

$$Rn_0 = \frac{\varepsilon \cdot C_{Ra} \cdot \rho_s}{\theta_t} \qquad \text{Eq. 2.6}$$

where ε (-) is the Rn emanation coefficient, C_{Ra} is the ^{226}Ra concentration of the solids (Bq kg^{-1}), ρ_s is the dry soil bulk density (kg m^{-3}) and θ_t is the soil porosity (-). Given the

coexistence of water and gas in soil pores, the following relationship can be written (Semprini et al., 2000):

$$Rn_0 = Rn_{w,b} \cdot S_{w,b} + Rn_b \cdot S_{g,b} \quad \text{Eq. 2.7}$$

Where $Rn_{w,b}$ (Bq m^{-3}), and Rn_b (Bq m^{-3}) are respectively the Rn activity concentration in equilibrium conditions in the water and gas, and $S_{w,b}$ (-) and $S_{g,b}$ (-) are respectively the water and gas saturations in the soil in the background area, related to each other as follows, if only two fluids are present in the system:

$$S_{g,b} = 1 - S_{w,b} \quad \text{Eq. 2.8}$$

Water and gas saturations can be calculated from the volumetric content of water and gas in the soil, respectively, as follows:

$$S_{w,b} = 1 - \theta_{w,b} \quad \text{Eq. 2.9}$$

$$S_{g,b} = 1 - \theta_{g,b} \quad \text{Eq. 2.10}$$

Considering a linear repartition between water and gas Rn partition coefficient $k_{w/g}$ can be introduced:

$$k_{\frac{w}{g}} = \frac{Rn_w}{Rn} \quad \text{Eq. 2.11}$$

Eq. 2.7 can be written as:

$$Rn_0 = Rn_b \cdot (k_{\frac{w}{g}} \cdot S_{w,b} + S_{g,b}) \quad \text{Eq. 2.12}$$

By combining Eq. 2.6 and Eq. 2.12, Rn activity in the soil gas within a volume of soil, Rn_b (Bq m^{-3}), can be described as (Cecconi et al., 2023a):

$$Rn_b = \frac{\varepsilon \cdot C_{Ra} \cdot \rho_s}{\theta_t \cdot (k_{\frac{w}{g}} \cdot S_{w,b} + S_{g,b})} \quad \text{Eq. 2.13}$$

All terms in the equation depend on soil characteristics. Therefore, assuming a homogeneous medium, the concentration of Rn in soil gas should remain constant, except for seasonal fluctuations caused mainly by variations in the emanation coefficient or for the decrease of Rn activity in the surface layers due to exhalation. Changes in Rn values in space or time can indicate processes or conditions affecting

Rn distribution in the subsurface, such as the presence of NAPL. Schubert et al. (2001) developed an equation to describe the equilibrium Rn activity in the soil pores within a volume of NAPL-contaminated soil, Rn_0 (Bq m^{-3}).

When there are three phases present in the soil pores, namely water, gas, and NAPL, Eq. 2.7 be expressed as follows:

$$Rn_0 = Rn_w \cdot S_w + Rn \cdot S_g + Rn_N \cdot S_N \quad \text{Eq. 2.14}$$

Where Rn_w (Bq m^{-3}), Rn (Bq m^{-3}), and Rn_N (Bq m^{-3}) are respectively the Rn activity concentration in equilibrium conditions in the water, gas, and NAPL and S_w (-), S_g (-) and S_N (-) are respectively the water, gas, and NAPL saturations in the NAPL-contaminated soil. Note that the following equation applies:

$$S_g = 1 - S_w - S_N \quad \text{Eq. 2.15}$$

Combining Eq. 2.6 and Eq. 2.14, it is obtained (Schubert et al., 2001; Cecconi et al., 2023a):

$$Rn = \frac{\varepsilon \cdot A_{Ra} \cdot \rho_s}{\theta_t \cdot (k_{\frac{w}{g}} \cdot S_w + S_g + k_{\frac{N}{g}} \cdot S_N)} \quad \text{Eq. 2.16}$$

With $k_{N/g}$ (-) Rn NAPL-gas partition coefficient:

$$k_{\frac{N}{g}} = \frac{Rn_N}{Rn} \quad \text{Eq. 2.17}$$

Rn deficit D (-) can be defined as the ratio between the Rn activity concentration in soil gas in the NAPL zone and the Rn activity concentration in the background area.

$$D = \frac{Rn}{Rn_b} \quad \text{Eq. 2.18}$$

This can also be written, from the ratio of Eq. 2.13 to Eq. 2.16, as (Cecconi et al., 2023a):

$$D = \frac{1 + S_{w,b} \cdot (k_{\frac{w}{g}} - 1)}{1 + S_w \cdot (k_{\frac{w}{g}} - 1) + S_N \cdot (k_{\frac{N}{g}} - 1)} \quad \text{Eq. 2.19}$$

This model, initially proposed by Semprini et al. (2000) for groundwater and later expanded to the unsaturated zone by Schubert et al. (2001), is based on the

assumption of secular Rn equilibrium, linear partitioning, and neglecting Rn sorption to the solid matrix. It also assumes uniform mineralogy and emanation throughout the investigated area, including both contaminated and uncontaminated zones.

Figure 2.8 provides an example of the theoretical relationship between Rn deficit and NAPL saturation, for sandy soil in the vadose zone, for two different partition coefficient values, corresponding to NAPL with a typical composition of gasoline and diesel mixtures (Schubert et al., 2007b). It can be observed that the Rn deficit varies greatly for low values of NAPL saturation, and even a small change in the deficit value can result in large changes in S_N. As S_N increases, the Rn deficit tends asymptotically to zero. Therefore, the model is not sensitive to high NAPL saturations (Schubert et al., 2001).

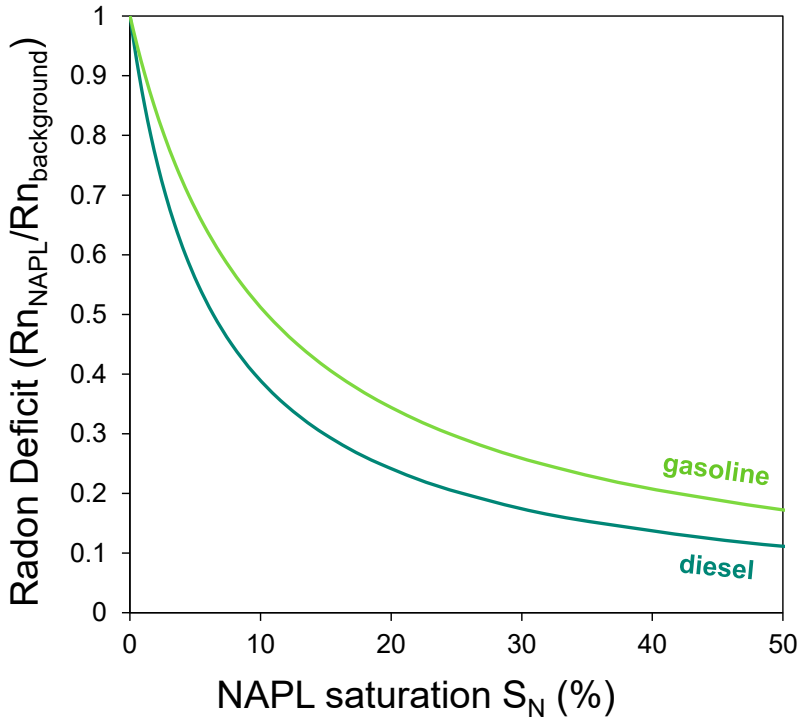

Figure 2.8. Theoretical relationship between Rn deficit and NAPL saturation, from Eq. 2.19, for sandy soil in the vadose zone, for two different NAPL with a typical composition of diesel and gasoline mixtures.

From Eq. 2.19 it is possible to derive the relationship for estimating the fraction of LNAPL in the subsoil, S_N (%), based on the observed Rn deficit (Cecconi et al., 2023a):

$$S_N = \frac{(1 - D) + \left(S_{w,b} - D \cdot S_w\right) \cdot \left(k_{\frac{w}{g}} - 1\right)}{D\left(k_{\frac{N}{g}} - 1\right)} \cdot 100 \qquad \text{Eq. 2.20}$$

The NAPL saturation can also be expressed in terms of TPH concentration C (mg kg^{-1}), using the following relation (Brost and De Vaull, 2000):

$$C = \frac{\theta_t \cdot \rho_N}{\rho_S} \cdot \frac{S_N}{100} \cdot 10^6 \qquad \text{Eq. 2.21}$$

where ρ_N is LNAPL density (g cm^{-3}) and S_N (%) is expressed in percentage.

The presented model describes the Rn activity concentration in the pores of a homogeneous soil under equilibrium conditions. However, it is rare to find uniform homogeneous formations in real site conditions. Identifying a Rn deficit caused by NAPL presence becomes more complex in heterogeneous areas. In fact, site heterogeneity greatly influences Rn production and transport, as the presence of distinct horizons and formations in the site lithography, such as clay lenses, alters the characteristic diffusion length and production rate of Rn.

2.3.2 Partition coefficients

The theoretical aspects described above demonstrate the importance of understanding the mechanisms of Rn partitioning between the liquid, gas, and separated phases in the soil. The distribution of Rn between water and air is a well-known phenomenon governed by the distribution coefficient $k_{w/g}$, which can be determined as the inverse of the value of Henry's constant (see section 2.1.2). The distribution of Rn between water or air and NAPL can still be described as linear. Literature values are available for the partition coefficients of Rn in pure organic compounds, while it is more difficult to find the same unique and established data for the partition in NAPL mixtures, due to the variability in their composition. For the Rn partition coefficient between NAPL and water $k_{N/w}$, for LNAPL with a typical diesel mixture composition, Hunkeler et al. (1997) found a value of 40 ± 2.3. Schubert et al. (2007a) proposed a value of 60 ± 1.3, and Le Meur et al. (2021) also found similar values (60.7 ± 6.1) for fresh diesel. Höhener and Surbeck (2004) used a value of 11.7 for the partition coefficient between diesel and air ($k_{N/g}$), which, considering a Henry's constant of 4.4 (Wilhelm et al., 2002) results in a $k_{N/W}$ of about 51.5. Furthermore,

considering the potential physical phenomena that can lead to an alteration of the diesel mixture (e.g., evaporation and UV-degradation) values ranging from 25.1 ± 2.5 to 74.8 ± 7.5 were found by Le Meur et al. (2021) for the diesel mixture studied. Similarly, for LNAPL with a typical gasoline mixture composition, Schubert et al. (2007a) proposed a value of 38.9 ± 0.9. Le Meur et al. (2021) also found similar results for fresh gasoline (37.4 ± 5.6) and observed a certain variability due to the above-mentioned degradation phenomena, finding $k_{N/W}$ values ranging between 30.8 ± 4.6 and 37.4 ± 5.6. Considering the data mentioned above, it may be considered reasonable to choose a range of values for $k_{N/W}$ between 30 and 60 for both diesel and gasoline, as also suggested by Le Meur et al. (2021). Table 2.4 presents a summary of the values of the Rn partition coefficient between NAPL and water, as reported in the literature for some pure compounds and some NAPL mixtures.

Table 2.4. Dimensionless Rn partition coefficient $K_{N/w}$ for some pure NAPL components and NAPL mixtures; dimensionless Rn partition coefficient $k_{N/g}$, derived by dividing the reported $k_{N/w}$ values for the dimensionless Henry's constant H (calculated using Eq. 2.2 at 20°C, unless otherwise noted)

Substance	**$k_{N/w}$ (-)**	**$k_{N/g}$ (-)**
Hexane	57.2 ± 3.1[a]	14.45 ± 0.8
Ethanol	27.9 ± 0.4[b]	7.05 ± 0.1
Benzene	40.8 ± 5.7[a]	10.31 ± 1.4
Toluene	42 (10°C) [e] 46.8 ± 0.4[a]	14.66 (10°C) 11.82 ± 0.1
Gasoline	30.8 ± 4.6 (evaporated)[d] 33 ± 4.9 (UV-degraded)[d] 37.4 ± 5.6 (fresh)[d] 38.9 ± 0.9[a] 50.9 ± 5.8[c]	7.78 ± 1.2 (evaporated) 8.34 ± 1.2 (UV-degraded) 9.45 ± 1.4 (fresh) 9.83 ± 0.2 12.86 ± 1.5
Kerosene	40.6 ± 8.3[c] 47.4 ± 0.2[a]	10.26 ± 2.1 11.98 ± 0.1
Diesel	25.1 ± 2.5 (evaporated)[d] 40 ± 2.3 (12°C) [e] 43.8 ± 4.6[c] 60.0 ± 1.3[a] 60.7 ± 6.1 (fresh)[d] 74.8 ± 7.5 (UV-degraded)[d]	6.34 ± 0.6 (evaporated) 13.03 ± 0.7 (12°C) 11.07 ± 1.2 15.16 ± 0.3 15.34 ± 1.5 (fresh) 18.90 ± 1.9 (UV-degraded)

a) Schubert et al., 2007a; b) Schubert et al., 2007b; c) Schubert et al., 2001; d) Le Meur et al., 2021; e) Hunkeler et al., 1997

2.4 APPLICATIONS

Theoretical and practical aspects of the Rn deficit technique were studied through laboratory experiments (e.g., Davis et al., 2002; Schubert et al., 2005, 2007a; De Simone et al., 2015; Cohen et al., 2019; Le Meur et al., 2021), modeling approaches (e.g., Semprini et al., 2000; Höhener and Surbeck, 2004; Cohen et al., 2016, 2019; Barrio-Parra et al., 2022), and field experiences (e.g., Schubert et al., 2001; García-González et al., 2008; Yoon et al., 2013; Barbosa et al., 2014; Cohen et al., 2016; De Simone et al., 2017; De Miguel et al., 2018, 2020; Mattia et al., 2020; Barrio-Parra et al., 2021; Briganti et al., 2023). This section presents an overview of the technique's utilization in soil gas, especially from a field perspective, and with some mention of modeling efforts. Some brief discussion of groundwater applications is also provided. A summary of the field applications included in this overview is given in Table 2.5.

Table 2.5 .Summary of Rn deficit technique field applications

Ref.	Application	Sampling	NAPL type	Soil type	Rn measure	Main results
(Hunkeler et al., 1997)	GW - Fuel station	GW-MW	LNAPL	Coarse	LSC	Rn reduction in MW within NAPL zone, and with dissolved HC. No quantitative correlations
(Semprini et al., 2000)	GW - Controlled test site	GW-MW	DNAPL	Coarse	LSC	Rn reduction (of a factor of 2-3) in NAPL zone. Rn downgradient re-equilibrated within a few meters to the upgradient value
(Schubert et al., 2001, 2002)	UZ a) Fuel station b) Military site	T-SGP	LNAPL	a) Fine b) Coarse	IC	Area of Rn deficit closely match the NAPL zone
(Davis et al., 2002, 2005)	GW - Former industrial site	In-well push-pull tests with tracers	LNAPL	Coarse	LSC	Higher Rn retardation in test in the NAPL zone. Uncertainty in estimated saturations. Research is needed to investigate the differences between injection and extraction-phase retardation factors
(Schubert et al., 2005)	UZ - a) Former airfield b) Radium bearing soil	a) T-SGP b) SSNTD	LNAPL	Coarse	a) IC b) SSNTD	a) Rn reduction (up to 10% of the background value) closely match the NAPL zone b) SSNTD can be used for Rn distribution patterns in upper soil

Ref.	Application	Sampling	NAPL type	Soil type	Rn measure	Main results
(Fan et al., 2007)	GW - Industrial site	GW-MW	LNAPL	Heterogeneous	LSC	Rn reduction found in MW within NAPL zone. NAPL concentration from Rn deficit agrees with soil chemical analysis. To effectively use the technique, Rn emanation rate must be virtually homogeneous in the aquifer
(Schubert et al., 2007c)	GW - Former fuel station	GW-MW	LNAPL	Heterogeneous; coarse aquifer	On-site stripping from GW samples + IC + LSC	Estimated NAPL saturation from Rn deficit agrees with chemical analysis. No Rn deficit in areas with only dissolved BTEX
(Schubert et al., 2007a)	GW - Industrial site	GW-MW	LNAPL	Heterogeneous; coarse aquifer	On-site stripping from GW samples + IC	Rn data allowed differentiation between NAPL source zone and NAPL plume (not possible by GW samples alone). NAPL quantification was possible, but complicated by mineralogical heterogeneities
(García-González et al., 2008)	UZ - Fuel station	T-SGP	LNAPL	Heterogeneous	SC	Rn reduction (5 - 10 times lower) in soil gas above accumulations of HC. Uncertainty in Rn background value
(Galhardi and Bonotto, 2012)	GW - Fuel station	GW-MW	LNAPL	Heterogeneous	Laboratory stripping from GW samples + IC	Dissolved HC tend to increase Rn concentration in water, due to the preferential partition. Rn can indicate the dissolved plume, but it did not provide information on residual concentrations
(Yoon et al., 2013)	GW - Industrial site	GW-MW	DNAPL	Heterogeneous	LSC	Low correlation between TCE concentration in GW and Rn, reflecting the local heterogeneity of the aquifer

Ref.	Application	Sampling	NAPL type	Soil type	Rn measure	Main results
(Barbosa et al., 2014)	UZ - Fuel station	T-SGP	LNAPL	Fine	IC	No significant correlation between Rn and VOCs, but the ratio between the minimum and maximum Rn values indicates that Rn near the fuel leak is 85% lower than in the upstream areas
(Yang et al., 2014)	GW - Industrial site	GW-MW	DNAPL	Backfill soil over bedrock	SC in closed loop mode	The changing trend of Rn activities in relation to the relative contaminant concentrations can be useful tool in residual contaminant tracing
(Mateus and Pecequilo, 2015)	UZ - Former Industrial site	SSNTD	LNAPL	Heterogeneous	SSNTD	Rn reduction (from 92% to 98%) found within NAPL zone. No correlation for second contaminated location
(Ponsin et al., 2015)	GW	GW-MW	LNAPL	Coarse over fine	SC in closed loop mode	Rn was measured successfully when a pump-and-skim system was active. Low Rn activities suggest zones of good recovery, while high activities were not always related to poor recovery. Large uncertainties in quantification of residual contamination based on Rn
(Cohen et al., 2016)	UZ - Railway site	T-SGP	LNAPL	Heterogeneous	Scintillation + photomultiplier + scale count	Low correlation between Rn and NAPL lens, due to heterogeneity of the sediment. Also for VOC, O2, CO2, CH4, diffusive gas transfer is locally restricted

Ref.	Application	Sampling	NAPL type	Soil type	Rn measure	Main results
(De Simone et al., 2017)	UZ	T-SGP	LNAPL	Coarse	Two SC in series	Residual NAPL estimation from Rn deficit agreed with direct determination of HC concentrations. Estimated saturations from very high deficits can be affected by large uncertainties (high errors from Rn measurements)
(Castelluccio et al., 2018)	UZ	T-SGP	LNAPL	a) Coarse b) Heterogeneous	SC	Rn reduction found within contaminated zone, but the estimation was influenced by seasonal soil conditions. Direct correlation between Rn deficit at shallow depth and highest electrical resistivity at greater depth
(De Miguel et al., 2018)	UZ - Industrial site	T-SGP	LNAPL	Fractured system (active fault)	Portable α monitors	Rn reduction in one section respond to a discontinuity in the subsurface rather than NAPL contamination. Rn reduction in other section suggest possible NAPL contamination. Rn emanation above background levels explained with presence of a fractured system (co-advective transport)
(Briganti et al., 2020)	GW - Former fuel station	GW-MW	LNAPL	Backfill soil over ignimbrites	Laboratory stripping from GW samples + SC	Rn deficit allowed to identify areas with residual NAPL after 15 years from the spill. No realistic evaluation of saturation was possible because required assumptions of aquifer homogeneity are not respected
(Cho et al., 2020)	GW - Industrial site	GW-MW	DNAPL	Backfill soil over fractured bedrock	Laboratory stripping from GW samples. α	Rn measurements were not successful to characterize residual TCE because of the heterogeneity of the fractured bedrock. Other noble gases (Ne, Ar, Xe) could be useful for characterization of the TCE contaminated site

Ref.	Application	Sampling	NAPL type	Soil type	Rn measure	Main results
(De Miguel et al., 2020)	UZ - Former industrial site	P-SGP	DNAPL	Heterogeneous	Pulse IC	Rn deficits corresponds with contamination hot spots obtained using standard direct and indirect prospecting techniques and are coherent with location of historical pollution sources
(Mattia et al., 2020)	GW - Fuel station	GW-MW	LNAPL	Backfill soil over ignimbrites	Laboratory stripping from GW samples + SC	Minimum Rn values corresponded to highest dissolved concentrations and describe the residual source zone. Low Rn levels detected downstream of the recharge wells, possibly due to the injection of treated GW treated, depleted in Rn
(Barrio-Parra et al., 2021)	UZ - Former industrial site	T-SGP	DNAPL	Heterogeneous	Pulse IC	Rn measurements dependent of atmospheric temperature. Negative spatial correlation of rescaled Rn and contaminant load in the upper layers. Inability to detect deep DNAPL
(Mattia et al., 2023)	GW and UZ – Fuel station	GW-MW P-SGP	LNAPL	a) Backfill soil over ignimbrites b) alluvial deposits	Laboratory stripping from GW samples + SC	Rn deficit validated with multi-parameter monitoring (Rn, NAPL, GW levels) and chemical analysis. Rn deficit in GW and SG allowed to identify areas with residual NAPL. NAPL saturation estimated based on GW Rn deficit values
(Briganti et al., 2024)	UZ and GW - Active fuel stations	PDMS-AC in MW, in UZ and GW	LNAPL	a) Heterogeneous b) fractured system	Passive accumulators	PDMS-AC passive accumulators can be useful to determine Rn vertical variations in UZ and GW

Groundwater; UZ: Unsaturated zone; MW: Monitoring well; GW-MW: Groundwater samples from monitoring wells; T-SGP: temporary soil gas probes; P-SGP: Permanent soil gas probes; LSC: Liquid scintillation counting of water samples, IC: Ionization chamber portable Rn detector; SC: Semiconductor portable Rn detector; α: alpha spectroscopy; PDMS-AC: polydimethylsiloxane + activated carbon; HC: hydrocarbons.

2.4.1 Groundwater applications

The first theoretical and practical studies of this technique focused on identifying NAPL in the saturated zone of the subsurface. Initial studies on the use of Rn as a partitioning tracer for the detection and quantification of NAPL contamination date back to the 1990s (Semprini et al., 1993, 1995; Hunkeler et al., 1997). Hunkeler et al. (1997) applied the Rn deficit technique to detect diesel contamination in aquifers. The research involved laboratory experiments with quartz sand contaminated with diesel fuel, to determine the diesel-water partition coefficient, as well as field observations in a diesel fuel-contaminated aquifer. The results from the laboratory experiments and field observations showed, as expected, a decrease in Rn activity in the water phase in the presence of NAPL contamination. This decrease was used to estimate the average diesel fuel saturation in the aquifer, with the calculated values aligning with those found in excavated aquifer material. Semprini et al. (2000) developed a steady state Rn partitioning model, useful to predict residual NAPL saturation from the theoretical Rn deficit in the aquifer. They also presented a one-dimensional flow and transport model, illustrating the response of Rn concentration as groundwater flows through a zone of residual NAPL contamination in the aquifer. Their simulations showed a reduction in Rn concentration as groundwater flows through the NAPL-contaminated zone. They also observed that Rn concentration to gradually returned to background levels, leaving the contaminated zone, due to the continued Rn emanation from the aquifer solids.

In the field application of this technique, Rn is measured in groundwater samples collected from wells installed at sites with known or suspected NAPL contamination (Cho et al., 2020). This is done in both the contaminated and unaffected areas to determine background Rn activity concentrations for the site. In this context, Rn activity in groundwater samples collected on site is typically measured not in the field, but through laboratory analysis (Davis et al., 2002; Fan et al., 2007; Yoon et al., 2013; Ponsin et al., 2015; Briganti et al., 2020), although also field-based techniques that enable the direct analysis of collected samples can be used (Schubert et al., 2007a; Wang et al., 2019). The results of the different field surveys (e.g., Fan et al., 2007; Schubert et al., 2007a, 2007c; Galhardi and Bonotto, 2012; Yoon et al., 2013; Briganti et al., 2020) confirmed the general applicability of Rn as a naturally occurring partitioning tracer to detect residual NAPL source zone in the saturated zone. Davis

et al. (2002, 2005) evaluated the use of single-well, “push–pull” tracer tests using Rn as a natural partitioning tracer to quantify NAPL saturations, finding that the test has the potential to provide a low-cost alternative to inter-well partitioning tracer tests.

2.4.2 Soil gas applications

Höhener and Surbeck (2004) conducted an experimental and theoretical study on a soil gas application for the technique. They observed a decrease in Rn in soil gas, measured as a result of the increase in n-Dodecane (chosen as a model NAPL) in alluvial sand in batch experiments. Additionally, they developed a one-dimensional analytical reactive transport model to derive Rn profiles for homogeneous and heterogeneous soil profiles with NAPL at selected depths. The authors compared the modeled results with those obtained from lysimeter experiments with positive outcomes. They concluded that NAPL can be effectively used as a tracer in the vadose zone, provided that the contamination level is sufficient, and the site can be assumed to have a uniform Rn production.

Regarding the field applications, different configurations were developed and successfully applied to evaluate the presence of residual LNAPL also in the vadose zone and the smear zone (Schubert et al., 2002; García-González et al., 2008; Barbosa et al., 2014; Mateus and Pecequilo, 2015; Castelluccio et al., 2018; De Miguel et al., 2018, 2020; Barrio-Parra et al., 2021). Rn activity can be analyzed directly in the soil gas, using different configurations depending on the equipment employed, the sampling method selected, and the features of the site being studied.

2.4.2.1 Active measurements

The prevailing technique for soil gas sampling involves the use of temporary soil gas probes, which consist of stainless-steel hollow rods equipped with free, sharpened lower ends (“lost” tips). These probes are inserted into the ground, either manually or with equipment such as electric drill hammers, to a depth of 0.7 - 1 m (Schubert et al., 2001; García-González et al., 2008; Castelluccio et al., 2018; De Miguel et al., 2018; Barrio-Parra et al., 2021). This is the typical sampling depth range when using temporary probes, and it is dictated primarily by the need to sample soil gas at a depth that minimizes the impact of atmospheric variables (e.g., temperature, atmospheric pressure, wind speed). On the other hand, it is important to consider the practicality

of temporary probe installation (Neznal et al., 2004), as the insertion of a hollow probe to greater depths may not be possible depending on the characteristics of the soil or in the presence of underground infrastructures (García-González et al., 2008).

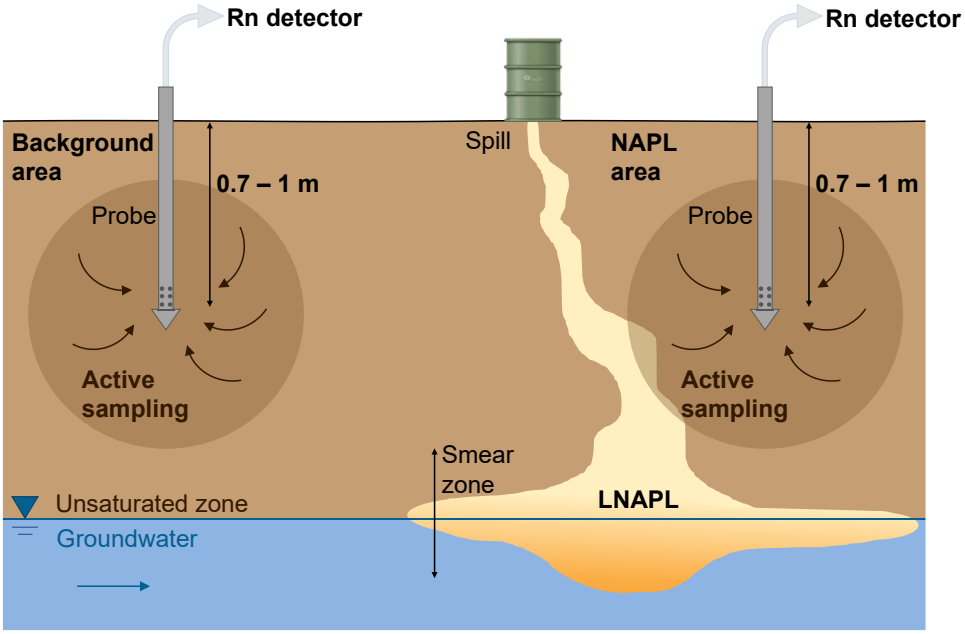

Figure 2.9. Schematic of soil gas Rn active detection using temporary probes for the application of the soil gas Rn deficit technique.

Schubert et al. (2001, 2002) conducted some field experiments to test the use of soil gas Rn concentration to detect NAPL contamination using this configuration. In particular, three sites contaminated with petroleum and kerosene with the presence of floating NAPL were chosen. These sites had previously been investigated to delineate the NAPL plumes. For the Rn surveys, a grid of soil gas sampling points was installed at each site using temporary soil gas probes. Soil gas samples were collected at a depth of 70 cm, and Rn concentrations were measured using a pulsed ionization chamber mobile Rn monitor. The results showed that the minimum Rn concentrations detected matched the respected NAPL plumes previously traced by conventional means, highlighting, however, the limitations related to geological complexities and the characteristic diffusion length of Rn.

During the blind field test conducted by García-González et al. (2008) soil gas was collected using a stainless-steel hollow probe that was inserted into the soil to a depth of 75-100 cm. Rn in soil gas was measured with a semiconductor detector. Data from

eight monitoring wells were used to estimate the location of the subsurface plume of free product. Although the map of free-product thickness is uncertain, there is a clear inverse correlation between the thickness of free product in the subsurface and Rn concentration in soil gas. Despite its simplicity, cost-effectiveness, and good reproducibility, the authors note that emanometry revealed some limitations during field trials, such as the need to ensure low humidity conditions to ensure good instrument performance or the potential problem of inserting the hollow probe into the ground.

In a field test performed by Barbosa et al. (2014), soil gas data was collected at a gas station using ten temporary soil gas probes to investigate the correlation between Rn activity and VOC concentrations in the subsurface soil. Over the entire survey area, there was no significant correlation between Rn and VOC concentrations in soil gas. However, the area near the fuel leak showed the highest VOC concentration and the lowest Rn activity.

Castelluccio et al. (2018) used a multi-method approach to monitor NAPL contamination in two study areas in Italy and India. They performed soil gas Rn measurements at a depth of 80 cm using a semiconductor Rn monitor connected to a hollow probe. The Rn activity concentration was measured by counting the decay of Rn daughters after the soil gas was collected, dried, and filtered. The extent of contamination in the upper part of the unsaturated aquifers was determined by deriving the Rn deficit through comparison with average soil Rn in reference to unpolluted areas. Additionally, residual fractions of contaminants in the vadose zone were estimated using the measurements. A direct correlation was found between the Rn deficit at shallow depths and the highest electrical resistivity at greater depths, which increases the reliability of the results of the methods.

De Miguel et al. (2018) used temporary soil gas probes to measure soil gas Rn through hollow rods buried 75–100 cm in the subsoil, at a site with lithological discontinuities through a blind test. Rn was measured using alpha spectroscopy monitors, following a regular sampling design with a 20 m^2 grid and adding some external points to assess the background Rn concentration in soil gas at the site. Although the soil gas Rn concentration was primarily influenced by the possible path of a fault and a lithologic discontinuity, characterization of the background emission in each lithologic unit allowed the identification of areas that may be impacted by NAPL.

Cohen et al. (2016) compared the potential of several in situ gas measurements to soil coring for LNAPL source delineation at a contaminated site with limited diffusion potential due to the presence of fine sands and silts. They used a network of gas probes at a depth of approximately 1 meter and analyzed VOCs, O_2, CO_2, CH_4, and Rn, comparing the results to independent LNAPL analysis by coring at the site. Rn monitoring was conducted using scintillation vials placed under vacuum to collect soil gases directly from the soil gas probes on site, and a photomultiplier. The data suggested that O_2, CO_2, and CH_4 have longer diffusion lengths and provide a clearer indication of the presence of LNAPL at the site, while migration of VOCs and Rn did not show a strong correlation with LNAPL, probably because it only occurs over short distances in such heterogeneous media. In the same study, numerical simulations were performed using a code for flow and reactive transport in variably saturated media (Mayer et al., 2002), to characterize the production and transport processes of the studied gas in the vadose zone. The simulations aim to understand the role of the presence of NAPL on gas profiles, using simplified scenarios. This modeling approach was then further explored in a following paper (Cohen et al., 2019), to better understand the applicability of Rn gas method for identifying LNAPL sources in chemically heterogeneous unsaturated media, and to determine the relevant parameters that affect the field application of this method.

The performance of the soil gas Rn deficit technique was also evaluated by Barrio-Parra et al. (2021, 2022) at a site where a complex DNAPL mixture contaminated the soil profile. Soil gas samples were collected using a syringe and introduced into a previously vacuumed ionization chamber. Samples were collected using hollow rods at two depths (0.8 m and 1.7 m) and purged to prevent dilution effects due to atmospheric air. Rn measurements were performed using a pulse ionization detector. A negative spatial correlation was found between soil gas Rn concentrations and organic contaminant levels in the top layers of the soil profile, indicating that the method correctly identified surface contaminant hotspots at the site. However, the same correlations were not found for deeper contamination, which is the typical location of DNAPL in the aquifer. Therefore, according to the authors, the inability to describe the deeper vertical profile of contaminant concentration along the soil profile using only shallow soil gas samples likely invalidates the Rn deficit technique as a screening tool for deep DNAPL accumulations.

Barrio-Parra et al. (2022) developed a numerical multilayer model of Rn production-partitioning-diffusion in unsaturated porous media. They also included a laboratory protocol to obtain site specific input parameters for the model. The model predictions were compared with field information obtained from sampling campaigns measuring soil gas Rn at a site where the vadose zone was affected by the presence of a DNAPL mixture. The model successfully predicted the vertical profile of soil gas Rn concentrations, including the effects of soil moisture, which varied due to water table fluctuations, and soil temperature.

For other applications involving soil gas measurements, such as vapor intrusion studies, permanent soil gas probes can also be used for soil gas monitoring. These probes consist of PVC or stainless-steel pipes, inserted into the unsaturated soil to the desired depth, using direct push drilling techniques (ASTM, 2012) or using previously excavated boreholes (ITRC, 2006). The borehole is then packed with filler material, consisting of clean sand near the probe tip, and of a sealing material, such as bentonite, for the rest of the borehole length (CalEPA, 2015). Probes are typically equipped with a gas-tight fitting that can be connected to the sampling tube. This configuration is usually not cost-effective and does not offer significant advantages in terms of data quality compared to the temporary probe approach, for the application of the soil gas Rn deficit technique, which requires a relatively large number of monitoring points to delineate the LNAPL source. In this view, an alternative to the traditional method was proposed by De Miguel et al. (2020) who employed PVC pipes directly inserted into the ground, with the bottom perforated to allow soil gas to enter the probe, and equipped with an air-tight outlet valve that is only opened during purging and sampling. This configuration was applied in a blind field test, conducted to evaluate the performance of the Rn deficit technique for a complex mixture of organic contaminants. The results obtained with this approach were comparable to those obtained in other studies that used temporary probes For the area investigated by De Miguel et al. (2020), the pollution hotspots inferred from the Rn campaigns aligned with the analytical data on the location of the pollution source zones obtained from traditional sampling campaigns. However, the authors identified the variation of Rn concentrations with diurnal changes in ground-level air temperature and the maximum depth of the investigation as limitations to the applicability of the technique. According to the authors, for an effecting application of the Rn deficit technique, the influence of temperature can be accounted for and minimized by averaging replicated

measurements during different days. Regarding the maximum depth of investigation, the authors concluded that variations in soil gas Rn concentrations are spatially correlated with changes in soil contamination only if the depth of the sampling point is within the maximum diffusion radius of Rn from the source zone. This latter limitation was considered statistically significant only if no significant advective or co-advective transport of Rn in soil gas is assumed at the site.

Mattia et al. (2023) measured Rn in soil gas by extracting it from two vapor extraction wells from a Soil Vapor Extraction (SVE) system, at different depths, and analyzing the samples in the laboratory using a semiconductor detector connected in a closed loop. Rn deficit observed in soil gas was used together with the more abundant Rn data obtained from groundwater sampling from the wells at the site, to identify the location of residual NAPL. Soil gas samples were not used for quantitative estimations due to their lower abundance compared to groundwater samples.

2.4.2.2 Passive measurements

Another approach is to use solid-state nuclear track detectors, which are passive, low-cost, and compact devices that do not require a power supply or suction systems (see section 2.4.2.2). The detectors are exposed for a variable period (days or weeks) before being analyzed to determine the average Rn activity for the exposure period. Schubert et al. (2005) conducted a soil gas Rn survey using solid-state nuclear track detectors LR-115. The purpose was to evaluate the efficiency of these instruments as a cost-effective method for the application of the technique. At the field site, the detectors were exposed for 8 days inside samplers buried in the soil at a depth of 70 cm. After exposure, all detectors were etched with a NaOH solution to reveal the alpha particle impacts as etching tracks. The resulting Rn distribution pattern indicated areas with concentrations at least 90% lower than the local background level, spatially matching the NAPL contamination present in the subsurface.

Mateus and Pecequilo (2015) evaluated the Rn deficit technique in soil gas by passive detection methodology with CR-39 solid state nuclear track detectors. The method was tested by placing the detectors inside special diffusion chambers within 1 m long PVC tubes buried in the soil. The detector was suspended inside the PVC pipe at a depth of 70 cm, together with a permeable bag containing silica gel, to prevent moisture, which can complicate alpha particle interactions. After 20 days of exposure,

the detectors were removed and analyzed to obtain track densities and the relative Rn activity concentrations. For the monitoring points assumed as contaminated locations Rn concentrations diminished in a range from 92% to 98% when compared with the results for the non-contaminated areas. The authors discovered that the monitoring point with the lowest Rn concentration was located outside the NAPL area estimated by classical environmental investigation techniques. However, during additional excavation in the area, evidence of oil-impregnated soil was found, confirming the results of the Rn monitoring technique.

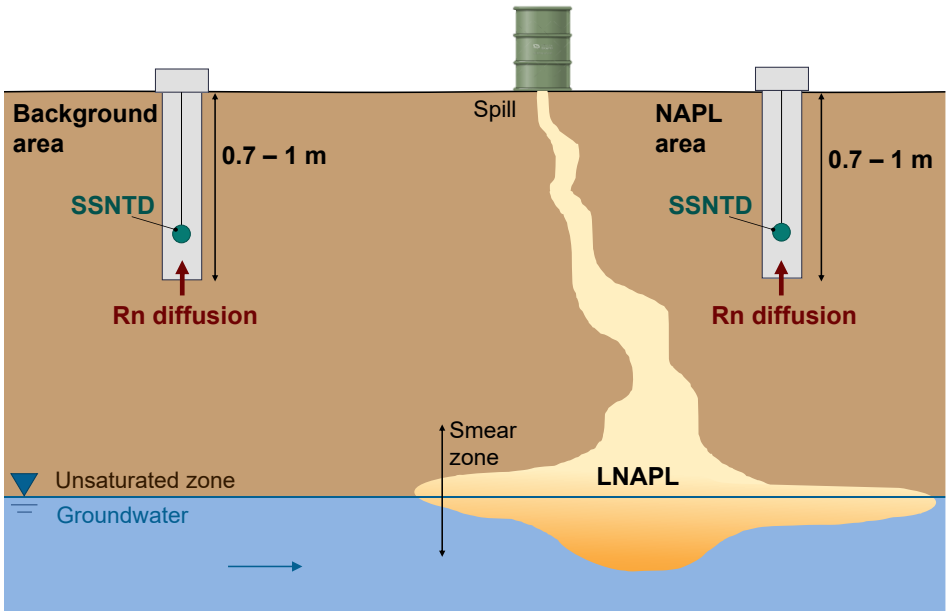

Figure 2.10. Schematic of soil gas Rn passive detection for the application of the soil gas Rn deficit technique.

Briganti et al. (2023) conducted a study to evaluate the feasibility of determining the vertical distribution of Rn at various soil depths to detect LNAPL contamination, using the passive Rn accumulator proposed by Voltaggio and Spadoni (2013). These passive accumulators, made of polydimethylsiloxane (PDMS) mixed with activated carbon (AC) were designed to measure Rn in both soil gas and groundwater due to the water-impermeable (PDMS) and Rn-adsorbing (AC) properties of the two materials. The accumulators were inserted at varying depths into monitoring wells and left inside for two weeks to absorb ambient Rn that diffuses within the material. After the recovery process, each sample was counted in the laboratory using a high-resolution gamma spectrometer equipped with a HPGe detector. These experimental

results appear to be consistent with the presence of residual LNAPL in the vadose zone, also indicated by detected peaks of VOC. From this initial field test, the authors found that PDMS-AC passive accumulators yielded positive results for environmental Rn sampling.

Based on the results presented in the above studies, passive samplers appear to be an adequate and less expensive tool for determining Rn distribution patterns in the upper soil.

2.4.3 Limitations identified and need for further study

The Rn deficit technique has proven to be an effective tool for the preliminary evaluation of sites contaminated with complex mixtures of organic contaminants with the presence of non-aqueous phases. The results obtained with different applications of the technique, in terms of identifying the location of NAPL contamination hotspots, were often consistent with those obtained using standard direct and indirect exploration techniques or with historical information about the site's contamination sources (Hunkeler et al., 1997; Fan et al., 2007; García-González et al., 2008; Schubert, 2015; De Miguel et al., 2018; Barrio-Parra et al., 2021; Briganti et al., 2024). Compared to conventional investigation tools such as drilling and soil groundwater sampling and analysis, Rn measurements can provide nearly real-time results with the potential for much higher spatial density and at a lower cost (De Miguel et al., 2020; Sukanya et al., 2022). Furthermore, the method can detect the presence of LNAPL in the subsurface even when it exists in residual phase (Briganti et al., 2020). which is usually more challenging since, unlike the free product, it cannot be detected by conventional monitoring of groundwater wells at the site (see section 1.4.2). Similarly, it may be useful to distinguish areas of pure dissolved phase plume from areas of actual separate phase presence (Schubert et al., 2007a, 2007c).

In spite of the favorable outcomes observed with each of the configurations mentioned in the previous section, certain limitations still exist concerning the applicability of the Rn deficit technique. Published work on the subject has identified different categories of limitations, mostly related to the variability of Rn activity in the soil over time and space, and to the distance between the soil gas measurement point and LNAPL depth.

Schubert et al. (2001, 2002, 2007c); Cohen et al. (2016); De Miguel et al. (2020); Briganti et al. (2020), among others, highlighted that the detection of Rn activity concentrations in the field may be affected by the geochemical, granulometric, and mineralogical characteristics of the soil. This may be due to the uneven distribution of ^{226}Ra, from which Rn originates, in the soil, and to variations in the emanation mechanism based on soil characteristics. Specifically, the concentration of ^{226}Ra can vary significantly among different rock types. For instance, granites (acidic igneous rocks), some types of bituminous shales, and phosphate rocks typically have higher average activity concentrations (see Table 2.1) (Nazaroff, 1992). Therefore, variations in Rn activity concentrations may arise due to heterogeneities in lithostratigraphic units, and not necessarily be related to the presence of LNAPL in the subsoil. As an example, Cohen et al. (2016) performed Rn measurements in soil gas in a site characterized by a significant heterogeneity of the subsurface and did not find a clear pattern in Rn concentrations above the LNAPL zone. Additionally, the characteristics of the soil matrix, such as grain size and permeability affect both Rn emanation and soil gas transport, and therefore its concentration in soil gas along soil profiles. These latter aspects can also complicate the application of the method in identifying the appropriate area to use as the reference Rn background value for the site for estimating the deficit.

Another important consideration in the application of this technique is the possible temporal variability of Rn measurements. Soil gas behavior in the shallowest soil layers, specifically those less than 1 meter deep, is affected by weather conditions such as temperature, atmospheric pressure, and wind speed (Scanlon et al., 2002). Concerning pressure, it was not observed a consistent Rn variability with the diurnal variation of barometric pressure (Barrio-Parra et al., 2021). It has been assumed in various applications that measuring Rn down to a depth of 75-100 cm can minimize the influence of atmospheric factors (Schubert et al., 2005; García-González et al., 2008; De Miguel et al., 2018; Barrio-Parra et al., 2021). However, temperature was found to have a significant effect on Rn concentrations in surface soils, to varying degrees depending on the sampling and measurement methods used (Schubert and Schulz, 2002; De Miguel et al., 2020; Barrio-Parra et al., 2021). It was also observed that the vertical temperature gradient in the soil may have an influence on depths around 1 meter, which is typical of the method's application (Barrio-Parra et al., 2021). If not properly accounted for, the thermal effect can result in a confounding effect in

the interpretation of Rn deficits. To avoid this effect on Rn concentration measurements in surface soil gas, Barrio-Parra et al. (2021) recommends using the arithmetic mean of the data set for each campaign. Passive instruments, such as SSNTDs, could be considered as an alternative option for Rn measurement, as they integrate Rn activity concentrations over a longer exposure time, flattening out some of the possible variability. It is important to account for the temperature effect when comparing the results of different field campaign, as seasonal variations as well as diurnal may also be relevant (King and Minissale, 1994; Hutter, 1996).

Although the soil gas Rn method has shown positive qualitative results in most tested cases for identifying zones with LNAPL presence in the subsurface, there are still few studies related to quantifying NAPL contamination using this technique in the unsaturated zone (Castelluccio et al., 2018; Schubert, 2015). In fact, the quantification of the extent of the contamination requires a greater knowledge of subsurface characteristics, nature and composition of the contaminant, and overall site-specific parameters. In this context, an important aspect to consider is the variability of the partition coefficient value depending on the composition of the LNAPL and the possible degradation phenomena it may have undergone over time (Le Meur et al., 2021).

Another factor that can impact the performance of the Rn deficit technique in the unsaturated zone is the distance of the Rn measurement point from the LNAPL source zone. In the case of deep contamination or of inhibited Rn transport, e.g., for a low soil permeability or higher water content, the characteristic gas diffusion length of Rn can be reduced, and thus the application of the Rn deficit method can become limited (Schubert et al., 2001; Höhener and Surbeck, 2004; Schubert, 2015; Castelluccio et al., 2015; De Miguel et al., 2018, 2020). For instance, Schubert et al. (2002) reported a successful performance of the method to identify an area with the presence of free phase kerosene, but highlighted the limitations related to the geological complexity and the characteristic diffusion length of Rn. A further example are the results of seven field campaigns carried out at one site, described by Barrio-Parra et al. (2021), which showed a good correlation between the points of low Rn concentration and the areas of highest contamination in the upper soil layers, although the same conclusions could not be drawn for the contamination of the deeper soil layers. This aspect is particularly relevant in cases where transport is purely or almost exclusively diffusive. Some

authors (De Miguel et al., 2020, 2018) have suggested that the presence of a fractured system that enhances Rn migration through co-advective transport in the subsurface can modify these dynamics. However, this aspect has not yet been thoroughly explored from either a modeling or application perspective. In this view, a systematic study evaluating the feasibility and effectiveness of using Rn measurements under different site-specific conditions for subsurface LNAPL detection would be beneficial, either by considering the more typical case of diffusive-only transport in soil gas or by including advective transport in the evaluations. These aspects have been evaluated and addressed, as part of this thesis, through modeling (Chapters 3 and 4) and through field application perspectives (Chapters 5 and 6).

CHAPTER 3

3 MODELING OF SOIL GAS RADON AS AN IN SITU PARTITIONING TRACER FOR LNAPL CONTAMINATION

Most of this chapter is taken from "Cecconi, A., Verginelli, I., Baciocchi, R., 2022. Modeling of soil gas radon as an in situ partitioning tracer for quantifying LNAPL contamination. Sci. Total Environ. 806, 150593. https://doi.org/10.1016/j.scitotenv.2021.150593"

ABSTRACT

This work examines the feasibility of using soil gas data collected at some distance from the source zone for the application of the Rn deficit technique for the identification and quantification of NAPL contamination. To this end, we used a steady-state 1-D analytical solution that is based on a 3-layer model that allows to simulate the transport and distribution of Rn in the source zone, capillary fringe and overlying unsaturated soil. The analytical solution was first validated against a more detailed numerical model available in the literature. Then, a series of simulations were carried out to evaluate the vertical concentration profiles of Rn in soil gas above the source zone and in background location not impacted by NAPL. Simulation results showed that the parameters that most influence the migration and distribution of Rn in the subsurface are the distance of the soil gas probe from the source zone and, to a lower extent, the type of contamination (e.g. diesel or gasoline) and the soil texture. On the basis of these results, we developed some easy-to-use nomographs to estimate the residual NAPL phase based on the observed Rn deficit in soil gas and on the probe to source distance and soil and NAPL characteristics. According to the obtained results, the Rn deficit technique results a feasible method for a qualitative identification of residual NAPL when Rn in soil gas is measured at distances lower than 2 m from the contaminated zone. However, for an accurate quantitative estimation of the NAPL phase content, soil gas probes should be preferably located at distances lower than 1 m from the source zone.

3.1 INTRODUCTION

In the field application of the soil gas Rn deficit technique one of the key aspects that can affect the performance of the method in detecting LNAPL in the subsurface is the distance of the soil gas probe from the LNAPL source zone. Indeed, if the contamination is deep or if the soil has lower permeability or higher water content, the characteristic gas diffusion length of Rn can be reduced and thus the application of the Rn deficit method can become less significant. Although this aspect was highlighted by some authors (e.g., Höhener and Surbeck, 2004; De Miguel et al., 2020) to our knowledge there is no systematic study assessing the feasibility and effectiveness of using Rn measurements in soil gas for the detection of LNAPL in the subsurface. In order to fill this gap, in this work we developed a model to examine how Rn concentration in the soil gas varies in the presence of LNAPL, considering different soil textures, volumetric NAPL contents, source depths and vertical distances of the soil gas probe from the source of contamination. The model is based on an analytical 1-D solution for Rn transport in the subsurface, obtained following an approach similar to the one previously adopted by Höhener and Surbeck (2004). The developed analytical solution allows to estimate the vertical concentration profiles of Rn in soil gas at steady state in a stratified soil assuming a diffusion dominated transport of Rn. To this end, we developed a 3-layer analytical solution that can be used to describe the transport of Rn in the capillary fringe, source zone and in the overlying unsaturated soil. After a description of the analytical solution, the results of several simulations are reported and discussed. In particular, the capability of the analytical solution is first tested by comparing its results with those obtained by a more sophisticated numerical model (Cohen et al., 2019). Then, a sensitivity analysis of the parameters that may influence the estimate of the volumetric LNAPL content (e.g. thickness of the source zone or depth of aquifer) is reported. Finally, we provide some nomographs that can be easily used to estimate the residual LNAPL phase as a function of the Rn deficit observed in soil gas and of the site-specific conditions such as the soil gas probe depth or the soil type.

3.2 MATERIAL AND METHODS

3.2.1 Governing equation and assumptions

The analytical model used in this work was derived following an approach similar to the one previously applied by Höhener and Surbeck (2004). Specifically, the 1-D steady state analytical solution for Rn transport in the subsurface was obtained assuming a homogenous soil with a constant diffusion coefficient and considering a uniform and constant Rn emanation from the solid matrix. Like previous modeling studies (e.g., Höhener and Surbeck, 2004; Cohen et al., 2019), Rn decay was assumed to be the only reaction occurring and was described by a first-order decay constant (λ). The partitioning of Rn in soil gas, water and NAPL was assumed to be instantaneous and reversible and was described using linear equilibrium partitioning constants (Werner and Höhener, 2002).

Under these assumptions, the governing equation for Rn diffusive transport at steady state in a homogeneous layer i of unsaturated soil, can be written as:

$$f_i \cdot D_{e,i} \cdot \frac{\partial^2 Rn}{\partial z^2} - \lambda \cdot Rn + f_i \cdot P_i = 0 \qquad \text{Eq. 3.1}$$

Where Rn is the Rn activity concentration in soil gas (Bq m^{-3}); f_i (-) is the fraction of Rn in the air phase of the layer i; P_i is the Rn production rate in the pore space in the layer i (Bq m^{-3} s^{-1}); $D_{e,i}$ is the effective diffusion coefficient of Rn in the layer i (m^2 s^{-1}), which can be written as (Millington and Quirk, 1961):

$$D_{e,i} = D_{m,g} \cdot \frac{\theta_{g,i}^{10/3}}{\theta_{t,i}^2} + D_{m,w} \cdot \frac{\theta_{w,i}^{10/3}}{k_{g/w}\theta_{t,i}^2} \qquad \text{Eq. 3.2}$$

where $D_{m,g}$ and $D_{m,w}$ are Rn molecular diffusion coefficients (m^2 s^{-1}) in gas phase and water respectively, $\theta_{g,i}$ is the volumetric gas content in the layer i, $\theta_{w,i}$ is the volumetric water content in the layer i, $\theta_{t,i}$ is the total soil porosity in the layer i and $k_{g/w}$ is Rn partition coefficient between gas phase and water phase (i.e. the dimensionless Henry's law constant).

The Rn production rate in the pore space in the layer i, P_i (Bq m^{-3} s^{-1}) is related to ^{226}Ra activity concentration of the solids, which corresponds to the number of Rn atoms produced per unit mass and time, and can be expressed in terms of Rn activity

considering Rn radioactive decay constant λ. P_i (Bq m^{-3} s^{-1}) can then be written as (Van Der Spoel et al., 1997):

$$P_i = \frac{C_{Ra} \cdot \lambda \cdot \varepsilon \cdot \rho_s \cdot (1 - \theta_{t,i})}{\theta_{g,i}} \quad \text{Eq. 3.3}$$

with C_{Ra} the ^{226}Ra concentration of the solids (Bq kg^{-1}), λ the Rn first order decay constant (s^{-1}), ε (-) the Rn emanation coefficient and ρ_s the solid density (kg m^{-3}).

The fraction of Rn in the air phase of the layer i, f_i (-), can be calculated as follows (Werner and Höhener, 2002):

$$f_i = \frac{1}{1 + \frac{\rho_s \cdot (1 - \theta_{t,i}) \cdot k_{s/w}}{k_{g/w} \cdot \theta_{g,i}} + \frac{\theta_{w,i}}{k_{g/w} \cdot \theta_{g,i}} + \frac{\theta_{N,i}}{k_{g/N} \cdot \theta_{g,i}}} \quad \text{Eq. 3.4}$$

where $\theta_{N,i}$ is the volumetric NAPL content of the layer i, $k_{s/w}$ is the partition coefficient of Rn between the solid and water phase and $k_{g/N}$ the partition coefficient of Rn between gas phase and NAPL.

Note that all parameters with the subscript i are dependent on the characteristics of the soil layer considered.

3.2.2 Analytical solution

Van Der Spoel et al. (1997) provided the analytical solution of Eq. 3.1 for a homogeneous vadose zone in the absence of NAPL. For heterogeneous layered soils, Eq. 3.1 has been solved analytically by Höhener and Surbeck (2004). Specifically, they provided an analytical solution for a 2-layer model to describe the transport of Rn in the presence of NAPL that they have obtained using a mathematics-based software. In this work, we present an analytical solution for a 3-layer model that can be used to describe the transport of Rn in the capillary fringe, source zone and in the overlying unsaturated layer. It is worth noting that also Höhener and Surbeck (2004), using a mathematics-based software, proposed a 3-layer model although they did not provide the analytical solution they obtained for sake of brevity. The domain of the 3-layer model developed in this work is depicted in Figure 3.1. The domain was divided into three zones: a non-contaminated layer of the vadose zone (denoted by the subscript V), a layer of the vadose zone with presence of residual NAPL (denoted

by the subscript VN), and a third layer represented by the capillary fringe, with presence of residual NAPL (denoted by the subscript CF).

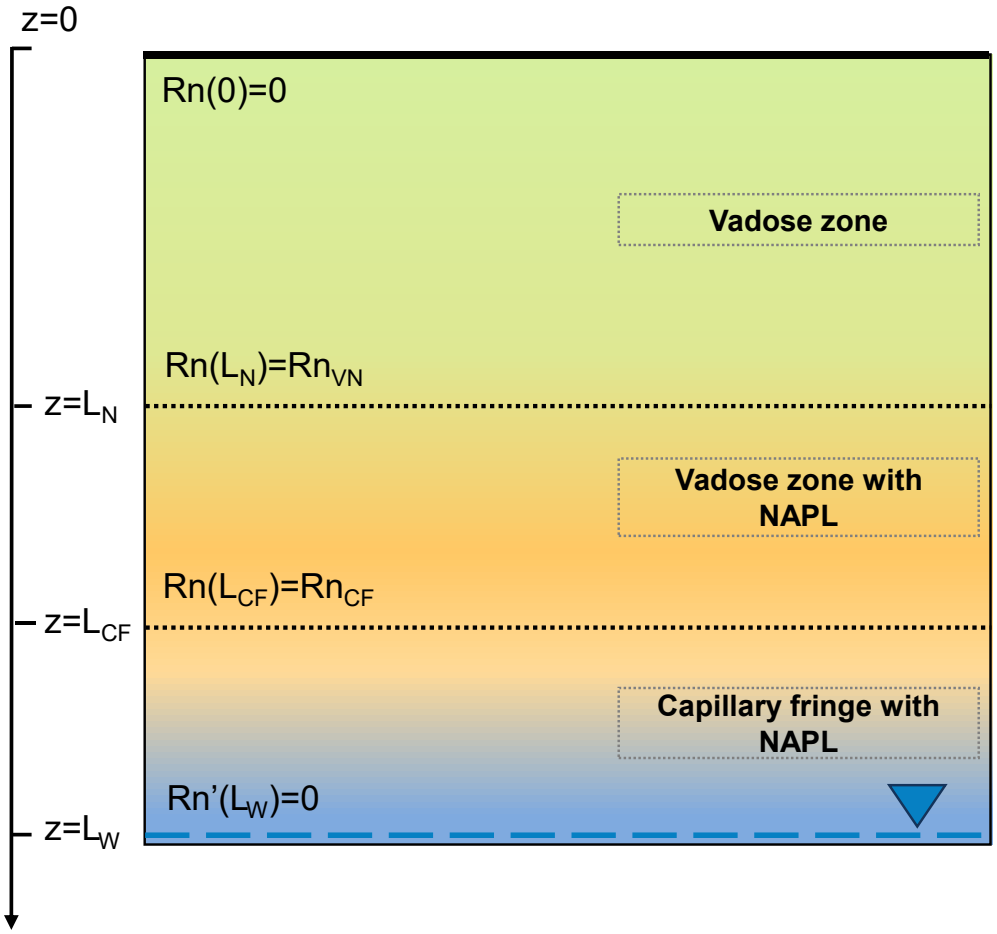

Figure 3.1. Domain of the model, consisting of three soil layers: uncontaminated vadose zone, vadose zone with presence of NAPL, and capillary fringe with presence of NAPL. The origin of axis z is placed at the ground level, and it is positive with increasing depth. In the figures are also described the boundary conditions assumed to derive the analytical solution.

To solve Eq. 3.1, four boundary conditions were considered.

The Rn concentration was considered zero in air, so Rn was imposed equal to zero at the soil surface (z = 0):

$$\mathrm{Rn} = 0 \text{ at } z = 0 \qquad \text{Eq. 3.5}$$

The Rn concentration at the interfaces for z = L_N and for z = L_{CF} was imposed as follows:

$$Rn = Rn_{VN} \text{ at } z = L_N \quad \text{Eq. 3.6}$$

$$Rn = Rn_{CF} \text{ at } z = L_{CF} \quad \text{Eq. 3.7}$$

Since the presence of the water table is simulated for z = L_W, no Rn flux was assumed at this location, giving:

$$\frac{\partial Rn}{\partial z} = 0 \text{ at } z = L_W \quad \text{Eq. 3.8}$$

By imposing these boundary conditions, the following solutions, describing the Rn concentration profile in the domain, were derived:

- For $0 < z \leq L_N$:

$$Rn(z) = Rn_{VN} \cdot \left[1 - \frac{\sinh\left(\frac{z}{L_{c,V}}\right)}{\sinh\left(\frac{L_N}{L_{c,V}}\right)}\right] + \frac{P_V \cdot f_V}{\lambda}\left[1 - \frac{\sinh\left(\frac{L_N - z}{L_{c,V}}\right) + \sinh\left(\frac{z}{L_{c,V}}\right)}{\sinh\left(\frac{L_N}{L_{c,V}}\right)}\right] \quad \text{Eq. 3.9}$$

- For $L_N < z \leq L_{CF}$:

$$Rn(z) = \frac{\left(Rn_{VN} - \frac{P_{VN} \cdot f_{VN}}{\lambda}\right) \cdot \sinh\left(\frac{L_{CF} - z}{L_{c,VN}}\right) + \left(Rn_{CF} - \frac{P_{VN} \cdot f_{VN}}{\lambda}\right) \sinh\left(\frac{z - L_N}{L_{c,VN}}\right)}{\sinh\left(\frac{L_{CF} - z_N}{L_{c,VN}}\right)} \quad \text{Eq. 3.10}$$

- For $L_{CF} < z \leq L_W$:

$$Rn(z) = \frac{\left(Rn_{CF} - \frac{P_{CF} \cdot f_{CF}}{\lambda}\right) \cdot \cosh\left(\frac{L_W - z}{L_{c,CF}}\right)}{\cosh\left(\frac{L_W - z_{CF}}{L_{c,CF}}\right)} + \frac{P_{CF} \cdot f_{CF}}{\lambda} \quad \text{Eq. 3.11}$$

With $L_{c,i}$ the characteristic diffusion length of Rn in the layer i:

$$L_{c,i} = \sqrt{\frac{f_i \cdot D_{e.i}}{\lambda}} \quad \text{Eq. 3.12}$$

Next, by imposing the continuity of the fluxes at the interface of the contiguous layers, the expressions of the concentrations Rn_{VN} (at z = L_N) and Rn_{CF} (at z = L_{CF}) were derived.

In particular, the concentration at the interface between the vadose zone with residual NAPL and the capillary fringe with residual NAPL, Rn_{CF}, is given by:

$$Rn_{CF} = \frac{A + B + X + \Delta}{E + \Phi} \quad \text{Eq. 3.13}$$

With:

$$A = \frac{D_V \cdot D_{VN}}{L_{C,V} \cdot L_{C,VN}} \cdot \frac{P_V \cdot f_V}{\lambda} \cdot \tanh\left(\frac{L_N}{2L_{C,V}}\right) \cdot \operatorname{csch}\left(\frac{L_{CF} - L_N}{L_{C,VN}}\right) \quad \text{Eq. 3.14}$$

$$B = \frac{D_{VN}}{L_{C,VN}} \cdot \frac{P_{VN} \cdot f_{VN}}{\lambda} \cdot \tanh\left(\frac{L_{CF} - L_N}{2L_{C,VN}}\right) \cdot \left[\frac{D_{VN}}{L_{C,VN}} \cdot \operatorname{csch}\left(\frac{L_{CF} - L_N}{2L_{C,VN}}\right) + \frac{D_V}{L_{C,V}} \cdot \coth\left(\frac{L_N}{L_{C,V}}\right)\right] \quad \text{Eq. 3.15}$$

$$\Gamma = \frac{D^2_{VN}}{L^2_{C,VN}} \cdot \frac{P_{VN} \cdot f_{VN}}{\lambda} \cdot \coth\left(\frac{L_{CF} - L_N}{L_{C,VN}}\right) \cdot \tanh\left(\frac{L_{CF} - L_N}{2L_{C,VN}}\right) \quad \text{Eq. 3.16}$$

$$\Delta = \frac{D_{CF}}{L_{C,CF}} \cdot \frac{P_{CF} \cdot f_{CF}}{\lambda} \cdot \tanh\left(\frac{L_W - L_{CF}}{L_{C,CF}}\right) \cdot \left[\frac{D_V}{L_{C,V}} \cdot \coth\left(\frac{L_N}{L_{C,V}}\right) + \frac{D_{VN}}{L_{C,VN}} \cdot \coth\left(\frac{L_{CF} - L_N}{L_{C,VN}}\right)\right] \quad \text{Eq. 3.17}$$

$$E = \frac{D^2_{VN}}{L^2_{C,VN}} + \frac{D_V \cdot D_{VN}}{L_{C,V} \cdot L_{C,VN}} \cdot \coth\left(\frac{L_N}{L_{CV}}\right) \cdot \coth\left(\frac{L_{CF} - L_N}{L_{C,VN}}\right) \quad \text{Eq. 3.18}$$

$$\Phi = \frac{D_{CF}}{L_{C,CF}} \cdot \tanh\left(\frac{L_W - L_{CF}}{L_{C,CF}}\right) \cdot \left[\frac{D_V}{L_{C,V}} \cdot \coth\left(\frac{L_N}{L_{C,V}}\right) + \frac{D_{VN}}{L_{C,VN}} \cdot \coth\left(\frac{L_{CF} - L_N}{L_{C,VN}}\right)\right] \quad \text{Eq. 3.19}$$

The concentration at the interface between the vadose zone and the vadose zone with residual NAPL, Rn_N, can be calculated as follows:

$$Rn_{VN} = \frac{\Lambda + M}{N} \quad \text{Eq. 3.20}$$

With:

$$\Lambda = \frac{D_{VN}}{L_{C,VN}} \cdot Rn_{CF} \cdot \operatorname{csch}\left(\frac{L_{CF} - L_N}{L_{C,VN}}\right) + \frac{D_V}{L_{C,V}} \cdot \frac{P_V \cdot f_V}{\lambda} \cdot \tanh\left(\frac{L_N}{2L_{C,V}}\right) \quad \text{Eq. 3.21}$$

$$M = \frac{D_{VN}}{L_{C,VN}} \cdot \frac{P_{VN} \cdot f_{VN}}{\lambda} \cdot \tanh\left(\frac{L_{CF} - L_N}{2L_{C,VN}}\right) \quad \text{Eq. 3.22}$$

$$N = \frac{D_V}{L_{C,V}} \cdot \coth\left(\frac{z_N}{L_{C,V}}\right) + \frac{D_{VN}}{L_{C,VN}} \cdot \coth\left(\frac{L_{CF} - L_N}{L_{C,VN}}\right) \quad \text{Eq. 3.23}$$

In the absence of NAPL, the domain is reduced to only two layers, i.e. a non-contaminated layer in the vadose zone and the capillary fringe. In this case, Eq. 3.9, Eq. 3.10 and Eq. 3.11 reduce to the following:

- For $0 < z \leq L_{CF}$:

$$Rn(z) = Rn_{CF} \cdot \left[1 - \frac{\sinh\left(\frac{z}{L_{c,V}}\right)}{\sinh\left(\frac{L_{CF}}{L_{c,V}}\right)}\right] + \frac{P_V \cdot f_V}{\lambda} \cdot \left[1 - \frac{\sinh\left(\frac{L_{CF} - z}{L_{c,V}}\right) + \sinh\left(\frac{z}{L_{c,V}}\right)}{\sinh\left(\frac{L_{CF}}{L_{c,V}}\right)}\right] \quad \text{Eq. 3.24}$$

- For $L_{CF} < z \leq L_W$:

$$Rn(z) = \left[\frac{\left(Rn_{CF} - \frac{P_{CF} \cdot f_{CF}}{\lambda}\right) \cdot \cosh\left(\frac{L_W - z}{L_{c,CF}}\right)}{\cosh\left(\frac{L_W - L_N}{L_{c,CF}}\right)}\right] + \frac{P_{CF} \cdot f_{CF}}{\lambda} \quad \text{Eq. 3.25}$$

with:

$$Rn'_{CF} = \frac{\frac{D_V}{L_{c,V}} \cdot \frac{P_V \cdot f_V}{\lambda} \cdot \tanh\left(\frac{L_{CF}}{2L_{c,V}}\right) + \frac{D_{CF}}{L_{c,CF}} \cdot \frac{P_{CF} \cdot f_{CF}}{\lambda} \cdot \tanh\left(\frac{L_W - L_{CF}}{L_{c,CF}}\right)}{\frac{D_V}{L_{c,V}} \cdot \coth\left(\frac{L_{CF}}{L_{c,V}}\right) + \frac{D_{CF}}{L_{c,CF}} \cdot \tanh\left(\frac{L_W - L_{CF}}{L_{c,CF}}\right)} \quad \text{Eq. 3.26}$$

This latter 2-layer analytical solution is analogous to the one previously obtained by Höhener and Surbeck (2004).

3.3 RESULTS

3.3.1 Comparison with a numerical model

To confirm the validity of the 3-layer model proposed in this work, we compared the analytical results with the ones previously obtained by Cohen et al. (2019) using the numerical code MIN3P (Mayer et al., 2002) adapted to account for Rn production, dissolution of Rn into NAPL, and Rn decay in the gas and NAPL phases. In particular, Cohen et al. (2019) simulated a column configuration with four different NAPL distributions. All configurations represent a 1.9 m alluvial sand column, with the first 12 cm at the bottom consisting of saturated sand. The top of the column was simulated open to the atmosphere.

In the first configuration (Case 1), above the first layer of saturated sand, the authors simulated a 50 cm sand layer with NAPL occupying the entire water-free porosity (θ_N = 0.37). In the second realization (Case 2), the contaminated layer was characterized by a NAPL content of 0.25 over a thickness of 74 cm. Case 3 contains a layer of residual NAPL (θ_N = 0.12) of 15 cm of thickness that was located on the top of a fully saturated NAPL layer (θ_N = 0.37) of 45 cm. Similarly, in Case 4, a layer of residual NAPL (θ_N = 0.12) of 52 cm was located above a 33 cm of a fully saturated NAPL layer. For these configurations, Cohen et al. (2019) provided the Rn concentration vertical profiles obtained by the numerical simulations.

Figure 3.2 shows the concentration profiles obtained by Cohen et al. (2019) with the numerical model (points) and the ones simulated with the analytical solution presented in this work (continuous lines) using the same input data (see Table 3.1). Note that these results refer to the concentration profiles obtained in the unsaturated zone (i.e. not considering the 12 cm of saturated layer simulated in the numerical model). The four scenarios considered by Cohen et al. (2019) were simulated with the analytical model using Eq. 3.24 and Eq. 3.25 for Case 1 and Case 2 and Eq. 3.9, Eq. 3.10 and Eq. 3.11 for Case 3 and Case 4.

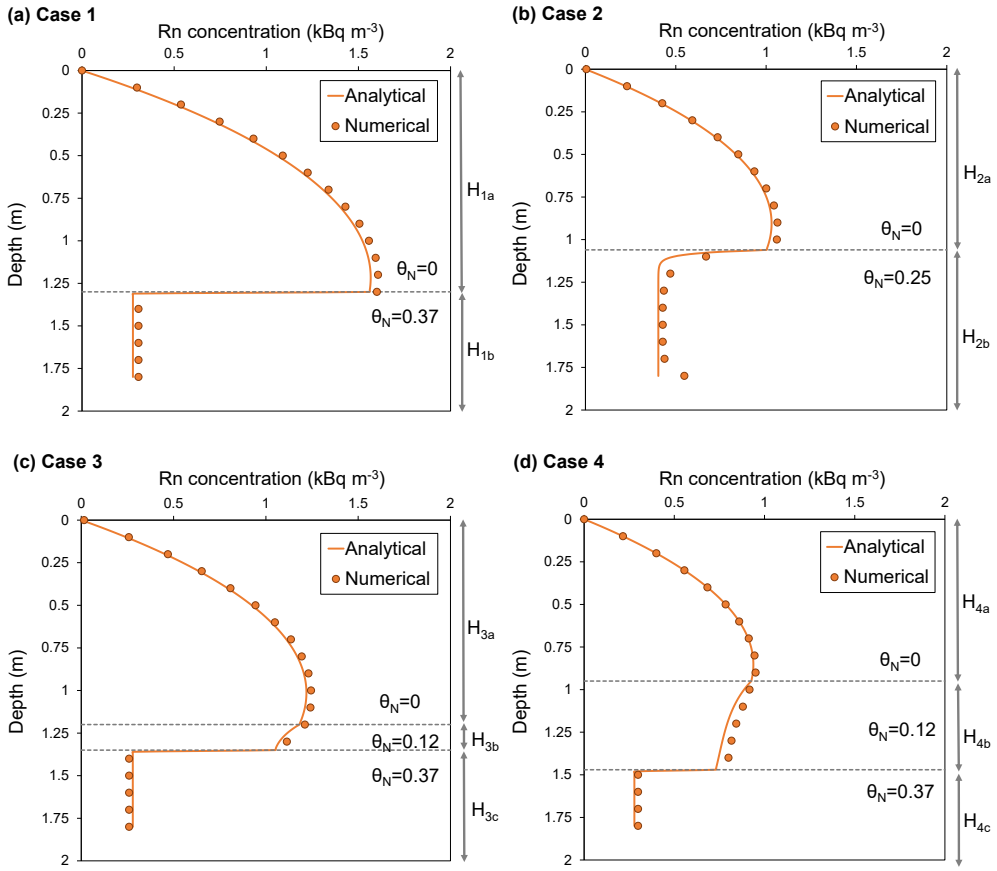

Figure 3.2. Rn concentration profiles for different NAPL distributions calculated with the analytical model (continuous lines) and the numerical model (dots) from Cohen et al. (2019). The dashed lines represent the depths of the layers with NAPL in the different configurations (Case 1, Case 2, Case 3 and Case 4 respectively in figure a, b, c and d).

Table 3.1. Parameters used for the validation of the model (see Figure 3.2).

PARAMETER	SYMBOL	UNIT	VALUE (Figure 3.2)
Solid density	ρ_s	kg m^{-3}	2550
Total porosity	θ_t	-	0.4
Residual water saturation	S_{wr}	-	0.08
Rn partition coefficient between gas and water (Henry's law constant)	$k_{g/w}$	-	4.4
Rn partition coefficient between NAPL and water	$k_{N/w}$	-	60
Rn first order decay constant	λ	s^{-1}	$2.1 \cdot 10^{-6}$
^{226}Ra concentration of the solids multiplied by Rn emanation coefficient	$C_{Ra}\varepsilon$	Bq kg^{-1}	0.92
Rn molecular diffusion coefficient in gas phase	D_{mg}	$m^2\ s^{-1}$	$1.1 \cdot 10^{-5}$
Rn molecular diffusion coefficient in water phase	D_{mw}	$m^2\ s^{-1}$	$1.1 \cdot 10^{-9}$
Van Genuchten parameters	α	m^{-1}	80
	n	-	2.7
	m	-	0.6
Case 1	H_{1a}	m	1.3
	θ_{N1a}	-	0
	θ_{w1a}	-	0.032
	H_{1b}	m	0.48
	θ_{N1b}	-	0.37
	θ_{w1b}	-	0.061
Case 2	H_{2a}	m	1.06
	θ_{N2a}	-	0
	θ_{w2a}	-	0.032
	H_{2b}	m	0.72
	θ_{N2b}	-	0.25
	θ_{w2b}		0.051

PARAMETER	SYMBOL	UNIT	VALUE (Figure 3.2)
Case 3	H_{3a}	m	1.2
	θ_{N3a}	-	0
	θ_{w3a}	-	0.032
	H_{3b}	m	0.15
	θ_{N3b}	-	0.12
	θ_{w3b}	-	0.033
	H_{3c}	m	0.43
	θ_{N3c}	-	0.37
	θ_{w3c}	-	0.054
Case 4	H_{4a}	m	0.950
	θ_{N4a}	-	0.032
	θ_{w4a}	-	0.52
	H_{4b}	m	0.12
	θ_{N4b}	-	0.033
	θ_{w4b}	-	0.31
	H_{4c}	m	0.37
	θ_{N4c}	-	0.065
	θ_{w4c}	-	

The volumetric gas content $\theta_{g,i}$ and the volumetric water content $\theta_{w,i}$ of each layer of the simulated porous media were calculated using the equation (Genuchten and Th., 1980):

$$\theta_w(h) = \theta_{wr} + \frac{(\theta_{ws} - \theta_{wr})}{[1 + (\alpha \cdot |h|)^n]^m} \quad \text{Eq. 3.27}$$

where h is the elevation above the steady state groundwater level; θ_{wr} is the residual water content; θ_{ws} is the saturated water content; α, n and m are the soil hydraulic retention parameters with m = 1 − 1/n.

The Van Genuchten parameters used in these simulations are reported in Table 3.1. Next, for the analytical solution the vertical moisture profile has been discretized using a vertical step of 0.1 m. Then, $\theta_{w,i}$ was calculated, for each layer, as the geometric

mean of the volumetric water contents of the layer. Hence, $\theta_{g,i}$ was calculated as the difference between the total porosity θ_t and the sum of the NAPL content of the layer $\theta_{N,i}$ and the water content of the layer $\theta_{w,i}$. D_i, P_i, f_i and $L_{c,i}$ were then calculated using Eq. 3.2, Eq. 3.3, Eq. 3.4 and Eq. 3.12 respectively.

Note that in both the numerical and analytical model the Rn partition coefficient between the solids and water ($k_{s/w}$) was considered negligible.

Referring to Figure 3.2 , it can be noticed that the concentration profiles of Rn obtained by the analytical solution proposed in this work are very close to the results obtained by Cohen et al. (2019). These slight differences are ascribed to the fact that the analytical solution proposed in this work does not allow to simulate a vertical heterogeneous moisture profile that as discussed earlier was discretized assuming the geometric mean of the moisture content representative of each layer. In any case, the differences between the two solutions are on average for all the simulated cases of about 5% and in almost all cases within 10%. Considering the purpose of this work (i.e. to provide a screening tool for the Rn behavior in the presence of NAPL) these slight deviations are negligible.

3.3.2 Sensitivity analysis

The developed analytical solution was applied to assess how the different site-specific parameters can influence the vertical Rn concentration profiles. Namely, the Rn profile was calculated above the NAPL zone and compared to the one expected in the same conditions but at a background location not impacted by NAPL. This allowed to calculate the expected deficit profiles in the different scenarios examined. Unless otherwise noted, the site parameters used in the simulations are those reported in Table 3.2. Then, a one-way sensitivity analysis was carried out by varying within the ranges expected in the field the various parameters that may affect the migration and distribution of Rn in the subsurface. The obtained results are discussed in the next sections.

Table 3.2. Parameters used to derive the vertical Rn concentration profiles and the saturation-deficit curves (unless otherwise indicated in the figures).

PARAMETER	Symbol	Unit	VALUES (Figure 3.3-3.8)
Solid density	ρ_s	kg m^{-3}	2650
Soil type	-	-	sand
Total porosity	θ_t	-	0.375
Residual water content	θ_{wr}	-	0.053
Water content in the vadose zone	$\theta_{w,v}$	-	0.054
Water content in the capillary fringe	$\theta_{w,cf}$	-	0.253
Rn partition coefficient between gas and water (Henry's law constant)	$k_{g/w}$	-	4.4
Contamination	-	-	diesel
Rn partition coefficient between NAPL and water	$k_{N/w}$	-	60
Rn partition coefficient between solid phase and water	$k_{s/w}$	-	$1.4 \cdot 10^{-5}$
Rn first order decay constant	λ	s^{-1}	$2.1 \cdot 10^{-6}$
^{226}Ra concentration of the solids multiplied by Rn emanation coefficient	$C_{Ra} \cdot \varepsilon$	Bq kg^{-1}	0.92
Rn molecular diffusion coefficient in gas phase	D_{mg}	$m^2\ s^{-1}$	$1.1 \cdot 10^{-5}$
Rn molecular diffusion coefficient in water phase	D_{mw}	$m^2\ s^{-1}$	$1.1 \cdot 10^{-9}$
Thickness of the source zone	H_N	m	0.5
Thickness of the capillary fringe	H_{CF}	m	0.2
Depth of the source zone	L_N	m	4.5
Depth of the capillary fringe	L_{CF}	m	4.8
Depth of the groundwater table	L_W	m	5

3.3.2.1 NAPL saturation

Figure 3.3 shows the vertical profiles of Rn concentrations calculated using Eq. 3.9, Eq. 3.10 and Eq. 3.11 as a function of different NAPL saturation (5-20%).

In the same figure the vertical profiles of Rn concentrations calculated using the same input parameters but in the absence of NAPL (Eq. 3.24 and Eq. 3.25) are also reported. Finally, based on the ratio of these two concentration profiles the deficit curve is also represented for each simulation. Rn deficit was calculated at each depth as:

$$\mathrm{Deficit(z)} = \frac{\mathrm{Rn_{NAPL(z)}}}{\mathrm{Rn_{NONAPL(z)}}} \qquad \text{Eq. 3.28}$$

where $Rn_{NAPL}(z)$ is the Rn concentration at the depth z in the presence of NAPL and $Rn_{NONAPL}(z)$ is the Rn concentration at the same depth z in the absence of NAPL.

Note that the soil water content in the vadose zone $\theta_{w,v}$ and in the capillary fringe $\theta_{w,cf}$ were taken from US EPA (2004) but they were adapted to account for the porosity filled by NAPL.

It can be noticed that the Rn concentrations in the NAPL zone are lower than the concentrations expected at the same depth at a background location with the same characteristics but not impacted by NAPL. This is because of the affinity of Rn to NAPL. Indeed, the higher the NAPL saturation the lower the Rn concentration in the soil gas. For instance, in all the four cases of Figure 3.3, at a depth of 4.5 m, i.e., at the beginning of the NAPL zone, a Rn concentration of about 5 kBq m^{-3} can be observed on the Rn curve in the absence of NAPL.

Instead, for case (b), i.e. 5% saturation, at the same depth, a Rn concentration of 3 kBq m^{-3} can be observed on the Rn curve in the presence of NAPL, while a Rn concentration of about 2 kBq m^{-3} can be observed in case (d) corresponding to 20% saturation. With increasing distance from the NAPL zone, in all simulated cases the two Rn profiles (NAPL and No NAPL) approach each other and overlap at a distance of approximately 3 m from the source zone. This behavior is also reflected on the deficit curve that at distances above 3 m from the source tends to 1. These results highlight that the deficit technique is not working anymore (i.e. no more sensitive) if

the Rn in soil gas is analyzed at distances higher than 2-3 m from the area interested by the presence of contamination.

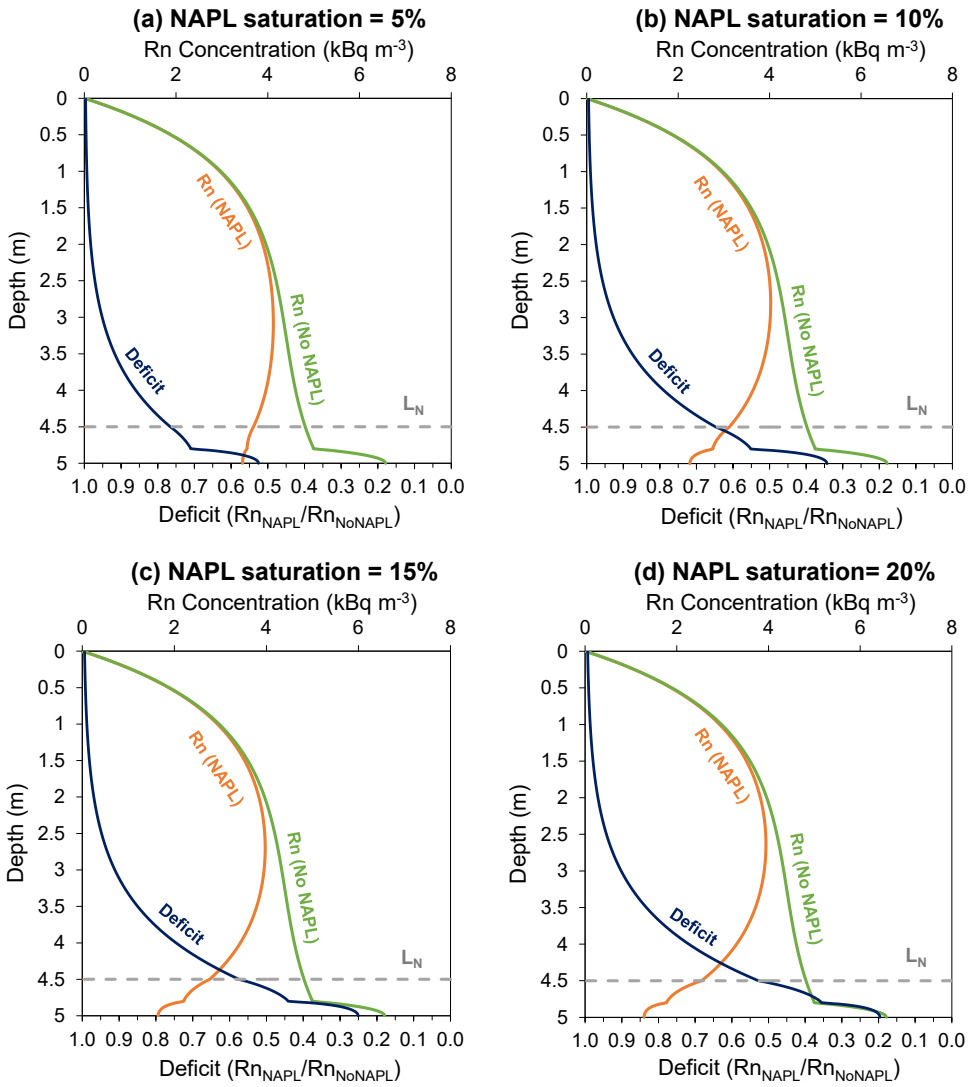

Figure 3.3. Rn vertical concentration profile in the presence of NAPL, in the absence of NAPL, and the associated Rn deficit, calculated for different NAPL saturation: (a) S_N = 5%, (b) S_N = 10%, (c) S_N = 15%, i (d) S_N = 20%. The dashed lines represent the depth of the top of the source zone (L_N) in the different configurations.

3.3.2.2 Influence of NAPL composition

To understand the influence of the type of NAPL mixture on Rn profiles, four simulations were performed, varying the value of the partition coefficient between NAPL and water ($k_{N/w}$) from 20 to 80. Note that Schubert et al. (2007b) assumed a

$k_{N/w}$ of around 38 for gasoline and 60 for a diesel contamination and also that the range of $k_{N/w}$ between 20 and 80 matches well the variations observed during the weathering of diesel and gasoline by evaporation (Le Meur et al., 2021). The results of these simulations, in terms of Rn concentration profiles and Rn deficit curves, are shown in Figure 3.4.

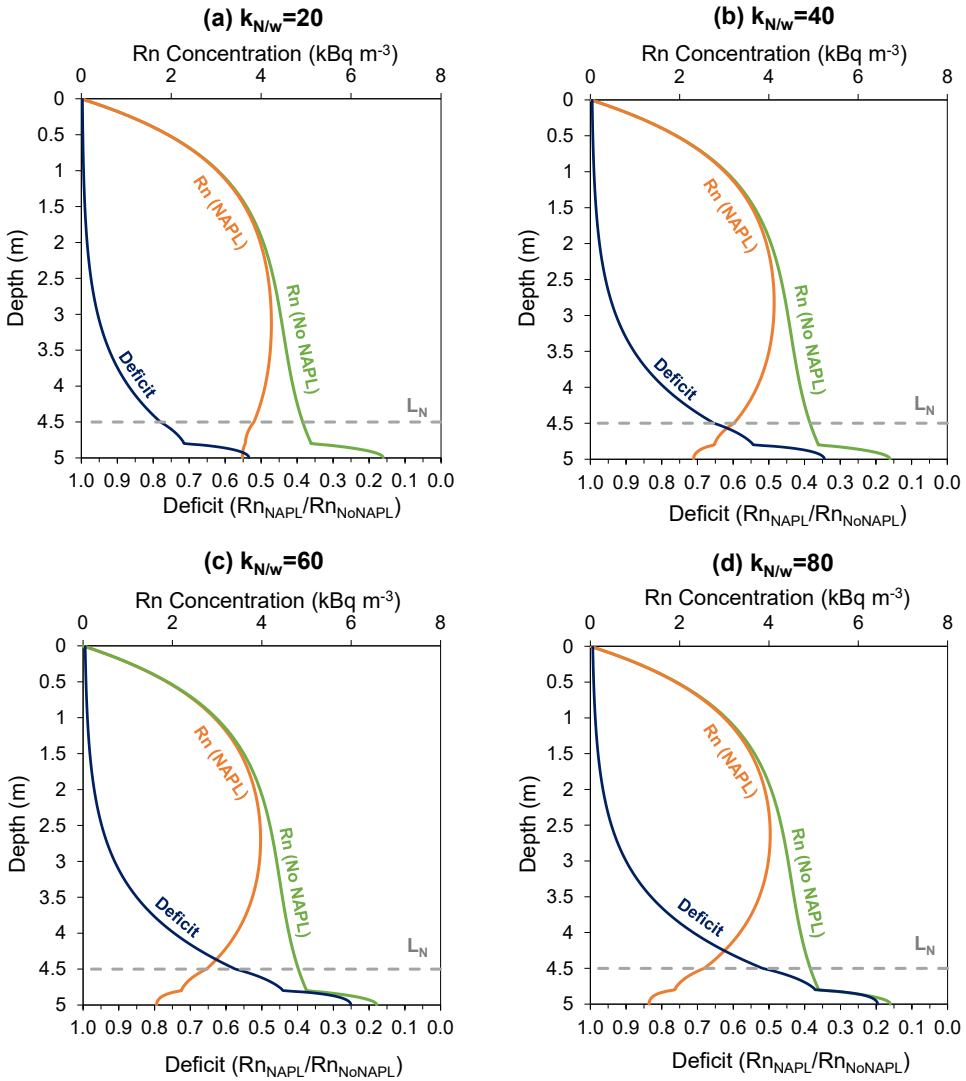

Figure 3.4. Rn vertical concentration profile in the presence of NAPL (saturation of 15%), in the absence of NAPL, and the associated Rn deficit calculated for different Rn partition coefficient ($k_{N/w}$) of the NAPL mixture (a) $k_{N/w}$ = 20, (b) $k_{N/w}$ = 40, (c) $k_{N/w}$ = 60, (d) $k_{N/w}$ = 80. The dashed lines represent the depth of the top of the source zone (L_N) in the different configurations.

It can be observed that the Rn concentration curve representative of the site background values clearly remains unchanged in the different configurations. In

contrast, the Rn concentrations in the presence of NAPL (NAPL saturation of 15%) decreases with increasing values of the partition coefficient. As a result, the Rn deficit curve (see Eq. 3.28) is also modified. Namely, for a higher $k_{N/w}$, Rn will have a greater affinity to NAPL, and the deficit will be more pronounced. For instance, at a distance of 0.5 m from the source zone (i.e., a depth of 4 m), a deficit value of 0.8 can be observed on the deficit curve for case (b), while the observed deficit at the same depth is about 0.7 in case (d). These differences are more evident near to the contaminated zone, while become less important in the most superficial layers, far away from the source zone.

3.3.2.3 Influence of soil texture

Another parameter that can influence the vertical profiles of Rn concentration in soil gas, is the soil texture. Here, four different soil textures were considered (Sand, Loamy Sand, Sandy Loam and Loam). For each soil textures, we varied the porosity, the water content, and the thickness of the capillary fringe according to the values suggested by US EPA (2004). The resulting profiles and the Rn deficit curves are shown in Figure 3.5.

In this case it can be observed that the soil textures influences not only the Rn concentration profile in the presence of NAPL, but also the profile in the case of absence of contamination. Soil properties indeed influences on one hand the fraction of Rn in the air phase and the Rn production rate in the pore space but on the other hand they affect the effective diffusion coefficient ($D_{e,i}$) and consequently the characteristic diffusion length ($L_{c,i}$). All the values of Rn diffusion length obtained from Eq. 3.12 for the different simulations are reported in Table 3.3. For example, considering again a distance from the source zone of 0.5 m (i.e., a depth of 4 m), the deficit observed in case (b) would be approximately 0.75, while in case (d) it would be higher than 0.8. These differences are more pronounced in correspondence of the capillary fringe.

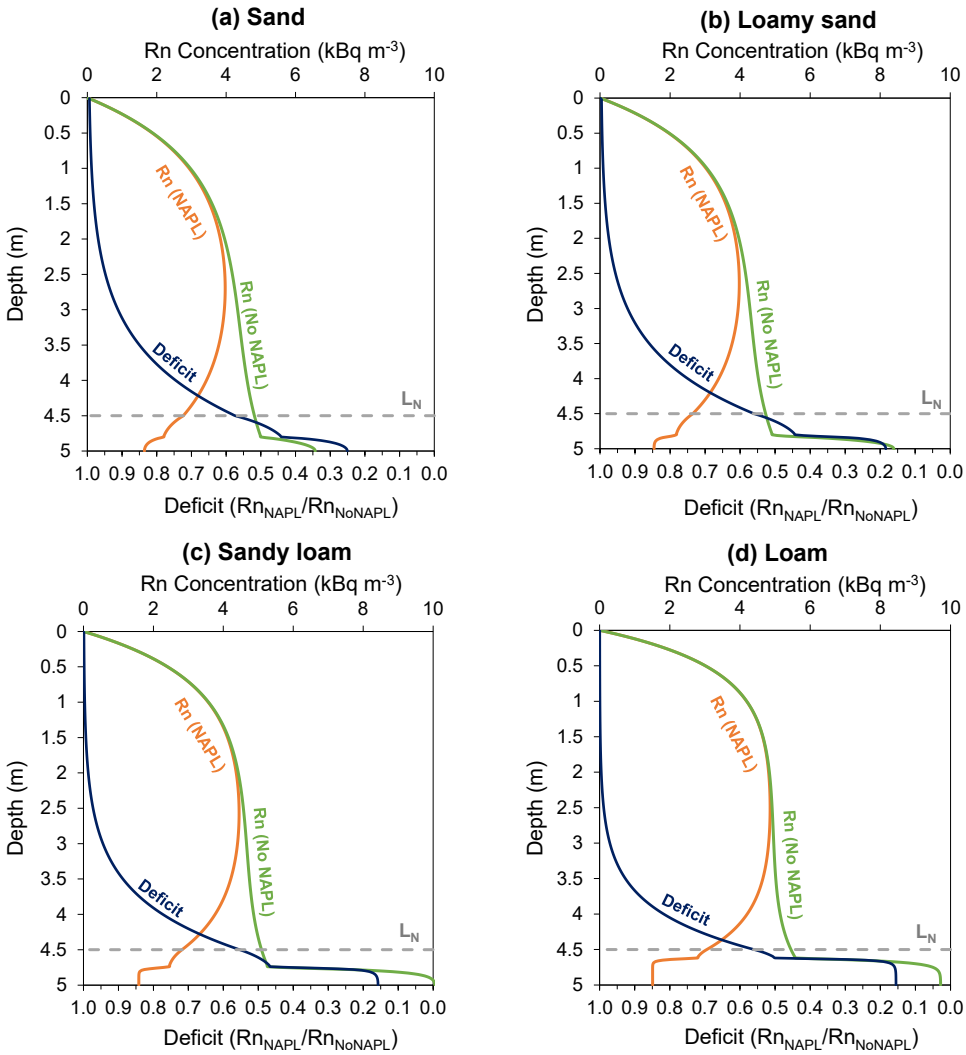

Figure 3.5. Rn vertical concentration profile in the presence of NAPL (NAPL saturation of 15%), in the absence of NAPL, and the associated Rn deficit calculated for different types of soil: (a) sand (θ_t = 0.375, θ_w = 0.054, h_{cap} = 0.17m), (b) loamy sand (θ_t = 0.39, θ_w = 0.076, h_{cap} = 0.19m) (c) sandy loam (θ_t = 0.387, θ_w = 0.103, h_{cap}= 0.25m), (d) loam (θ_t = 0.399, θ_w = 0.148, h_{cap} = 0.38m). The dashed lines represent the depth of the top of the source zone (L_N) in the different configurations.

Table 3.3. Characteristic diffusion length of Rn calculated with Eq. 3.12 for each layer of the simulation in figures 3.3 - 3.7.

Characteristic diffusion length (m)				
	Case a	**Case b**	**Case c**	**Case d**
		Figure 3.3		
NO NAPL, layer 1	0.89	0.89	0.89	0.89
NO NAPL, layer 2	0.15	0.15	0.15	0.15
NAPL, layer 1	0.89	0.89	0.89	0.89
NAPL, layer 2	0.61	0.44	0.34	0.26
NAPL, layer 3	0.1	0.08	0.07	0.06
		Figure 3.4		
NO NAPL, layer 1	0.89	0.89	0.89	0.89
NO NAPL, layer 2	0.15	0.15	0.15	0.15
NAPL, layer 1	0.89	0.89	0.89	0.89
NAPL, layer 2	0.47	0.39	0.34	0.30
NAPL, layer 3	0.10	0.08	0.07	0.06
		Figure 3.5		
NO NAPL, layer 1	0.89	0.82	0.69	0.53
NO NAPL, layer 2	0.15	0.07	0.04	0.04
NAPL, layer 1	0.89	0.82	0.69	0.53
NAPL, layer 2	0.34	0.36	0.37	0.27
NAPL, layer 3	0.07	0.03	0.02	0.02

Figure 3.6 – 3.7				
NO NAPL, layer 1	0.89	0.89	0.89	0.89
NO NAPL, layer 2	0.15	0.15	0.15	0.15
NAPL, layer 1	0.89	0.89	0.89	0.89
NAPL, layer 2	0.34	0.34	0.34	0.34
NAPL, layer 3	0.07	0.07	0.07	0.07

3.3.2.4 Influence of source zone thickness

Further simulations were carried out by varying the thickness of the NAPL source zone (H_N) from 0.2 to 2.5 m. Here, with source zone we mean both the vadose zone and capillary fringe with the presence of NAPL. The results of the simulations are shown in Figure 3.6.

It can be observed that the Rn profile in the presence of NAPL (and consequently the deficit curve) varies with increasing thickness of the source zone. However, it is interesting to note that the deficit value observed in the different configurations at the same distance from the top of the source zone (L_N), remains almost unchanged. For instance, considering case (b), at a distance of 0.5 m from the source zone (i.e., a depth of 4 m), the deficit observed is approximately 0.75, i.e. almost coincident with the deficit observed at the same distance (i.e., a depth of 2 m) in case (d). This means that the deficit of Rn concentration between impacted, and background location depends on the NAPL saturation and distance of the soil gas probe from the source but not on the thickness of the zone impacted by NAPL.

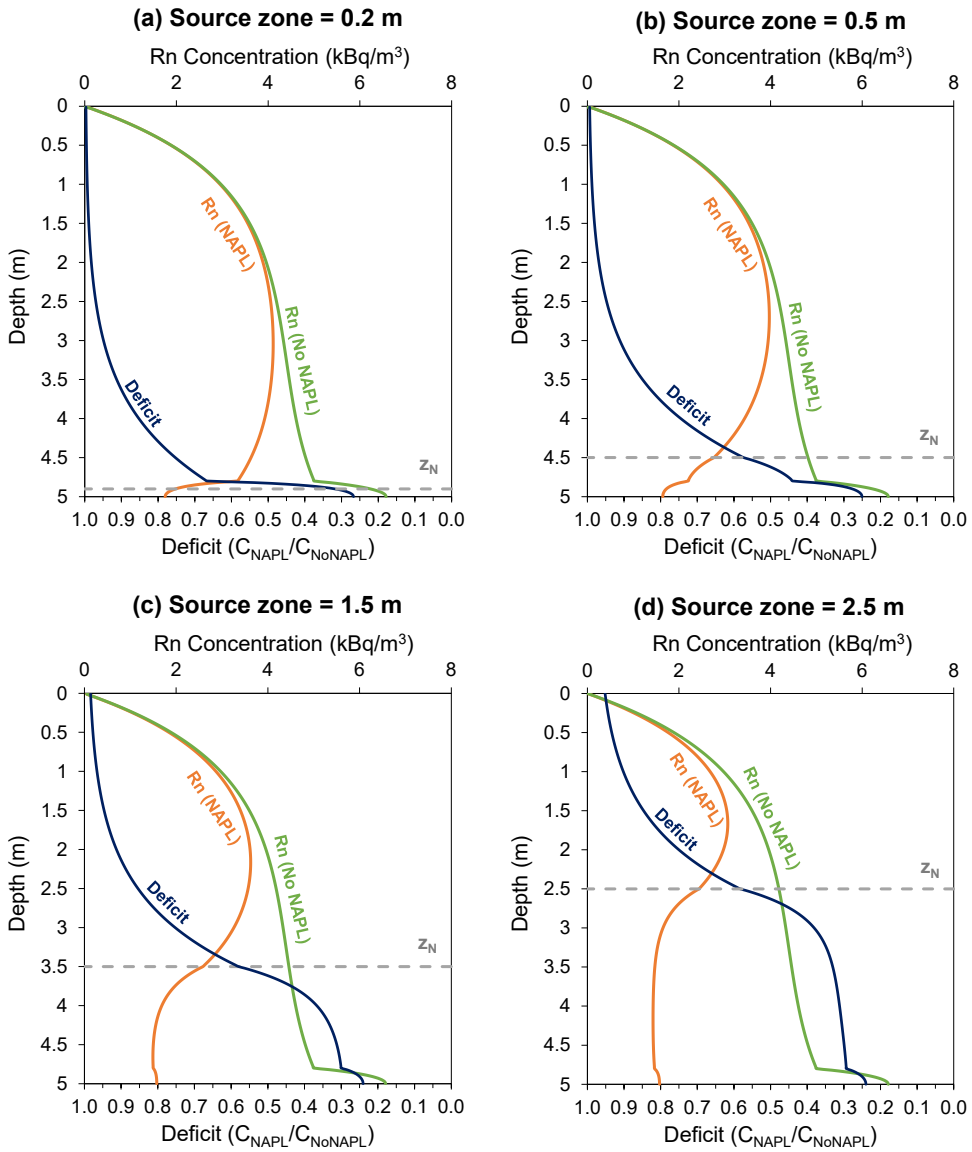

Figure 3.6. Rn vertical concentration profile in the presence of NAPL (NAPL saturation of 15%), in the absence of NAPL, and the associated Rn deficit, calculated for different thicknesses of the source zone: (a) H_N = 0.2 m, (b) H_N = 0.5 m, (c) H_N = 1.5 m, (d) H_N = 2.5 m. The dashed lines represent the depth of the top of the source zone (L_N) in the different configurations.

3.3.2.5 Influence of groundwater depth

Another parameter investigated was the depth of groundwater. In this case, the simulations were carried out by varying the depth of the aquifer from 3 to 10 m. The curves obtained are shown in Figure 3.7.

In this case, the Rn concentration curves do not present particular variations if not those obviously due to the variation of the maximum depth considered in the domain of the model. Specifically, it can be noticed that the deficit value observed at the same distance from the top of the source zone (L_N), remains nearly unaltered. For example, considering cases (b) and (d), the deficit observed at a distance of 0.5 m from the source zone (i.e., a depth of 4 m for case (b) and a depth of 9 m for case (d)), is about 0.75. We can then state that the estimation of NAPL saturation from Rn measurements taken at a certain distance from the NAPL zone will not be influenced by the depth of the groundwater table at the site.

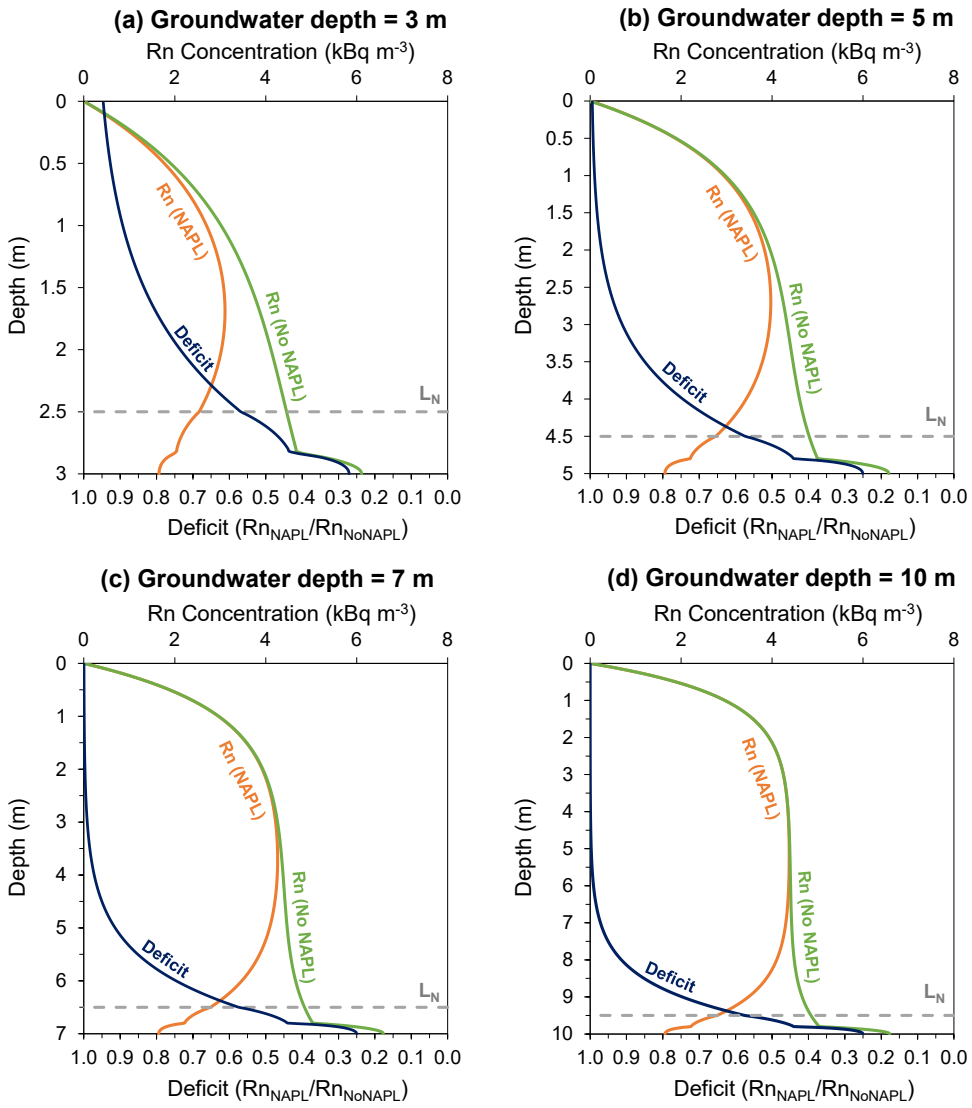

Figure 3.7. Rn vertical concentration profile in the presence of NAPL (NAPL saturation of 15%), in the absence of NAPL, and the associated Rn deficit, calculated for different depths of the aquifer: (a) L_W = 3 m, (b) L_W = 5 m, (c) L_W = 7 m, (d) L_W = 10m. The dashed lines represent the depth of the top of the source zone (L_N) in the different configurations.

3.3.2.6 Sensitivity analysis results

As shown in the previous sections, the key parameter that affects the effectiveness of the Rn deficit technique is the distance of the soil gas probe from the source zone. To examine the influence of the other parameters on the Rn transport and distribution, in Table 3.4 we summarized the results of the different simulation discussed earlier. Namely, Table 3.4 reports the Rn deficit (see Eq. 3.28) estimated in the different

simulations within the capillary fringe zone (i.e. in the source at a distance of 0.1 m above the water table) and in the unsaturated zone at a distance of 0.1 m, 0.5 m and 1 m above LNAPL. To evaluate the influence of each parameter on the Rn deficit value, the percentage of variation of the deficit value observed in each case was calculated.

It can be observed that the parameters with most affect the Rn transport and distribution in the subsurface are the NAPL saturation (variation of the Rn deficit of 10% to 157%) and the Rn partition coefficient between NAPL and water ($k_{N/w}$) (variation of 11% to 159%). To a lower extent, also the soil texture affects the calculated Rn deficit (3%-79%). In relation to the latter, it can be observed, also from Figure 3.5, that the greatest variation (79%) occurs in the capillary fringe. Less important, and in nearly all cases negligible, are the contributions given by the thickness of the contaminated zone (4%-27%) and the depth of the water table (2%-11%).

Table 3.4. Results of the sensitivity analysis in terms of Rn deficit observed in the simulations at a distance of 0.1 m above the water table (in the capillary fringe) and 0.1m, 0.5m and 1m from the contaminated zone for cases a,b,c,d in Figures 3.3, 3.4, 3.5, 3.6, 3.7. The variation is calculated as the difference between the maximum deficit and the minimum deficit over the minimum deficit value observed in the four cases considered for each parameter.

Parameter	Figure	Deficit value case a	Deficit value case b	Deficit value case c	Deficit value case d	Variation (%)
Source zone @ 0.1 m above the water table (capillary fringe)						
Influence of NAPL saturation	Figure 3.3	0.56	0.38	0.28	0.22	**157**
Influence of NAPL composition	Figure 3.4	0.57	0.38	0.28	0.22	**159**
Influence of soil texture	Figure 3.5	0.28	0.20	0.16	0.16	**79**
Influence of source zone thickness	Figure 3.6	0.32	0.28	0.25	0.25	**27**
Influence of groundwater depth	Figure 3.7	0.31	0.28	0.28	0.28	**11**
@ 0.1 m from the source zone (unsaturated zone)						
Influence of NAPL saturation	Figure 3.3	0.79	0.68	0.61	0.57	**38**
Influence of NAPL composition	Figure 3.4	0.8	0.68	0.61	0.56	**43**
Influence of soil texture	Figure 3.5	0.61	0.61	0.61	0.63	**3**
Influence of source zone thickness	Figure 3.6	0.69	0.61	0.62	0.6	**15**
Influence of groundwater depth	Figure 3.7	0.61	0.61	0.62	0.62	**2**

Parameter	Figure	Deficit value case a	Deficit value case b	Deficit value case c	Deficit value case d	Variation (%)
@ 0.5 m from the source zone (unsaturated zone)						
Influence of NAPL saturation	Figure 3.3	0.86	0.79	0.75	0.72	**20**
Influence of NAPL composition	Figure 3.4	0.87	0.79	0.75	0.71	**23**
Influence of soil texture	Figure 3.5	0.75	0.75	0.77	0.82	**9**
Influence of source zone thickness	Figure 3.6	0.79	0.75	0.75	0.75	**5**
Influence of groundwater depth	Figure 3.7	0.73	0.75	0.75	0.75	**3**
@ 1 m from the source zone (unsaturated zone)						
Influence of NAPL saturation	Figure 3.3	0.92	0.88	0.85	0.83	**10**
Influence of NAPL composition	Figure 3.4	0.92	0.87	0.85	0.83	**11**
Influence of soil texture	Figure 3.5	0.85	0.86	0.89	0.93	**9**
Influence of source zone thickness	Figure 3.6	0.88	0.85	0.85	0.85	**4**
Influence of groundwater depth	Figure 3.7	0.83	0.85	0.85	0.85	**2**

3.3.3 Nomographs

To aid the determination of the NAPL saturation, starting from the 1-D analytical solution of the Rn transport diffusive equation we developed some nomographs that can be used for the application of Rn deficit technique, starting from soil gas Rn

concentration data collected at some distance from the source zone. Figure 3.8 shows the NAPL saturation calculated as a function of the Rn deficit and the distance of the soil gas probes from the source zone. The figures also report, as reference, the results obtained with the model proposed by Schubert et al. (2001), without depth dependence. The nomographs were developed for two soil types (Sand and Loam) with the values suggested by US EPA (2004) and for two types of contamination (diesel and gasoline) with the corresponding values of $k_{N/w}$ equal to 60 and 40, respectively, suggested by Schubert et al. (2007b).

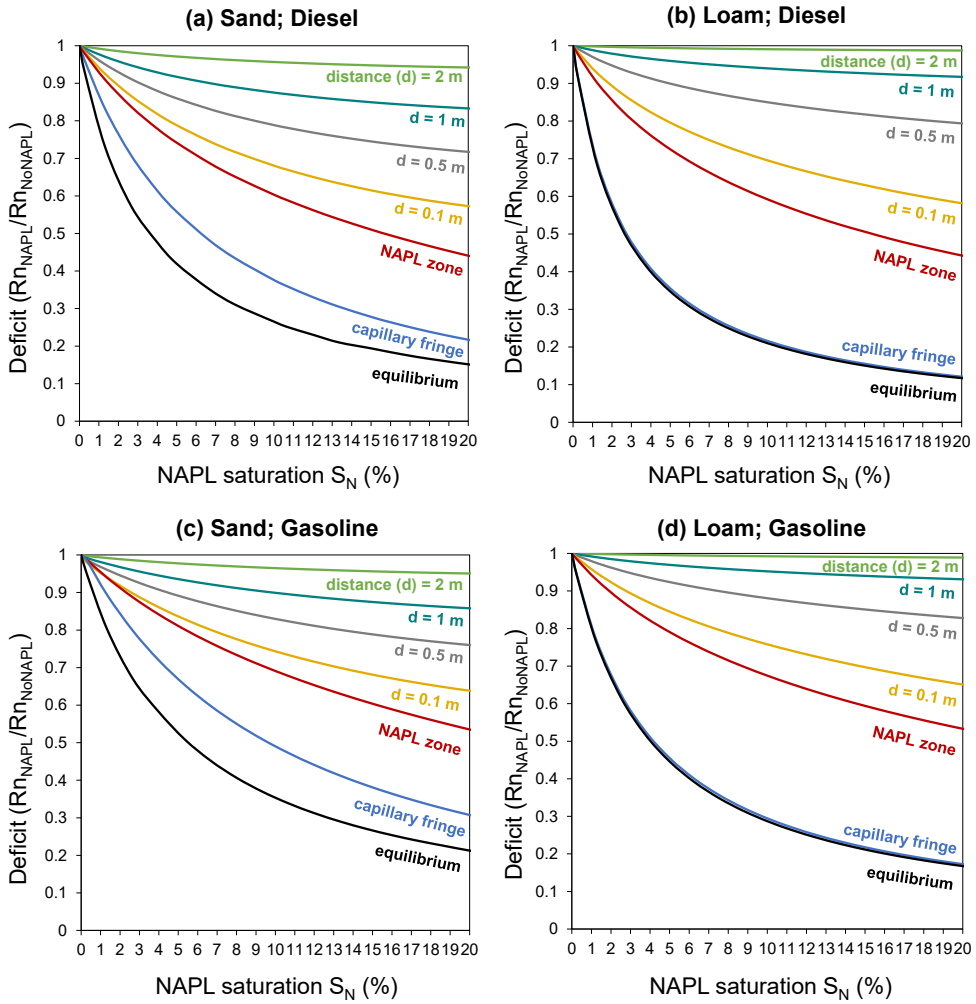

Figure 3.8. NAPL saturation - Rn deficit curves calculated as a function of the vertical distance (d) between the Rn measurement point and the top of NAPL zone (L_N). The NAPL zone curve is calculated 0.1 m below L_N. The capillary fringe curve is calculated 0.1 m above the water table. The four nomographs (a), (b), (c), (d) are calculated for different soil types and contamination types, as reported in figure. The curve obtained applying the model proposed by Schubert et al. (2001) is also shown.

From the nomographs shown in Figure 3.8 it can be observed that, as expected, the Rn deficit decreases (i.e., Rn decreases in the impacted area compared to the value obtained in the background location) as NAPL saturation increases. It is also clear that the deficit is more evident as the measurement point approaches the source zone. Namely, in all the cases considered the deficit is no longer appreciable at a distance of 2 m from the source zone. It should also be noted that for distances greater than 1 m, even a small variation in measured deficit can lead to large differences in the estimation of NAPL saturation. For this reason, in case of measurements made beyond 1 m from the source zone, the results can be considered reliable only from a qualitative point of view. This behavior is related to the characteristic diffusion length of Rn, whose values, as can be seen in Table 3.3, are in the range of 0.02 to 0.9 m, i.e. less than 1 m. From these results it can be also observed that the NAPL saturation calculated with the model proposed by Schubert et al. (2001) tend to be significantly underestimated with increasing distance of the soil gas probes form the source zone. For instance, considering case (a) and assuming a deficit of 0.9 observed at a distance of 1 m from the source zone, using the approach proposed by Schubert et al. (2001) the NAPL saturation would be of about 0.5%, while considering the derived solution that accounts for the Rn diffusion in the vadose zone the calculated NAPL saturation would result about 6.5%. Hence, this highlights the importance of considering the dynamic transport and partition of Rn for the interpretation of the observed deficit.

CHAPTER 4

4 INFLUENCE OF ADVECTION ON THE SOIL GAS RADON DEFICIT TECHNIQUE

Most of this chapter is taken from "Cecconi, A., Verginelli, I., Barrio-Parra, F., De Miguel, E., Baciocchi, R., 2023b. Influence of advection on the soil gas radon deficit technique for the quantification of LNAPL. Sci. Total Environ. 875, 162619. https://doi.org/10.1016/j.scitotenv.2023.162619"

ABSTRACT

The Radon (Rn) deficit technique is a rapid, low-cost, and non-invasive method to identify and quantify light non-aqueous phase liquids (LNAPL) in the soil. LNAPL saturation is typically estimated from Rn deficit using Rn partition coefficients, assuming equilibrium conditions. This work examines the applicability of this method in the presence of local advective fluxes that can be generated by groundwater fluctuations or biodegradation processes in the source zone. To this end, a one-dimensional analytical model was developed to simulate the steady-state diffusive-advective transport of soil gas Rn in the presence of LNAPL. The analytical solution was first validated against an existing numerical model adapted to include advection. Then a series of simulations to study the effect of advection on Rn profiles were carried out. It was found that in high-permeability soils (such as sandy soils), advective phenomena can significantly affect Rn deficit curves in the subsurface compared with those expected, assuming either equilibrium conditions or a diffusion-dominated transport. Namely, in the presence of pressure gradients generated by groundwater fluctuations, applying the traditional Rn deficit technique (assuming equilibrium conditions) can lead to an underestimation of LNAPL saturation. Furthermore, in the presence of methanogenesis processes (e.g. in the case of a fresh LNAPL of petroleum hydrocarbons) local advective fluxes can be expected above the source zone. In such cases, Rn concentrations above the source zone can be higher than those above background areas without advective phenomena, resulting in Rn deficits higher than 1 (i.e., Rn excess), and thus leading to a wrong interpretation regarding the presence of LNAPL in the subsurface if advection is not considered. Overall, the results obtained suggest that advection should be considered in the presence of pressure gradients in the subsurface to ensure an effective application of the soil gas Rn-deficit technique for a quantitative estimation of LNAPL saturation.

4.1 INTRODUCTION

Over the years, the theoretical study of the Rn deficit technique has also focused on modeling Rn in the subsurface. In particular, in this context, major efforts have focused on predicting Rn profiles in water (see e.g., Semprini et al., 2000; Davis et al., 2005; Schubert et al., 2007c) and soil gas (see e.g., Höhener and Surbeck, 2004; Cohen et al., 2019; Barrio-Parra et al., 2022; Cecconi et al., 2022) under various site-specific conditions, focusing on the issues of Rn emanation, partition, and transport. Diffusion is commonly considered the dominant transport process for the migration of gases in the vadose zone (Hillel, 1982). Indeed, on a long-term average basis, available evidence suggests that Rn transport from the soil into the atmosphere occurs predominantly by molecular diffusion (Nazaroff, 1992). However, under certain conditions, pressure-driven advection may also be significant (Alzaydi et al., 1978; Thorstenson and Pollock, 1989; Massmann and Farrier, 1992; US EPA, 2015). In particular, advection may be the locally dominant flow in the presence of high average pressure or when intermolecular collisions prevail over collisions between gas molecules and pore walls (Cunningham and Williams, 1980). The latter condition can occur when the average free path of gas molecules is much smaller than the pore size of the medium, e.g., in dry, coarse-grained media (Scanlon et al., 2002). Several factors can induce a local pressure gradient in the soil that causes an advective flow (Molins and Mayer, 2007; US EPA, 2015). Cyclic fluctuations in barometric pressure (caused by diurnal temperature variations and the passage of high- and low-pressure fronts) cause an inward and outward advective motion of subsurface air (Forde et al., 2019), known as barometric pumping (Auer et al., 1996). However, this phenomenon only affects the surface soil layers, typically around the first meter. According to Neznal et al. (2004), a sampling depth of 0.8 m is a good compromise between reducing the effect of atmospheric phenomena and the practicality of measurements with temporary probes. Assuming, therefore, that Rn measurements are performed at these or greater depths, the influence of barometric fluctuations and the resulting advective flow can be considered irrelevant to the application under discussion. Another phenomenon that can lead to the generation of an advective flow in the subsurface is the fluctuations of the water table induced by various periodic natural forces (Man et al., 2021). Groundwater fluctuations can cause upward and downward advection of soil gas within the vadose zone, promoting the transport of soil gases and accelerating the vapor phase transport through the unsaturated zone and their

release into the atmosphere (Qi et al., 2020). In fact, a drop in the water table level can create a reduction in total gas pressure, producing a suction effect that can limit the gas flow, while the upward movement of groundwater creates an increase in total gas pressure, resulting in a piston effect that pushes the soil gases toward the surface (Cavelan et al., 2022). Choi and Smith (2005) investigated the effects of water table fluctuations on advective and diffusive fluxes of volatile organic compounds under natural atmospheric conditions and suggested that water table fluctuation with an amplitude of 0.1 m can create pressure gradients in the soil similar in magnitude to those caused by atmospheric pressure variations, which could significantly affect the advective flux. Man et al. (2021) showed that soil texture plays a significant role in the advective transport of soil gas. Other phenomena that can create a local advective flow in the subsurface can be related to LNAPL contamination (Ma et al., 2012; Yao et al., 2015; Verginelli and Baciocchi, 2021). A significant in-situ generation of CH_4 can make advection the dominant local gas transport mechanism (Yao et al., 2015; CRC CARE, 2018). Methanogenesis is now accepted as one of the dominant attenuation processes of LNAPL sources (e.g., Lundegard and Johnson, 2006; Ng et al., 2015; CRC CARE, 2018; ITRC, 2018). Significant methanogenesis can occur, under anaerobic conditions, in the saturated zone and at the bottom of the unsaturated zone, which results in direct outgassing and ebullition of methane and carbon dioxide (ITRC, 2018). The combined gas fluxes migrate vertically upward through the unsaturated zone, where methane is oxidized (Amos et al., 2005). In accordance with field observations, the zones of CH_4 generation (near the water table and oil body) correlate with slightly elevated total gas pressures, while above the methanogenic zone, in the methanotrophic zone, CH_4 and O_2 consumption causes gas pressure to decrease marginally below atmospheric levels (Molins et al., 2010). Furthermore, the solubility of CO_2, produced in the methane oxidation reaction, is higher than that of O_2 or CH_4, so even more gas is removed from the gas phase by the dissolution of the produced gas into water (Amos et al., 2005). Since advection, compared to diffusion, can transfer Rn over a wide range of distances it is important to account for this phenomenon when applying the soil gas Rn deficit technique. Indeed, if not properly considered, the existence of advective phenomena can result in a further confounding factor for the interpretation of the Rn deficit detected in soil gas. For instance, De Miguel et al. (2018) found, during a field campaign, Rn concentrations above background values in an area where other evidence indicated the presence of NAPL.

Mateus and Pecequilo (2015) successfully identified NAPL contamination in some areas by monitoring Rn in the upper soil, but also found high Rn values, compared to the site average, in some areas where a NAPL plume was estimated to exist. Cohen et al. (2016) found unclear correlations between Rn and NAPL at another site where methane was also found in the soil gas, explaining these results by the presence of stratigraphic heterogeneities. Although the anomalous behavior observed in the above-mentioned works would require further investigations to be explained, as suggested by De Miguel et al. (2018), a possible partial explanation could be given by the establishment of advective phenomena, especially in cases where other parameters might indicate its possible occurrence (e.g. the methane detected in the field campaigns carried out by Cohen et al. (2016). To account for the aspects described above, this work aims to evaluate the impact of the advective term on the transport of Rn in the soil gas in soils characterized by the presence of LNAPL. For this purpose, a 1-D steady-state analytical solution of the equation for the diffusive-advective transport of Rn in the subsurface in a two-layer soil was developed. To our knowledge, no analytical models that allow to account for both diffusion and advection of Rn in the subsurface in the presence of LNAPL are available in the literature. The developed 2-layer analytical solution estimates the vertical concentration profiles of Rn in soil gas at a steady state in a two-layer soil, assuming a diffusive-advective transport of Rn. The validity of the solution has been tested by comparing the results with an already existing numerical model (Barrio-Parra et al., 2022), that was adapted in this work to include the advective term. The analytical solution was then used to study the influence of the advective term on Rn profiles and, consequently, on the Rn deficit, carrying out simulations under different conditions of pressure gradient and contamination, and considering the influence of other site-specific parameters.

4.2 MATERIAL AND METHODS

4.2.1 Governing equation and assumptions

The analytical model was developed assuming a 1-D steady-state advective-diffusion transport of Rn in homogenous soils. The solution was obtained under assumptions consistent with previous Rn modeling studies (e.g., Höhener and Surbeck, 2004; Cohen et al., 2019). In particular, a homogeneous soil, a constant diffusion coefficient, and a constant advective velocity were considered for each layer. A constant and uniform emanation of Rn from the solid matrix was also considered. Furthermore, Rn decay was assumed to be the only reaction to occur and was described by a first-order decay constant (λ). The phenomenon of Rn partitioning between soil phases (solid phase, gas, water, and LNAPL) was considered instantaneous and reversible and was described by linear equilibrium partitioning constants (Höhener and Surbeck, 2004).

Under the above assumptions, the governing equation for the diffusive and advective steady-state transport of Rn in a homogeneous layer i of unsaturated soil is:

$$f_i \cdot D_{e,i} \cdot \frac{\partial^2 Rn}{\partial z^2} - f_i \cdot u_i \cdot \frac{\partial Rn}{\partial z} - \lambda \cdot Rn + f_i \cdot P_i = 0 \qquad \text{Eq. 4.1}$$

where Rn is the Rn activity concentration in soil gas (Bq m^{-3}); $D_{e,i}$ is the effective diffusion coefficient of Rn in layer i ($m^2\ s^{-1}$); f_i (-) is the fraction of Rn in the air phase of layer i; u_i is the soil gas velocity (m s^{-1}); P_i is the Rn production rate in the pore space in layer i (Bq $m^{-3}\ s^{-1}$).

The effective diffusion coefficient of Rn in layer i, $D_{e,i}$ can be calculated using the expression proposed by Millington and Quirk (1961), reported in Eq. 3.2.

The expression for the fraction of Rn in the air phase of layer i, f_i (-), is reported in Eq. 3.4 (Werner and Höhener, 2002).

The Rn production rate in the pore space in layer i, P_i (Bq $m^{-3}\ s^{-1}$) can be calculated as indicated in Eq. 3.3 (Van Der Spoel et al., 1997).

The soil gas velocity u can be estimated using the following equation (Scanlon et al., 2002):

$$u_i = \frac{k_{g_i}}{\mu} \cdot \frac{dp_i}{dz} \qquad \text{Eq. 4.2}$$

where $k_{g,i}$ (m^2) is the effective permeability to soil gas flow, μ (kg m^{-1} s^{-1}) is the dynamic viscosity of soil gas, and dp_i/dz (kg m^{-2} s^{-2}) is the pressure variation, also synthetically denoted by ∇p_i. The effective permeability $k_{g,i}$ can be calculated as the product of the intrinsic permeability $k_{int,i}$ (m^2) and the relative air permeability $k_{rg,i}$ (-) at the soil water-filled porosity $\theta_{w,i}$:

$$k_{g,i} = k_{int,i} \cdot k_{rg,i} \qquad \text{Eq. 4.3}$$

Note that all parameters with the subscript i depend on the soil layer's characteristics.

4.2.2 Analytical solution

For heterogeneous layered soils, but without the advective term, Eq. 4.1 has been solved analytically Höhener and Surbeck (2004) and Cecconi et al. (2022) (see section 3.2.2). In this work, we present an analytical solution for a 2-layer model that can be used to describe both the diffusive and advective transport of Rn in a contaminated layer (source zone) and the overlying unsaturated layer. The domain of the 2-layer model developed in this work is depicted in Figure 4.1. The domain was divided into two zones: a non-contaminated layer of the vadose zone and an underlying layer of the vadose zone with LNAPL.

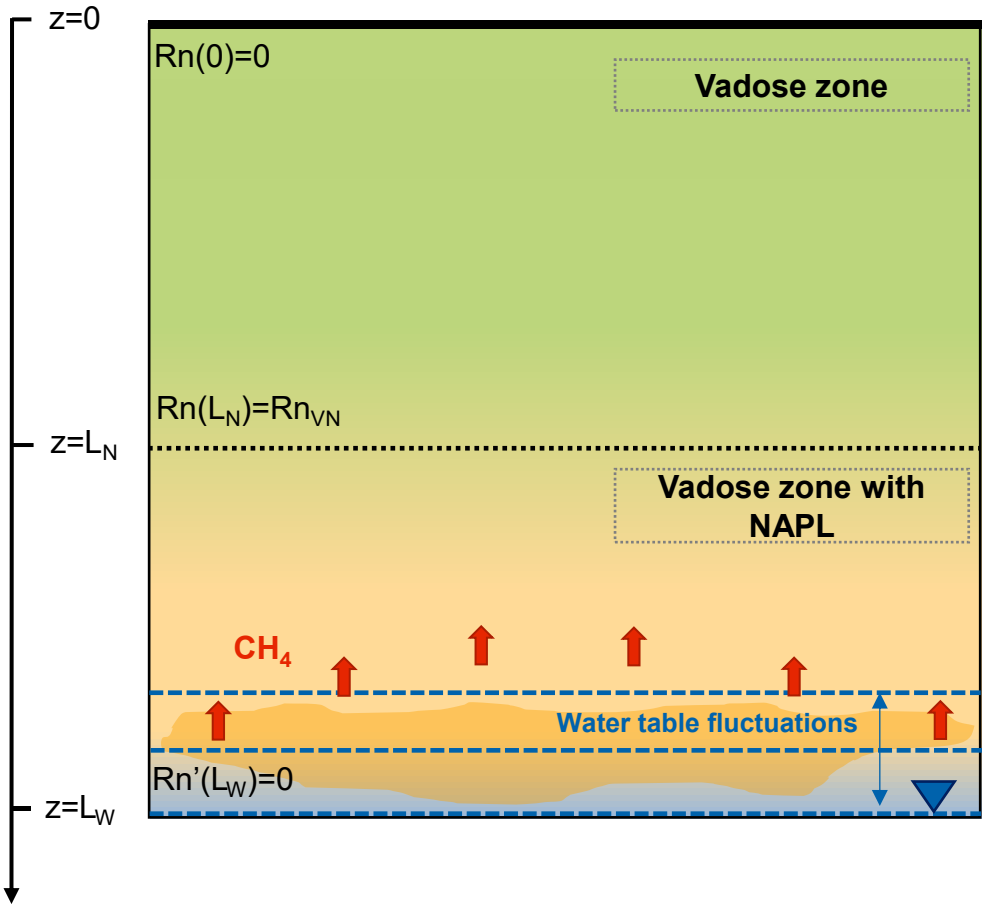

Figure 4.1. Domain of the 2-layer model consisting of an upper layer of uncontaminated vadose zone and a deeper layer of vadose zone with the presence of LNAPL. The origin of axis z is placed at ground level and is positive with increasing depth. The figure also describes the boundary conditions assumed to derive the analytical solution and the conditions that may cause advective phenomena in the soil (water table fluctuations and methanogenesis processes).

To solve Eq. 4.1, three boundary conditions were considered (see Figure 4.1). Specifically, the Rn concentration was considered zero in air (Höhener and Surbeck, 2004), the continuity of concentration was imposed at the interface between the two layers and no Rn flux was assumed at the water table depth ($z = L_W$).

By imposing these boundary conditions, the following solutions describing the Rn concentration profile in the domain were derived.

For $0 \leq z \leq L_N$:

$$Rn(z) = \Xi + O \quad \text{Eq. 4.4}$$

With:

$$\Xi = Rn_{VN} \cdot \left(\frac{e^{-k_V \cdot (L_N - z)} \cdot \sinh(\gamma_V \cdot z)}{\sinh(\gamma_V \cdot L_N)} \right) \quad \text{Eq. 4.5}$$

$$O = \frac{P_V \cdot f_V}{\lambda} \cdot \left(1 - \frac{e^{k_V \cdot z} \cdot \sinh(\gamma_V \cdot (L_N - z)) + e^{-k_V \cdot (L_N - z)} \cdot \sinh(\gamma_V \cdot z)}{\sinh(\gamma_V \cdot L_N)} \right) \quad \text{Eq. 4.6}$$

For $L_N < z \leq L_w$

$$Rn(z) = \left[\frac{e^{-k_N \cdot (L_N - z)} \cdot \Pi}{\Phi} \right] + \frac{P_N \cdot f_N}{\lambda} \quad \text{Eq. 4.7}$$

With:

$$\Pi = [k_N \cdot \sinh(\gamma_N \cdot (L_w - z)) + \gamma_N \cdot \cosh(\gamma_N \cdot (L_w - z))] \quad \text{Eq. 4.8}$$

$$\Phi = [k_N \cdot \sinh(\gamma_N \cdot (L_w - L_N)) + \gamma_N \cdot \cosh(\gamma_N \cdot (L_w - L_N))] \quad \text{Eq. 4.9}$$

And where k_i is calculated as:

$$k_i = \frac{u}{2D_{e,i}} \quad \text{Eq. 4.10}$$

and γ_i calculated as:

$$\gamma_i = \sqrt{\frac{u^2}{4D^2_{e,i}} + \frac{\lambda}{f_i \cdot D_{e,i}}} = \sqrt{{k_i}^2 + \frac{1}{L^2_{c,i}}} \quad \text{Eq. 4.11}$$

with $L_{c,i}$ the characteristic diffusion length of Rn in layer i (Eq. 3.12):

Next, by imposing the continuity of the fluxes at the interface of the contiguous layers, the expression of the concentration Rn_N (at $z = L_N$) was derived. The resulting expression is given in the following equation:

$$Rn_{VN} = \frac{D_{e,V} \cdot \frac{P_V \cdot f_V}{\lambda} \cdot \left(k_V + \gamma_V \cdot \coth(\gamma_V \cdot L_N) - \frac{\gamma_V \cdot e^{k_V \cdot L_N}}{\sinh(\gamma_V \cdot L_N)} \right) - D_{e,N} \cdot \frac{P_N \cdot f_N}{\lambda} \cdot \Psi}{D_{e,V} \cdot (k_V + \gamma_V \cdot \coth(\gamma_V \cdot L_N)) - D_{e,N} \cdot \Psi} \quad \text{Eq. 4.12}$$

With:

$$\Psi = \frac{k_N \cdot k_N - \gamma_N \cdot \gamma_N}{\left[k_N + \gamma_N \cdot \coth(\gamma_N \cdot (L_w - L_N))\right]} \quad \text{Eq. 4.13}$$

The developed analytical solution was applied to calculate the vertical Rn concentration profiles under different scenarios. In particular, the Rn profile in the NAPL zone was calculated and compared to that expected under the same conditions but at a background location not impacted by the LNAPL. From the ratio of these two concentration profiles, the expected deficit profiles under the specific conditions of each case were derived. Rn deficit was calculated at each depth as:

$$\text{Deficit}(z) = \frac{Rn_{NAPL}(z)}{Rn_{NONAPL}(z)} \quad \text{Eq. 4.14}$$

where $Rn_{NAPL}(z)$ is the Rn concentration at depth z in the presence of LNAPL and $Rn_{NONAPL}(z)$ is the Rn concentration at the same depth z in the absence of LNAPL.

4.2.3 Estimation of the intrinsic permeability and of the relative air permeability

The intrinsic permeability $k_{int,i}$ (m^2) values used in this work were chosen based on the range of values suggested by Freeze and Cherry (1979), according to soil texture (see Table 4.1).

The relative air permeability of soil $k_{rg,i}$ (-) was calculated considering the effects of water saturation on air permeability. Parker et al. (1987) extended the relative air permeability model of van Genuchten (1980) to allow the estimation of the relative permeabilities of air and water in a two or three-phase system (US EPA, 2004):

$$k_{rg,i} = (1 - S_{we,i})^{1/2} \cdot (1 - S_{we,i}{}^{1/m})^{2m} \quad \text{Eq. 4.15}$$

with $S_{we,i}$ the effective water saturation (-) and m the van Genuchten shape parameter (-).

The effective water saturation $S_{we,i}$ can be calculated as:

$$S_{we,i} = \frac{(\theta_{w,i} - \theta_{r,i})}{(\theta_{t,i} - \theta_{r,i})} \quad \text{Eq. 4.16}$$

Where $\theta_{t,i}$ is the total soil porosity in layer i, $\theta_{w,i}$ is the volumetric water content in layer i and θ_r the residual water content.

The effective permeability $k_{g,i}$ (m^2) was then calculated as the product of the intrinsic permeability $k_{int,i}$ and the relative air permeability $k_{rg,i}$ at the soil water-filled porosity $\theta_{w,i}$.

The values of characteristic soil parameters (e.g., porosity, water content) are given by US EPA (2004). Note that all parameters with the subscript i depend on the soil layer's characteristics.

Table 4.1 shows the values of the parameters used to calculate effective permeability for three soil textures.

Table 4.1. Parameters used to calculate effective permeability for three soil textures.

Parameter	**Symbol**	**Unit**	**Medium sand (Figs. 4.3-4.12)**	**Fine sand (Fig. 4.10)**	**Loam (Fig. 4.10)**
Total porosity	θ_t	-	0.375	0.387	0.399
Water content	θ_w	-	0.054	0.103	0.148
Residual water content	θ_r	-	0.053	0.039	0.061
Van Genuchten parameter	m	-	0.685	0.310	0.321
Intrinsic permeability	k_{int}	m^2	10^{-10}	10^{-12}	10^{-13}
Relative air permeability	k_{rg}	-	0.998	0.901	0.854
Effective permeability	k_g	m^2	$9.98 \cdot 10^{-11}$	$9.01 \cdot 10^{-13}$	$8.54 \cdot 10^{-14}$

4.2.4 Simulated scenarios and Input parameters

The analytical solution was applied to assess the role of advection in different scenarios where, under certain conditions, a subsurface pressure gradient can be expected. The scenarios investigated comprise the condition of a rising water table, which creates a positive pressure gradient and a resultant advective flux toward the surface (Figure 4.2b), the condition of a falling water table, with a negative pressure gradient creating a downward advective flux (Figure 4.2c), and the case of the presence of fresh LNAPL, with a positive pressure gradient in the zone with LNAPL due to methanogenesis and a negative pressure gradient in the overlying zone of methane oxidation (Figure 4.2d). In this latter case, since the pressure gradient affects

only the contaminated zone, a purely diffusive transport was considered in the background area. The case of purely diffusive transport will be used as a comparison (see Figure 4.2a). The scenarios described in Figure 4.2b and Figure 4.2c are more likely to occur at sites near coastal areas or in tropical climates subject to heavy rainfall in short periods of time. The scenario described in Figure 4.2d, on the other hand, can be considered characteristic of areas with high NAPL saturation levels and fresh NAPL, which are more likely to result in high methane production.

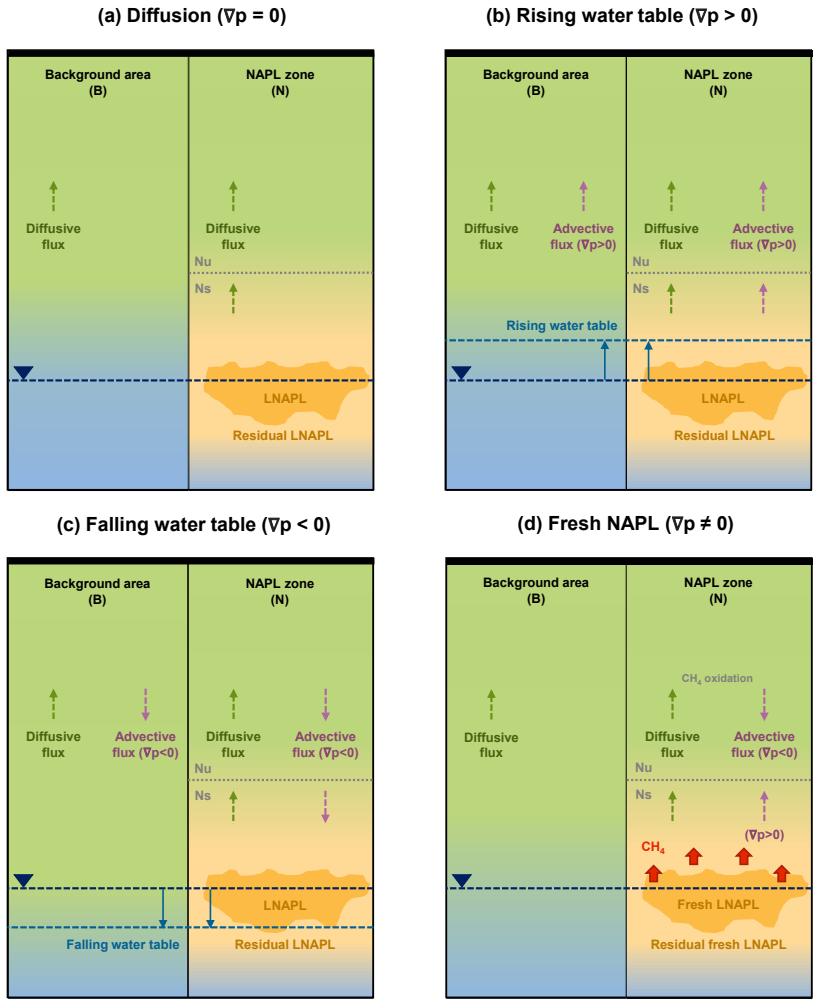

Figure 4.2. Conceptual model of the four simulated scenarios: a) purely diffusive transport both in the LNAPL zone and background area, b) rising water table both in the LNAPL zone and background area (positive pressure gradient, advective flux toward the surface), c) falling water table both in the LNAPL zone and background area (negative pressure gradient, downward advective flux), d) presence of fresh LNAPL in the LNAPL zone (positive pressure gradient in the LNAPL source zone (Ns) due to CH_4 production and negative pressure gradient in the overlying zone (Nu) due to CH_4 oxidation) and no advective flux in the background zone (diffusive flux only).

The input parameters listed in Table 4.2 and Table 4.3 were used for the simulations shown in the following sections. The values of characteristic soil parameters (e.g. porosity, density, water saturation) given by US EPA (2004) were used in all simulations. Details regarding the estimation of the intrinsic permeability and the relative air permeability are given in section 4.2.3.

Table 4.2. Parameters used for the validation of the analytical model (Fig.4.3) and to derive the vertical Rn concentration profiles and the Rn deficit curves in Figs.4.4-4.12 (unless otherwise indicated in the figures).

Parameter	**Symbol**	**Unit**	**Values (Figs. 4.3-4.12)**
Solid density	ρ_s	kg m^{-3}	1660
Soil type	-	-	sand
Total porosity	θ_t	-	0.375
Water saturation	θ_w	-	0.054
Relative air permeability	k_{rg}	-	0.998
Intrinsic permeability	k_i	m^2	10^{-10}
Effective permeability	k_g	m^2	$9.98 \cdot 10^{-11}$
Dynamic viscosity of soil gas	μ	kg m^{-1} s^{-1}	$1.8 \cdot 10^{-6}$
Rn partition coefficient between soil and water	$k_{s/w}$	-	$1.4 \cdot 10^{-5}$
Rn partition coefficient between gas and water (Henry's law constant)	$k_{g/w}$	-	4.4
Contamination	-	-	Diesel
Rn partition coefficient between NAPL and water	$k_{N/w}$	-	60
Rn first order decay constant	λ	s^{-1}	$2.1 \cdot 10^{-6}$
^{226}Ra concentration of the solids	C_{Ra}	Bq kg^{-1}	30

Parameter	Symbol	Unit	Values (Figs. 4.3-4.12)
Rn emanation coefficient	ε	-	0.2
Rn molecular diffusion coefficient in the gas phase	D_{mg}	$m^2\ s^{-1}$	$1.1 \cdot 10^{-5}$
Rn molecular diffusion coefficient in the water phase	D_{mw}	$m^2\ s^{-1}$	$1.1 \cdot 10^{-9}$
Total profile length	L	m	5
Source zone depth	L_N	m	4
Thickness of the source zone	H_N	m	1
NAPL saturation	S_N	%	10
Time interval (numerical model)	dt	s	60
Depth interval (numerical model)	dz	m	0.05
Simulation duration (numerical model)	t_{max}	days	30
Lower boundary (numerical model)	boundary	-	Open

Table 4.3. Surface pressure gradient conditions in the subsurface considered to derive the vertical Rn concentration profiles and the Rn deficit curves in Figures 4.4-4.8 (unless otherwise indicated in the figures).

Scenario	Zone	Symbol	Unit	Pressure gradient values (Figs. 4.4-4.12)		
				Low	Medium	High
Rising water table (Fig. 4.2b)	NAPL zone, upper layer	$\nabla p\ N_u$	Pa m^{-1}	0.01	0.05	0.1
	NAPL zone, source zone	$\nabla p\ N_s$	Pa m^{-1}	0.01	0.05	0.1
	Background area	$\nabla p\ B$	Pa m^{-1}	0.01	0.05	0.1
Falling water table (Fig. 4.2c)	NAPL zone, upper layer	$\nabla p\ N_u$	Pa m^{-1}	-0.01	-0.05	-0.1
	NAPL zone, source zone	$\nabla p\ N_s$	Pa m^{-1}	-0.01	-0.05	-0.1
	Background area	$\nabla p\ B$	Pa m^{-1}	-0.01	-0.05	-0.1
Fresh LNAPL (Fig. 4.2d)	NAPL zone, upper layer	$\nabla p\ N_u$	Pa m^{-1}	-0.0025	-0.0125	-0.025
	NAPL zone, source zone	$\nabla p\ N_s$	Pa m^{-1}	0.01	0.05	0.1
	Background area	$\nabla p\ B$	Pa m^{-1}	0	0	0

4.3 RESULTS

4.3.1 Comparison with a numerical model

Figure 4.3 shows a comparison of the steady-state Rn concentration profiles predicted by the analytical solution developed in this work (continuous lines) with the results obtained using the numerical model (points) developed by Barrio-Parra et al. (2022). For the analytical model, the solution previously described was used (Eq. 4.4 - Eq. 4.12). For the numerical model, the original Matlab® code developed by Barrio-Parra et al. (2022) has been adapted to account for the advective transport (the full Matlab® code is available in the Supplementary Material of Cecconi et al. (2023b)). Four scenarios representing different pressure gradient conditions were simulated using the same input parameters reported in Table 4.2. Note that for the transient numerical model, the Rn concentration profiles represent the results obtained assuming a 30-day simulation which, according to preliminary simulations, was found to be representative of steady-state conditions. From Figure 4.3, it can be observed that there is a good agreement between the numerical results and those predicted with the analytical model developed in this work. The performance of the analytical model was evaluated by the coefficient of determination R^2 and the normalized root mean square error (NRMSE). Specifically, the R^2 value was 0.999 for all simulations, and the NRMSE was always lower than 1.5% (0.015) (see Figure 4.3).These values indicate an accurate model simulation, thus confirming the validity of the analytical model to simulate the expected Rn concentration profiles in the presence of a pressure gradient in the subsurface.

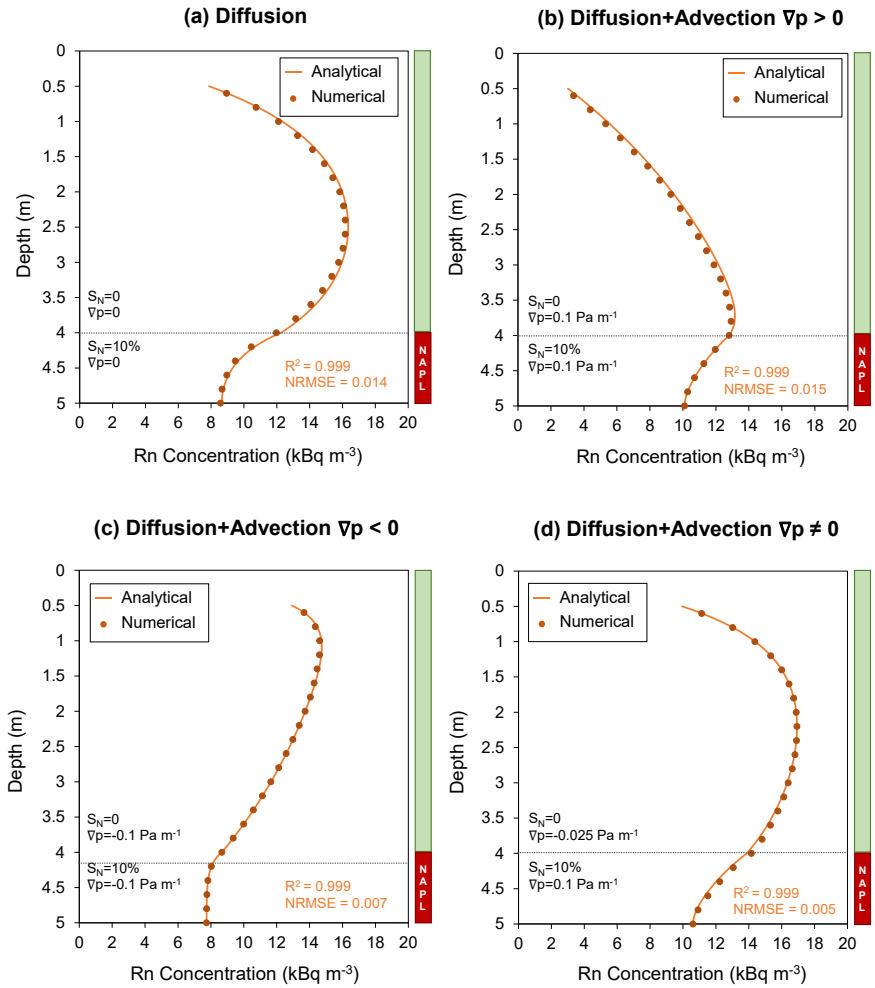

Figure 4.3. Rn concentration profiles for different imposed pressure gradients calculated with the analytical model (continuous lines) and the numerical model (dots) adapted from Barrio-Parra et al. (2022). Four imposed pressure gradients are shown: zero pressure gradient, i.e., diffusion-dominated transport (figure a); constant positive pressure gradient of +0.1 Pa m^{-1} (figure b), constant negative pressure gradient of -0.1 Pa m^{-1} (figure c); variable pressure gradient of +0.1 Pa m^{-1} in the LNAPL layer and of -0.025 in the overlying vadose zone layer (figure d). The dashed lines represent the beginning of the layer with the presence of LNAPL. A LNAPL saturation of 10% in the deepest layer was imposed. The performance of the analytical model is shown for each simulation in terms of coefficient of determination R^2 and normalized root mean square error NRMSE.

4.3.2 Influence of the pressure gradient on Rn deficit profiles

The developed analytical solution was used to examine the Rn concentration profiles expected in the presence of pressure gradients in the subsurface at LNAPL-impacted areas and in background locations not impacted by LNAPL. From the ratio of these two concentration profiles, the expected Rn deficit curves were also calculated (see

Eq. 4.14). Unless otherwise stated, the site-specific parameters used in the simulations are those reported in Table 4.2, and the pressure gradient conditions considered are those summarized in Table 4.3.

4.3.2.1 Positive pressure gradient (rising water table)

Figure 4.4 shows the Rn concentration profiles and the relative Rn deficits obtained assuming a positive pressure gradient in the subsurface (see Figure 4.2b).

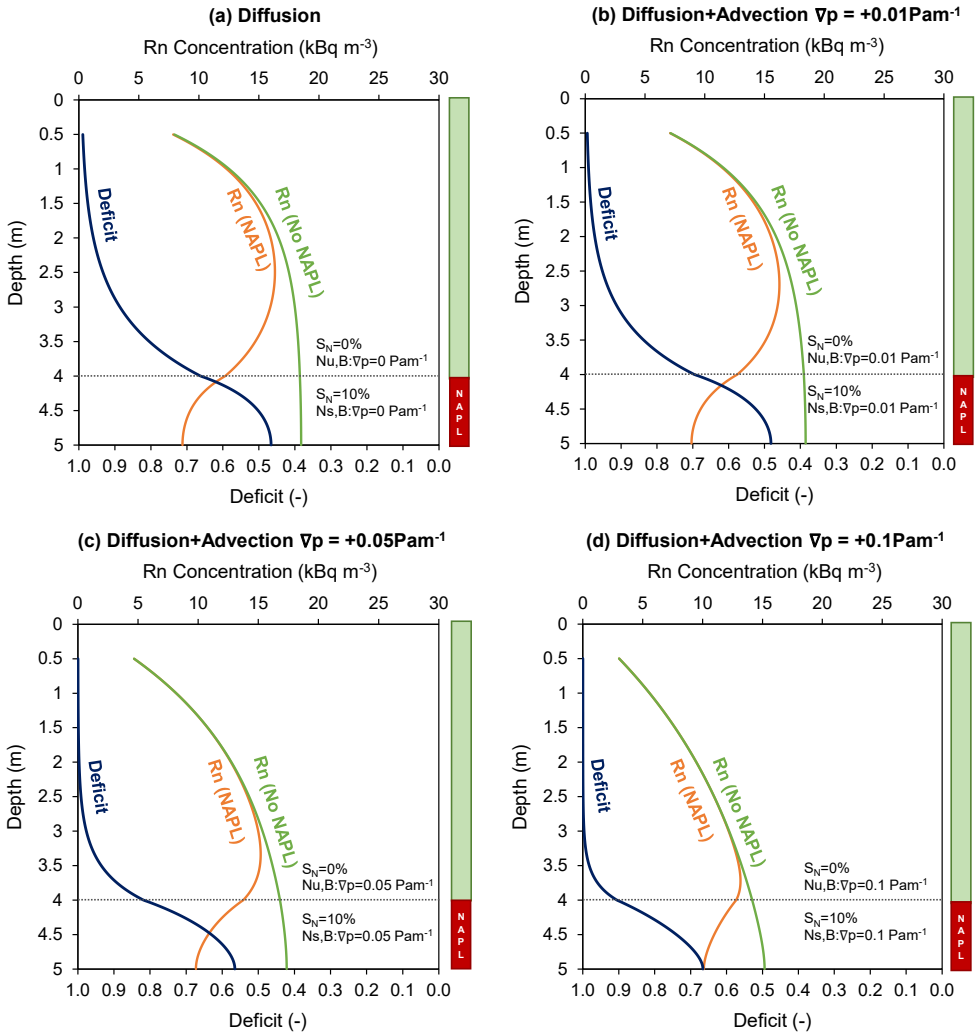

Figure 4.4. Rn concentration profiles and Rn deficit curves for different imposed pressure gradients, simulating the condition of groundwater level elevation in both the LNAPL zone (denoted with N_u for the upper layer and N_s for the LNAPL source zone) and background (denoted with B). Four pressure gradient values are shown: zero pressure gradient, i.e., purely diffusive transport (figure a); a pressure gradient of 0.01 Pa m^{-1} (figure b), 0.05 Pa m^{-1} (figure c) and 0.1 Pa m^{-1} (figure d). The dashed lines represent the beginning of the layer with the presence of LNAPL. LNAPL saturation in the deepest layer is imposed at 10%.

The pressure gradient values simulated in Figure 4.4b, Figure 4.4c and Figure 4.4d, (see Table 4.3) are representative of a water table rise between approximately 0.3 cm and 3 cm in a period of 0.5 days, assuming a sandy soil ($k_g = 4.04 \cdot 10^{-12}$ m^2, $\theta_{a,cap} = 0.045$) and according to the method reported by Choi and Smith (2005). In Figure 4.4a the Rn profiles in the case of a purely diffusive transport over the whole soil thickness (zero-pressure gradient i.e., no advective transport) are shown. As can be observed, the Rn concentration profiles obtained assuming a pressure gradient in the subsurface can be substantially different from the one expected assuming a purely diffusive transport. It can also be observed that as the pressure gradient increases there is a smaller deviation between the Rn concentration curves in the contaminated zone and the background zone (i.e. Rn deficit tends to 1). Indeed, a positive pressure gradient increases the velocity of soil gas flow towards the soil surface, reducing the attenuation of Rn caused by its partitioning into the LNAPL. It may be assumed, for example, to sample soil gas in proximity of the LNAPL source, e.g. considering the top of the source zone (in the present case at a distance of 1 m from the water table). Although, depending on soil type, temporal probes can be used at depths up to 4-5 m, typically soil gas samples collected at depths greater than 2 m are not cost-effective with commonly used direct-push techniques. At 2 m depth, the Rn deficit expected in the simulated scenario for a diffusive-only transport is approximately equal to 0.66 (Figure 4.4a), while in the case of a diffusive-advective transport the Rn deficit is 0.69, 0.82 and 0.9 in Figure 4.4b, Figure 4.4c and Figure 4.4d, respectively. This implies that, under the conditions considered, the deficit values observable at the top of the source zone, assuming a positive subsurface pressure gradient, can be up to 1.3 - 1.4 times higher than the deficit observed at the same depth in the case of diffusive transport only. Note that these deficits result from Rn concentrations in the NAPL zone of approximately 12.2 - 13.7 kBq m^{-3} (corresponding to maximum differences of about 15%) and Rn background concentrations of 18.4 - 14.1 kBq m^{-3} (corresponding to maximum differences of about 25%) (for Figure 4.4a, Figure 4.4b, Figure 4.4c and Figure 4.4d respectively). It is worth mentioning, that Rn concentration values can be significantly different, depending on the radium content and the Rn emanation coefficient (among other parameters) characteristic of the soil under investigation. It is also worth recalling that the deficit observed at a certain depth is used in the Rn deficit technique to estimate the subsurface residual LNAPL saturation. From these first results, it is evident that the presence of advective transport has a

relevant impact on the interpretation of Rn monitoring data for the quantification of LNAPL contamination.

4.3.2.2 Negative pressure gradient (falling water table)

Figure 4.5 shows Rn concentration profiles and the relative Rn deficits for a negative pressure gradient in the subsurface (see Figure 4.2c). Figure 4.5a shows the case of purely diffusive transport, while the profiles for diffusive-advective transport are shown in Figure 4.5b, Figure 4.5c and Figure 4.5d, respectively. The simulated pressure gradient values (see Table 4.3) are representative of a drop in the groundwater level between 0.3 cm and 3 cm for a period of 0.5 days, assuming a sandy soil ($k_g = 4.04 \cdot 10^{-12}$ m^2, $\theta_{a,cap} = 0.045$), using the method described by Choi and Smith (2005). As can be observed in Figure 4.5, a negative pressure gradient limits the gas flow towards the surface, and thus leads to an increase of Rn attenuation due to the partitioning effect of Rn in the LNAPL present in the source zone. Therefore, it can be observed that as the negative pressure gradient increases, there is a more significant deviation between the Rn concentration profiles expected above the source and background zone. Considering, for example, the deficit value at the top of the source zone (at 1 m from the groundwater level), the Rn deficit expected in the simulated scenario for a diffusive transport (Figure 4.5a) is approximately 0.66, while introducing a pressure gradient of respectively -0.01, -0.05 and -0.1 Pa m^{-1} (Figure 4.5b, Figure 4.5c and Figure 4.5d), the Rn deficit is 0.63, 0.52 and 0.46 (i.e. up to 1.4 times lower than the deficit expected for a diffusion-dominated transport). The effect of advection is less pronounced in the source zone, where the deficit profiles for a diffusion-dominated transport and for a diffusive-advective transport approach each other. This suggests that performing soil gas Rn measurements in proximity of the source zone can potentially be helpful in reducing the confounding effect of advection on the interpretation of Rn data for the identification and quantification of LNAPL in the subsoil. It should be noted, however, that drilling at great depths to collect soil gas samples could be practically complicated and/or economically unfeasible. To reach these depths, an alternative way may consist in measuring Rn soil gas concentration in the headspace of groundwater monitoring wells. This approach could, for example, be useful for monitoring the evolution of LNAPL contamination during natural attenuation processes or during active remediation.

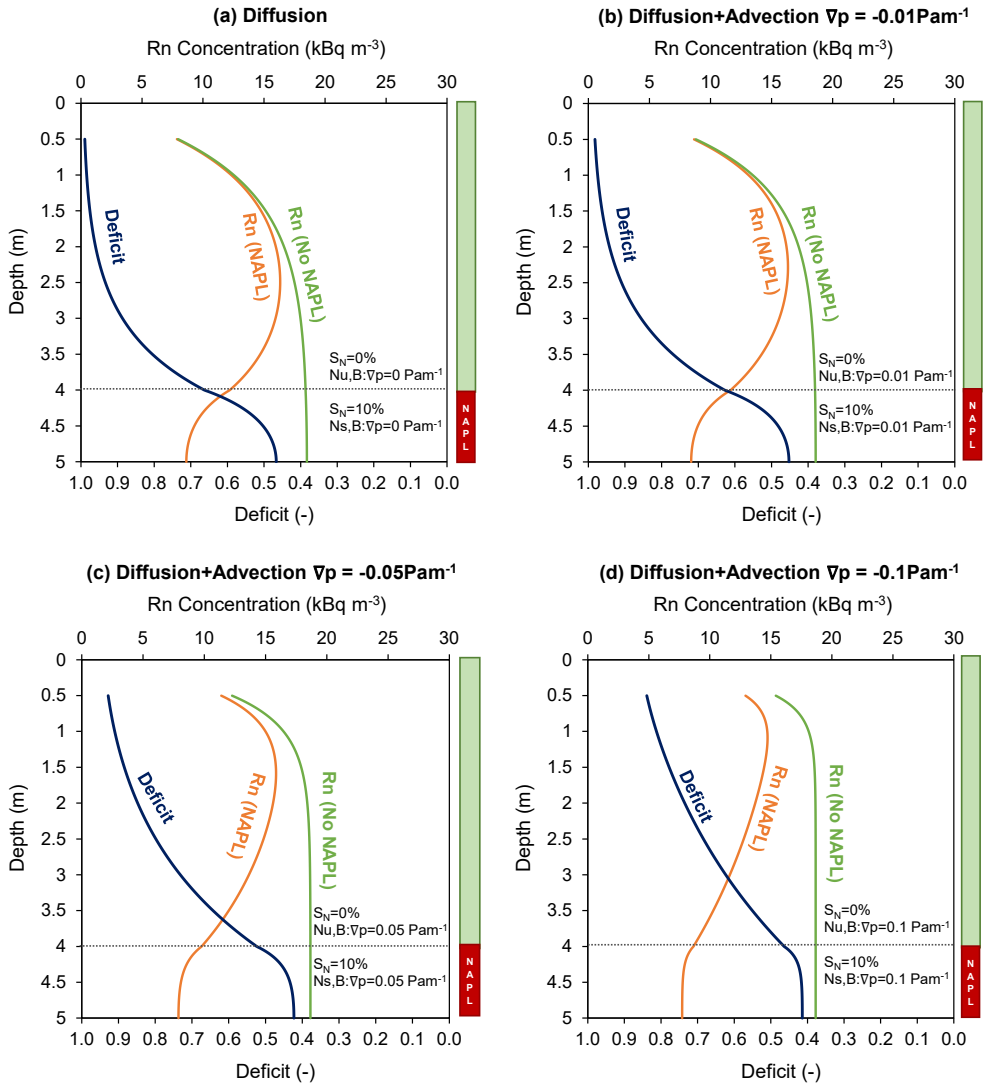

Figure 4.5. Rn concentration profiles and Rn deficit curves for different imposed pressure gradients, simulating the condition of lowering groundwater level in both the LNAPL zone (denoted with N_u for the upper layer and N_s for the LNAPL source zone) and background (denoted with B). Four pressure gradient values are shown: zero pressure gradient, i.e., purely diffusive transport (figure a); a pressure gradient of -0.01 Pa m^{-1} (figure b), -0.05 Pa m^{-1} (figure c) and -0.1 Pa m^{-1} (figure d). The dashed lines represent the beginning of the layer with the presence of LNAPL. LNAPL saturation in the deepest layer is imposed at 10%.

4.3.2.3 Variable pressure gradient (fresh LNAPL)

Figure 4.6 shows Rn concentration profiles simulated in the presence of fresh LNAPL (see Figure 4.2d).

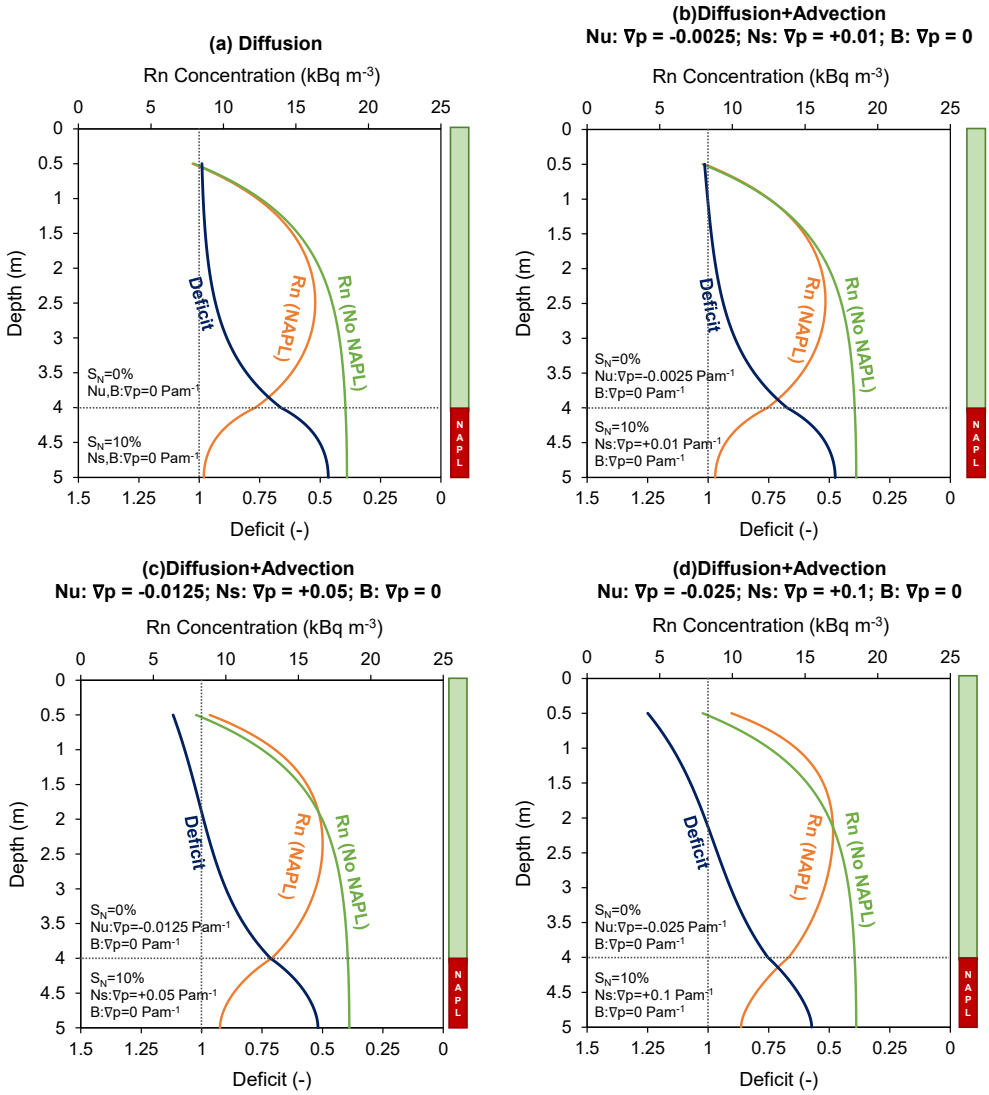

Figure 4.6. Rn concentration profiles and Rn deficit curves for different imposed pressure gradients, simulating the condition of the presence of fresh LNAPL. Four pressure gradient conditions are shown: zero pressure gradient, i.e., purely diffusive transport in both the LNAPL (denoted with N_u for the upper layer and N_s for the LNAPL source zone) and background (denoted with B) zones (figure a); a pressure gradient of +0.01 Pa m^{-1} in the LNAPL zone and -0.0025 Pa m^{-1} in the upper layer, and a zero pressure gradient in the background location (figure b), a pressure gradient of +0.05 Pa m^{-1} in the LNAPL zone and -0.0125 Pa m^{-1} in the upper layer, and a zero pressure gradient in the background location (figure c), a pressure gradient of +0.1 Pa m^{-1} in the LNAPL zone and -0.025 Pa m^{-1} in the upper layer, and a zero pressure gradient in the background location (figure d). The dashed lines represent the beginning of the layer with the presence of LNAPL. LNAPL saturation in the deepest layer is imposed at 10%.

In particular, Figure 4.6b, Figure 4.6c and Figure 4.6d show the Rn deficit curves obtained by considering a diffusion-only transport in the background zone and a

diffusive-advective transport in the area with the presence of LNAPL. The pressure gradient values assumed in the two zones for each figure are summarized in Table 4.3, and are consistent with literature values (Molins et al., 2010; Ma et al., 2014). Figure 4.6a shows the case of diffusive-only transport in both zones as a reference. It can be observed that for shallow sampling depths, the values of Rn concentration in the LNAPL zone exceed the values of Rn concentration in the background zone, in contrast with what is typically expected. Considering that the Rn deficit is calculated (see Eq. 4.14) as the ratio of the Rn concentration in the presence of LNAPL to the concentration of Rn in the background zone, the deficit value becomes at some depths greater than 1. It can be observed that as the pressure gradient is higher, the increase of Rn deficit values over 1 is observable at increasing depths. For the lower pressure gradient values (Figure 4.6b), for instance, this effect is no longer visible for depths greater than 1 m, and even at those depths, the effect is almost negligible. This scenario highlights how the influence of advective transport can be significant and such that Rn profiles can, in some cases, be reversed from those expected. In such situations, using the Rn deficit technique without taking advection into account could entail the risk of misinterpreting the state of soil contamination. Also in these cases, however, performing Rn measurements at greater depths (ideally in the proximity of the LNAPL source zone) can reduce the risk of misinterpreting Rn deficit data for LNAPL detection and localization.

4.3.3 Influence of pressure gradient on the estimation of LNAPL saturation

4.3.3.1 Positive pressure gradient (rising water table)

Figure 4.7 shows the Rn deficit curves calculated assuming a LNAPL saturation of 5% (Figure 4.7a), 10% (Figure 4.7b) and 20% (Figure 4.7c) (typical residual saturation range according to Brost and De Vaull, (2000)), considering the pressure gradient conditions of a rising water table (i.e., a positive pressure gradient), as described in Figure 4.2b and assuming the relative values indicated in Table 4.3.

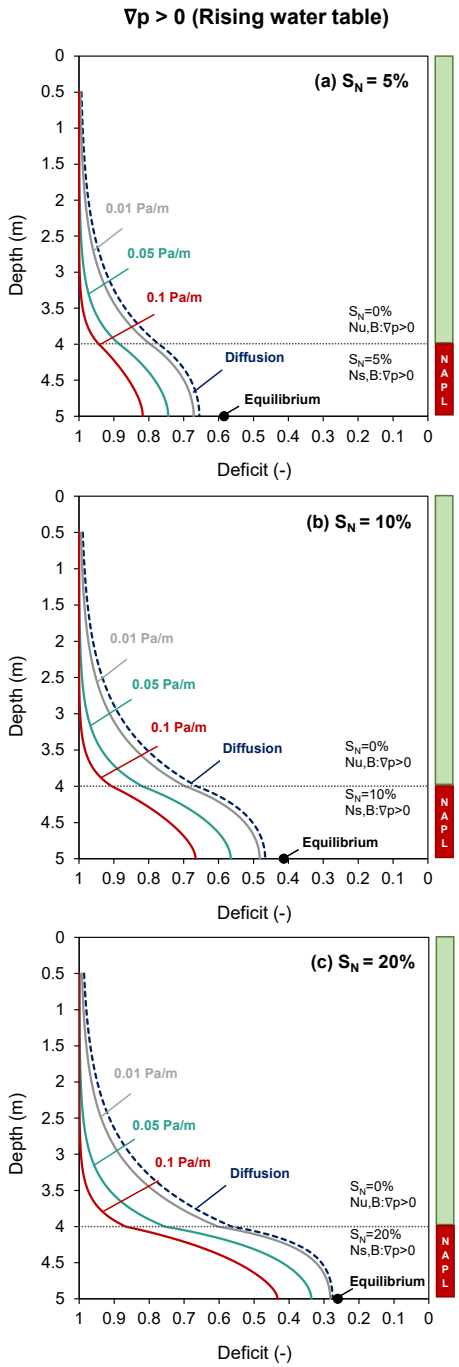

Figure 4.7. Rn deficit profiles for different imposed pressure gradients and different LNAPL saturations. Three LNAPL saturation conditions are considered: S_N = 5%, S_N = 10% and S_N = 20% for figures a, b and c respectively. In each graph, three values for a positive, constant pressure gradient are shown: low (+0.01 Pa m^{-1}), medium (+0.05 Pa m^{-1}) and high (+0.1 Pa m^{-1}). The deficit profile of the only diffusive transport case is also shown (dashed curve). The deficit expected at equilibrium conditions is also reported as a reference. The dotted lines represent the beginning of the layer with LNAPL.

The diffusive Rn deficit curve and three diffusive-advective deficit curves (lower, intermediate and higher pressure gradient value) are shown in each graph. It can be observed that the deficit at the top of the source zone (at 1 m from the water table) is less pronounced for diffusive-advective transport than for purely diffusive transport (shown in the same figures with the dashed line) by a factor up to 1.2, 1.4 and 1.5 (LNAPL saturations of 5%, 10% and 20% respectively). Considering, for example, the deficit curve in Figure 4.7a (S_N = 5%) representing a positive pressure gradient of 0.05 Pa m^{-1}, the observed deficit in the upper part of the source zone is approximately 0.88. If the advective term was ignored, using this deficit value would lead to estimating a LNAPL saturation of about 2% (using the nomographs presented in section 3.3.3 (Cecconi et al., 2022)). This means that in the proposed example, ignoring the presence of advective transport would result in underestimating LNAPL saturation by more than 2 times. It should also be noted that the Rn deficit technique is typically applied (e.g., Schubert et al., 2001; Schubert, 2015; De Simone et al., 2017; Castelluccio et al., 2018) assuming equilibrium conditions (i.e. neglecting both diffusion and advection):

$$\mathrm{Deficit}_{\mathrm{eq}} = \frac{\theta_{\mathrm{g,NONAPL}} + \frac{\theta_{\mathrm{w,NONAPL}}}{k_{\mathrm{g/w}}}}{\theta_{\mathrm{g,NAPL}} + \frac{\theta_{\mathrm{w,NAPL}}}{k_{\mathrm{g/w}}} + \frac{\theta_{\mathrm{N}}}{k_{\mathrm{g/N}}}} \qquad \text{Eq. 4.17}$$

By comparing the deficits obtained in Figure 4.7a, Figure 4.7b and Figure 4.7c, with the expected deficit at equilibrium conditions (shown as reference in each figure), it can be noticed that in the case of positive pressure gradients the presence of advection compared to diffusion alone causes the deficit values to deviate even further from equilibrium conditions. For example, using again a Rn deficit of 0.88 at the source zone (relative to a positive pressure gradient of 0.05 Pa m^{-1} for a LNAPL saturation of 5%), would result in an estimated LNAPL saturation of 0.5% (Eq. 4.17) considering equilibrium conditions. These considerations indicate that, in the proposed example, assuming equilibrium conditions and thus ignoring the presence of both diffusive and advective transport would result in an estimate of LNAPL saturation 10 times lower than the actual one. The same conclusions can be drawn by considering the curves in Figure 4.8, which show LNAPL saturation calculated as a function of the Rn deficit obtained considering soil gas Rn measurements carried out at a fixed distance from the water table.

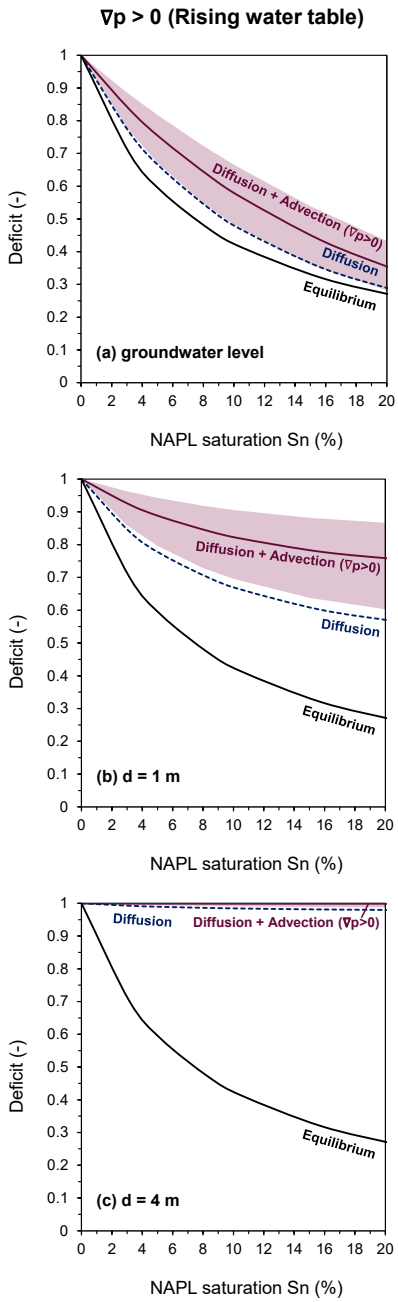

Figure 4.8. LNAPL saturation – Rn deficit curves for a positive pressure gradient and different vertical distances from the water table. Three distances between the soil gas Rn measuring point and the water table are shown: a zero distance (i.e., at the water table) for figure a; a distance of 1 m for figure b; and a distance of 4 m for figure c. The colored area indicates the variation of the diffusion-advection curve when varying the pressure gradient intensity from a lower to a higher value (see Table 4.3), while the curve at the middle of the area represents a medium value (see Table 4.3).The curve of the only diffusive transport case is also shown (dashed curve) in each figure. The deficit expected at equilibrium conditions is also reported as a reference.

In particular, different saturation-deficit curves are shown assuming a rising water table and performing Rn measurements at the water table (Figure 4.8a), at a vertical distance of 1 m from it (Figure 4.8b) and at a distance of 4 m (Figure 4.8c). Each graph shows three saturation-deficit curves: under equilibrium conditions (using Eq. 4.17), under diffusive transport conditions, and under diffusive-advective transport conditions. It can be observed that for a positive pressure gradient and for a fixed deficit observed from Rn measurements, if purely diffusive transport or equilibrium conditions are considered, an underestimation of the actual LNAPL saturations (considered as those of the diffusive-advective curve) is reached. It is also clear that, if Rn measurements are performed at a certain distance from the source, i.e., closer to the surface, the risk of misinterpreting LNAPL saturation increases because the differences between the curves become much more pronounced at shallower depths. By moving the measurement point too far away from the LNAPL source, the deficits become no longer observable with varying saturations (Figure 4.8c), making the technique no longer applicable.

4.3.3.2 Negative pressure gradient (falling water table)

Figure 4.9 shows the Rn deficit curves calculated assuming a LNAPL saturation of 5% (Figure 4.9a), 10% (Figure 4.9b) and 20% (Figure 4.9c) (typical residual saturation range according to Brost and De Vaull, (2000)), considering the pressure gradient conditions of a falling water table (i.e., a negative pressure gradient), as described in Figure 4.2c and assuming the relative values indicated in Table 4.3. It can be observed that the deficit at the source zone in Figure 4.9a (S_N = 5%) for a pressure gradient of -0.05 Pa m^{-1} is approximately 0.67. Assuming a diffusion-dominated transport, the same deficit value at the same depth would lead to an estimated LNAPL saturation value of about 7% (using the nomographs presented in section 3.3.3 (Cecconi et al., 2022)), while under equilibrium conditions it would be around 2% (using Eq. 4.17). Therefore, it can be stated that ignoring the presence of advective transport, assuming it to be purely diffusive, results in an overestimation of LNAPL saturation, while assuming equilibrium conditions leads to an underestimation of LNAPL saturation.

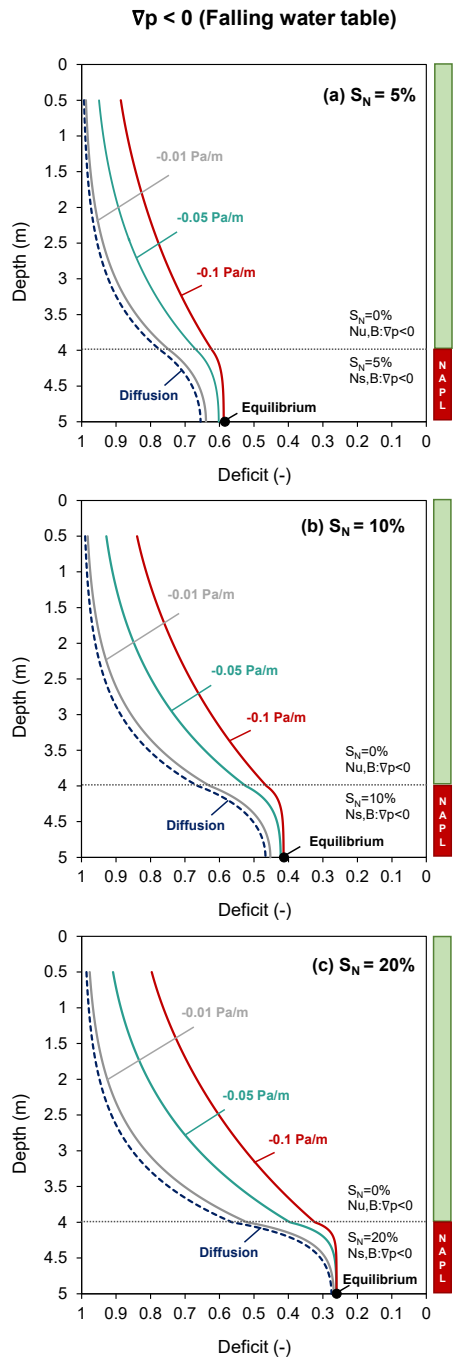

Figure 4.9. Rn deficit profiles for different imposed pressure gradients and different LNAPL saturations. Three LNAPL saturation conditions are considered: S_N = 5%, S_N = 10% and S_N = 20% for figures a, b and c respectively. In each graph, three values for a negative, constant pressure gradient are shown: low (-0.01 Pa m^{-1}), medium (-0.05 Pa m^{-1}) and high (-0.1 Pa m^{-1}). The deficit profile of the only diffusive transport case is also shown (dashed curve). The deficit expected at equilibrium conditions is also reported as a reference. The dotted lines represent the beginning of the layer with LNAPL.

The same conclusions can be drawn observing the curves in Figure 4.10, which show LNAPL saturation calculated as a function of the Rn deficit obtained considering soil gas Rn measurements carried out at a fixed distance from the water table. It can indeed be observed that the Rn deficit curves for negative pressure gradients lie between the diffusive deficit curve and the deficit value obtained assuming equilibrium conditions. It should be noted again that, also for this scenario, performing Rn measurements near the source zone (Figure 4.10a) helps to reduce the uncertainty of the method, since at these depths the curves are significantly closer to each other and to the equilibrium deficit value, compared to the cases shown in Figure 4.10b and Figure 4.10c.

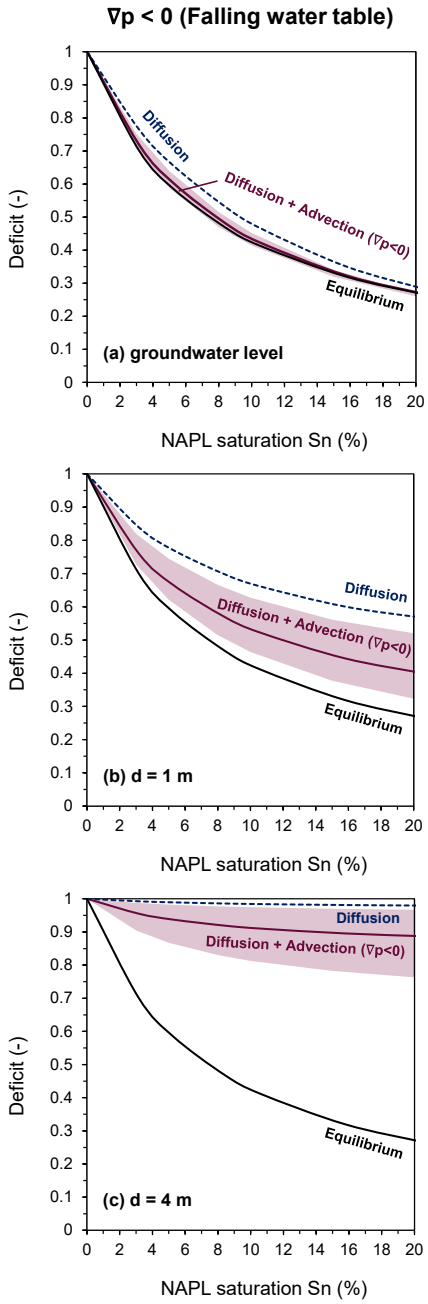

Figure 4.10. LNAPL saturation – Rn deficit curves for a negative pressure gradient and different vertical distances from the water table. Three distances between the soil gas Rn measuring point and the water table a shown: a zero distance (i.e., at the water table) for figure a; a distance of 1 m for figures b; and of 4 m for figure c. The colored area indicates the variation of the diffusion-advection curve when varying the pressure gradient intensity from a lower to a higher value (see Table 4.3), while the curve at the middle of the area represents a medium value (see Table 4.3).The curve of the only diffusive transport case is also shown (dashed curve) in each figure. The deficit expected at equilibrium conditions is also reported as a reference.

4.3.3.3 Variable pressure gradient (fresh LNAPL)

Figure 4.11 shows the Rn deficit curves calculated assuming a LNAPL saturation of 5% (Figure 4.11a), 10% (Figure 4.11b) and 20% (Figure 4.11c) (typical residual saturation range according to Brost and De Vaull, (2000)), considering the pressure gradient conditions a diffusion-only transport in the background zone and a diffusive-advective transport in the area with the presence of LNAPL, as described in Figure 4.2d. The pressure gradient values assumed in the two zones are summarized in Table 4.3. It can be observed that diffusion and diffusion-advection deficit prove to be much closer to each other. In this case the most important deviations occur considering the Rn deficits at higher distances from the source zone (i.e., approaching the surface), where Rn deficit exceeds the value of 1 for some shallow depths. This is also evident in the graphs in Figure 4.12, which show LNAPL saturation calculated as a function of the Rn deficit obtained considering soil gas Rn measurements carried out at a fixed distance from the water table. In particular, Figure 4.12c shows that the diffusive-advective curve obtained from Rn measurements performed at shallower depths (4 m from the water table) presents Rn deficits values that exceed 1. Obtaining deficit values greater than 1 in the application of the technique would lead not only (as in previous cases) to an erroneous estimation of LNAPL saturations but even to the risk of confusing areas with LNAPL as background areas.

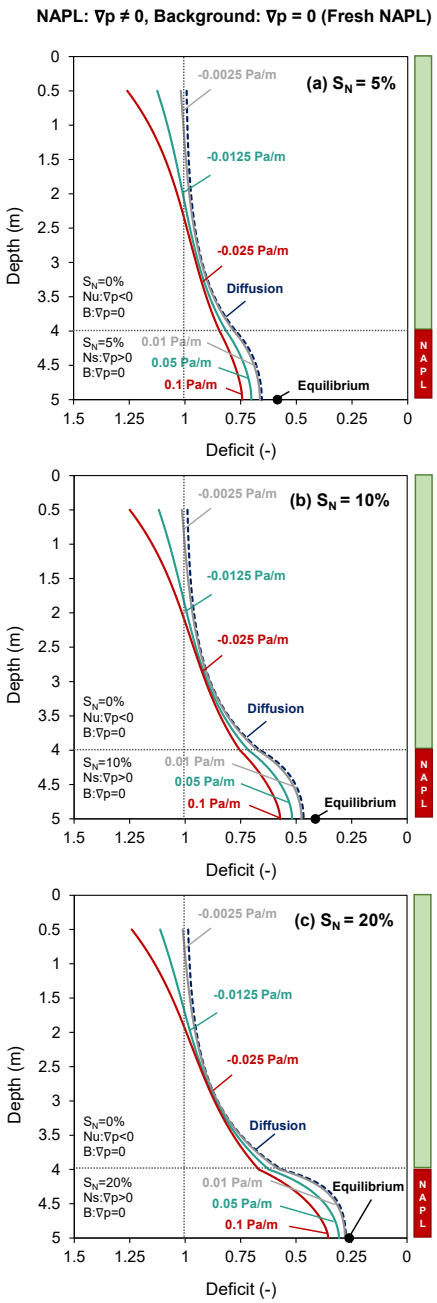

Figure 4.11. Rn deficit profiles for different imposed pressure gradients and different LNAPL saturations. Three LNAPL saturation conditions are considered: S_N = 5%, S_N = 10% and S_N = 20% for figures a, b and c respectively. Three conditions of variable pressure gradient in the LNAPL zone are shown in each graph. Positive (+0.01, +0.05, +0.1 Pa m^{-1}) in the LNAPL source zone (N_s) and negative (-0.0025, -0.0125, -0.025 Pa m^{-1}) in the upper layer (N_u), compared with a zero pressure gradient in the background area (B). The deficit profile of the only diffusive transport case is also shown (dashed curve) in each figure. The deficit expected at equilibrium conditions is also reported as a reference. The dotted lines represent the beginning of the layer with LNAPL.

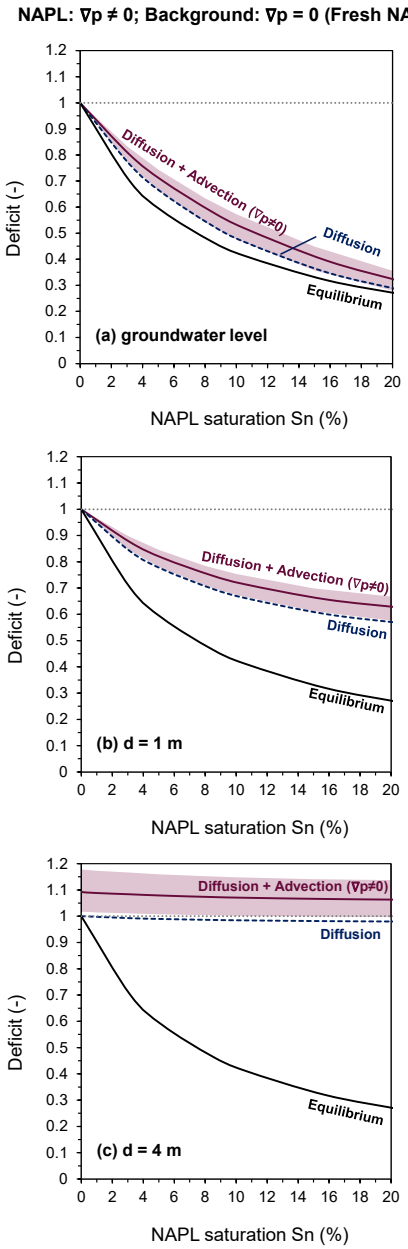

Figure 4.12. LNAPL saturation – Rn deficit curves for different imposed pressure gradients and different vertical distances from the water table. Three distances between the soil gas Rn measuring point and the water table a shown: a zero distance (i.e., at the water table) for figure a; a distance of 1 m for figures b; and of 4 m for figure c. The pressure gradient conditions are representative of a variable pressure gradient in the LNAPL zone, positive in the LNAPL source zone and negative in the upper layer, compared with a zero pressure gradient in the background area. The colored area indicates the variation of the diffusion-advection curve when varying the pressure gradient intensity from a lower to a higher value (see Table 4.3), while the curve at the middle of the area represents a medium value (see Table 4.3).The curve of the only diffusive transport case is also shown (dashed curve) in each figure. The deficit expected at equilibrium conditions is also reported as a reference.

4.3.4 Influence of site-specific parameters on Rn deficit profiles

The extent of the influence of advective fluxes on Rn transport in soil gas depends on the site-specific parameters. Therefore, the effect of LNAPL composition, soil texture, source zone thickness, and groundwater table depth on the Rn deficit curve was analyzed by considering three different pressure gradient conditions and varying only one of the investigated parameters each time. For each of the pressure gradient conditions (see Figure 4.2 and Table 4.3) considered, in Figure 4.13, Figure 4.14, Figure 4.15 and Figure 4.16, the diffusive Rn deficit curve and three diffusive-advective deficit curves (calculated for three pressure gradient values: a lower, an intermediate and a higher value) will be shown in each graph. It was found that the parameter to have the greatest influence on Rn deficit profiles is soil textures (Figure 4.14), since the effect of advection results important for coarse-grained rather than fine-grained soils, and, at a lower extent, also LNAPL composition (Figure 4.13). Instead, both the source zone thickness (Figure 4.15) and the water table depth (Figure 4.16) do not seem to significantly influence the Rn deficit values measured at a certain distance from the water table, even in the presence of a pressure gradient in the subsurface, considering the same pressure gradient simulation scenario. A more detailed discussion is given below.

4.3.4.1 Influence of NAPL composition on the Rn deficit curves

Figure 4.13 shows the Rn deficits calculated assuming contamination by gasoline (characterized by a partition coefficient between NAPL and water $k_{N/W}$ of about 40), kerosene ($k_{N/W}$ approximately 50) and diesel ($k_{N/W}$ of 60) (Schubert et al., 2007b).

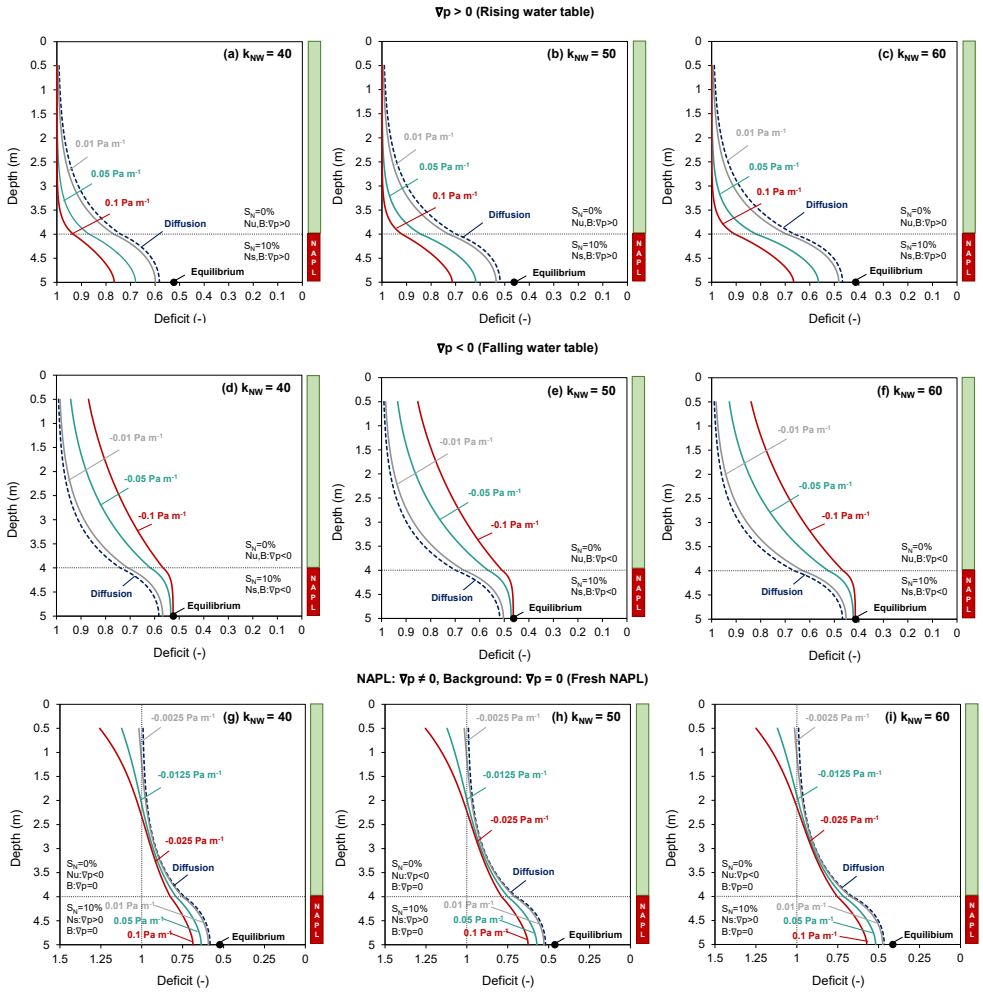

Figure 4.13. Rn deficit profiles for a medium sand soil type for different imposed pressure gradients and different NAPL compositions. Three NAPL composition conditions are considered: Gasoline ($k_{N/W}$ = 40) for figures a, d, g, Kerosene ($k_{N/W}$ = 50) for figures b, e, h and Diesel ($k_{N/W}$ = 60) for figures c, f, i. Three conditions for the pressure gradient are shown (low, medium, high): a constant positive pressure gradient (+0.01, +0.05, +0.1 Pa m^{-1}) (figures a-c), a constant negative pressure gradient (-0.01, -0.05, -0.1 Pa m^{-1}) (figures d-f), and a variable pressure gradient in the NAPL zone, positive (+0.01, +0.05, +0.1 Pa m^{-1}) in the source zone (N_s) and negative (-0.0025, -0.0125, -0.025 Pa m^{-1}) in the upper layer (N_u), compared with a zero pressure gradient in the background area (B) (figures g-i). The deficit profile of the only diffusive transport case is also shown (dashed curve) in each figure. The deficit expected at equilibrium conditions is also reported as a reference. The dotted lines represent the beginning of the layer with LNAPL. NAPL saturation in the deepest layer is imposed at 10%.

It can be observed that by increasing the partition coefficient $k_{N/W}$, the Rn deficit value decreases either assuming a diffusion-dominate transport or considering also an advective component. In fact, Rn deficit values in the range of 0.74-0.66 ($k_{N/W}$ = 40-60) are obtained for diffusive-only transport at the source zone (i.e., at 1 m from

groundwater), against deficit of 0.93-0.66 ($k_{N/W}$ = 40-60) for a positive pressure gradient (Figure 4.13a, d, g), of 0.71-0.46 ($k_{N/W}$ = 40-60) for a negative pressure gradient (Figure 4.13b, e, h) and of 0.82-0.66 ($k_{N/W}$ = 40-60) for a variable pressure gradient (Figure 4.13c, f, i). Thus, the composition of NAPL (for the considered range of values) affects the deviation of the Rn deficit expected in the diffusive and diffusive-advective cases, with a slight decrease in the differences between the simulated curves for the three different pressure gradient values as the partition coefficient decreases. This result is in agreement with the literature about the recognized influence of NAPL composition on the value of the NAPL-water partition coefficient (and that between NAPL and soil gas) (Le Meur et al., 2021) and thus on Rn behavior in the subsoil. Consequently, depending on the NAPL composition, different soil gas Rn vertical profiles and, thus, Rn deficit can be expected.

4.3.4.2 Influence of soil texture on the Rn deficit curves

Figure 4.14 shows the Rn deficit curves calculated assuming a medium sand (Figure 4.14a, d, g), fine sand (Figure 4.14b, e, h) and loam (Figure 4.14c, f, i) soil type (see Table 4.1). It can be observed that the soil texture significantly influences the advective-diffusive deficit curves. Indeed, for a loam (Figure 4.14c, f, i) and a fine sand (Figure 4.14b, e, h) soil type, the advective-diffusive curves and the diffusive curves are overlapped, while in the case of medium sand (Figure 4.14a, d, g) the differences are more pronounced. Thus, it can be stated that for loam and fine sand soil types, the predominant transport mechanism appears to be diffusion, even for higher simulated values of the pressure gradient. This is also evidenced by the value of the Peclet number, which for most of the above cases, is indeed lower than 1 (for Pe<1 it can be assumed that the dominant transport mechanism is diffusion). It is recalled that the Peclet number can be calculated by:

$$Pe_i = \frac{u_i \cdot L_i}{D_{e_i}} \qquad \text{Eq. 4.18}$$

With L_i the length of the layer.

It is also noted that for a medium sand soil type, the Peclet number for the lowest value of imposed pressure gradient is also low (<5). In fact, it can be observed that the curve is close to that of diffusive-only transport.

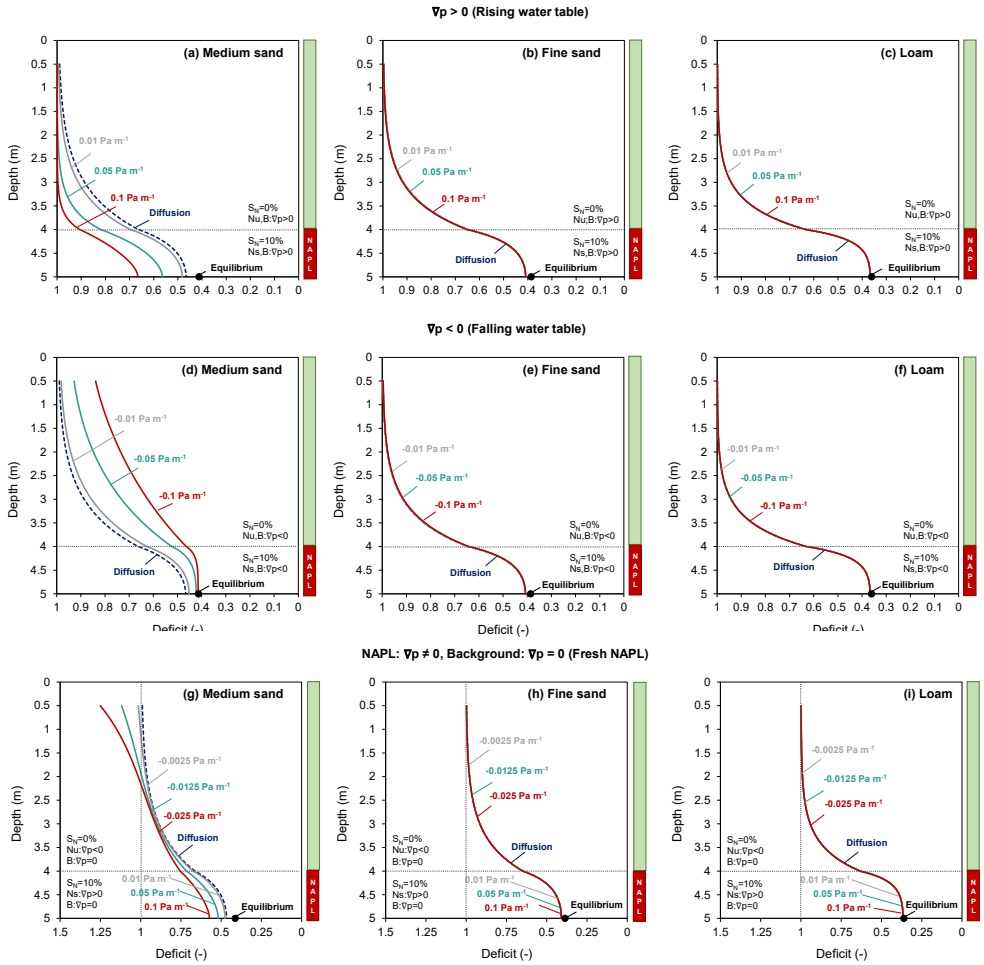

Figure 4.14. Rn deficit profiles for different imposed pressure gradients and different soil types. Three soil texture conditions are considered: a medium sand for figures a, d, g, a fine sand for figures b, e, h, and loam for figures c, f, i. Three conditions for the pressure gradient are shown (low, medium, high): a constant positive pressure gradient (+0.01, +0.05, +0.1 Pa m^{-1}) (figures a-c), a constant negative pressure gradient (-0.01, -0.05, -0.1 Pa m^{-1}) (figures d-f), and a variable pressure gradient in the NAPL zone, positive (+0.01, +0.05, +0.1 Pa m^{-1}) in the source zone (N_s) and negative (-0.0025, -0.0125, -0.025 Pa m^{-1}) in the upper layer (N_u), compared with a zero pressure gradient in the background area (B) (figures g-i). The deficit profile of the only diffusive transport case is also shown (dashed curve) in each figure. The deficit expected at equilibrium conditions is also reported as a reference. The dotted lines represent the beginning of the layer with LNAPL. NAPL saturation in the deepest layer is imposed at 10%.

4.3.4.3 Influence of source zone thickness on the Rn deficit curves

Figure 4.15 shows the Rn deficit profiles simulated assuming a source thickness of 0.5 m (Figure 4.15a, d, g), 1 m (Figure 4.15b, e, h), and 2 m (Figure 4.15c, f, i), considering a constant positive pressure gradient (representative, for instance, of a rising groundwater level), a constant negative pressure gradient (e.g., lowering

groundwater level), and the case of the presence of fresh NAPL, with a positive pressure gradient in the NAPL source due to methanogenesis and a negative pressure gradient in the overlying zone of methane oxidation, compared with a zero pressure gradient in the background area.

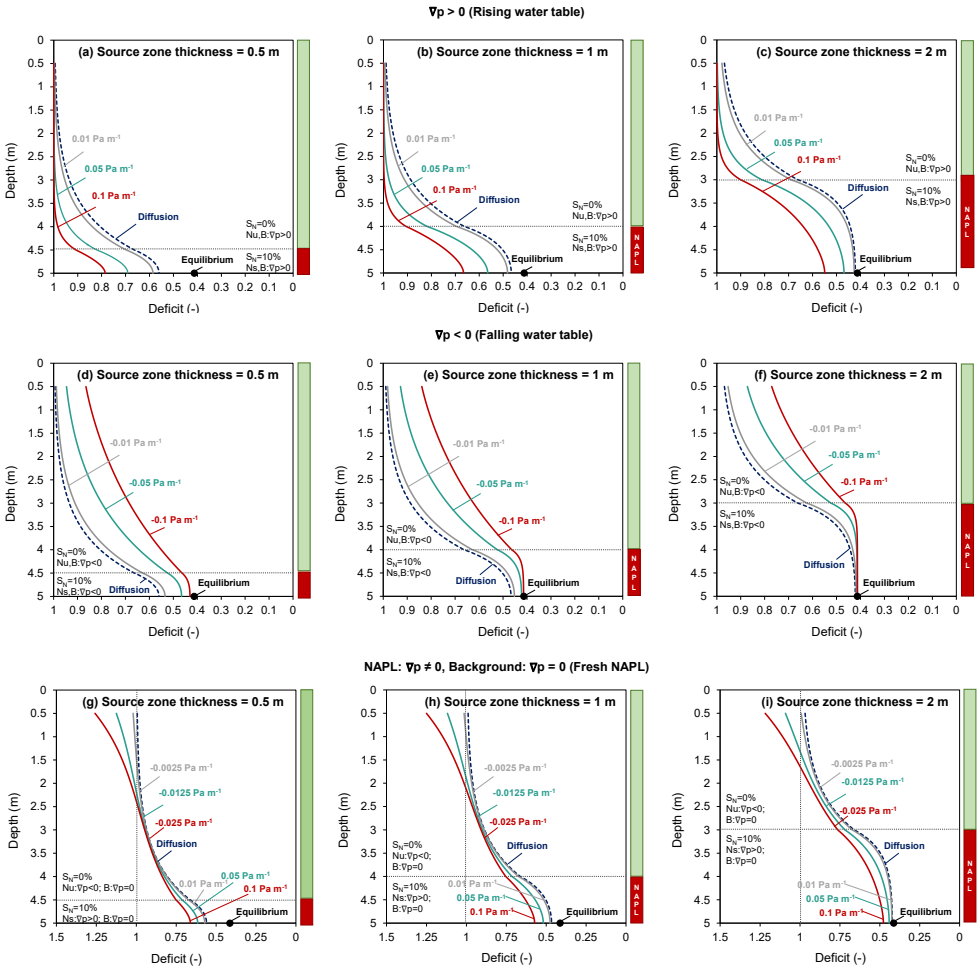

Figure 4.15. Rn deficit profiles for a medium sand soil type for different imposed pressure gradients and different source zone thicknesses. Three source zone thickness conditions are considered: 0.5 m (figures a, d, g), 1 m (figures b, e, h) and 2 m (figures c, f, i). Three conditions for the pressure gradient are shown (low, medium, high): a constant positive pressure gradient (+0.01, +0.05, +0.1 Pa m^{-1}) (figures a-c), a constant negative pressure gradient (-0.01, -0.05, -0.1 Pa m^{-1}) (figures d-f), and a variable pressure gradient in the NAPL zone, positive (+0.01, +0.05, +0.1 Pa m^{-1}) in the source zone (N_s) and negative (-0.0025, -0.0125, -0.025 Pa m^{-1}) in the upper layer (N_u), compared with a zero pressure gradient in the background area (B) (figures g-i). The deficit profile of the only diffusive transport case is also shown (dashed curve) in each figure. The deficit expected at equilibrium conditions is also reported as a reference. The dotted lines represent the beginning of the layer with LNAPL. NAPL saturation in the deepest layer is imposed at 10%.

The diffusive-advective deficit curves in each figure are calculated for a lower, an intermediate, and a higher pressure gradient value (see Table 4.3). By comparing the diffusive-advective Rn deficit curves obtained in each scenario, it can be noted that there are no substantial variations between the curves. In support of this statement, it can be observed that the deficit values at the beginning of the source zone (i.e., at a depth of 4.5 m, 4 m, and 3 m respectively for a source zone thickness of 0.5 m, 1 m and 2 m) for the diffusive-advective transport cases are 0.69, 0.82 and 0.91 (low, intermediate and high pressure gradients intensities) for a positive pressure gradient (Figure 4.15a-c), 0.63, 0.52 and 0.46 for a negative pressure gradient (Figure 4.15d-f), and 0.67, 0.71 and 0.75 for the fresh NAPL simulation (Figure 4.15g-i). From these observations, it can be concluded that the thickness of the source zone does not significantly affect the Rn deficit values measured at the same distance from the contaminated zone, assuming the same pressure gradient scenario.

4.3.4.4 Influence of groundwater table depth on the Rn deficit curves

Figure 4.16 Rn deficit curves were derived considering an aquifer depth of 3 m, 5 m and 10 m for the different pressure gradient cases adopted in the previous section. From the comparison of the obtained deficit curves, it can be noted that the curves for a water table at a depth of 3 m (Figure 4.16a, d, g) do not differ significantly from the curves shown for the water table assumed at 5 m (Figure 4.16b, e, h) and 10 m (Figure 4.16c, f, i). Rn deficits at the beginning of the source zone (i.e. at 1 m from the groundwater table) are, in fact, approximately 0.69, 0.82, 0.91 for a positive pressure gradient (Figure 4.16a-c), 0.63, 0.52, 0.46 for a negative pressure gradient (Figure 4.16d-f), and 0.67, 0.71, 0.75 for the variable pressure gradient representative of the presence of fresh NAPL in the source zone (Figure 4.16g-i). Thus, it can be concluded that the depth of the water table does not seem to influence the Rn deficit values measured at a certain distance from the source zone, assuming the same conditions of pressure gradient in the subsurface.

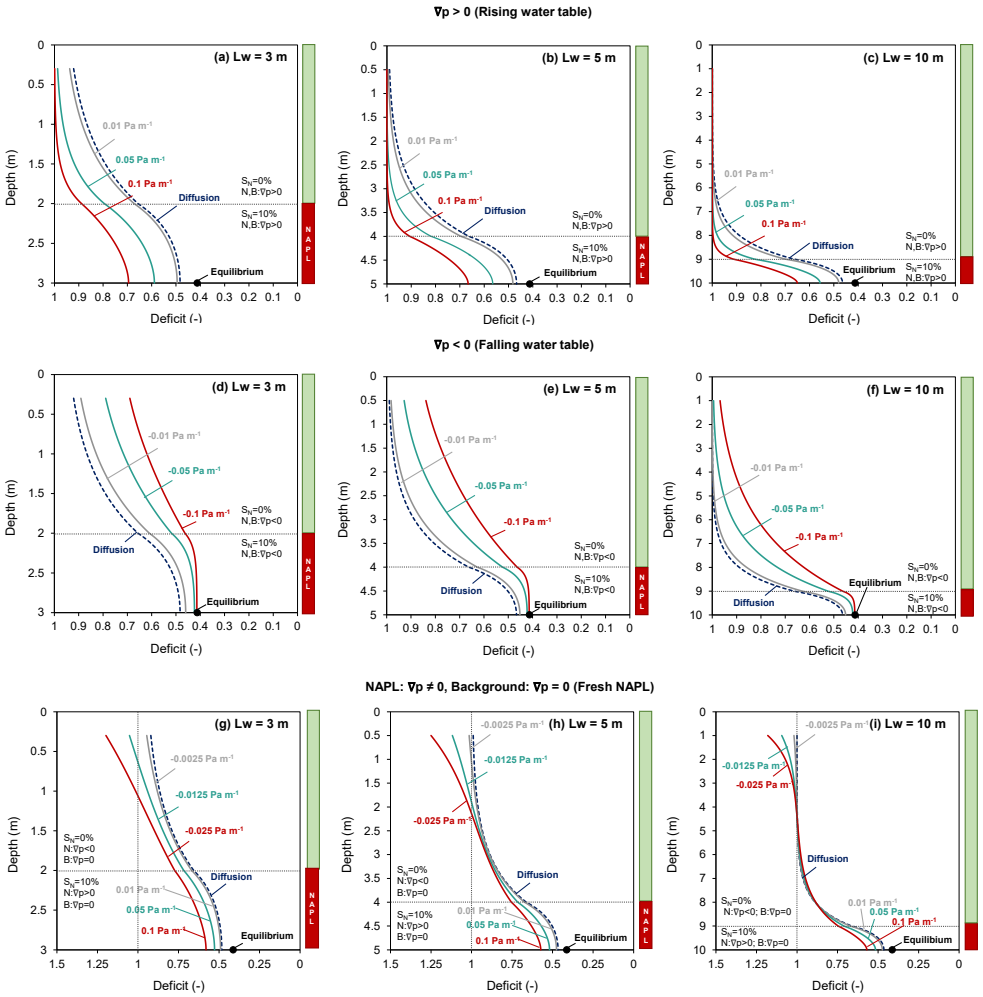

Figure 4.16. Rn deficit profiles for a medium sand soil type for different imposed pressure gradients and different water table depths. Three water table depths conditions are considered: 3 m (figures a, d, g), 5 m (figures b, e, h) and 10 m (figures c, f, i). Three conditions for the pressure gradient are shown (low, medium, high): a constant positive pressure gradient (+0.01, +0.05, +0.1 Pa m^{-1}) (figures a-c), a constant negative pressure gradient (-0.01, -0.05, -0.1 Pa m^{-1}) (figures d-f), and a variable pressure gradient in the NAPL zone, positive (+0.01, +0.05, +0.1 Pa m^{-1}) in the source zone (N_s) and negative (-0.0025, -0.0125, -0.025 Pa m^{-1}) in the upper layer (N_u), compared with a zero pressure gradient in the background area (B) (figures g-i). The deficit profile of the only diffusive transport case is also shown (dashed curve) in each figure. The deficit expected at equilibrium conditions is also reported as a reference. The dotted lines represent the beginning of the layer with LNAPL. NAPL saturation in the deepest layer is imposed at 10%.

CHAPTER 5

5 USING GROUNDWATER MONITORING WELLS FOR RAPID APPLICATION OF SOIL GAS RADON DEFICIT TECHNIQUE

Most of this chapter is taken from "Cecconi, A., Verginelli, I., Baciocchi, R., Lanari, C., Villani, F., Bonfedi, G., 2023a. Using groundwater monitoring wells for rapid application of soil gas radon deficit technique to evaluate residual LNAPL. J. Contam. Hydrol. 258, 104241. https://doi.org/10.1016/j.jconhyd.2023.104241"

ABSTRACT

The application of the ^{222}Radon (Rn) deficit technique using subsurface soil gas probes for the identification and quantification of light non-aqueous phase liquids (LNAPL) has provided positive outcomes in recent years. This study presents an alternative method for applying this technique in the headspace of groundwater monitoring wells. The developed protocol, designed for groundwater monitoring wells with a portion of their screen in the vadose zone, is based on the use of portable equipment that allows rapid measurement of the Rn soil gas activity in the vadose zone close to the water table (i.e., smear zone) where LNAPL is typically expected. The paper first describes the step-by-step procedure to be followed for the application of this method. Then, a preliminary assessment of the potential of the method was carried out at two Italian sites characterized by accidental gasoline and diesel spills into the subsurface from underground storage tanks. Although the number of tests conducted does not allow for definitive conclusions, the results obtained suggest that, from a qualitative point of view, Rn monitoring in the headspace of monitoring wells is a promising, fast, and minimally invasive screening method that could also potentially reduce the costs associated with field data acquisition. This method proves to be suitable for detecting the presence of LNAPL in both the mobile and residual phases with results consistent with the other lines of evidence available at the sites, such as groundwater and soil gas monitoring. Future efforts should be directed toward evaluating the accuracy of this method for a quantitative assessment of residual LNAPL saturations.

5.1 INTRODUCTION

Several works and experiments conducted in recent decades have highlighted the positive potential of the Rn deficit technique. Favorable results have been observed with each of the tested configurations (see section 2.4). In spite of these favorable outcomes, certain limitations still exist concerning the applicability of the Rn deficit technique in the soil gas (see also section 2.4.3). A crucial aspect emphasized by several authors (Cohen et al., 2016; De Miguel et al., 2020; Cecconi et al., 2023b) is the vertical distance up to which NAPL contamination at a certain depth can be indirectly detected using the Rn deficit in soil gas as an indicator. This distance depends on various factors, such as soil texture characteristics, NAPL saturation of soil pores and Rn diffusion coefficient in the soil. In dry, sandy soils, Rn diffusion length can reach approximately 2 meters (Schubert et al., 2001), but it can be significantly smaller in finer, wetter materials (Cecconi et al., 2022). Additionally, a heterogeneous geological setting can complicate the interpretation of the collected Rn data (Cohen et al., 2016, 2019; Cho et al., 2020). Therefore, if gas transport in the soil is purely diffusive, the technique's application would be limited to cases where the distance between NAPL contamination and the depth at which the soil gas samples are taken falls within the range of the Rn characteristic diffusion length in the soil (Schubert et al., 2001; De Miguel et al., 2020; Cecconi et al., 2022). Furthermore, Cecconi et al. (2023b) highlighted that performing Rn measurements in soil gas at a depth close to the LNAPL source zone can enhance the method's performance also in the occurrence of local advective fluxes, due to groundwater level fluctuations, or methanogenesis phenomena that may occur in the proximity of LNAPL, which can complicate the interpretation of Rn data for the application of the Rn deficit technique. In this view, it is worth considering that a common characteristic of the LNAPL-contaminated sites being investigated is the presence of monitoring wells, typically screened across part of the vadose zone, through the smear zone and some portion of the aquifer (Lenhard and Parker, 1990; Steffy et al., 1995; CalEPA, 2014; Sweeney and Ririe, 2017). However, installing the soil gas probes at the depth of the smear zone is not technically feasible as close to the water table, as low-flow conditions might be encountered due to the high moisture content (CalEPA, 2015). In light of these observations, Jewell and Wilson (2011) developed a method that allows for soil gas sampling to be carried out using monitoring wells without the need for invasive installation of soil gas probes. Sweeney and Ririe (2017) proposed some

modifications to the method, which have been applied by other authors (Sookhak Lari et al., 2017; Smith et al., 2021; Ririe and Sweeney, 2022) to investigate phenomena such as vapor intrusion and natural source zone depletion (NSZD). It is worth noting that, although this method proved to be promising, it still must undergo further validation and obtain regulatory acceptance.

The objective of this study was to develop and evaluate a methodology for the application of the Rn deficit technique in soil gas by using the headspace of groundwater monitoring wells screened across the smear zone, installed at sites with LNAPL presence. In this work, we first defined the developed field protocol and then employed it at two Italian sites characterized in the past by accidental gasoline and diesel spills in the subsurface from underground storage tanks. At the first site, the developed protocol was compared with the results obtained using soil gas probes. The campaign carried out at the second site involved the use of groundwater monitoring wells to evaluate Rn data over a more significant number of monitoring points, also examining the temporal variability of Rn gas activity values through repeated measurements within the same day. Based on the obtained results, general recommendations on the use of monitoring wells for the application of soil gas Rn deficit technique to evaluate residual LNAPL are provided.

5.2 MATERIALS AND METHODS

5.2.1 Field protocol

This section describes a simple procedure developed for a rapid application of the Rn deficit technique in soil gas, to assess LNAPL contamination, analyzing the headspace of groundwater monitoring wells using portable equipment. This application can be suitable for sites with wells installed both in an area with presumed, or proven, presence of LNAPL, as well as in an area considered uncontaminated, to determine also the background value of Rn activity, necessary for the interpretation of the data. Note that, as for groundwater sampling, proper design and installation of the well is crucial to ensure the quality of the soil gas data obtained with the protocol outlined below. Considering the possible deterioration of the well's materials over time, conducting regular checks on the well's integrity and visual inspections can help ensure conformity with this last aspect. Note also that the method is best suited to typical LNAPL distributions in the subsurface, where the contamination is mainly found in the area comprising the shallower portion of the aquifer, the capillary fringe and some portion of the vadose zone, where the presence of LNAPL-gas interfaces allows the Rn deficit in the soil gas to be observed. Therefore, the protocol is suitable for groundwater monitoring wells that have a portion of their screen in the vadose zone. The configuration of the procedure follows some of the aspects proposed by Sweeney and Ririe (2017), in a modification of the US EPA protocol (Jewell and Wilson, 2011) for soil gas sampling from the headspace of monitoring wells. Figure 5.1 shows a schematic representation of the method.

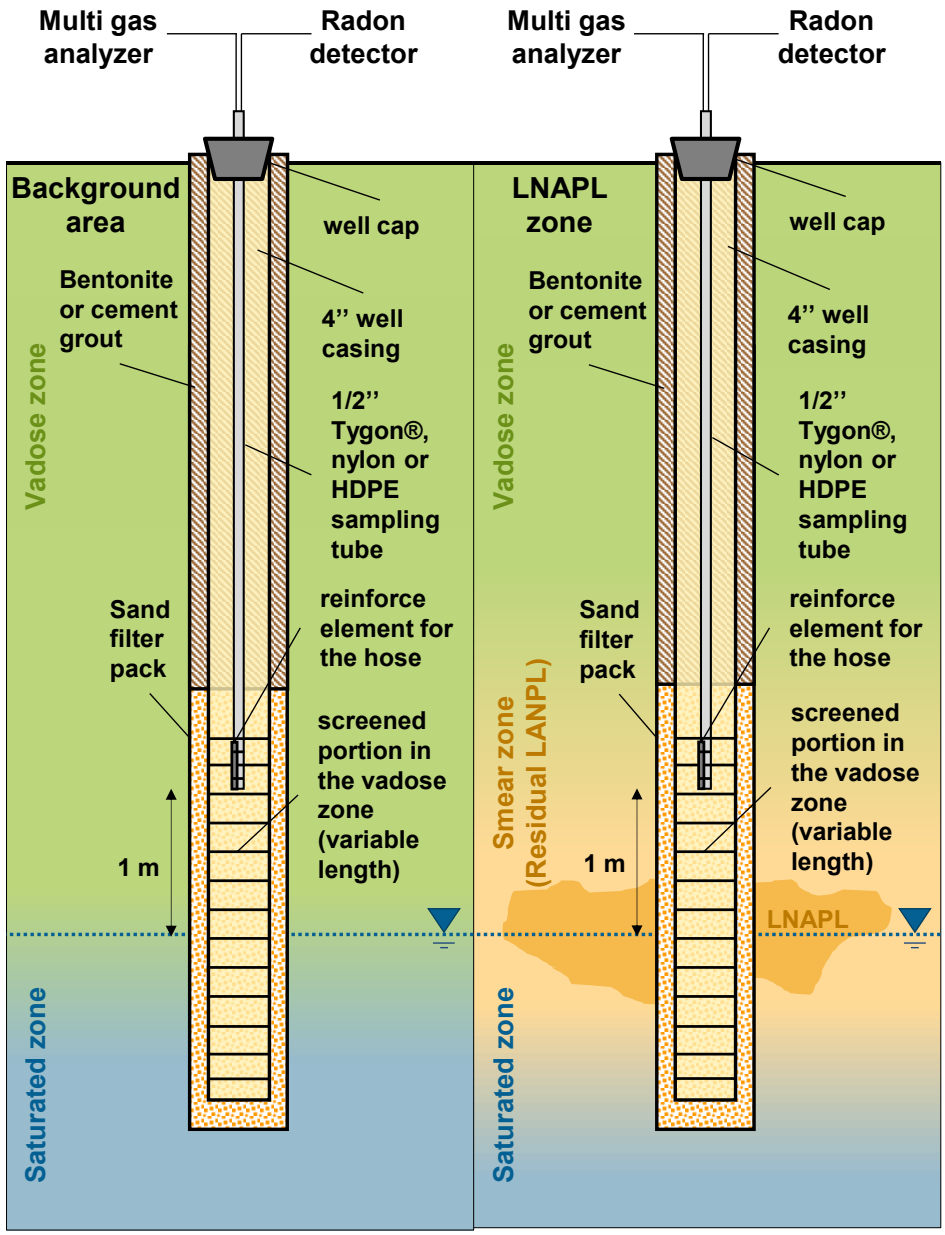

Figure 5.1. Schematic of the method for the application of the Rn deficit technique in monitoring wells, located both in the LNAPL area and background zone.

For each monitoring point, both in the contaminated and the background area, the following steps can be followed:

- The well protective cap of the well is opened, and a sampling tube (typically of the size of ½ inch, of materials such as Tygon®, nylon or HDPE) is dropped into the well under investigation to a depth of approximately 1 m above the

top of groundwater or LNAPL in the well. To ensure measurement in the gas phase without reaching the liquid interface, the liquid phase level should be measured ideally immediately before the sampling tube is inserted. In this case, the sampling tube can be brought even closer to the groundwater level to ensure the reliability of the monitored data. It is suggested that the end of the sampling tube, being flexible, is attached to a reinforcement that allows the tube to be extended to the desired depth.

- The wellhead is sealed with a well cap, fitted with an opening for the sampling tube, to prevent the ingress of air and the dilution of the soil gas to be sampled.

- The purge of the system can be carried out with the built-in pump of a portable gas detector or with an external pump. Using the gas detector to purge the system is considered the simplest approach and also provides an analysis of the soil gas sample from the well immediately after the purging phase (Sweeney and Ririe, 2017). The time for this phase can be calculated by dividing the purge volume by the flow rate of the instrument used, typically 0.5-1 L min^{-1} if field gas detectors are used. The purge volume can be considered as the sum of the internal volume of the well and of the sampling and connection tubes. It is worth noting that the use of a packer can help reduce the purge volume and select the well portion to be monitored.

- A multi-gas detector is used immediately after purging for a first sampling phase, for the analysis of CH_4, and CO_2, to provide supplementary information on the composition of the soil gas pumped from the bottom of the vadose zone and to highlight any ongoing attenuation processes of LNAPL sources (ITRC, 2009). High concentrations of CH_4 and CO_2 may be indicative of biodegradation phenomena. Measurements can be taken for approximately 5 minutes, after the monitored concentrations stabilize.

- The gas detector is then disconnected from the sampling line and replaced by a portable, active Rn gas detector (e.g., RAD7 manufactured by DURRIDGE or AlphaGUARD, manufactured by Bertin Instruments). To select the best setting and time for Rn analysis, reference must be made to the specific characteristics of the Rn monitor used and, if available, to the manufacturer's instructions for analysis in soil gas.

- At the end of the survey, the sampling tube is removed, and the well is closed with its own cap before proceeding to the following monitoring point and repeating the procedure.

The procedure should be followed, following the protocol described, for both groundwater wells located in the LNAPL-impacted area and in the background area.

5.2.2 Interpretation of Rn data

From the ratio of the Rn activity detected in the LNAPL area and background zone, the Rn deficit, D (-), can be derived using the following relationship:

$$D = \frac{Rn(NAPL)}{Rn_b} \qquad \text{Eq. 5.1}$$

Where Rn is the Rn concentration in the monitoring point in the LNAPL zone and Rn_b is the mean Rn activity detected in the monitoring points located in the assumed uncontaminated area. Note that the term deficit indicates a depletion ratio of Rn activity, so the greater the difference between the background values and those in the LNAPL region, the closer the value of the deficit to zero.

Note that Rn might have a different partitioning behavior within soil pores and inside the well casing, which could lead to a potential dilution of the soil gas within the well casing. This potential dilution factor DF is represented by the ratio of the Rn concentration in soil gas to that in the well headspace, and can be expressed as the ratio of the total headspace volume of the well, V_{HS} (L), to the volume aspirated for Rn detection, as indicated as follows:

$$DF = \frac{V_{HS}}{Q \cdot t} \qquad \text{Eq. 5.2}$$

where Q (L min^{-1}) is the flow rate of the Rn detector's pump and t (min) is the soil gas sampling duration for Rn measurement. This could be accounted for in the interpretation of Rn data. As will be shown later, for the typical flow rates and duration adopted for Rn monitoring the expected dilution factor is relatively small and thus can be neglected.

It is then possible to estimate the fraction of LNAPL in the subsurface based on the observed Rn deficit, using different approaches. To take into account the vertical

distance of the measurement point from the LNAPL source, the method proposed by (Cecconi et al., 2022, 2023b) can be used, assuming respectively diffusive and diffusive-advective transport. If Rn measurements are carried in proximity of the LNAPL source (as in the case proposed here) more simplified approaches based on the assumption of equilibrium conditions can be used. Schubert et al. (2001) developed an equation to describe the equilibrium Rn activity in the soil gas within a volume of NAPL-contaminated soil. According to the equations described in section 2.3.1, the Rn deficit D can be described as follows:

$$D = \frac{1 + S_{w,b} \cdot (k_{\frac{w}{g}} - 1)}{1 + S_w \cdot (k_{\frac{w}{g}} - 1) + S_N \cdot (k_{\frac{N}{g}} - 1)} \quad \text{Eq. 5.3}$$

where $S_{w,b}$ (-) and S_w (-) are respectively the water saturations in the soil in the background area and the NAPL impacted zone, S_N (-) is NAPL saturation, $k_{w/g}$ (-) is the Rn partition coefficient between water and gas and $k_{N/g}$ (-) is the Rn partition coefficient between NAPL and gas.

From Eq. 5.3 (see also Eq. 2.19) it is then possible to derive the relationship for estimating the fraction of LNAPL in the subsoil, S_N (%), based on the observed Rn deficit, as described in Eq. 2.20.

$$S_N = \frac{(1 - D) + \left(S_{w,b} - D \cdot S_w\right) \cdot \left(k_{\frac{w}{g}} - 1\right)}{D \cdot \left(k_{\frac{N}{g}} - 1\right)} \cdot 100 \quad \text{Eq. 5.4}$$

The LNAPL saturation can also be expressed in terms of total petroleum hydrocarbons (TPH) concentration, C (mg kg^{-1}), using the relation in Eq. 2.21 (Brost and De Vaull, 2000), also given below:

$$TPH = \frac{\theta_t \cdot \rho_N}{\rho_S} \cdot \frac{S_N}{100} \cdot 10^6 \quad \text{Eq. 5.5}$$

where ρ_N is LNAPL density (g cm^{-3}) and S_N (%) is expressed in percentage.

5.3 FIELD TESTS

To test the performance of the method described above, the protocol was applied in two field campaigns, conducted between March 2021 and June 2022, at two contaminated sites located in Italy.

5.3.1 First campaign (site 1)

The first site, located in central Italy, was characterized in the past by accidental spills of diesel from an underground storage tank with a consequent contamination of the unsaturated soil and groundwater by hydrocarbons. A portion of the site was previously affected by the presence of free LNAPL in groundwater, which is located about 3-4 m below ground surface, with a thickness of about 3 m. The site is characterized by a rather homogeneous geology, with the presence of a layer of silty sands at the most superficial layer and weakly silty sands at greater depth, up to approximately 7 m from the surface, overlying a layer of clays.

The field test at the first site was conducted in March 2021. The activities consisted of the application of the Rn deficit technique in two groundwater wells and two soil gas probes to verify the feasibility of the proposed method. The operating procedure followed for gas analysis in the headspace of the monitoring wells is the described in the previous section. For the two soil gas probes, the instruments (see section 5.3.3) were instead connected directly to the sampling tube of the probes, installed to a depth of 1.2 m. The monitoring points were selected based on the contamination present at the site. In particular, free LNAPL was found in the past at the monitoring well named MW-L, in proximity of the soil gas probe SGS-L and were therefore selected for the application of the method. The area near the monitoring well MW-B and the soil gas probe SGS-B, instead, was always uncontaminated, and was considered suitable to obtain the Rn background activity expected in the absence of contamination, also considering the stratigraphic homogeneity of the site. Figure 5.2 schematically shows the locations of the selected monitoring points. Table 5.1 shows the characteristics, in terms of water table depth, screening and contamination, of the 4'' monitoring wells selected for the first site.

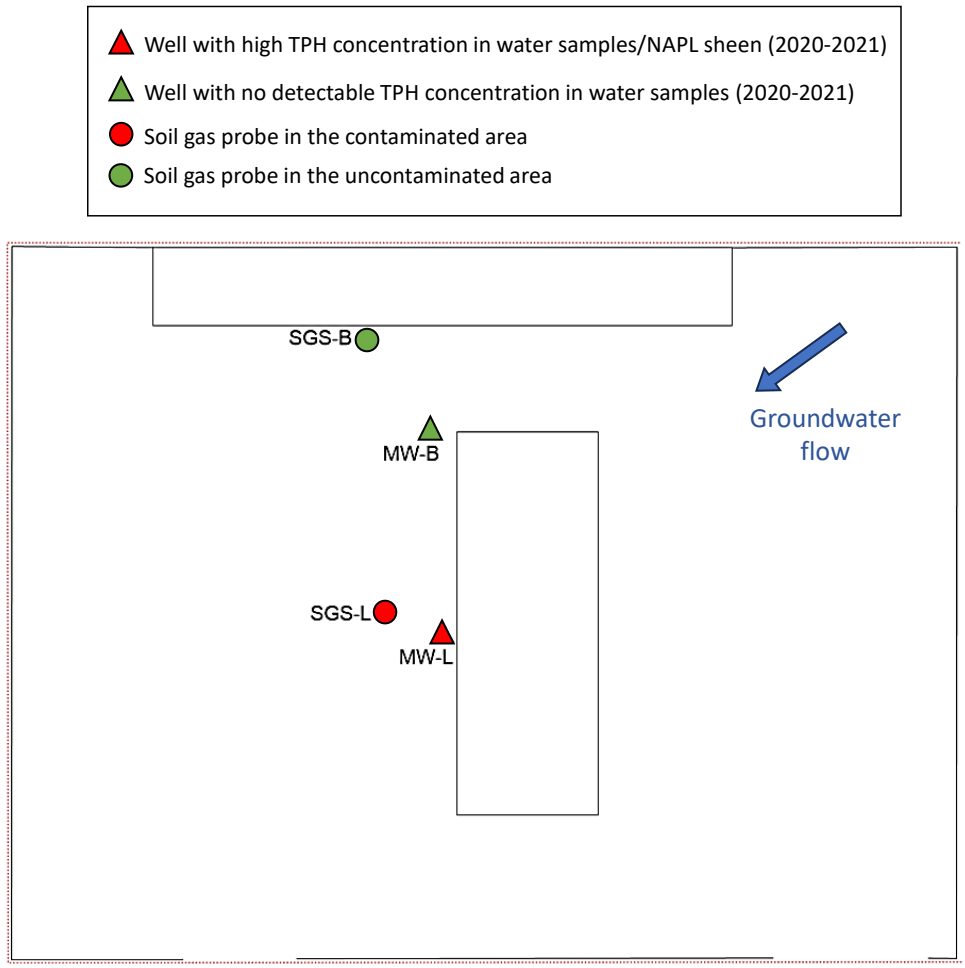

Figure 5.2. Schematic representation of site 1, representing the location of the soil gas probes (SGS) and monitoring wells (MW) selected for the monitoring campaign. TPH = Total Petroleum Hydrocarbons.

Table 5.1. Characteristics of the monitoring wells (MW) selected at site 1. The monitoring well indicated with the letter B (MW-B) is in the background area, while the one indicated with the letter L (MW-L) is in the contaminated zone. TPH = Total Petroleum Hydrocarbons.

MW	Water table depth (m from surface) March 2021	Top of the MW screen (m from surface)	Free LNAPL thickness (mm)		Groundwater TPH tot (µg L^{-1}) June 2020
			Min - Max value 2018-2020	Last measure March 2021	
MW-B	3.5	2	-	-	< 30
MW-L	3.1	2	0 - 40	- (sheen)	16,100

5.3.2 Second campaign (site 2)

The second site, located in central Italy, was characterized in the past by accidental spills of gasoline from an underground storage tank with consequent contamination of the unsaturated soil and groundwater by light (C ≤ 12) and heavy (C > 12) hydrocarbons. A portion of the site was previously affected by the presence of free LNAPL in groundwater, which is located about 4-6 m below ground surface. The site is characterized by a heterogeneous stratigraphy that presents a more superficial layer of backfill sands and gravels (up to about 2 m from ground level) and a layer of compact silts or clays with possible inclusions of medium-fine sand and gravel layers (up to about 12 m from the surface), laying on a layer of clays.

The investigation conducted at the second site aimed to evaluate the applicability of the proposed method in a larger number of monitoring points, as well as to assess the temporal variability of Rn activity. The groundwater wells were selected based on the contamination found in different areas of the site, on the local stratigraphy, and on the possible presence of skimmers or pumps in the wells. In particular, MW-B1 and MW-B2, located upgradient of the contamination source zone with respect to the direction of the groundwater flux, were chosen as background monitoring points. These two monitoring points showed no evidence of contamination during the characterization and the concentrations of hydrocarbons in groundwater were always below the detection limit. Instead, the groundwater wells MW-L1, MW-L2, MW-L3 and MW-L4 were chosen as monitoring points for the LNAPL area. Specifically, they were chosen for the presence of free product (or high concentrations of hydrocarbons and a sheen of LNAPL). The location of the selected monitoring points for the site is shown in Figure 5.3

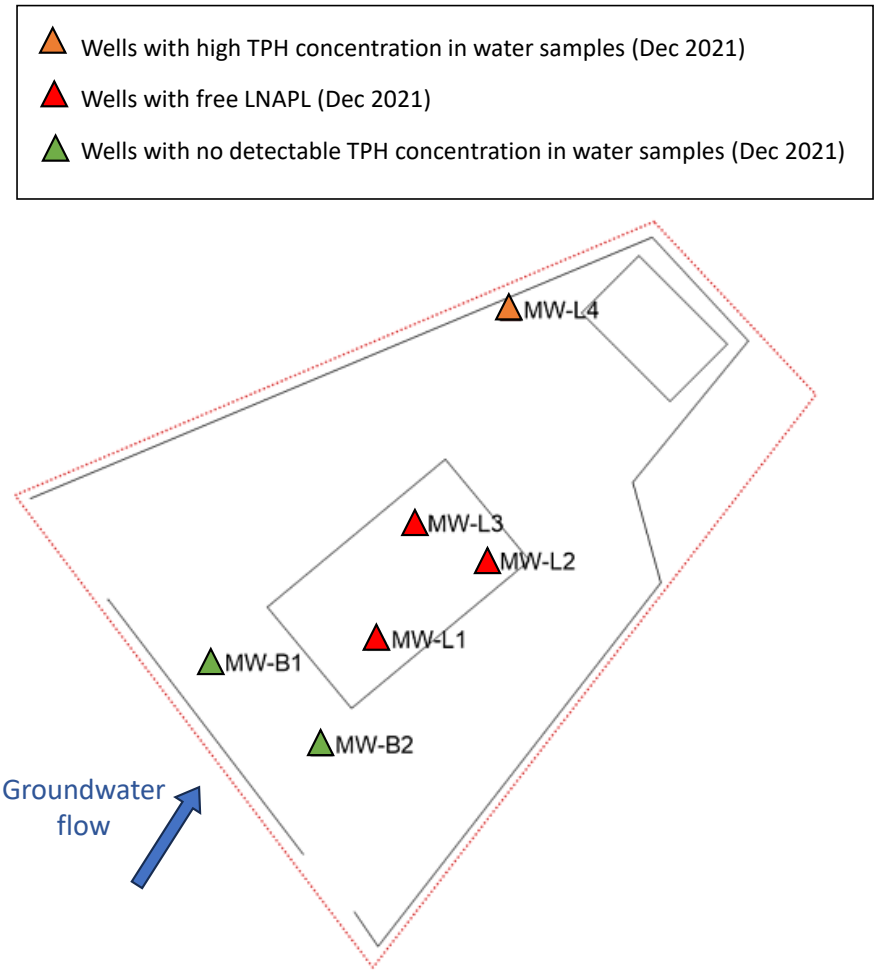

Figure 5.3. Schematic representation of site 2, representing the location of the monitoring wells (MW) selected for the monitoring campaign. TPH = Total Petroleum Hydrocarbons.

Note that the monitoring wells with installed total fluid or electric submersible pumps were excluded from the test. The background point MW-B2 and the contaminated point MW-L3 were selected to assess how the daily variability of Rn emissions from the subsurface may affect the estimation of LNAPL concentrations, repeating the procedure for three times within the same day. The characteristics of the selected monitoring wells, all with a diameter of 4'', are summarized in Table 5.2. It is worth noting that in the wells MW-L1 and MW-L3 the skimmers were turned off the early morning of the test date, so that possible interference with the activities could be minimized.

Table 5.2. Characteristics of the monitoring wells (MW) selected at site 2. Monitoring wells indicated with the letter B are in the background zone, those indicated with the letter L are in the contamination zone. TPH = Total Petroleum Hydrocarbons.

MW	Water table depth (m from surface) Dec 2021	Top of the MW screen (m from surface)	Free LNAPL thickness (mm)		Groundwater TPH tot (µg L^{-1}) Dec 2021	Active measures
			Min - Max value 2021	Last measure Dec 2021		
MW-B1	4.4	3	-	-	< 30	-
MW-B2	4.2	3	-	-	< 30	-
MW-L1	4.3	3	0 - 220	2	not sampled (Free LNAPL)	skimmer
MW-L2	4.1	3	0 - 2	2	not sampled (Free LNAPL)	-
MW-L3	6.2	3	0 - 608	13	not sampled (Free LNAPL)	skimmer
MW-L4	4.5	3	0 - 0.5	-	1,600	-

5.3.3 Instruments used in the field campaigns

The instrument used for both the purging of the well and the subsequent sampling phase was the portable multi-gas detector Eagle 2 (RKI Instruments Inc., California, USA). The purge was carried out with a flow rate of 0.9 L min^{-1} for 10 minutes. For the analysis of CH_4 and CO_2 the measurements were taken at the stabilization of the monitored concentrations, at a maximum of 5 minutes after the purge.

For the analysis of Rn activity an electronic active Rn monitor (RAD7, DURRIDGE Company Inc., Massachusetts, USA) was used. The detector is equipped with a built-in pump to collect a gas sample at a flow rate of 0.8 L min^{-1}, that decays inside the instruments chamber, producing positively charged progeny, used by a solid-state alpha detector to determine Rn activity. The Rn detector was connected to a small tube containing 30 grams of drierite (provided by DURRIDGE Co.), a desiccant that reduces the moisture content of the gas sample before it is pumped into the Rn monitor. Before the connection to the sampling line, a warm-up of the instrument of about 10 minutes is required, during which the internal pump runs continuously. As

suggested by the RAD7 instrument manual for soil gas analysis, the "Sniff" protocol was set for the measurements. This protocol involves readings (hereinafter referred to as cycles) of Rn activity every 5 minutes and the continuous operation of the instrument's pump. The 5 minutes measurement cycles were repeated for each well until a stabilization of the detected Rn activity was reached, for a total measurement duration for each point of about 30 minutes. To obtain a representative value of Rn activity at the investigated well, the first two five-minute readings were excluded, following the instrument manual's recommendation, while the last three measurement cycles were averaged.

Figure 5.4. Use of the Rad-7 Rn detector and Eagle 2 multi-gas analyzer.

5.4 RESULTS AND DISCUSSION

5.4.1 First campaign (site 1)

Table 5.3 provides a summary of the results obtained from the first field campaign carried out at site 1, in which the proposed method was applied in two monitoring wells and, for comparison, in two soil gas probes.

Table 5.3. Results of the first campaign carried out on site 1. The Rn mean activity and the standard deviation was calculated considering the results of the last three 5-minute Rn measurement cycles. The mean Rn deficit was calculated using Eq. 5.1, LNAPL saturation and the relative TPH concentration in the soil were calculated using Eq. 5.4 and Eq. 5.5, respectively. The method of uncertainty propagation was used to derive the uncertainty values for Rn deficit, LNAPL saturation and TPH concentration.

Parameter	Symbol	Unit	Soil gas probes		Monitoring wells	
			SGS-L	SGS-B	MW-L	MW-B
CH_4 concentration	CH_4	$\%_{vol}$	0.05	0	0.05 - 0.1	0.05
CO_2 concentration	CO_2	$\%_{vol}$	0.2 - 0.3	0.1	0.7	0.7 - 0.8
Radon mean activity	**Rn**	**Bq m^{-3}**	**7,604**	**8,206**	**6,362**	**7,768**
Radon standard deviation	σ Rn	Bq m^{-3}	1,819	1,058	406	560
Radon coefficient of variation	CV Rn	%	24	13	6	7
Radon deficit	**D**	**-**	**0.93 ± 0.34**		**0.82 ± 0.11**	
LNAPL saturation	**S_N**	**%**	**0.5 ± 2.53 ($K_{N/w}$ = 60)**		**0.78 ± 0.59 ($K_{N/w}$ = 60)**	
			1.09 ± 5.45 ($K_{N/w}$ = 30)		**1.68 ± 1.26 ($K_{N/w}$ = 30)**	
TPH concentration	**TPH**	**mg kg^{-1}**	**1,071 ± 5,376 ($K_{N/w}$ = 60)**		**1,656 ± 1,243 ($K_{N/w}$ = 60)**	
			2,307 ± 11,580 ($K_{N/w}$ = 30)		**3,567 ± 2,678 ($K_{N/w}$ = 30)**	

Specifically, for each monitoring point, the detected soil gas concentrations of CH_4, CO_2 and Rn are provided. The Rn activity reported in the table refers to the average activity obtained in the last three measurement cycles (the first two measurement cycles, as suggested by the manufacturer of the Rn instrument, were discarded). The standard deviation and the associated coefficient of variation of the three Rn measurement cycles are also reported as a reference. The Rn deficit (D) in the probes and monitoring wells was calculated based on the ratio of average activity obtained in the two areas using Eq. 5.1. The expected dilution factor was evaluated using Eq. 5.2. Considering sampling times of approximately 30 minutes for Rn measurement, with a flow rate of 0.8 L min^{-1}, and considering the geometry of site's wells (i.e., 4'' diameter, and 3.5 m height above the water table level), it was estimated a dilution factor of about 1.2, which was considered negligible. LNAPL saturation (S_N) and the relative TPH concentration in the soil (C) were calculated using Eq. 5.4 and Eq. 5.5, respectively. To derive the uncertainty values for Rn deficit, LNAPL saturation and TPH concentration the uncertainty propagation method was used.

In this campaign, the analysis of the gases associated with LNAPL depletion did not yield relevant information on the subsurface contamination, either in the probes or the wells. In particular, low values of CO_2 were observed at the site, both in the probes and the wells. This can be an indication of the absence of significant free-phase LNAPL in the monitored area, as this would result in higher concentrations of CO_2 or CH_4 due to hydrocarbon degradation processes. Consequently, the soil gas measurements did not exhibit distinctive patterns that would indicate the extent of contamination. However, Rn measurements proved to be informative in this regard, as it was observed that the Rn activities detected in the contaminated area were, on average, lower than those measured in the background zone. The deficit was approximately 90% in the soil gas probes and around 80% in the monitoring wells. Note that accounting for the standard deviation, the deficit values obtained in the soil gas probes result close to the unit or even higher, indicating that there is no statistically significant difference between the Rn activity values obtained from the background zone and the NAPL zone. The observed difference between the results obtained with the two systems could be attributed in part to the variation in contamination levels at the two measurement points (SGS-L and MW-L are approximately 10 m apart) and to the fact that Rn measurements in the wells reflect Rn activity at the depth likely to be affected by the presence of LNAPL (smear zone), whereas measurements in the soil

gas probes were taken at a vertical distance of nearly 2 m from the source zone. At this distance, the effect of Rn adsorption in the LNAPL could have been partially obscured due to Rn emissions from the clean soil layers between the impacted zone and the probe depth, also considering the typical characteristic diffusion length of Rn (Schubert et al., 2001; Cohen et al., 2019; De Miguel et al., 2020; Cecconi et al., 2022). It should also be noted that the data obtained from the wells exhibited smaller coefficients of variation (6-7%) compared to those measured in the soil gas probes (13-24%), indicating lower variability.

The fraction of LNAPL in the subsoil was estimated based on the observed Rn deficit, using Eq. 5.4. The latter equation requires site-specific measurements of water saturation in the NAPL-affected area. Since for site 1 this site-specific information is not available, an average literature value of water saturation, based on soil texture, was used. This implies that the same level of water saturation was assumed for both the background zone and the LNAPL-impacted zone (i.e. $S_w = S_{w,b}$). Specifically, for the application of Eq. 5.4 in the soil gas probes, a water saturation (S_w) of 0.144, determined as the ratio of soil moisture ($\theta_w = 0.054$) to soil porosity ($\theta_t = 0.375$) for a sandy soil (US EPA, 2004), was used. For the application of Eq. 5.4 in the groundwater monitoring wells, a water saturation (S_w) of 0.675, representative of the value expected in the capillary fringe for a sandy soil ($\theta_w = 0.253$ and $\theta_t = 0.375$), always according to the values provided by US EPA (2004), was instead adopted. Note that while this assumption may provide a reasonable estimate, it may not fully account for the variations in water saturation between the two zones, leading to some level of uncertainty in the results, i.e., assuming that water saturation in the contaminated area is reduced due to the presence of LNAPL, leading to a slight overestimation of LNAPL saturation. The Rn water-gas partition coefficient ($k_{w/g}$) was assumed equal to 0.25 (calculated at 20°C from (Kiliari and Pashalidis, 2008)).

The Rn NAPL-gas partition coefficient ($k_{N/g}$) was calculated as the product of $k_{w/g}$ and the NAPL-water partition coefficient $k_{N/w}$. Regarding the value of this last parameter, it should be noted that $k_{N/w}$ does not have a unique and recognized value. Considering the data mentioned in section 2.3.2, it was deemed appropriate to choose a range of values for $k_{N/W}$ between 30 and 60 for both diesel and gasoline, as also suggested by Le Meur et al. (2021). Based on these assumptions, the estimated average LNAPL fraction (S_N) was found to be between 0.5% and 1%, according to the results obtained

in the soil gas probes. Note that, as shown in Table 5.3, the variability of the Rn measurements for the soil gas probes brought to a high uncertainty in the estimation of LNAPL saturation and TPH concentrations. The S_N estimated from the average Rn data obtained for the monitoring wells was between 0.8 and 1.7% (see Table 5.3). TPH concentrations in the range of 1,500–3,500 mg kg^{-1} (see Table 5.3) were then obtained using Eq. 5.5, assuming a soil bulk density of 1.66 g cm^{-3} (US EPA, 2004) and NAPL density of 0.94 g cm^{-3} (density of a diesel mixture provided by Brost and De Vaull (2000)). These concentrations are higher than the saturation concentration (C_{sat}) typically expected for diesel contamination, which is in the range of 18 mg kg^{-1} (Brost and De Vaull, 2000). However, considering the residual concentration (C_{res}) value suggested by Brost and De Vaull (2000) for diesel and sandy soil, which is around 7,700 mg kg^{-1}, it can be inferred that the concentrations estimated using the Rn deficit technique are below this threshold. This result is consistent with the other field investigations (see Table 5.4).

Table 5.4. Comparison of different lines of evidence on LNAPL contamination at well MW-L at site 1.

Free LNAPL thickness (mm)		Groundwater TPH (µg L^{-1}) June 2020	TPH from soil samples (mg kg^{-1}) 2012	CO_2 (%vol) March 2021	CH_4 (%vol) March 2021	LNAPL saturation from Rn deficit (%) March 2021	TPH from Rn deficit (mg kg^{-1}) March 2021
Min - Max value 2018-2020	Last measure March 2021						
0 - 40	- (sheen)	16,100	~ 4,800	0.7	0.05 - 0.1	0.78 ± 0.59 ($K_{N/w}$ = 60) 1.68 ± 1.26 ($K_{N/w}$ = 30)	1,656 ± 1,243 ($K_{N/w}$ = 60) 3,567 ± 2,678 ($K_{N/w}$ = 30)

No measurable product thickness was indeed detected in MW-L with the water-oil probe, although traces of sheen were observed in the well water samples collected with a bailer, indicating the possible presence of residual immobile LNAPL in the saturated zone. Furthermore, soil samples taken during the site characterization (conducted prior to this work) in the survey carried out for the installation of MW-L, revealed concentrations of hydrocarbons C<12 of approximately 4,000 mg kg^{-1} and hydrocarbons C>12 of approximately 800 mg kg^{-1}, thus with a TPH concentration of

about 4,800 mg kg^{-1}. These values are consistent, although slightly higher, with those estimated from Rn deficits for the monitoring wells.

5.4.2 Second campaign (site 2)

The results obtained in the second campaign, using the proposed protocol in the headspace of the six selected monitoring wells of site 2, are presented in Table 5.5 and Table 5.6.

Table 5.5. Results of the first campaign carried out on site 2. The Rn mean activity and the standard deviation was calculated considering the results of the last three 5-minute Rn measurement cycles. The mean Rn deficit was calculated using Eq. 5.1, LNAPL saturation and the relative TPH concentration in the soil were calculated using Eq. 5.4 and Eq. 5.5, respectively. The method of uncertainty propagation was used to derive the uncertainty values for Rn deficit, LNAPL saturation and TPH concentration.

Parameter	Symbol	Unit	MW-B1	MW-L1	MW-L2	MW-L4
CH_4 concentration	CH_4	$\%_{vol}$	0.05	0.2	0.1	0
CO_2 concentration	CO_2	$\%_{vol}$	0	0.8	0.3	0
Radon mean activity	**Rn**	**Bq m^{-3}**	**85,167**	**48,867**	**43,000**	**43,400**
Radon standard deviation	σ Rn	Bq m^{-3}	4,336	3,686	1,732	2,946
Radon coefficient of variation	CV Rn	%	5	8	4	7
Radon deficit	**D**	**-**	**-**	**0.57 ± 0.07**	**0.50 ± 0.05**	**0.51 ± 0.06**
LNAPL saturation	**S_N**	**%**	**-**	**1.64 ± 0.49 ($K_{N/w}$ = 60)** **3.52 ± 1.04 ($K_{N/w}$ = 30)**	**2.16 ± 0.4 ($K_{N/w}$ = 60)** **4.65 ± 0.86 ($K_{N/w}$ = 30)**	**2.12 ± 0.51 ($K_{N/w}$ = 60)** **4.57 ± 1.11 ($K_{N/w}$ = 30)**
TPH concentration	**TPH**	**mg kg^{-1}**	**-**	**3,015 ± 894 ($K_{N/w}$ = 60)** **6,494 ± 1,925 ($K_{N/w}$ = 30)**	**3,980 ± 733 ($K_{N/w}$ = 60)** **8,573 ± 1,579 ($K_{N/w}$ = 30)**	**3,906 ± 946 ($K_{N/w}$ = 60)** **8,413 ± 2,038 ($K_{N/w}$ = 30)**

Table 5.6. Results of the second campaign, carried out on site 2, for the wells MW-B2 and MW-L3. The Rn mean activity and the standard deviation was calculated considering the results of the last three 5-minute Rn measurement cycles. The mean Rn deficit was calculated using Eq. 5.1 and LNAPL saturation was calculated using Eq. 5.4. The method of uncertainty propagation was used to derive the uncertainty values for Rn deficit and LNAPL saturation.

Parameter	Symbol	Unit	1° measure (morning)		2° measure (mid-day)		3° measure (afternoon)	
			MW-L3	MW-B2	MW-L3	MW-B2	MW-L3	MW-B2
CH_4 concentration	CH_4	$\%_{vol}$	1.2	0.1	1.3	0.15	0.65	0.35
CO_2 concentration	CO_2	$\%_{vol}$	0.7	0.5	0.8	0.3	0.4	0.1
Radon mean activity	**Rn**	**Bq m^{-3}**	**3,840**	**77,967**	**7,367**	**92,267**	**9,723**	**97,933**
Radon standard deviation	σ Rn	Bq m^{-3}	173	7,315	220	7,433	585	2,875
Radon coefficient of variation	CV Rn	%	5	9	3	8	6	3
Radon deficit	**D**	**-**	**0.05 ± 0.01**		**0.08 ± 0.01**		**0.10 ± 0.01**	
LNAPL saturation	**S_N**	**%**	**42.53 ± 6.21 ($K_{N/w}$ = 60)** **91.6 ± 13.38 ($K_{N/w}$ = 30)**		**25.39 ± 3.05 ($K_{N/w}$ = 60)** **54.69 ± 6.56 ($K_{N/w}$ = 30)**		**19.99 ± 1.99 ($K_{N/w}$ = 60)** **43.05 ± 4.28 ($K_{N/w}$ = 30)**	

As for the first campaign, the tables show the detected soil gas concentrations of CH_4, CO_2 and Rn activity for each monitoring point. It should be noted that the Rn activity values measured at site 2 are about one order of magnitude higher than those measured at site 1. The background Rn activity in soil gas can vary considerably between different locations, as it is the result of several mechanisms, all influenced by site-specific parameters. In particular, the main mechanisms that can affect Rn activity in soil gas, excluding migration processes in soil pores, are Rn generation from the decay of radium (influenced by radium content in rocks and soil and by its distribution), Rn emanation process (influenced e.g., by moisture, temperature and grain size), and Rn partitioning process between the soil phases (Nazaroff, 1992). This emphasizes the importance of measuring Rn activity in a background area for the application of the Rn deficit technique, as this value is strongly site-specific. For

this site as well, considering a well diameter of 4'' and a height of about 5 m above the water table, and considering the use of the same Rn detector with the same protocol as for site 1, the dilution factor from Eq. 5.2 is about 1.5 and can therefore be considered negligible.

Table 5.5 and Table 5.6 also show the deficits obtained for each monitoring point with contamination, in relation to the background Rn activity found in the background wells (see Eq. 5.1), together with the corresponding LNAPL saturation (see Eq. 5.4). For the determination of these latter value, values representative of a sandy clay were considered, since site-specific data were not measured. As for site 1, the same value of water saturation was assumed for both the background and the LNAPL-impacted zone. Specifically, a water saturation (S_w) of 0.92, determined as the ratio of soil moisture of the capillary fringe (θ_w = 0.355) to soil porosity (θ_t = 0.385) for a sandy clay soil (US EPA, 2004) was used. The Rn water-gas partition coefficient ($k_{w/g}$) was assumed equal to 0.25 (calculated at 20°C from Kiliari and Pashalidis (2008)) and the Rn NAPL-gas partition coefficient ($k_{N/g}$) was calculated as the product of $k_{w/g}$ and the NAPL-water partition coefficient $k_{N/w}$. As discussed in the previous section, $k_{N/w}$ was ranged between 30 and 60. Finally, a soil bulk density 1.63 g cm^{-3} (US EPA, 2004) and a NAPL density of 0.78 g cm^{-3} were used.

Referring to the results of the investigations performed in the background well MW-B1 and in the MW-L1, MW-L2 and MW-L4 wells in the contaminated zone (Table 5.5), it can be observed that some traces of CH_4 and CO_2 were observed in the wells located in the impacted zone, thus providing first evidence on the presence of LNAPL in these monitoring points. More robust evidence for the presence of LNAPL was instead provided by the average Rn activity found in the contaminated area, which resulted significantly lower (approximately half) than that found in the background. The TPH concentrations estimated from the Rn deficit (3,000 – 9,000 mg kg^{-1}) are in line with the residual concentration (C_{res}) of 10,000 mg kg^{-1}, indicated by Brost and De Vaull (2000) for silt to fine sand soil type contaminated by gasoline. Therefore, these results indicate the presence of residual LNAPL and potential free-phase LNAPL in the selected wells. This result is consistent with the investigations carried out in wells MW-L1 and MW-L2 (see Table 5.7), in which the occasional presence of mobile product was observed during the previous conventional groundwater monitoring (a few millimeters in the most recent).

Table 5.6 shows Rn activity and the concentrations of the other gases detected in the three measurements repeated within the same day in the headspace of the groundwater wells MW-B2 (background area) and MW-L3 (LNAPL zone). Elevated levels of CH_4 were observed in MW-L3, reaching up to approximately 1.3%vol, indicating the potential occurrence of methanogenesis processes commonly associated with areas contaminated with LNAPL. Note that also MW-B2 showed the presence of CH_4, although in lower concentrations compared to MW-L3. This suggests that petroleum hydrocarbons may be present even in areas considered not impacted by the contamination, which could result in an inaccurate assessment of the Rn background values for the area. The repeated measurements carried out during the day revealed a considerable Rn variability, with a tendency to increase during the day. This could be related to the increase in atmospheric temperature during the daytime hours, in agreement with observations by other studies (Minkin and Shapovalov, 2016; De Miguel et al., 2020; Barrio-Parra et al., 2021), who found a positive correlation between air temperature and Rn exhalation. This resulted in variability in the Rn deficit by a factor of about 2, with a value of 0.05 detected in the morning sampling compared to the value of 0.1 detected in the afternoon. It is first observed that these deficit values are rather pronounced. This could be due to the fact that the Rn measurements in the headspace of the wells were carried out at greater depth, closer to the area with LNAPL, compared to the more shallow measurements typically carried out with soil gas probes. Furthermore, measuring Rn in the headspace of a well that shows a layer of free product, could lead to a modification of Rn partition behavior. In particular, the observed deficit could be also influenced by the presence of free product in the well besides the residual saturation in the surrounding vadose zone. The pronounced deficit values detected have indeed led to the estimation of very high LNAPL saturations, especially in the first measurement in the morning (S_N estimates even exceeding 90%), that suggest that mobile LNAPL is present in the area of MW-L3. This conclusion is also supported by the elevated methane values detected in well MW-L3, as well as by the results of previous water monitoring campaigns (see Table 5.7).

Table 5.7. Comparison of different lines of evidence on LNAPL contamination at site 2.

MW	Free LNAPL thickness (mm)		Groundwater TPH (µg L^{-1}) Dec 2021	Active measures	CO_2 ($\%_{vol}$) 2022	CH_4 ($\%_{vol}$) 2022	LNAPL saturation from Rn deficit (%) 2022
	Min - Max value 2021	Last measure Dec 2021					
MW-L1	0 - 220	2	not sampled (Free LNAPL)	skimmer	0.8	0.2	1 – 4
MW-L2	0 - 2	2	not sampled (Free LNAPL)	-	0.3	0.1	2 – 5
MW-L3	0 - 608	13	not sampled (Free LNAPL)	skimmer	0.1 – 0.8	0.6 – 1.3	20 – 90 (Free LNAPL)
MW-L4	0 - 0.5	-	1,600	-	0	0	2 – 5

CHAPTER 6

6 APPLICATION OF SOIL GAS RADON DEFICIT TECHNIQUE USING PASSIVE DOSIMETERS IN GROUNDWATER MONITORING WELLS

ABSTRACT

The objective of this study was to develop and evaluate a methodology for the application of the Rn deficit technique in soil gas using passive dosimeters installed in the headspace of groundwater monitoring wells screened across the LNAPL smear zone, installed at sites with LNAPL presence. The design chosen for the application of the method is based on a recently proposed approach, based on application of the Rn deficit technique in soil gas using groundwater monitoring wells, using active portable Rn monitors. This configuration was chosen based on the promising, albeit preliminary, results obtained in the previous work, which showed that the use of groundwater monitoring wells has the potential to offer several improvements compared to the more traditional technique using soil gas probes. Despite the potential benefits, one of the main concerns that emerged from the previous work was the temporal variability of Rn concentrations detected in the headspace of groundwater monitoring wells using portable Rn detectors. In the approach proposed in this work, the use of passive equipment to carry out the Rn measurement in the headspace of the wells is evaluated, in order to reduce the influence of these oscillations on the effectiveness of NAPL detection and quantification. The field protocol is outlined and tested in a fist campaign conducted at a site in Italy affected by gasoline contamination. The results obtained were compared with the evidence of LNAPL presence in monitoring wells from traditional groundwater monitoring. Interpretation of the results showed that the area affected by the lowest Rn measurements corresponded well with the area of wells where the presence of free product was detected. The method appears therefore to be an affordable alternative to Rn monitoring with active instrumentation, although further investigation is required in order to use it for an accurate quantification of contamination.

6.1 INTRODUCTION

An alternative approach to the application of the soil gas Rn deficit technique, to identify LNAPL in the subsurface and obtain a quantitative estimate of its concentration, has recently been developed, tested, and proposed (Cecconi et al., 2023a). As also described in Chapter 5, this method involves monitoring Rn in the headspace of monitoring wells, typically already present at site impacted by LNAPL, using portable Rn analyzers. Although the number of experiments conducted was limited, the results were encouraging, highlighted how monitoring Rn in the headspace of wells can be a fast and minimally invasive screening method for the identification of areas impacted by LNAPL both in free and residual phase. On of the main advantages of this approach is that it allows for gas sampling in the unsaturated zone, closest to the NAPL source zone, which could result in a more accurate measurement of Rn at the area of interest. Some limitations were found in the quantitative estimation of the extent of contamination. One of the main uncertainties identified during the first tests was related to the temporal variability of the Rn activity concentrations monitored in the field. Significant variability in Rn values and estimated deficit (up to a factor of 2) was observed within the same day during the tests. It should be noted that these types of uncertainties are likely not related to the use of groundwater monitoring wells for the application of the method, since they have also been observed with the more traditional approach that comprise the use of temporary soil gas probes (Schubert and Schulz, 2002; De Miguel et al., 2020; Barrio-Parra et al., 2021). Daily fluctuations in Rn activities are partially influenced by atmospheric parameters, especially for measurements taken at shallow depths. Several authors have highlighted the influence of atmospheric and soil temperature on Rn concentrations measured in the field, assessing its significant effect on Rn concentrations (Schubert and Schulz, 2002; De Miguel et al., 2020; Barrio-Parra et al., 2021). If not addressed, these effects may lead to misinterpretation of the detected Rn deficits.

To consolidate the results obtained in these previous experiments and overcome the limitations associated with instant Rn measurement using portable equipment, additional activities were planned to test a new approach to Rn analysis in soil gas based on the use of passive dosimeters, based on solid-state nuclear track detectors (SSNTD), in the headspace of monitoring wells. Passive dosimeters are systems

composed of a small diffusion chamber and a sensitive element. The chamber allows the entry of gas by diffusion while prevents the entry of dust and Rn decay products. The sensitive element is constituted by a material (e.g., polyallyldiglycol carbonate or cellulose nitrate) sensitive to alpha radiation, also known as SSNTD. Rn, decaying inside the device, produces alpha radiation that creates traces (tracks) in the sensitive material structure (Nikezic and Yu, 2004). The density of the tracks, analyzed in laboratory, is directly proportional to the Rn concentration of the environment in which the SSNTD was exposed, and to the exposure time (Khan et al., 1993). This type of equipment has already been tested for the application of the Rn deficit technique, although with a different configuration, involving the exposure of the SSNTD in PVC containers buried in the soil at a depth of 0.7 - 1 m from the surface (Schubert et al, 2005, Mateus and Pecequilo, 2015).

This work describes the field methodology adopted for the installation of passive dosimeters for the measurement of Rn in the headspace of wells for the long-term monitoring of Rn activity concentrations, to be used for the identification and quantification of LNAPL in the subsurface. It also describes the activities carried out in the month of June 2023 for a first application of this approach in a gasoline-contaminated site located in Italy. The activity consisted in the installation of the passive dosimeters in the headspace of 14 wells of the site, its subsequent removal at the end of the exposure time, and in the interpretation of the average Rn concentration data (provided by a specialized laboratory) together with its comparison with the evidence of LNAPL presence in the monitoring wells obtained from traditional groundwater monitoring.

6.2 MATERIALS AND METHODS

6.2.1 Field protocol

This section provides a detailed description of the procedure used to apply the soil gas Rn deficit technique, to assess LNAPL contamination, by monitoring Rn in the headspace of groundwater monitoring wells using passive dosimeters. The method design closely follows that described in the previous chapter (section 5.2.1) (Cecconi et al., 2023). As with the previous configuration, this approach is applicable to sites with wells that have a portion of their screen in the vadose zone, installed in both the LNAPL zone and the uncontaminated zone. It is assumed that the site is characterized by a typical LNAPL distribution that includes the presence of NAPL not only in groundwater, but also in the capillary fringe and some portion of the vadose zone. A schematic of the method is shown in Figure 6.1.

The main difference with the approach previously followed is the instrumentation and measurement method used, which affects the time required to obtain the result. In fact, passive Rn monitoring involves the use of devices that are placed in contact with the environment to be monitored for a given period of time. At the end of the exposure, the dosimeter is analyzed in a specialized laboratory to determine the average Rn concentration over the exposure period. The operating procedure involved placing dosimeters in the headspace of monitoring wells located in both contaminated (with the presence of free or residual LNAPL) and uncontaminated areas of the site. The devices were placed in the headspace of the screened interval of the well, above the piezometric level. The well headspace was sealed with appropriate end caps throughout the exposure period. The activities required the presence of operators at the site for two days: the first dedicated to positioning the dosimeters, and the second day to retrieving them.

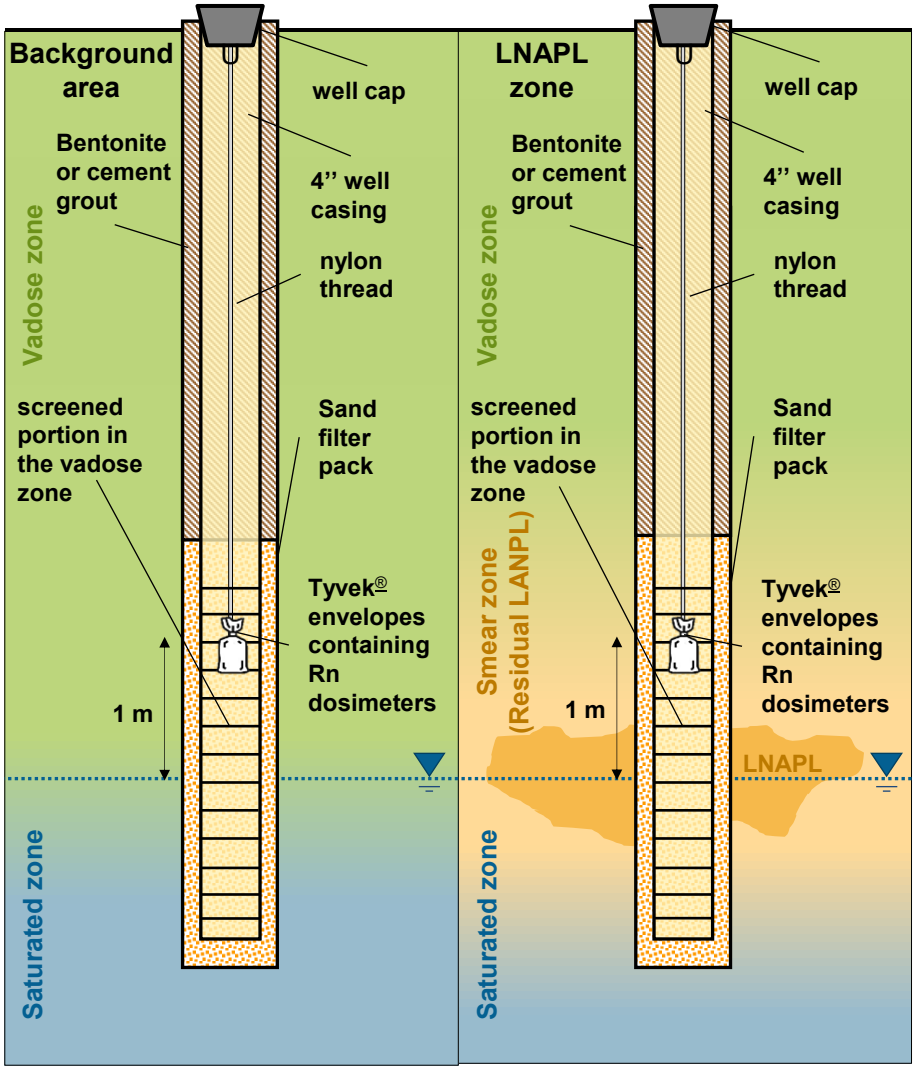

Figure 6.1. Schematic of the method for the application of the Rn deficit technique in monitoring wells, located both in the LNAPL area and background zone, using passive dosimeters.

The protocol used to position the dosimeters at the site is described below:

- A nylon thread is cut to the appropriate length to allow the instrument to be exposed to the desired depth in the well. The thread is connected at one end to the well plug (4" PVC expansion plug with isoprene seal) and at the other end to a stainless-steel carabiner (Figure 6.2).

Figure 6.2. 4" PVC expansion well plug used to seal the head of the well and connection to the dosimeter with a nylon thread and a stainless steel carabiner.

- The cap of the well to be monitored is opened.
- To prepare the dosimeter for use, its own protective bag is opened at the time of use and the device is attached to the carabiner. It is then placed in a Tyvek envelope to protect it from dust and moisture, along with silica gel (for additional moisture protection). The envelope is sealed with tape. As recommended by the manufacturer, the protective bag of the dosimeter should be kept to store it at the end of the exposure period.
- The dosimeter, inside the Tyvek bag, is inserted into the headspace of the well to be monitored (Figure 6.3) up to a depth that allows it to be exposed at the beginning of the screened zone of the well, and above the water table level, in order to ensure measurement in the gas phase without reaching the water table. When the dosimeter is inserted, in addition to the identification

number of each device, the date and time of the start of the exposure are recorded.

- The well is sealed with the plug to which the dosimeter is connected.

The exposure time of each dosimeter in the well headspace should be selected by considering the measurement range of the analytical method used by the specialized laboratory (as indicated by the instrument supplier) and the maximum Rn concentration values expected at the site under investigation.

Figure 6.3. Installation of the dosimeter, enclosed in Tyvek protection, in the headspace of the well.

The following procedure was used to retrieve the dosimeters:

- The well plug, used as a wellhead seal and for attaching the dosimeters, is opened, and the envelope containing the dosimeter is retrieved from the well.

- the Tyvek bag is opened, and the dosimeter is removed and immediately stores in the protective bag provided by the manufacturer of the devices. At the time of extraction, in addition to checking the identification number of each device, the date and time of the end of exposure shall be recorded (to be provided to the laboratory for the elaboration of the data).

- The well is again sealed with its own cap.

For the test site, the dosimeters were installed in the wells at a depth of 3 m from the ground surface, as the depth of the groundwater table at the site is about 4 - 5 m. In a selected number of wells, a second dosimeter was also placed in the same Tyvek envelope at a depth of 3 m as a blind duplicate (Figure 6.4). Additionally, in a selected number of wells, a second nylon thread was also attached to the plug to expose a second dosimeter (again in a Tyvek envelope with silica gel) at a depth of 1.5 m from ground level, in the blind portion of the well.

The dosimeter used for the field test were Radout® CR-39. These devices consist of a Radout® model external plastic frame designed by Mi.am S.r.l. and contain a CR-39 type passive Solid State Nuclear Tracks Detector (SSNTD), which is the sensitive part of the device. Rn diffuses into the device and the alpha radiation resulting from the decay of Rn and its progeny (Po-218 and Po-214) damages the structure of the detector, creating visible "tracks" that are counted during the analysis. The number of tracks is proportional to the concentration of Rn gas in the environment and the exposure time. The CR-39 detectors have been analyzed in the Mi.am laboratories using the Politrack® automated system developed by Mi.am in collaboration with the Politecnico di Milano.

Figure 6.4. Dosimeter and double blind connected to the carabiner.

6.2.2 Interpretation of Rn data

To interpret the Rn data obtained in the Rn monitoring field campaign, the same approach as described in section 5.2.2 can be used. Specifically, the Rn deficit can be determined using Eq. 5.1, and from that, the fraction of NAPL in the area and the relative TPH concentration are estimated using Eq. 5.4 and Eq. 5.5, respectively. For more details and for the specific equations, please refer to section 5.2.2.

6.3 FIELD TESTS

To evaluate the effectiveness of the method, the described protocol was applied in a field campaign conducted in June 2023 at a contaminated site in Italy.

6.3.1 Site description

The site selected for the first test was subject to a contamination event due to the leakage of a tank used for the storage of gasoline. In order to verify the qualitative state of the environmental matrices, the site was therefore subjected to an environmental characterization between 2020 and 2021, which involved the drilling of 27 boreholes, of which 20 were equipped with wells.

Some surveys have detected the presence of BTEX, light hydrocarbons C ≤ 12 and heavy hydrocarbons C > 12 in the unsaturated soil. In particular, for light hydrocarbons C ≤ 12, in the surveys equipped with wells MW7, MW11 and in the surveys S4, S6 (Figure 6.5) were found concentrations higher than the contamination threshold concentrations (in Italian *Concentrazione Soglia di Contaminazione,* CSC) in the context of contaminated sites in Italian legislation (Col. B, Tab.1, All.5, Part IV, Title V of the Legislative Decree 152/06)

During the groundwater monitoring campaign in March 2023, the presence of Total Petroleum Hydrocarbons (TPH), again higher that the relative contamination threshold concentrations CSC value, was detected in wells MW9 and MW10. Supernatant product was also found in groundwater wells MW3, MW5, MW7, MW8, MW11 and MW20 (Figure 6.6).

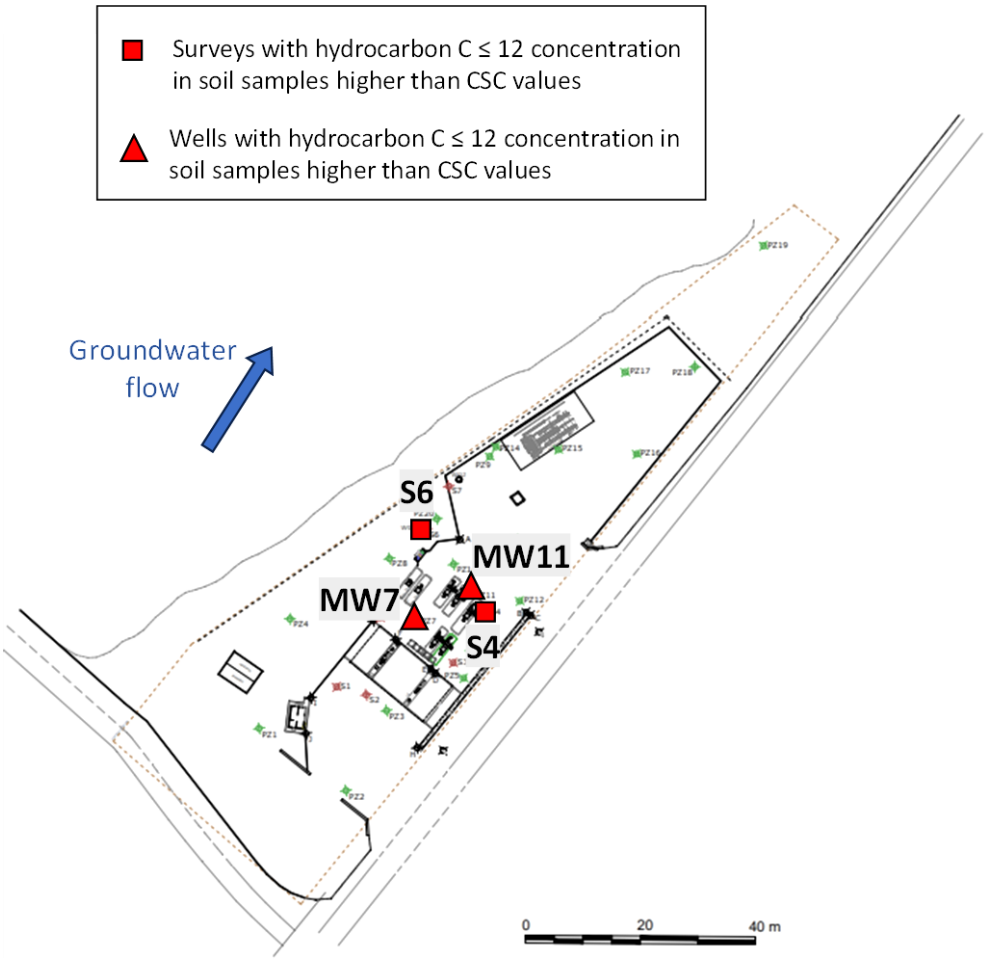

Figure 6.5. Surveys that revealed concentrations exceeding the CSC values in soils for the parameter hydrocarbons C≤12.

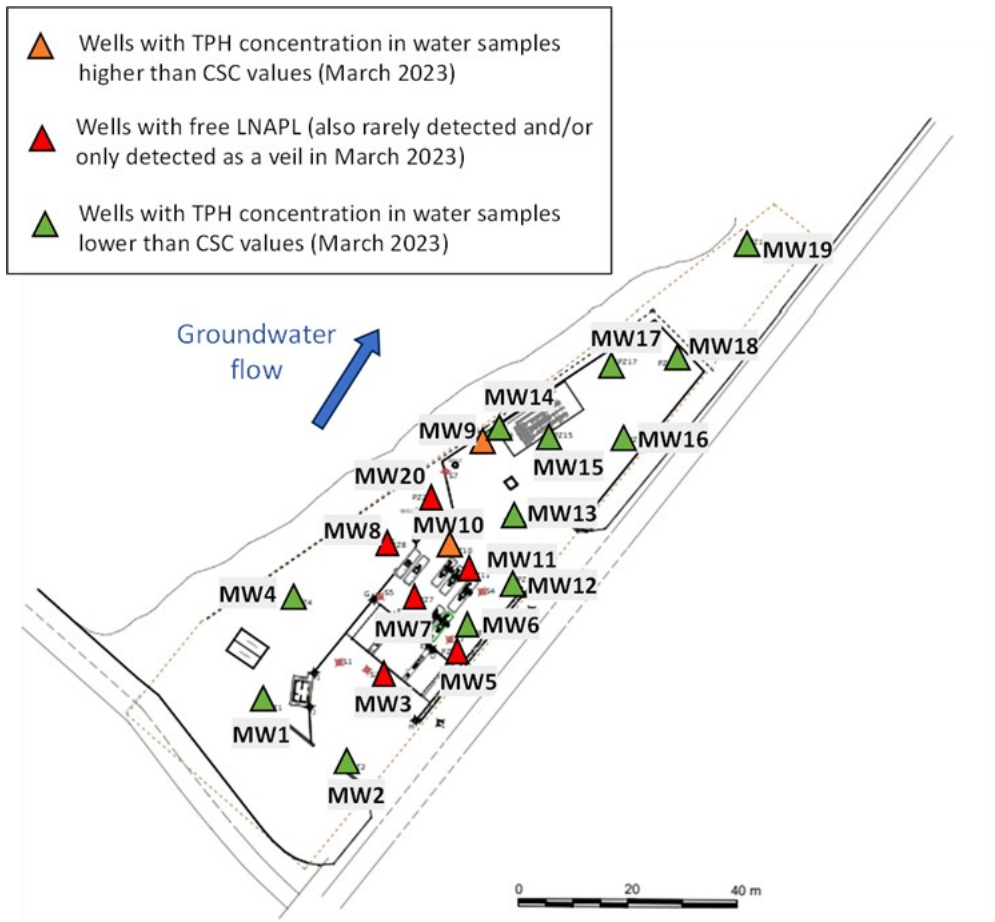

Figure 6.6. Groundwater wells that revealed concentrations exceeding the CSC values in soils for TPH, and wells in which free product was detected, in March 2023.

The data on the characteristics of the available wells on the site are shown in Table 6.1, in terms of concentrations of hydrocarbons analyzed in soil samples, in groundwater samples (in the most recent water monitoring campaign) and the eventual presence of a free product. Table 6.1 also shows the depth of the water table measured during the most recent groundwater monitoring campaign and the resulting thickness of the screened portion of the well in the unsaturated zone, obtained from the depth of the water table and the properties of the screen (starting at 3 m above ground level for all the wells at the site).

It should be noted that in the fall of 2021, active skimmers were installed in MW3 and MW7 wells, electro-submersible pumps were installed in MW8, MW13, MW14 and MW20 wells, while a total fluid pump was installed in MW11.

Table 6.1. C≤12 and C>12 hydrocarbons (HC) and Total Petroleum Hydrocarbons (TPH) concentrations and characteristics of monitoring wells (MW). < loq indicates cases with concentrations below the limit of quantification.

MW	Soil HC C≤12 (mg kg^{-1}) max at 3-7 m	Soil HC C>12 (mg kg^{-1}) max at 3-7 m	Water TPH (µg L^{-1}) 23/3/23	Free LNAPL (mm) 24/5/23	Free LNAPL (mm) max 2021-2023	Water table level (m b.g.l.) 24/05/23	Screened portion in unsaturated zone (m) 24/05/23
1	< loq	13.4	<30	0	0	4.650	1.65
2	< loq	10.7	<30	0	0	4.385	1.39
3*	23.8	82	LNAPL	2	274	4.644	1.64
4	< loq	10.7	<30	0	2	5.054	2.05
5	14.2	13.1	LNAPL	1	2	4.373	1.37
6	49	42	260	0	2	4.253	1.25
7*	420	580	LNAPL	2	608	4.717	1.72
8**	12	89	LNAPL	0	1	4.853	1.85
9	38	131	520	0	0	4.847	1.85
10	133	179	9,500	0	4	4.758	1.76
11*	630	600	LNAPL	2	56	4.634	1.63
12	< loq	21.5	<30	0	0	4.157	1.16
13**	8.3	32	48	0	1	4.047	1.05
14**	223	49	<30	0	0	4.974	1.97
15	< loq	10.1	<30	0	0	4.372	1.37

MW	Soil HC C≤12 (mg kg^{-1}) max at 3-7 m	Soil HC C>12 (mg kg^{-1}) max at 3-7 m	Water TPH (µg L^{-1}) 23/3/23	Free LNAPL (mm) 24/5/23	Free LNAPL (mm) max 2021-2023	Water table level (m b.g.l.) 24/05/23	Screened portion in unsaturated zone (m) 24/05/23
16	< loq	< loq	<30	0	1	4.325	1.33
17	< loq	< loq	<30	0	1	4.493	1.49
18	< loq	14.5	<30	0	0	4.615	1.62
19	< loq	18.4	<30	0	1	4.463	1.46
20**	237	215	LNAPL	0	5	5.547	2.55

* skimmer
** electro-submersible pump
*** total fluid pump

The site has a heterogeneous stratigraphy, with a superficial layer of sand/gravel fill up to approximately 2 meters from the surface. Below this, there is a layer of compact silt or clay with possible inclusions of medium sand layers, fine and gravel, up to approximately 12 meters from the ground level, resting on a layer of clay. The average depth of the water table from the ground level is approximately 4 - 6 meters.

6.3.2 Field activities

The field test, conducted on June 22 and 27, 2023, consisted of Rn passive monitoring in the headspace of 14 selected wells at the site. The exposure time of each dosimeter was chosen based on the measurement range of the test method used by the specialized laboratory. Based on the values provided by the laboratory and the maximum expected Rn activity at the site, as determined by previous portable instrument Rn analysis, a monitoring period of 5 days was deemed appropriate.

On June 22, 2023, the dosimeters were installed following the protocol outlined in section 6.2.1. A total of 25 devices were installed on the site:

- In 14 groundwater monitoring wells, denominated MW1, MW2, MW3, MW4, MW5, MW6, MW7, MW8, MW9, MW10, MW11, MW12, MW16 and MW18, a

dosimeter was installed at a depth of 3 m from ground level (at the beginning of the screened portion of the well and above the water table level).

- In 7 of the selected monitoring wells (MW4, MW5, MW8, MW9, MW11, MW12, MW18), a second dosimeter was inserted in the same Tyvek bag at a depth of 3 m as a blind duplicate (a duplicate to which a fictitious name was assigned before sending the dosimeter to laboratory for Rn analysis).
- In 4 of the wells (MW2, MW3, MW5, MW7), a dosimeter was also exposed to a depth of 1.5 m from ground level in the blind section of the well.

Figure 6.7 shows the location of the groundwater wells selected for the monitoring campaign, and Table 6.1 presents their characteristics.

On June 27, 2023, the retrieval operations for the previously installed dosimeters were carried out following the protocol described in section 6.2.1. The dosimeters were sent to a specialized laboratory for analysis of Rn decay traces on the sensitive element of the device and for the quantification of Rn concentration in the headspace of the well in which the dosimeter was exposed, in accordance with the supplier’s indications.

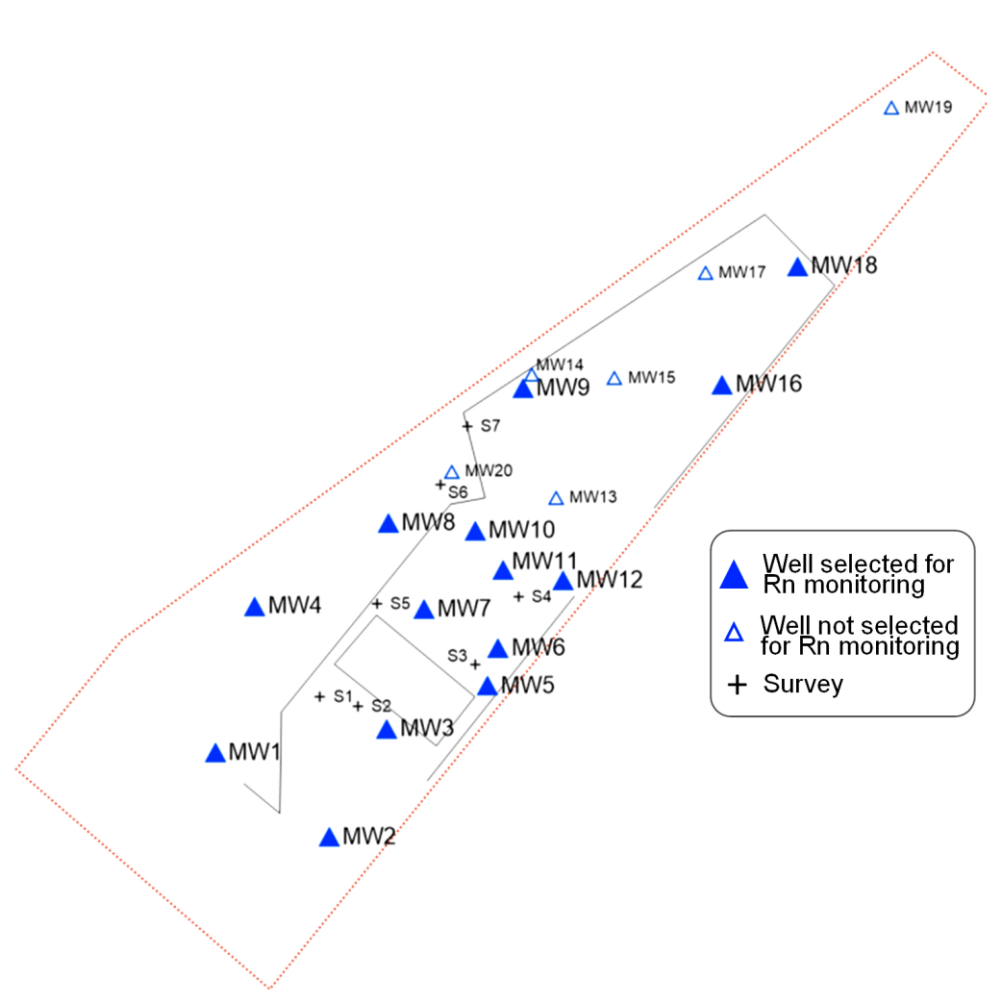

Figure 6.7. Wells selected for the monitoring campaign using passive dosimeters.

6.4 RESULTS AND DISCUSSION

The results of the test carried out are shown in Table 6.2 in terms of Rn exposure (kBq h m^{-3}) and Rn activity concentration (Bq m^{-3}). It can be observed that Rn concentration values obtained in the headspace of the wells at the greatest depth of investigation (3 m b.g.l.) are on average higher than those observed at a depth of 1.5 m. Since the wells are screened from 3 m b.g.l., it is likely that the results obtained at 1.5 m are not indicative of Rn activities at that depth in the subsurface. These results therefore highlight the significance of the dosimeter's location within the wells headspace to obtain a representative estimate of Rn emissions from the subsoil. Note that further data evaluation in this chapter refers to the data obtained at 3 m depth from ground level, corresponding to the screened area of the wells. In terms of data variability, it can be observed the standard deviation compared to the mean value is quite small, as the coefficients of variation, calculated as the ratio between the standard deviation and the mean value of Rn activities, typically fall below 20%. The measurements replicability is confirmed by consistent values obtained in the blind duplicates (indicated with an asterisk), with maximum coefficients of variation of 7%.

Table 6.2. Dosimeter exposure points, exposure times, and average Rn concentrations provided by the specialized laboratory.

MW	Depth (m b.g.l.)	Start time 22/6/23	End time 27/6/23	Rn exposure (kBq h m^{-3})	Mean Rn Activity (Bq m^{-3})	Standard deviation (Bq m^{-3})
1	3	11:15	12:40	14,472	**119,600**	19,480
2	1.5	11:21	10:45	15,898	**133,597**	21,752
2	3	11:21	10:45	21,666	**182,065**	29,631
3	1.5	14:19	13:15	3,717	**31,236**	5,137
3	3	14:19	13:15	5,731	**48,159**	7,882
4	3	14:35	12:34	11,404	**96,641**	15,753
4*	3	14:35	12:34	11,017	**93,366**	15,222
5	1.5	12:25	11:26	2,786	**2,412**	3,868

MW	Depth (m b.g.l.)	Start time 22/6/23	End time 27/6/23	Rn exposure (kBq h m^{-3})	Mean Rn Activity (Bq m^{-3})	Standard deviation (Bq m^{-3})
5	3	12:25	11:26	6,003	**50,443**	8,253
5*	3	12:25	11:26	5,814	**48,857**	7,996
6	3	11:04	12:30	12,670	**104,708**	17,058
7	1.5	13:20	12:23	8,859	**74,446**	12,148
7	3	13:20	12:23	11,279	**94,785**	15,448
8	3	13:00	11:40	13,399	**113,548**	18,497
8*	3	13:00	11:40	13,545	**114,788**	18,698
9	3	11:56	11:06	17,382	**144,847**	23,566
9*	3	11:56	11:06	15,835	**131,957**	21,474
10	3	12:13	12:10	17,860	**148,832**	24,216
11	3	12:42	12:05	1,948	**16,233**	2,704
11*	3	12:42	12:05	1,799	**14,993**	2,503
12	3	11:00	11:59	19,215	**160,124**	26,061
12*	3	11:00	11:59	19,627	**163,561**	26,619
16	3	10:45	11:47	20,619	**170,409**	27,729
18	3	10:41	11:14	12,509	**103,379**	16,845
18*	3	10:41	11:14	12,232	**101,094**	16,475

* blind duplicate

The Rn activity concentration values obtained from the wells at a depth of 3 m below the surface are reported in Table 6.3.

Table 6.3. Rn deficit values obtained using Eq. 5.5, from Rn activity concentrations shown in Table 6.2. For the blind duplicates the mean Rn activity obtained from the two exposed devices, is shown. As Rn background activity concentration, the mean Rn activity between MW1 and MW2 was considered.

MW	Mean Rn Activity (Bq m^{-3})	Rn deficit (-) (obtained from background Rn value*)
1	119,600	**-**
2	182,065	**-**
3	48,159	**0.319**
4	95,004	**0.630**
5	49,650	**0.329**
6	104,708	**0.694**
7	94,785	**0.628**
8	114,168	**0.757**
9	138,402	**0.918**
10	148,832	**0.987**
11	15,613	**0.104**
12	161,843	**1 (1.073)****
16	170,409	**1 (1.130)****
18	102,237	**0.678**

* mean Rn activity concentration between those obtained in wells MW1 and MW2
** mean Rn values similar to the ones considered as the site background

These values were mapped onto the site under investigation, as shown in Figure 6.8. For wells MW4, MW5, MW8, MW9, MW11, MW12, and MW18, in which a blind duplicate was inserted, the average of the values obtained from the two exposed devices, both representative of the analyzed point, is considered. The map highlights

an area, marked by colors tending towards red, corresponding to wells MW3, MW5, MW7, and MW11, where the Rn concentration values are significantly lower than the higher values of the areas (shown in blue) corresponding to MW1 and MW16.

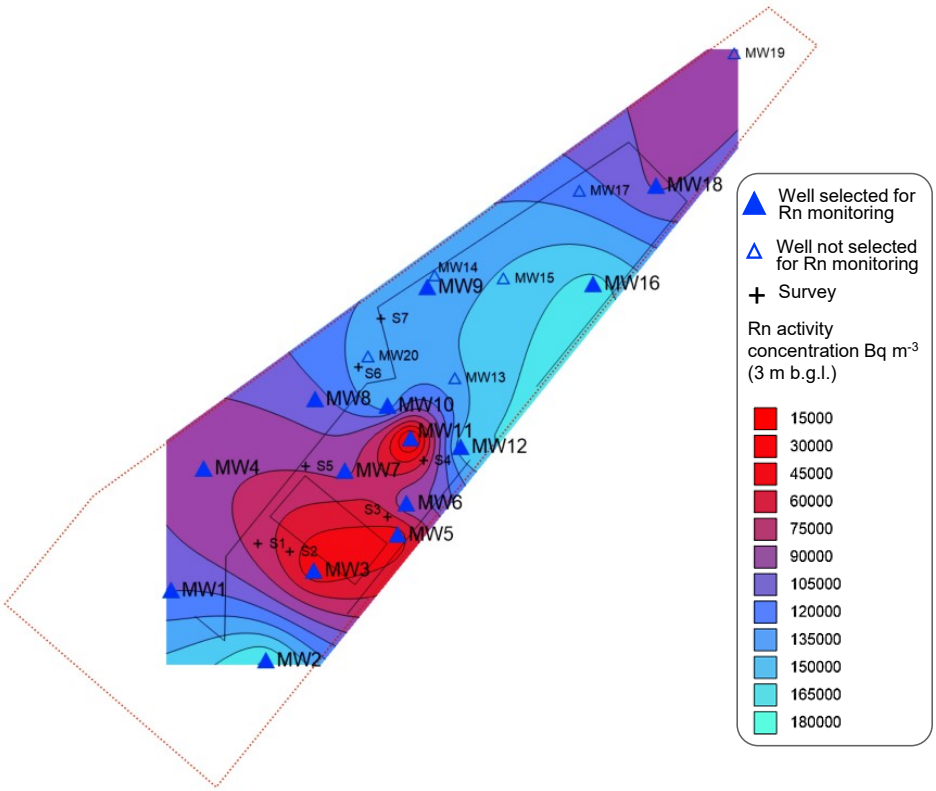

Figure 6.8. Map of Rn activity concentrations (Bq m^{-3}) obtained from Rn monitoring, in the headspace of groundwater monitoring wells, at 3 m from ground level, using passive dosimeters.

Rn deficit values were obtained for each monitored point by comparing the observed Rn concentrations at a depth of 3 m from ground level to the background values. The background values considered for the examined site were those obtained in the wells that were not affected by hydrocarbon contamination and were located upstream of the area where LNAPL and/or hydrocarbons were found in water. In particular, the mean Rn concentrations obtained at 3 m from ground level in wells MW1 and MW2 was chosen as the reference value for Rn activity concentration in the background zone (see Figure 6.7 and Table 6.1, respectively, for the location and characteristics of the wells). The difference between the two Rn activity concentration values in the two wells selected as background could be due to the stratigraphic heterogeneities

characterizing the site. The geology of the site in fact is characterized by an alternance of gravel and silty clays or silty sands layers.

The deficit values were obtained using Eq. 5.5, and are reported in Table 6.3. The deficit values were mapped on the site, as shown in Figure 6.9. As can be observed, the higher deficit values, those approaching zero (reported in red-violet) were observed in the area of the wells MW3, MW5 and MW11. Figure 6.9 also shows the map of the thickness of the free LNAPL measured in the wells at the site in the groundwater monitoring campaign carried out in May 2023 (24/05/2023). The comparison of the two maps shown in the figure reveals a strong correlation between the areas affected by the free product (albeit with a thickness of a few millimeters) and the areas with a more pronounced Rn deficit. Specifically, the contaminated area appears to correspond with wells MW3, MW5, MW7, and MW11. Furthermore, Eq. 5.1 allows to estimate, from the observed Rn deficits in the contaminated area (D), the fraction of NAPL in an unsaturated soil with a degree of water saturation in the background area $S_{w,b}$ and the water saturation in the area with LNAPL S_w (calculated as the ratio between soil moisture θ_w and soil porosity θ_e in the two areas). For the site under investigation, in particular, the same value of water saturation (S_w = 0.512) was considered for both areas, assuming a sandy-clay soil texture for the entire area (θ_w = 0.197 and θ_e = 0.385; source US EPA, 2004).

A Rn partition coefficient of approximately 0.23 was calculated as the inverse of the dimensionless Henry constant at 25°C of approximately 4.4 (Lee et al., 2010) between water and soil gas ($k_{w/g}$). For gasoline, a Rn partition coefficient between LNAPL and water ($k_{N/w}$) of approximately 40 was assumed (Le Meur et al., 2021). The value of the Rn partition coefficient between LNAPL and soil gas ($k_{N/g}$), of approximately 9, was obtained as the product of $k_{w/g}$ and $k_{N/w}$.

To derive TPH concentrations, by Eq. 5.5, a soil density ρ_s of 1.63 kg L^{-1} (USEPA, 2004), a LNAPL density ρ_N of 0.780 kg L^{-1} (Brost and De Vaull, 2000), and an effective porosity θ_e of 0.385 (USEPA, 2004) were considered for a sandy clay soil.

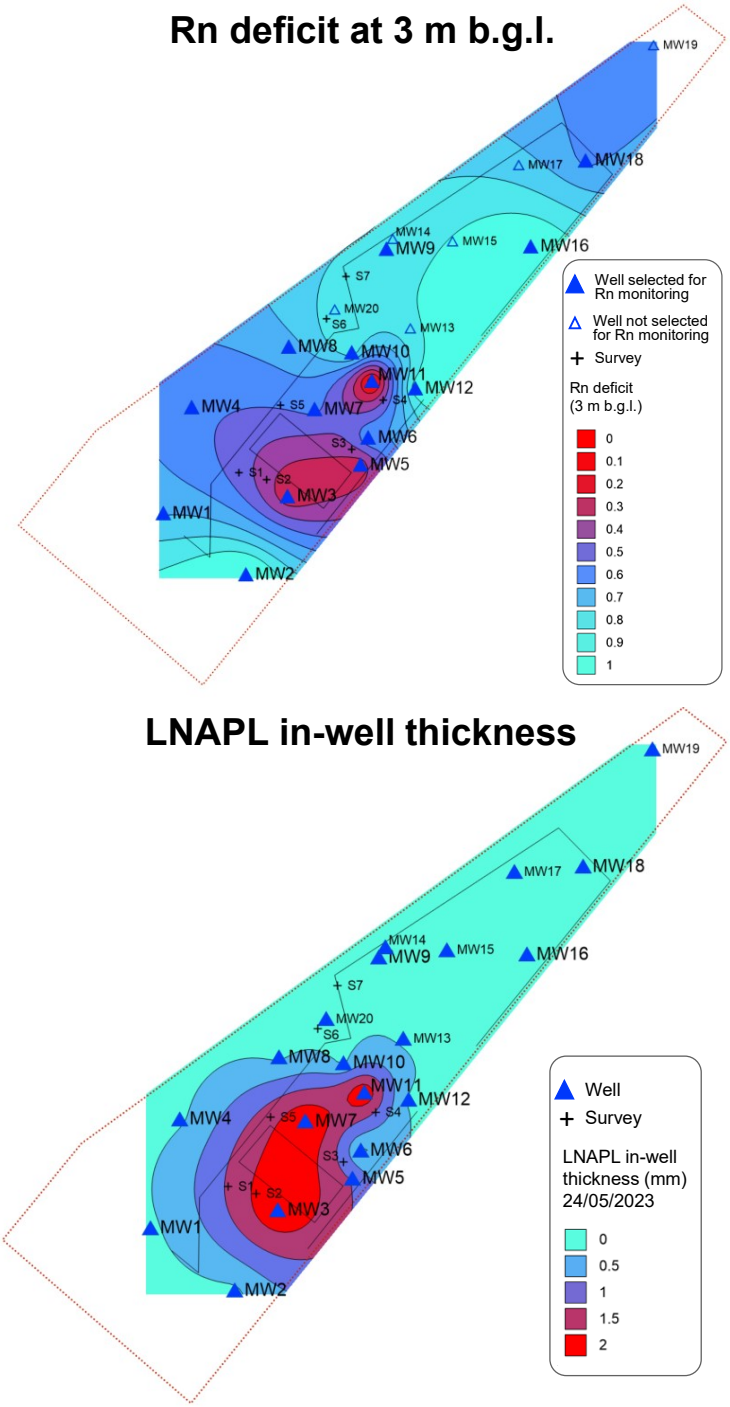

Figure 6.9. Top: Map of the deficit Rn values obtained with Rn monitoring in the headspace of groundwater monitoring wells at 3 m b.g.l., carried out from 22/06/2023 to 27/06/2023. Bottom: map pf the free LNAPL thickness observed in the wells in date 24/05/2023.

Table 6.4 shows the values obtained in terms of LNAPL saturation and TPH concentrations, using equations 2 and 3, respectively, in the areas identified as affected by the presence of the product (MW3, MW5, MW7 and MW11). It should be noted that in MW11 two dosimeters were exposed to the same depth (blind duplicate), therefore the Rn concentration for the well refers to the average between the two values provided by the analytical laboratory. To determine the deficit, we used the average of the values observed in MW01 and MW02, which was 150832 Bq m^{-3}, as the reference background concentration.

Table 6.4. Estimation of LNAPL saturation (Eq. 5.4) and total petroleum hydrocarbon (TPH) concentrations (Eq. 5.5) in the zones identified as affected by the free LNAPL. The mean background concentration (average between MW01 and MW02) is 150832 Bq m^{-3}

MW	Mean Rn activity (Bq m^{-3})	Rn deficit (-)	LNAPL saturation (%)	TPH (mg kg^{-1})
	Rn	D	S_N	C
3	48,159	0.319	15.9	29,351
5	49,650	0.329	15.2	28,056
7	94,785	0.628	4.4	8,140
11	15,613	0.104	64.7	119,233

The estimated TPH concentrations can be compared to the reference values of residual concentration (C_{res}), which represents the mechanical absorption capacity of the soil, beyond which the free product becomes mobile and can generate the presence of floating LNAPL in the wells. The TPH concentrations estimated from the Rn deficit (8,000-30,000 mg kg^{-1}) exceed the C_{res} of 10,000 mg kg^{-1}, as indicated by API (2000) for silt to fine sand soils contaminated by gasoline. These results suggest the presence of LNAPL as free phase in the investigated wells, which is consistent with the results of the traditional groundwater monitoring (a few millimeters of LNAPL were identified in the examined wells). The quantitative data regarding the extent of contamination in the mentioned wells should be considered a rough estimate due to the heterogeneous geological nature of the site, which can affect Rn activities. Additionally, the active interventions in some of the selected points, such as the

skimmer in wells MW3 and MW7 and the total fluid pump in the MW11 monitoring well, can also influence the state of contamination.

Based on these results, it appears that the two different lines of evidence based on the thickness of the free product in the wells, and Rn monitoring, are in agreement, confirming that the tested approach for the application of the Rn deficit technique is suitable, from a qualitative point of view, for defining areas with the presence of LNAPL. The same approach described in section 5.2.1, to derive a quantitative estimation of the entity of the contamination, can also be used with this alternative field approach, and it provided results consistent with other lines of evidence. Although this approach excluded uncertainty related to temporal oscillations of Rn activities detected in the subsoil, the quantitative data obtained should still be considered an estimate rather than accurate values due to the remaining uncertainties related to the heterogeneities of the subsoil, which are strictly site dependent.

CONCLUSIONS

This thesis examined the topic of the soil gas Rn deficit technique as a tool to identify and quantify LNAPL contamination in the subsurface. This document first provides an overview on the issue of characterization of petroleum hydrocarbon contaminated sites with the presence of LNAPL (Chapter 1), and a focus on theoretical and technical aspects of Rn deficit method as well as a review of the literature on practical approaches in the vadose zone (Chapter 2). As a contribution to the current scientific knowledge on the topic, further research was conducted to refine the analytical modeling of Rn transport in soil gas, to aid in the interpretation of Rn deficit data (Chapters 3 and 4). Based on the results of the modeling efforts, new approaches for applying the technique in the field were defined and tested (Chapters 5 and 6).

MODELING WORKS

MODELING OF SOIL GAS RADON AS AN IN SITU PARTITIONING TRACER FOR LNAPL CONTAMINATION

The results obtained with the first modeling work (Chapter 3) (Cecconi et al., 2022) showed that the parameter that most affects the effectiveness of the Rn deficit technique using soil gas data for the quantification of the NAPL content in the subsurface is the distance of the soil gas probe from the source zone. At distances higher than 2 m the method is indeed not more sensitive to the presence of LNAPL and for distances higher than 1 m the method can provide only a qualitative evidence on the presence of NAPL as even small uncertainties associated to the deficit can result in significant variation of the estimated NAPL content. These results are ascribed to the characteristic diffusion length of Rn that is typically less than 1 m. In this view, to ensure a direct measurement of the Rn soil gas concentrations within the source zone, the measurement of the headspace of groundwater monitoring wells used in other applications (e.g., see Sweeney and Ririe, 2017) could be a good alternative to permanent or temporary soil gas probes. To a lower extent, also the soil texture and the type of contamination (e.g., diesel or gasoline) can affect the expected Rn profiles above the source of contamination. Thus, for an accurate estimation of the NAPL content these two aspects should be carefully examined and identified. Other

parameters such as the thickness of the source zone or the depth of the water table do not significantly affect the estimated NAPL content. Thus, the nomographs provided in this work, which allow the estimation of NAPL saturation as a function of the distance of soil gas probes from the source zone and of the type of soil and contamination, are generally applicable to all sites involving relatively homogenous soils. Conversely, in the case of heterogeneous soils involving geological barriers or stratified contaminations, more sophisticated numerical model should be preferred (see e.g., Cohen et al. (2019)). The presence of heterogeneous layers can indeed influence the migration and distribution of Rn in the subsurface making the application of the deficit technique more complicated. Other aspects not addressed in this work are the diurnal and seasonal variations that can be expected in shallow soil gas samples because of barometric pumping. In this view, the results obtained in this work should be used for soil gas data collected at depths greater than 1 m where these effects become less relevant (Neznal et al., 2004).

INFLUENCE OF ADVECTION ON THE SOIL GAS RADON DEFICIT TECHNIQUE

The modeling work was further developed by simulating also less traditional scenarios where the influence of Rn transport by advection becomes non-negligible compared to that by diffusion. The analytical modeling work presented in Chapter 4 (Cecconi et al., 2023b) highlighted that for most of the simulated conditions, advective phenomena in the subsurface can significantly influence the Rn profiles and deficits in the subsurface compared to the ones expected assuming a diffusion-dominated transport or assuming equilibrium conditions. Advection can be neglected when the Peclet number is lower than 1, and thus a purely diffusive transport model can be applied. In these cases, LNAPL saturation can be estimated using the nomograms provided by Cecconi et al. (2022). For higher values of the Peclet number, i.e. in cases where the influence of advective transport is comparable to or greater than diffusive transport, Rn deficit profiles are strongly influenced by local advection. In particular, it was found that in high-permeability soils (such as sandy soils), in the presence of local advective fluxes in the same direction of diffusive fluxes (e.g., in the case of a rising groundwater level), the Rn deficit can be higher than would be expected in the presence of a diffusion-dominated transport. This implies that in those cases, applying the Rn deficit technique neglecting advection can lead to an underestimation of the expected LNAPL saturation in the subsurface. This underestimation becomes more significant

when the traditional Rn deficit technique (assuming equilibrium condition) is applied to soil gas Rn measurements carried out at some vertical distance from the LNAPL source zone. Assuming the occurrence of local advective fluxes in the opposite direction of diffusive fluxes (e.g., in the case of a falling water table), the observed Rn deficit is expected to be smaller than that in the case of diffusion-dominated transport, but higher than the one expected under equilibrium conditions. This implies that in those cases, applying the Rn deficit technique neglecting advection can lead to overestimations of the expected LNAPL saturation in the subsurface, while applying the traditional Rn deficit technique, assuming equilibrium conditions, there is a tendency to slightly underestimate LNAPL saturation values. In both cases, by approaching the Rn measurement point to the depths of the LNAPL source zone, the error in saturation estimation can be significantly reduced. Furthermore, in the case of the occurrence of methanogenesis processes in the LNAPL zone, a local advection can be expected only in the LNAPL-impacted zone (with a positive pressure gradient in the source zone and a negative pressure gradient in the overlying layer) and not in the adjacent areas considered for Rn background values. In such cases, the differences in deficit profiles can be so significant as to make the Rn deficit greater than 1, thus risking, on a practical level, a complete misinterpretation of Rn monitoring data. Even in this case, this confounding effect can be significantly reduced if soil gas Rn measurements are performed in the proximity of the LNAPL source and thus at greater depths compared to typical soil gas analysis performed at depths of around 1 m. In any case, when using the model proposed in this work, attention must be paid to the site conditions being simulated, considering the different assumptions on which the analytical model is based (e.g. steady-state conditions, homogeneity of soil and contamination in the domain layers, and homogeneity of other site-specific parameters such as Rn production, diffusion coefficient or water content). For sites with pronounced heterogeneities, it may be more indicated to use a numerical model that better simulates these conditions, such as the one provided by (Cecconi et al., 2023b, modified from Barrio-Parra et al., 2022).

FIELD APPLICATIONS

Both modeling studies emphasized the significance of measuring Rn in soil gas near the LNAPL-affected area for the method to be most effective, especially when the possible occurrence of local advective transport is also present as an additional

confounding factor. In this view, to ensure a direct measurement of the Rn soil gas concentrations within the source zone, the measurement of the headspace of groundwater monitoring wells used in other applications (e.g., see Sweeney and Ririe, (2017)) was considered to be a good alternative to permanent or temporary soil gas probes. This approach could be used as an alternative to measurements in permanent or temporary soil gas probes, which typically do not allow for measurements at depths greater than 1.5 - 2 m (although greater depths can be reached in some cases depending on soil type). Namely, this option can be particularly indicated to assess and monitor the evolution of LNAPL contamination in the occurrence of natural source zone depletion processes or during active remediation.

USING GROUNDWATER MONITORING WELLS FOR A RAPID APPLICATION OF SOIL GAS RADON DEFICIT TECHNIQUE

Chapter 5 presents a method that has the potential to offer a rapid and low invasive approach for the application of the Rn deficit technique, using portable equipment to sample the soil gas in the headspace of groundwater monitoring wells already present at LNAPL-contaminated sites (Cecconi et al., 2023a). The protocol described is suitable for groundwater monitoring wells presenting a portion of the screen through the aquifer and in the overlying vadose zone (smear zone), so that gas can be sampled in the unsaturated zone closest to the groundwater table, where LNAPL is usually found. The proposed method can be applied using various Rn detectors and multi-gas analyzers and is not affected by the depth of the aquifer, but only requires adjustments to the depth of the measurement point based on aquifer depth. For this reason, it is recommended to measure the water table depth before the beginning of the protocol activities. A simple method for estimating LNAPL saturation and TPH concentration was also provided based on the measured Rn deficit. The equations were derived from previous works that are based on Rn equilibrium conditions (Schubert et al., 2001). Note that these relations may be inaccurate in cases where the probe to LNAPL vertical distance increases, and in such cases methods that account for the Rn transport in the subsurface (e.g., Cecconi et al., 2022, 2023) may be more appropriate. Also, the lack of site-specific data on water saturation in the investigated area can affect the accuracy of the results. To provide an initial insight into the method's potential as a tool for the detection of LNAPL, the proposed protocol was tested at a first site, in comparison to the more traditional application in soil gas

probes, yielding overall positive results from a qualitative point of view, and no complications related to the proposed configuration. In the second site, the method was applied in a more significant number of wells, showing results consistent with other lines of evidence, such as groundwater and soil gas monitoring. Overall, from these first evaluations, the proposed method has shown potential for a qualitative identification of LNAPL in the subsurface. Compared to the more traditional technique using soil gas probes, the proposed method has indeed the potential to offer several improvements, providing a rapid and non-invasive approach and eliminating the need to install additional gas probes at sites. Furthermore, although this sampling method is yet to be validated and is not yet regulated, the use of the headspace of monitoring wells may allow for gas sampling in the unsaturated zone, closest to the water table, where both free and residual phase LNAPL may be present (smear zone). This may allow for a more representative Rn measurement at the zone of interest, without the limitations associated with Rn diffusion distance, and reducing the potential errors caused by local advective phenomena. Furthermore, the proposed method has the potential to provide quantitative information on the subsurface contamination concentrations. Therefore, future investigations could be oriented to collect additional data to assess the accuracy of this approach for a quantitative assessment of LNAPL. In this view, it is worth recalling some limitations typically associated with the methods based on the Rn deficit technique. For instance, as highlighted by several authors, the heterogeneity of the soil matrix can have a significant impact on the distribution of Rn in the soil gas, independently of the presence of LNAPL (Fan et al., 2007; Cohen et al., 2016; De Miguel et al., 2018; Cho et al., 2020). Moreover, the almost instantaneous nature of the measurements may provide a Rn activity value strongly tied to the sampling moment without considering temporal fluctuations in Rn emissions, which could affect the estimation of the actual subsurface contamination (Winkler et al., 2001; Neznal et al., 2004; De Miguel et al., 2020).Therefore, spatial and temporal variability of contamination and Rn emissions from the subsurface implies that a higher spatial density of measuring points and a higher frequency of field campaigns are necessary for accurate determinations. These aspects should be addressed in future research efforts to advance the understanding and application of LNAPL detection using the soil gas Rn deficit.

APPLICATION OF SOIL GAS RADON DEFICIT TECHNIQUE USING PASSIVE DOSIMETERS IN GROUNDWATER MONITORING WELLS

To reduce uncertainties associated with the instantaneous nature of Rn measurement using active portable Rn monitors, an approach based on the use of passive dosimeters in the headspace of groundwater monitoring wells was tested for the application of the Rn deficit technique. The method has been applied in a field experiment at a site with detected LNAPL, consisting of Rn analysis in 14 wells located in both contaminated and uncontaminated areas. Twenty-five Radout® CR-39 passive dosimeters were used to monitor Rn levels. The devices were placed in the headspace at a depth of 3 m above ground level, at the beginning of the screened section of the wells, and approximately 1.5 m from the water table. The devices were left exposed in the headspace of the wells for five days. Afterwards, they were sent to a specialized laboratory to determine the average concentration values of Rn during the exposure period. A strong correlation was observed between the areas affected by the presence of NAPL according to the last groundwater monitoring campaign and the areas where a more pronounced Rn deficit was found. The percentage fraction of LNAPL and the concentration of total hydrocarbons were estimated at the locations affected by contamination. The estimated concentrations were higher than the residual concentration reference values (C_{res}), indicating the presence of free-phase LNAPL in the investigated wells, consistent with the evidence of traditional groundwater monitoring. Based on the obtained results, it can be concluded that Rn monitoring in the headspace of wells already present in LNAPL contaminated sites is a cost-effective and minimally invasive screening method for identifying the presence of mobile and residual product, which cannot always be achieved by only monitoring the supernatant product in wells or through traditional groundwater sampling. The use of passive dosimeters to measure Rn allowed the estimation of an average Rn concentration independent of daily Rn variations, thus eliminating one of the limiting factors in the application of the Rn deficit method for quantitative estimation of the extent of subsurface contamination. The technique for measuring Rn deficit in the headspace of monitoring wells was first proposed and tested using portable monitors for Rn measurement. These instruments have the advantage of providing a concentration value of Rn in the area of interest within about 30 minutes, compared to the exposure times of days or weeks required with passive devices. Furthermore,

portable active Rn monitors directly provide Rn concentration values, without the need for further analysis in specialized laboratories or the need to collect, ship, and/or analyze any sample. On the other hand, passive dosimeters have the advantage of being economical instruments (around €20/30 per analysis), small in size (around 50 mm in diameter by 20 mm in height), which do not require electricity, do not perturb the soil gas in the area to be monitored and do not require space on the surface of the site. Furthermore, compared to portable analyzers, the installation and recovery of these instruments from the wells is much quicker, allowing campaigns to be carried out with a much higher number of investigation points and therefore suitable for extensive screening and/or monitoring campaigns of the progress of remediation interventions.

CONCLUSIONS AND FUTURE DEVELOPMENTS

The outcomes of the theoretical and practical studies presented in this thesis can be considered as a contribution to some aspects of the evolving knowledge on the soil gas Rn deficit technique for LNAPL assessment in the subsurface.

The modeling results helped to identify the main parameters that can affect the method's effectiveness, providing some suggestions for both field workers and researchers on the practical application of the technique and the interpretation of the resulting data. However, in some cases, the assumptions required for analytical models can limit their ability to model complex scenarios. New numerical modeling developments may be useful in these circumstances and can help to further identify potential areas for improvement over current field approaches. Nevertheless, the results of the analytical modelling have allowed to identify a critical aspect in the distance between the Rn measurement point and the NAPL impacted area, and to propose an alternative approach for field investigations, consisting in measuring soil gas Rn in the headspace of existing monitoring wells at contaminated sites, using both active portable Rn detectors and passive Rn devices. The field tests conducted to evaluate the proposed methods had positive results in identifying areas of LNAPL, also demonstrating the method's potential to quantify the NAPL extent, although with significant uncertainties.

Based on the existing knowledge and on the results of this research, it is believed that the method has the potential to be used as a rapid, inexpensive, and minimally

invasive approach to subsurface LNAPL investigation, even in the presence of residual phase, for an initial screening during the site characterization, as well as for LNAPL monitoring over time and during remediation activities. Despite the method's promise for qualitative identification, challenges such as soil matrix heterogeneity (with both passive and active instrumentation) and temporal variation in Rn emissions (with active instrumentation) have been recognized to affect quantitative evaluations. In this view, future research, and collaboration among researchers and industry professionals, should aim to refine both established and emerging methods under diverse site specific conditions, addressing limitations associated with soil matrix heterogeneity and temporal Rn variability to improve the reliability and applicability of the technique for the assessment of LNAPL contamination.

Nomenclature

SYMBOL	PARAMETER	UNIT
C_g	Gas phase concentration	mg L^{-1}
C_{Ra}	^{226}Ra concentration of the solids	Bq kg^{-1}
C_{res}	Residual NAPL concentration	mg kg^{-1}
C_s	Sorbed phase concentration	mg kg^{-1}
C_{sat}	Soil saturation concentration	mg kg^{-1}
CSC	Contamination threshold concentrations for soil for Italian legislation (Col. B, Tab.1, All.5, Part IV, Title V of the Legislative Decree 152/06)	mg kg^{-1}
C_w	Aqueous phase concentration	mg L^{-1}
d	Vertical distance of the soil gas probe from the NAPL zone	m
D	Rn deficit	-
D_e	Effective diffusion coefficient of Rn	m^2 s^{-1}
DF	Dilution factor	-
D_{mg}	Rn molecular diffusion coefficient in gas phase	m^2 s^{-1}
D_{mw}	Rn molecular diffusion coefficient in water phase	m^2 s^{-1}
dp/dz ∇p	Pressure gradient	kg m^{-2} s^{-2}
f	Fraction of Rn in the gas phase	-
f_{oc}	Organic carbon fraction of the soil	-
h	Elevation above the steady state groundwater level	m

SYMBOL	PARAMETER	UNIT
H	Dimensionless Henry's constant ($k_{g/w}$)	-
J_{adv}	Volumetric advective flux	$m^3\ m^{-2}\ s^{-1}$
J_{diff}	Rn diffusive flux	$Bq\ m^{-2}\ s^{-1}$
J_{exh}	Rn exhalation rate	$Bq\ m^{-2}\ s^{-1}$
H_{CF}	Thickness of the capillary fringe	m
H_N	Thickness of the source zone	m
k_g	Effective permeability to soil gas flow	m^2
$k_{g/N}$	Rn partition coefficient between gas and NAPL (calculated as $k_{g/w}$ /$k_{N/w}$)	-
$k_{g/w}$	Rn partition coefficient between gas and water (Henry's law constant)	-
k_{int}	Intrinsic permeability	m^2
$k_{N/g}$	Rn partition coefficient between NAPL and gas	-
$k_{N/w}$	Rn partition coefficient between NAPL and water	-
K_{oc}	Organic carbon partition coefficient	$mL\ g^{-1}$
k_{rg}	Relative air permeability	m^2
K_{sw}	Soil-water partition coefficient	$L\ kg^{-1}$
$k_{s/w}$	Rn partition coefficient between the solid and water	-
$k_{w/g}$	Rn partition coefficient between water and gas	-
L_c	Rn characteristic diffusion length	m
L_{CF}	Capillary fringe depth	m

SYMBOL	PARAMETER	UNIT
L_N	Source zone depth	m
L_W	Total profile length (water table depth)	m
m	Van Genuchten parameter	-
MW	Groundwater monitoring well	-
n	Van Genuchten parameter	-
p	Vapor pressure	kg m^{-1} s^{-2}
P	Rn production rate in the pore space	Bq m^{-3} s^{-1}
p^0	Vapor pressure of pure compound	kg m^{-1} s^{-2}
p_N	NAPL interface pressure	kg m^{-1} s^{-2}
p_w	Water interface pressure	kg m^{-1} s^{-2}
Q	Pump flow rate	L min^{-1}
r	Pore entry radius	m
Rn	Rn activity concentration in soil gas	Bq m^{-3}
Rn_{CF}	Rn concentration at the interface between the vadose zone with residual NAPL and the capillary fringe	Bq m^{-3}
Rn_{NV}	Rn concentration at the interface between the vadose zone and the vadose zone with residual NAPL	Bq m^{-3}
Rn_N	Rn activity concentration in NAPL	Bq m^{-3}
Rn_0	Equilibrium Rn activity concentration in soil pores	Bq m^{-3}
Rn_w	Rn activity concentration in water	Bq m^{-3}
S	Pure compound solubility	mg L^{-1}

SYMBOL	PARAMETER	UNIT
S_e	Effective solubility	mg L^{-1}
S_g	Gas saturation	-
S_N	NAPL saturation	-
$S_{r,N}$	Residual NAPL saturation	-
S_{we}	Effective water saturation	-
S_w	Water saturation	-
T	Temperature	°C
TPH	Total Petroleum Hydrocarbon	mg kg^{-1}
u	Upward soil gas velocity	m s^{-1}
V_{HS}	Total headspace volume of the well	L
VOC	Volatile organic compounds	-
X	Mole fraction	-
α	Van Genuchten parameter	m^{-1}
α_c	Fluids interface contact	°
ε	Rn emanation coefficient	-
θ_g	Volumetric gas content	-
θ_N	Volumetric NAPL content	-
$\theta_{r,N}$	Residual volumetric NAPL content	-
θ_r	Residual volumetric water content	-

SYMBOL	PARAMETER	UNIT
θ_t	Total porosity	-
θ_w	Volumetric water content	-
λ	Rn first order decay constant	s^{-1}
μ	Dynamic viscosity of soil gas	kg m^{-1} s^{-1}
ρ_N	NAPL density	kg m^{-3}
ρ_s	Solid bulk density	kg m^{-3}
σ	Interface tension	kg s^{-2}

Bibliography

Alden, D.F., García-Rincón, J., Rivett, M.O., Wealthall, G.P., Thomson, N.R., 2024. Complexities of Petroleum Hydrocarbon Contaminated Sites, in: García-Rincón, J., Gatsios, E., Lenhard, R.J., Atekwana, E.A., Naidu, R. (Eds.), Advances in the Characterisation and Remediation of Sites Contaminated with Petroleum Hydrocarbons, Environmental Contamination Remediation and Management. Springer International Publishing, Cham, pp. 1–19. https://doi.org/10.1007/978-3-031-34447-3_1

Alzaydi, A.A., Moore, C.A., Rai, I.S., 1978. Combined pressure and diffusional transition region flow of gases in porous media. AIChE J. 24, 35–43. https://doi.org/10.1002/aic.690240105

Amos, R.T., Mayer, K.U., Bekins, B.A., Delin, G.N., Williams, R.L., 2005. Use of dissolved and vapor-phase gases to investigate methanogenic degradation of petroleum hydrocarbon contamination in the subsurface. Water Resour. Res. 41, 02001. https://doi.org/10.1029/2004wr003433

Andrews, J.N., Wood, D.F., 1972. Mechanism of radon release in rock matrices and entry into groundwaters. Inst Min. Met TransSect B 81 198-209Nov 1972.

Annable, M.D., Rao, P.S.C., Hatfield, K., Graham, W.D., Wood, A.L., Enfield, C.G., 1998. Partitioning Tracers for Measuring Residual NAPL: Field-Scale Test Results. J. Environ. Eng. 124, 498–503. https://doi.org/10.1061/(ASCE)0733-9372(1998)124:6(498)

API, 2007. NAPL Distribution and Recovery Model. Volume 1. Distribution and Recovery of Petroleum Hydrocarbon Liquids in Porous.

Arato, A., Wehrer, M., Biró, B., Godio, A., 2014. Integration of geophysical, geochemical and microbiological data for a comprehensive small-scale characterization of an aged LNAPL-contaminated site. Environ. Sci. Pollut. Res. 21, 8948–8963. https://doi.org/10.1007/s11356-013-2171-2

ASTM, 2012. Standard Practice for Active Soil Gas Sampling for Direct Push or Manual-Driven Hand-Sampling. ASTM D7648 - 12. https://doi.org/10.1520/D7648-12

ASTM, 2000. Standard Guide for Risk-Based Corrective Action.

ASTM E 1739-95, n.d. Guide for Risk-Based Corrective Action Applied at Petroleum Release Sites.

ASTM PS 104-98, n.d. Standard Standard Provisional Guide to Risk-Based Corrective Action.

Atteia, O., Palmier, C., Schäfer, G., 2019. On the influence of groundwater table fluctuations on oil thickness in a well related to an LNAPL contaminated aquifer. J. Contam. Hydrol. 223, 103476. https://doi.org/10.1016/j.jconhyd.2019.03.008

Auer, L.H., Rosenberg, N.D., Birdsell, K.H., Whitney, E.M., 1996. The effects of barometric pumping on contaminant transport. J. Contam. Hydrol. 24, 145–166. https://doi.org/10.1016/S0169-7722(96)00010-1

Ball, T.K., Cameron, D.G., Colman, T.B., Roberts, P.D., 1991. Behaviour of radon in the geological environment: a review. Q. J. Eng. Geol. 24, 169–182. https://doi.org/10.1144/GSL.QJEG.1991.024.02.01

Barbosa, E.Q., Galhardi, J.A., Bonotto, D.M., 2014. The use of radon (Rn-222) and volatile organic compounds in monitoring soil gas to localize NAPL

contamination at a gas station in Rio Claro, São Paulo State, Brazil. Radiat. Meas. 66, 1–4. https://doi.org/10.1016/j.radmeas.2014.04.024

Barrio-Parra, F., Hidalgo, A., Izquierdo-Díaz, M., Arévalo-Lomas, L., De Miguel, E., 2022. 1D_RnDPM: A freely available 222Rn production, diffusion, and partition model to evaluate confounding factors in the radon-deficit technique. Sci. Total Environ. 807, 150815. https://doi.org/10.1016/j.scitotenv.2021.150815

Barrio-Parra, F., Izquierdo-Díaz, M., Díaz-Curiel, J., De Miguel, E., 2021. Field performance of the radon-deficit technique to detect and delineate a complex DNAPL accumulation in a multi-layer soil profile. Environ. Pollut. 269, 116200. https://doi.org/10.1016/j.envpol.2020.116200

Baskaran, M., 2016. Radon: A tracer for geological, geophysical and geochemical studies. Basel: Springer.

Bertolla, L., Porsani, J.L., Soldovieri, F., Catapano, I., 2014. GPR-4D monitoring a controlled LNAPL spill in a masonry tank at USP, Brazil. J. Appl. Geophys. 103, 237–244. https://doi.org/10.1016/j.jappgeo.2014.02.006

Biosca, B., Arévalo-Lomas, L., Barrio-Parra, F., Díaz-Curiel, J., 2020. Application and limitations of time domain-induced polarization tomography for the detection of hydrocarbon pollutants in soils with electro-metallic components: a case study. Environ. Monit. Assess. 192, 115. https://doi.org/10.1007/s10661-020-8073-0

Boumaiza, L., Chesnaux, R., Walter, J., Lenhard, R.J., Hassanizadeh, S.M., Dokou, Z., Alazaiza, M.Y.D., 2022. Predicting Vertical LNAPL Distribution in the Subsurface under the Fluctuating Water Table Effect. Groundw. Monit. Remediat. 42, 47–58. https://doi.org/10.1111/gwmr.12497

Briganti, A., Tuccimei, P., Voltaggio, M., Carusi, C., Galli, G., Lucchetti, C., 2020. Assessing methyl tertiary butyl ether residual contamination in groundwater using radon. Appl. Geochem. 116, 104583. https://doi.org/10.1016/j.apgeochem.2020.104583

Briganti, A., Voltaggio, M., Rainaldi, E., Carusi, C., 2024. Vertical Light Non-Aqueous Phase Liquid (LNAPL) distribution by Rn prospecting in monitoring wells. Environ. Monit. Assess. 196. https://doi.org/10.1007/s10661-023-12154-0

Briganti, A., Voltaggio, M., Tuccimei, P., Soligo, M., Rainaldi, E., Carusi, C., 2023. Radiometric dating of Light Non-Aqueous Phase Liquids (LNAPLs) dispersed in soil: A low environmental impact tool for natural resource restorations and protection. Appl. Geochem. 159, 105817. https://doi.org/10.1016/j.apgeochem.2023.105817

Broecker, W.S., Peng, T.H., 1974. Gas exchange rates between air and sea1. Tellus 26, 21–35. https://doi.org/10.3402/tellusa.v26i1-2.9733

Brost, E.J., De Vaull, 2000. Non-aqueous phase liquid (NAPL) mobility limits in soil.

CalEPA, (California Environmental Protection Agency Department of Toxic Substances Control), 2015. Advisory: Active soil gas investigations.

CalEPA, (California Environmental Protection Agency Department of Toxic Substances Control), 2014. Well Design and Construction for Monitoring Groundwater at Contaminated Sites.

Castelluccio, M., Agrahari, S., De Simone, G., Pompilj, F., Lucchetti, C., Sengupta, D., Galli, G., Friello, P., Curatolo, P., Giorgi, R., Tuccimei, P., 2018. Using a multi-method approach based on soil radon deficit, resistivity, and induced polarization measurements to monitor non-aqueous phase liquid contamination in two study areas in Italy and India. Environ. Sci. Pollut. Res. 25, 12515–12527. https://doi.org/10.1007/s11356-018-1429-0

Castelluccio, M., De Simone, G., Lucchetti, C., Moroni, M., Salvati, F., Tuccimei, P., 2015. A new technique to measure in situ soil gas permeability. J. Geochem. Explor. 148, 56–59. https://doi.org/10.1016/j.gexplo.2014.08.002

Cavelan, A., Golfier, F., Colombano, S., Davarzani, H., Deparis, J., Faure, P., 2022. A critical review of the influence of groundwater level fluctuations and temperature on LNAPL contaminations in the context of climate change. Sci. Total Environ. 806, 150412. https://doi.org/10.1016/j.scitotenv.2021.150412

Cecconi, A., Verginelli, I., Baciocchi, R., 2024. Assessing LNAPL in the subsurface using the soil gas Rn deficit technique: a literature overview of field studies. Manuscript submitted for publication.

Cecconi, A., Verginelli, I., Baciocchi, R., 2022. Modeling of soil gas radon as an in situ partitioning tracer for quantifying LNAPL contamination. Sci. Total Environ. 806, 150593. https://doi.org/10.1016/j.scitotenv.2021.150593

Cecconi, A., Verginelli, I., Baciocchi, R., Lanari, C., Villani, F., Bonfedi, G., 2023a. Using groundwater monitoring wells for rapid application of soil gas radon deficit technique to evaluate residual LNAPL. J. Contam. Hydrol. 258, 104241. https://doi.org/10.1016/j.jconhyd.2023.104241

Cecconi, A., Verginelli, I., Barrio-Parra, F., De Miguel, E., Baciocchi, R., 2023b. Influence of advection on the soil gas radon deficit technique for the quantification of LNAPL. Sci. Total Environ. 875, 162619. https://doi.org/10.1016/j.scitotenv.2023.162619

Čeliković, I., Pantelić, G., Vukanac, I., Nikolić, J.K., Živanović, M., Cinelli, G., Gruber, V., Baumann, S., Ciotoli, G., Poncela, L.S.Q., Rábago, D., 2022. Overview of Radon Flux Characteristics, Measurements, Models and Its Potential Use for the Estimation of Radon Priority Areas. Atmosphere 13, 2005. https://doi.org/10.3390/atmos13122005

Chapelle, F.H., 1999. Bioremediation of Petroleum Hydrocarbon-Contaminated Ground Water: The Perspectives of History and Hydrology. Groundwater 37, 122–132. https://doi.org/10.1111/j.1745-6584.1999.tb00965.x

Chauhan, R.P., Nain, M., Kant, K., 2008. Radon diffusion studies through some building materials: Effect of grain size. Radiat. Meas., Proceedings of the 23rd International Conference on Nuclear Tracks in Solids 43, S445–S448. https://doi.org/10.1016/j.radmeas.2008.03.013

Cho, I., Ju, Y., Lee, S.-S., Kaown, D., Lee, K.-K., 2020. Characterization of a NAPL-contaminated site using the partitioning behavior of noble gases. J. Contam. Hydrol. 235, 103733. https://doi.org/10.1016/j.jconhyd.2020.103733

Choi, J.-W., Smith, J.A., 2005. Geoenvironmental Factors Affecting Organic Vapor Advection and Diffusion Fluxes from the Unsaturated Zone to the Atmosphere under Natural Conditions. Environ. Eng. Sci. 22, 95–108. https://doi.org/10.1089/ees.2005.22.95

Christensen, L.B., Larsen, T.H., 1993. Method for determining the age of diesel oil spills in the soil. Ground Water Monit. Remediat. U. S. 13:4. https://doi.org/10.1111/j.1745-6592.1993.tb00458.x

CL:AIRE, 2017. Petroleum Hydrocarbons in groundwater: Guidance on assessing petroleum hydrocarbons using existing hydrogeological risk assessment methodologies.

CL:AIRE, 2014. An illustrated handbook of LNAPL transport and fate in the subsurface.

CL:AIRE, 2002. Site characterisation in support of monitored natural attenuation of fuel hydrocarbons and MTBE in a chalk aquifer in Southern England, CL:AIRE Case Study Bulletin, CSB 1.

Cohen, G.J.V., Bernachot, I., Su, D., Höhener, P., Mayer, K.U., Atteia, O., 2019. Laboratory-scale experimental and modelling investigations of 222Rn profiles in chemically heterogeneous LNAPL contaminated vadose zones. Sci. Total Environ. 681, 456–466. https://doi.org/10.1016/j.scitotenv.2019.05.023

Cohen, G.J.V., Jousse, F., Luze, N., Höhener, P., Atteia, O., 2016. LNAPL source zone delineation using soil gases in a heterogeneous silty-sand aquifer. J. Contam. Hydrol. 192, 20–34. https://doi.org/10.1016/j.jconhyd.2016.06.001

Corapcioglu, M.Y., Baehr, A.L., 1987. A compositional multiphase model for groundwater contamination by petroleum products: 1. Theoretical considerations. Water Resour. Res. 23, 191–200. https://doi.org/10.1029/WR023i001p00191

CRC CARE, 2018. Technical Measurement Guidance for LNAPL Natural Source Zone Depletion.

Cunningham, R.E., Williams, R.J.J., 1980. Diffusion in Gases and Porous Media. Springer US, Boston, MA. https://doi.org/10.1007/978-1-4757-4983-0

Davis, B.M., Istok, J.D., Semprini, L., 2005. Numerical simulations of radon as an in situ partitioning tracer for quantifying NAPL contamination using push–pull tests. J. Contam. Hydrol. 78, 87–103. https://doi.org/10.1016/j.jconhyd.2005.03.003

Davis, B.M., Istok, J.D., Semprini, L., 2002. Push–pull partitioning tracer tests using radon-222 to quantify non-aqueous phase liquid contamination. J. Contam. Hydrol. 58, 129–146. https://doi.org/10.1016/S0169-7722(02)00010-4

De Miguel, E., Barrio-Parra, F., Elío, J., Izquierdo-Díaz, M., García-González, J.E., Mazadiego, L.F., Medina, R., 2018. Applicability of radon emanometry in lithologically discontinuous sites contaminated by organic chemicals. Environ. Sci. Pollut. Res. 25, 20255–20263. https://doi.org/10.1007/s11356-018-2372-9

De Miguel, E., Barrio-Parra, F., Izquierdo-Díaz, M., Fernández, J., García-González, J.E., Álvarez, R., 2020. Applicability and limitations of the radon-deficit technique for the preliminary assessment of sites contaminated with complex mixtures of organic chemicals: A blind field-test. Environ. Int. 138, 105591. https://doi.org/10.1016/j.envint.2020.105591

De Simone, G., Galli, G., Lucchetti, C., Tuccimei, P., 2015. Using Natural Radon as a Tracer of Gasoline Contamination. Procedia Earth Planet. Sci., 11th Applied Isotope Geochemistery Conference AIG-11 13, 104–107. https://doi.org/10.1016/j.proeps.2015.07.025

De Simone, G., Lucchetti, C., Pompilj, F., Galli, G., Tuccimei, P., Curatolo, P., Giorgi, R., 2017. Soil radon survey to assess NAPL contamination from an ancient spill. Do kerosene vapors affect radon partition ? J. Environ. Radioact. 171, 138–147. https://doi.org/10.1016/j.jenvrad.2017.02.014

Etiope, G., Lombardi, S., 1995. Evidence for radon transport by carrier gas through faulted clays in Italy. J. Radioanal. Nucl. Chem. 193, 291–300. https://doi.org/10.1007/BF02039886

Fan, K., Kuo, T., Han, Y., Chen, C., Lin, C., Lee, C., 2007. Radon distribution in a gasoline-contaminated aquifer. Radiat. Meas. 42, 479–485. https://doi.org/10.1016/j.radmeas.2006.12.012

Farr, A.M., Houghtalen, R.J., McWhorter, D.B., 1990. Volume Estimation of Light Nonaqueous Phase Liquids in Porous Media. Groundwater 28, 48–56. https://doi.org/10.1111/j.1745-6584.1990.tb02228.x

Fingas, M., 2022. 1 Introduction to oil chemistry, in: 1 Introduction to Oil Chemistry. De Gruyter, pp. 1–46. https://doi.org/10.1515/9783110694529-001

Forde, O.N., Cahill, A.G., Beckie, R.D., Mayer, K.U., 2019. Barometric-pumping controls fugitive gas emissions from a vadose zone natural gas release. Sci. Rep. 9, 14080. https://doi.org/10.1038/s41598-019-50426-3

Fortmann, R.C., 1993. Measurement Methods and Instrumentation, in: Radon. ASTM International.

Freeze, R.A., Cherry, J.A., 1979. Groundwater. Prentice-Hall, Inc., Englewood Cliffs, New Jersey.,.

Frollini, E., Petitta, M., 2018. Free LNAPL volume estimation by pancake model and vertical equilibrium model: Comparison of results, limitations, and critical points. Geofluids 2018. https://doi.org/10.1155/2018/8234167

Galhardi, J.A., Bonotto, D.M., 2012. Radon in groundwater contaminated by dissolved hydrocarbons in Santa Bárbara d´Oeste, São Paulo State, Brazil. Appl. Radiat. Isot. 70, 2507–2515. https://doi.org/10.1016/j.apradiso.2012.06.029

García-González, J.E., Ortega, M.F., Chacón, E., Mazadiego, L.F., Miguel, E.D., 2008. Field validation of radon monitoring as a screening methodology for NAPL-contaminated sites. Appl. Geochem. 23, 2753–2758. https://doi.org/10.1016/j.apgeochem.2008.06.020

García-Rincón, J., Gatsios, E., Rayner, J.L., McLaughlan, R.G., Davis, G.B., 2020. Laser-induced fluorescence logging as a high-resolution characterisation tool to assess LNAPL mobility. Sci. Total Environ. 725, 138480. https://doi.org/10.1016/j.scitotenv.2020.138480

Garg, S., Newell, C.J., Kulkarni, P.R., King, D.C., Adamson, D.T., Renno, M.I., Sale, T., 2017. Overview of Natural Source Zone Depletion: Processes, Controlling Factors, and Composition Change. Ground Water Monit. Remediat. 37, 62–81. https://doi.org/10.1111/gwmr.12219

Genuchten, van, Th., M., 1980. A closed-form equation for predicting the hydraulic conductivity of unsaturated soils. Soil Sci. Soc. Am. J. 44, 892–898. https://doi.org/10.2136/sssaj1980.03615995004400050002x

George, A.C., 1990. An overview of instrumentation for measuring environmental radon and radon progeny. IEEE Trans. Nucl. Sci. 37, 892–901. https://doi.org/10.1109/23.106733

George, A.C., 1984. Passive, Integrated Measurement of Indoor Radon Using Activated Carbon. Health Phys. 46, 867.

Gewali, J.P., Sheron, P., Thakur, A., Jaishy, B., 2021. Study of Radiation Interactions in Makrofol-E and LR-115 Detectors Using SSNTD Technique, in: Sengupta, S., Dey, S., Das, S., Saikia, D.J., Panda, S., Podila, R. (Eds.), Selected Progresses in Modern Physics, Springer Proceedings in Physics. Springer, Singapore, pp. 375–385. https://doi.org/10.1007/978-981-16-5141-0_40

Gieg, L.M., Fowler, S.J., Berdugo-Clavijo, C., 2014. Syntrophic biodegradation of hydrocarbon contaminants. Curr. Opin. Biotechnol., Energy biotechnology • Environmental biotechnology 27, 21–29. https://doi.org/10.1016/j.copbio.2013.09.002

Greenshields, J.B., Rossini, F.D., 2002. Molecular Structure and Properties of Hydrocarbons and Related Compounds [WWW Document]. ACS Publ. https://doi.org/10.1021/j150561a005

Griffin, T.W., Watson, K.W., 2002. A Comparison of Field Techniques for Confirming Dense Nonaqueous Phase Liquids. Groundw. Monit. Remediat. 22, 48–59. https://doi.org/10.1111/j.1745-6592.2002.tb00312.x

Gutiérrez Villanueva, J.-L.G.´rrez, 2008. Radon concentrations in air, soil, and water in a granitic area: instrumental development and measurements.

Hamper, M., Seyedabbasi, M., 2023. Update to the light nonaqueous phase liquid infiltration conceptual model. Remediat. J. 33, 227–231. https://doi.org/10.1002/rem.21756

Hassan, N.M., Hosoda, M., Ishikawa, T., Sorimachi, A., Sahoo, S.K., Tokonami, S., Fukushi, M., 2009. Radon Migration Process and Its Influence Factors; Review. Jpn. J. Health Phys. 44, 218–231. https://doi.org/10.5453/jhps.44.218

Henry, J.A., 1998. Composition and toxicity of petroleum products and their additives. Hum. Exp. Toxicol. 17, 111–123. https://doi.org/10.1177/096032719801700206

Hillel, D., 1982. Introduction to Soil Physics. Academic Press.

Hirao, S., Yamazawa, H., Moriizumi, J., 2010. Estimation of the Global ^{222}Rn Flux Density from the Earth's Surface. Jpn. J. Health Phys. 45, 161–171. https://doi.org/10.5453/jhps.45.161

Höhener, P., Surbeck, H., 2004. Radon-222 as a Tracer for Nonaqueous Phase Liquid in the Vadose Zone: Experiments and Analytical Model. Vadose Zone J. 3, 1276–1285. https://doi.org/10.2113/3.4.1276

Hunkeler, D., Hoehn, E., Höhener, P., Zeyer, J., 1997. 222Rn as a Partitioning Tracer To Detect Diesel Fuel Contamination in Aquifers: Laboratory Study and Field Observations. Environ. Sci. Technol. 31, 3180–3187. https://doi.org/10.1021/es970163w

Huntley, D., Beckett, G.D., 2002. Persistence of LNAPL sources: relationship between risk reduction and LNAPL recovery. J. Contam. Hydrol. 59, 3–26. https://doi.org/10.1016/s0169-7722(02)00073-6

Hutter, A.R., 1996. Spatial and temporal variations of soil gas 220Rn and 222Rn at two sites in New Jersey. Environ. Int. 22, 455–469. https://doi.org/10.1016/S0160-4120(96)00146-8

Iskandar, D., Yamazawa, H., Iida, T., 2004. Quantification of the dependency of radon emanation power on soil temperature. Appl. Radiat. Isot. 60, 971–973. https://doi.org/10.1016/j.apradiso.2004.02.003

ISO, 2019. ISO 11665-1:2019.

ITRC, 2019. Implementing Advanced Site Characterization Tools.

ITRC, 2018. LNAPL Site Management: LCSM Evolution, Decision Process, and Remedial Technologies.

ITRC, 2009. Evaluating Natural Source Zone Depletion at Sites with LNAPL.

ITRC, 2006. The Use of Direct Push Well Technology for Long-term Environmental Monitoring in Groundwater Investigations.

ITRC, 2000. Dense Non-Aqueous Phase Liquids (DNAPLs): Review of Emerging Characterization and Remediation Technologies.

Janik, M., Ishikawa, T., Omori, Y., Kavasi, N., 2014. Invited Article: Radon and thoron intercomparison experiments for integrated monitors at NIRS, Japan. Rev. Sci. Instrum. 85, 022001. https://doi.org/10.1063/1.4865159

Jewell, K.P., Wilson, J.T., 2011. A New Screening Method for Methane in Soil Gas Using Existing Groundwater Monitoring Wells. Ground Water Monit. Remediat. 31, 82–94. https://doi.org/10.1111/j.1745-6592.2011.01345.x

Johansson, S., Fiandaca, G., Dahlin, T., 2015. Influence of non-aqueous phase liquid configuration on induced polarization parameters: Conceptual models applied to a time-domain field case study. J. Appl. Geophys. 123, 295–309. https://doi.org/10.1016/j.jappgeo.2015.08.010

Johnson, P.C., Hertz, M.B., Byers, D.L., 1992. Estimates for Hydrocarbon Vapor Emissions Resulting from Service Station Remediations and Buried Gasoline-

Contaminated Soils, in: Principles and Practices for Petroleum Contaminated Soils.

Johnston, C.D., Trefry, M.G., 2010. Response of LNAPL fuel and groundwater to forcing by sea level and rainfall recharge. Presented at the Environmental Hydraulics - Proceedings of the 6th International Symposium on Environmental Hydraulics, pp. 673–678.

Karimi Askarani, K., Sale, T., Palaia, T., 2024. Natural Source Zone Depletion of Petroleum Hydrocarbon NAPL, in: García-Rincón, J., Gatsios, E., Lenhard, R.J., Atekwana, E.A., Naidu, R. (Eds.), Advances in the Characterisation and Remediation of Sites Contaminated with Petroleum Hydrocarbons, Environmental Contamination Remediation and Management. Springer International Publishing, Cham, pp. 113–138. https://doi.org/10.1007/978-3-031-34447-3_5

Kemblowski, M.W., Chiang, C.Y., 1990. Hydrocarbon Thickness Fluctuations in Monitoring Wells. Groundwater 28, 244–252. https://doi.org/10.1111/j.1745-6584.1990.tb02252.x

Khan, H.A., Qureshi, I.E., Tufail (INVITED), 1993. Passive Dosimetry of Radon and its Daughters Using Solid State Nuclear Track Detectors (SSNTDs). Radiat. Prot. Dosimetry. https://doi.org/10.1093/oxfordjournals.rpd.a081671

Kiliari, T., Pashalidis, I., 2008. Determination of aquatic radon by liquid scintillation counting and airborne radon monitoring system. Radiat. Meas. 43, 1463–1466. https://doi.org/10.1016/j.radmeas.2008.03.006

King, C.-Y., Minissale, A., 1994. Seasonal variability of soil-gas radon concentration in central California. Radiat. Meas. 23, 683–692. https://doi.org/10.1016/1350-4487(94)90004-3

King, R.W., 1988. Petroleum: its composition, analysis and processing. Occup. Med. Phila. Pa 3, 409–430.

Kitto, M.E., 2005. Interrelationship of indoor radon concentrations, soil-gas flux, and meteorological parameters. J. Radioanal. Nucl. Chem. 264, 381–385. https://doi.org/10.1007/s10967-005-0725-6

Kotrappa, P., Brubaker, T., Dempsey, J.C., Stieff, L.R., 1992. Electret Ion Chamber System for Measurement of Environmental Radon and Environmental Gamma Radiation. Radiat. Prot. Dosimetry 45, 107–110. https://doi.org/10.1093/rpd/45.1-4.107

Kotrappa, P., Dempsey, J.C., Hickey, J.R., Stieff, L.R., 1988. An Electret Passive Environmental 222Rn Monitor Based on Ionization Measurement. Health Phys. 54, 47.

Krishnaswami, S., Seidemann, D.E., 1988. Comparative study of 222Rn, 40Ar, 39Ar and 37Ar leakage from rocks and minerals: Implications for the role of nanopores in gas transport through natural silicates. Geochim. Cosmochim. Acta 52, 655–658. https://doi.org/10.1016/0016-7037(88)90327-4

Kulkarni, P.R., Walker, K.L., Newell, C.J., Askarani, K.K., Li, Y., McHugh, T.E., 2022. Natural source zone depletion (NSZD) insights from over 15 years of research and measurements: A multi-site study. Water Res. 225, 119170. https://doi.org/10.1016/j.watres.2022.119170

Kuppusamy, S., Maddela, N.R., Megharaj, M., Venkateswarlu, K., 2019. Total Petroleum Hydrocarbons: Environmental Fate, Toxicity, and Remediation, Total Petroleum Hydrocarbons: Environmental Fate, Toxicity, and Remediation. https://doi.org/10.1007/978-3-030-24035-6

L'Annunziata, M.F., 2012. Handbook of Radioactivity Analysis. Academic Press.

Lauer, N., Vengosh, A., 2016. Age Dating Oil and Gas Wastewater Spills Using Radium Isotopes and Their Decay Products in Impacted Soil and Sediment. Environ. Sci. Technol. Lett. 3, 205–209. https://doi.org/10.1021/acs.estlett.6b00118

Le Meur, M., Cohen, G.J.V., Laurent, M., Höhener, P., Atteia, O., 2021. Effect of NAPL mixture and alteration on 222Rn partitioning coefficients: Implications for NAPL subsurface contamination quantification. Sci. Total Environ. 791, 148210. https://doi.org/10.1016/j.scitotenv.2021.148210

Lee, K.Y., Yoon, Y.Y., Ko, K.S., 2010. Determination of the emanation coefficient and the Henry's law constant for the groundwater radon. J. Radioanal. Nucl. Chem. 286, 381–385. https://doi.org/10.1007/s10967-010-0730-2

Lenhard, R.J., García-Rincón, J., 2024. Historical Development of Constitutive Relations for Addressing Subsurface LNAPL Contamination, in: García-Rincón, J., Gatsios, E., Lenhard, R.J., Atekwana, E.A., Naidu, R. (Eds.), Advances in the Characterisation and Remediation of Sites Contaminated with Petroleum Hydrocarbons, Environmental Contamination Remediation and Management. Springer International Publishing, Cham, pp. 21–39. https://doi.org/10.1007/978-3-031-34447-3_2

Lenhard, R.J., Parker, J.C., 1990. Estimation of Free Hydrocarbon Volume from Fluid Levels in Monitoring Wells. Groundwater 28, 57–67. https://doi.org/10.1111/j.1745-6584.1990.tb02229.x

Li, Y., Gupta, G., 1994. Adsorption of hydrocarbons by clay minerals from gasoline. J. Hazard. Mater. 38, 105–112. https://doi.org/10.1016/0304-3894(94)00006-9

López-Coto, I., Mas, J.L., Bolivar, J.P., 2013. A 40-year retrospective European radon flux inventory including climatological variability. Atmos. Environ. 73, 22–33. https://doi.org/10.1016/j.atmosenv.2013.02.043

Lu, Q., Wang, Y., Li, H., 2021. GPR attribute analysis for the detection of LNAPL contaminated soils. IOP Conf. Ser. Earth Environ. Sci. 660, 012033. https://doi.org/10.1088/1755-1315/660/1/012033

Lucas, H.F., 1957. Improved Low-Level Alpha-Scintillation Counter for Radon. Rev. Sci. Instrum. 28, 680–683. https://doi.org/10.1063/1.1715975

Lundegard, P.D., Johnson, P.C., 2006. Source Zone Natural Attenuation at Petroleum Hydrocarbon Spill Sites—II: Application to a Former Oil Field. Groundw. Monit. Remediat. 26, 93–106. https://doi.org/10.1111/j.1745-6592.2006.00115.x

Ma, J., Luo, H., DeVaull, G.E., Rixey, W.G., Alvarez, P.J.J., 2014. Numerical Model Investigation for Potential Methane Explosion and Benzene Vapor Intrusion Associated with High-Ethanol Blend Releases. Environ. Sci. Technol. 48, 474–481. https://doi.org/10.1021/es403926k

Ma, J., Rixey, W.G., DeVaull, G.E., Stafford, B.P., Alvarez, P.J.J., 2012. Methane bioattenuation and implications for explosion risk reduction along the groundwater to soil surface pathway above a plume of dissolved ethanol. Environ. Sci. Technol. 46, 6013–6019. https://doi.org/10.1021/es300715f

Man, J., Wang, G., Chen, Q., Yao, Y., 2021. Investigating the role of vadose zone breathing in vapor intrusion from contaminated groundwater. J. Hazard. Mater. 416, 126272. https://doi.org/10.1016/j.jhazmat.2021.126272

Markkanen, M., Arvela, H., 1992. Radon Emanation from Soils. Radiat. Prot. Dosimetry 45, 269–272. https://doi.org/10.1093/rpd/45.1-4.269

Marshall, T.J., 1958. A Relation Between Permeability and Size Distribution of Pores. J. Soil Sci. 9, 1–8. https://doi.org/10.1111/j.1365-2389.1958.tb01892.x

Massmann, J., Farrier, D.F., 1992. Effects of atmospheric pressures on gas transport in the vadose zone. Water Resour. Res. 28, 777–791. https://doi.org/10.1029/91WR02766

Mateus, C., Pecequilo, B.R.S., 2015. Preliminary results of NAPL contamination in a disused industry in the city of São Paulo, Brazil, by radon evaluation with CR-39 detectors. Presented at the International Nuclear Atlantic Conference; meeting on nuclear applications, 12th; meeting on reactor physics and thermal hydraulics.

Mattia, M., Tuccimei, P., Ciotoli, G., Soligo, M., Carusi, C., Rainaldi, E., Voltaggio, M., 2023. Combining Radon Deficit, NAPL Concentration, and Groundwater Table Dynamics to Assess Soil and Groundwater Contamination by NAPLs and Related Attenuation Processes. Appl. Sci. 13, 12813. https://doi.org/10.3390/app132312813

Mattia, M., Tuccimei, P., Soligo, M., Carusi, C., 2020. Radon as a Natural Tracer for Monitoring NAPL Groundwater Contamination. Water 12, 3327. https://doi.org/10.3390/w12123327

Mayer, A.S., Miller, C.T., 1992. The influence of porous medium characteristics and measurement scale on pore-scale distributions of residual nonaqueous-phase liquids. J. Contam. Hydrol. 11, 189–213. https://doi.org/10.1016/0169-7722(92)90017-9

Mayer, K.U., Frind, E.O., Blowes, D.W., 2002. Multicomponent reactive transport modeling in variably saturated porous media using a generalized formulation for kinetically controlled reactions. Water Resour. Res. 38, 13-1-13–21. https://doi.org/10.1029/2001WR000862

McCall, W., Christy, T.M., Pipp, D.A., Jaster, B., White, J., Goodrich, J., Fontana, J., Doxtader, S., 2018. Evaluation and application of the optical image profiler (OIP) a direct push probe for photo-logging UV-induced fluorescence of petroleum hydrocarbons. Environ. Earth Sci. 77, 374. https://doi.org/10.1007/s12665-018-7442-2

McCoy, K., Zimbron, J., Sale, T., Lyverse, M., 2015. Measurement of Natural Losses of LNAPL Using CO2 Traps. Groundwater 53, 658–667. https://doi.org/10.1111/gwat.12240

Meng, J., Dong, Y., Xia, T., Ma, X., Gao, C., Mao, D., 2022. Detailed LNAPL plume mapping using electrical resistivity tomography inside an industrial building. Acta Geophys. 70, 1651–1663. https://doi.org/10.1007/s11600-022-00818-3

Mercer, J.W., Cohen, R.M., 1990. A review of immiscible fluids in the subsurface: Properties, models, characterization and remediation. J. Contam. Hydrol. 6, 107–163. https://doi.org/10.1016/0169-7722(90)90043-G

Miles, J.C.H., Sinnaeve, J., 1986. The performance of different types of etched-track radon dosemeters in two international intercomparisons. Int. J. Radiat. Appl. Instrum. Part Nucl. Tracks Radiat. Meas., Special Volume Solid State Nuclear Track Detectors 12, 735–738. https://doi.org/10.1016/1359-0189(86)90691-6

Millington, R.J., Quirk, J.P., 1961. Permeability of porous solids. Trans. Faraday Soc. 57, 1200–1207. https://doi.org/10.1039/TF9615701200

Millington, R.J., Shearer, R.C., 1971. Diffusion in aggregated porous media. Soil Sci. 111, 372.

Mineo, S., 2023. Groundwater and soil contamination by LNAPL: State of the art and future challenges. Sci. Total Environ. 874, 162394. https://doi.org/10.1016/j.scitotenv.2023.162394

Minkin, L., Shapovalov, A.S., 2016. Thermo-diffusional radon waves in soils. Sci. Total Environ. 565, 1–7. https://doi.org/10.1016/j.scitotenv.2016.04.131

Molins, S., Mayer, K.U., 2007. Coupling between geochemical reactions and multicomponent gas and solute transport in unsaturated media: A reactive transport modeling study. Water Resour. Res. 43. https://doi.org/10.1029/2006WR005206

Molins, S., Mayer, K.U., Amos, R.T., Bekins, B.A., 2010. Vadose zone attenuation of organic compounds at a crude oil spill site — Interactions between biogeochemical reactions and multicomponent gas transport. J. Contam. Hydrol., Frontiers in Reactive Transport: Microbial Dynamics nad Redox Zonation in the Subsurface 112, 15–29. https://doi.org/10.1016/j.jconhyd.2009.09.002

Morrison, R.D., 2000. Critical Review of Environmental Forensic Techniques: Part I. Environ. Forensics. https://doi.org/10.1006/enfo.2000.0017

Nazaroff, W., Moed, B., Sextro, R., Revzan, K., Nero, A., 1989. Factors influencing soil as a source of indoor radon: Framework for assessing radon source potential (No. LBL-20645, 5494347, ON: DE90002607). https://doi.org/10.2172/5494347

Nazaroff, W.W., 1992. Radon transport from soil to air. Rev. Geophys. 30, 137–160. https://doi.org/10.1029/92RG00055

NCRP, 1988. Measurement of Radon and Radon Daughters in Air. National Council on Radiation Protection and Measurements.

Negi, S., Batoye, S., Singh, K., Waraich, J., 2021. Environmental Pollution, Its Causes and Impact on Ecosystem. pp. 1–22. https://doi.org/10.1007/978-981-15-9239-3_1

Neznal, M., Matolín, M., Just, G., Turek, K., 2004. Short-term temporal variations of soil gas radon concentration and comparison of measurement techniques. Radiat. Prot. Dosimetry 108, 55–63. https://doi.org/10.1093/rpd/nch004

Ng, G.-H.C., Bekins, B.A., Cozzarelli, I.M., Baedecker, M.J., Bennett, P.C., Amos, R.T., 2014. A mass balance approach to investigating geochemical controls on secondary water quality impacts at a crude oil spill site near Bemidji, MN. J. Contam. Hydrol. 164, 1–15. https://doi.org/10.1016/j.jconhyd.2014.04.006

Ng, G.-H.C., Bekins, B.A., Cozzarelli, I.M., Baedecker, M.J., Bennett, P.C., Amos, R.T., Herkelrath, W.N., 2015. Reactive transport modeling of geochemical controls on secondary water quality impacts at a crude oil spill site near Bemidji, MN. Water Resour. Res. 51, 4156–4183. https://doi.org/10.1002/2015WR016964

Nikezic, D., Yu, K.N., 2004. Formation and growth of tracks in nuclear track materials. Mater. Sci. Eng. R Rep. 46, 51–123. https://doi.org/10.1016/j.mser.2004.07.003

NRC, 1999. Risk Assessment of Radon in Drinking Water, National Research Council (US) Committee on Risk Assessment of Exposure to Radon in Drinking Water. National Academies Press (US), Washington (DC).

NRC, 1966. Waste Management and Control; a Report to the Federal Council for Science and Technology.

Nunes, L.J.R., Curado, A., Lopes, S.I., 2023. The Relationship between Radon and Geology: Sources, Transport and Indoor Accumulation. Appl. Sci. 13, 7460. https://doi.org/10.3390/app13137460

O'Reilly, K.T., Magaw, R.I., Rixey, W.G., 2001. Predicting the effect of hydrocarbon and hydrocarbon-impacted soil on groundwater, API Bullettin No. 14.

Osin, O.A., Yu, T., Lin, S., 2017. Oil refinery wastewater treatment in the Niger Delta, Nigeria: current practices, challenges, and recommendations. Environ. Sci. Pollut. Res. 24, 22730–22740. https://doi.org/10.1007/s11356-017-0009-z

Ossai, I.C., Ahmed, A., Hassan, A., Hamid, F.S., 2020. Remediation of soil and water contaminated with petroleum hydrocarbon: A review. Environ. Technol. Innov. 17, 100526. https://doi.org/10.1016/j.eti.2019.100526

Oudijk, G., 2009. Age Dating Heating-Oil Releases, Part 2: Assessing Weathering and Release Time Frames Through Chemistry, Geology and Site History. Environ. Forensics 10, 120–131. https://doi.org/10.1080/15275920902945885

Panagos, P., Van Liedekerke, M., Yigini, Y., Montanarella, L., 2013. Contaminated sites in Europe: review of the current situation based on data collected through a European network. J. Environ. Public Health 2013, 158764. https://doi.org/10.1155/2013/158764

Papastefanou, C., 2007. Measuring radon in soil gas and groundwaters: a review.

Parker, J.C., 1989. Multiphase flow and transport in porous media. Rev. Geophys. 27(3). https://doi.org/doi:10.1029/rg027i003p00311

Parker, J.C., Lenhard, R.J., Kuppusamy, T., 1987. A parametric model for constitutive properties governing multiphase flow in porous media. Water Resour. Res. 23, 618–624. https://doi.org/10.1029/WR023i004p00618

Parker, J.C., Waddill, D.W., Johnson, J.A., 1996. UST corrective action technologies: Engineering design of free product recovery systems. Project report (No. PB-96-153556/XAB). Environmental Systems and Technologies, Inc., Blacksburg, VA (United States).

Penman, H.L., 1940a. Gas and vapour movements in the soil: I. The diffusion of vapours through porous solids. J. Agric. Sci. 30, 437–462. https://doi.org/10.1017/S0021859600048164

Penman, H.L., 1940b. Gas and vapour movements in the soil: II. The diffusion of carbon dioxide through porous solids. J. Agric. Sci. 30, 570–581. https://doi.org/10.1017/S0021859600048231

Perrier, F., Richon, P., Sabroux, J.-C., 2009. Temporal variations of radon concentration in the saturated soil of Alpine grassland: The role of groundwater flow. Sci. Total Environ. 407, 2361–2371. https://doi.org/10.1016/j.scitotenv.2008.12.018

Ponsin, V., Chablais, A., Dumont, J., Radakovitch, O., Höhener, P., 2015. 222Rn as Natural Tracer for LNAPL Recovery in a Crude Oil-Contaminated Aquifer. Groundw. Monit. Remediat. 35, 30–38. https://doi.org/10.1111/gwmr.12091

Qi, S., Luo, J., O'Connor, D., Wang, Y., Hou, D., 2020. A numerical model to optimize LNAPL remediation by multi-phase extraction. Sci. Total Environ. 718, 137309. https://doi.org/10.1016/j.scitotenv.2020.137309

Quindos Poncela, L.S., Sainz Fernandez, C., Fuente Merino, I., Gutierrez Villanueva, J.L., Gonzalez Diez, A., 2013. The use of radon as tracer in environmental sciences. Acta Geophys. 61, 848–858. https://doi.org/10.2478/s11600-013-0119-z

Rao, P.S.C., Annable, M.D., Kim, H., 2000. NAPL source zone characterization and remediation technology performance assessment: recent developments and applications of tracer techniques. J. Contam. Hydrol. 45, 63–78. https://doi.org/10.1016/S0169-7722(00)00119-4

Ririe, G.T., Sweeney, R.E., 2022. Rapid Field Approach to Evaluating Natural Source Zone Depletion for a Range of Light Non-Aqueous Phase Liquid Sites. Groundw. Monit. Remediat. 42, 67–77. https://doi.org/10.1111/gwmr.12535

Rivett, M.O., Thornton, S.F., 2008. Monitored natural attenuation of organic contaminants in groundwater: principles and application. Proc. Inst. Civ. Eng. - Water Manag. 161, 381–392. https://doi.org/10.1680/wama.2008.161.6.381

Robles, K.P.V., Yee, J.-J., Kee, S.-H., 2022. Electrical Resistivity Measurements for Nondestructive Evaluation of Chloride-Induced Deterioration of Reinforced Concrete—A Review. Materials 15, 2725. https://doi.org/10.3390/ma15082725

Rösch, F., 2019. The Basics of Nuclear Chemistry and Radiochemistry: An Introduction to Nuclear Transformations and Radioactive Emissions, in: Lewis, J.S., Windhorst, A.D., Zeglis, B.M. (Eds.), Radiopharmaceutical Chemistry. Springer International Publishing, Cham, pp. 27–61. https://doi.org/10.1007/978-3-319-98947-1_3

Sakoda, A., Ishimori, Y., Yamaoka, K., 2011. A comprehensive review of radon emanation measurements for mineral, rock, soil, mill tailing and fly ash. Appl. Radiat. Isot. 69, 1422–1435. https://doi.org/10.1016/j.apradiso.2011.06.009

Scanlon, B.R., Nicot, J.P., Massmann, J.W., 2002. 8 Soil Gas Movement in Unsaturated Systems.

Schery, S.D., Whittlestone, S., Hart, K.P., Hill, S.E., 1989. The flux of radon and thoron from Australian soils. J. Geophys. Res. 94, 8567–8576. https://doi.org/10.1029/jd094id06p08567

Schubert, M., 2015. Using radon as environmental tracer for the assessment of subsurface Non-Aqueous Phase Liquid (NAPL) contamination – A review. Eur. Phys. J. Spec. Top. 224, 717–730. https://doi.org/10.1140/epjst/e2015-02402-3

Schubert, M., Balcázar, M., Lopez, A., Peña, P., Flores, J.H., Knöller, K., 2007a. Combination of radon and stable isotope analysis as a tool for decision support concerning the remediation of NAPL-contaminated sites. Isotopes Environ. Health Stud. 43, 215–226. https://doi.org/10.1080/10256010701550708

Schubert, M., Freyer, K., Treutler, H.C., Weiss, H., 2002. Using radon-222 in soil gas as an indicator of subsurface contamination by non-aqueous phase-liquids (NAPLs). Geofísica Int. https://doi.org/10.22201/igeof.00167169p.2002.41.4.491

Schubert, M., Freyer, K., Treutler, H.-C., Weiß, H., 2001. Using the soil gas radon as an indicator for ground contamination by non-aqueous phase-liquids. J. Soils Sediments 1, 217–222. https://doi.org/10.1007/BF02987728

Schubert, M., Lehmann, K., Paschke, A., 2007b. Determination of radon partition coefficients between water and organic liquids and their utilization for the assessment of subsurface NAPL contamination. Sci. Total Environ. 376, 306–316. https://doi.org/10.1016/j.scitotenv.2006.12.050

Schubert, M., Paschke, A., Lau, S., Geyer, W., Knöller, K., 2007c. Radon as a naturally occurring tracer for the assessment of residual NAPL contamination of aquifers. Environ. Pollut., Ozone at the Intensive Monitoring Plots in SW Europe 145, 920–927. https://doi.org/10.1016/j.envpol.2006.04.029

Schubert, M., Pena, P., Balcazar, M., Meissner, R., Lopez, A., Flores, J.H., 2005. Determination of radon distribution patterns in the upper soil as a tool for the localization of subsurface NAPL contamination. Radiat. Meas. 40. https://doi.org/10.1016/j.radmeas.2005.04.020

Schubert, M., Schulz, H., 2002. Diurnal radon variations in the upper soil layers and at the soil-air interface related to meteorological parameters. Health Phys. 83, 91.

Semprini, L., Broholm, K., McDonald, M., 1993. Radon-222 deficit method for locating and quantifying NAPL contamination in the subsurface. EOS Trans Am. Geophys Union 74(43), 299.

Semprini, L., Hopkins, O.S., Gottipati, S., Tasker, B.R., 1995. Field, laboratory and, modeling studies of radon-222 as a natural tracer for detecting NAPL contamination in the subsurface and monitoring the progress of remediation. EOS Trans Am. Geophys Union 76(46), F276.

Semprini, L., Hopkins, O.S., Tasker, B.R., 2000. Laboratory, Field and Modeling Studies of Radon-222 as a Natural Tracer for Monitoring NAPL Contamination. Transp. Porous Media 38, 223–240. https://doi.org/10.1023/A:1006671519143

Sethy, N.K., Jha, V.N., Ravi, P.M., Tripathi, R.M., 2014. A simple method for calibration of Lucas scintillation cell counting system for measurement of 226Ra and 222Rn. J. Radiat. Res. Appl. Sci. 7, 472–477. https://doi.org/10.1016/j.jrras.2014.08.002

Shao, S., Guo, X., Gao, C., 2019. Fresh underground light non-aqueous liquid (LNAPL) pollution source zone monitoring in an outdoor experiment using cross-hole electrical resistivity tomography. Environ. Sci. Pollut. Res. 26, 18316–18328. https://doi.org/10.1007/s11356-019-05039-8

Sihota, N.J., Singurindy, O., Mayer, K.U., 2011. CO2-Efflux Measurements for Evaluating Source Zone Natural Attenuation Rates in a Petroleum Hydrocarbon Contaminated Aquifer. Environ. Sci. Technol. 45, 482–488. https://doi.org/10.1021/es1032585

Smith, J.J., Benede, E., Beuthe, B., Marti, M., Lopez, A.S., Koons, B.W., Kirkman, A.J., Barreales, L.A., Grosjean, T., Hjort, M., 2021. A comparison of three methods to assess natural source zone depletion at paved fuel retail sites. Q. J. Eng. Geol. Hydrogeol. 54, qjegh2021-005. https://doi.org/10.1144/qjegh2021-005

Sookhak Lari, K., Rayner, J.L., Davis, G.B., 2017. A computational assessment of representative sampling of soil gas using existing groundwater monitoring wells screened across the water table. J. Hazard. Mater. 335, 197–207. https://doi.org/10.1016/j.jhazmat.2017.04.006

Stacks, A.M., 2015. Radon: Geology, environmental impact and toxicity concerns, Radon: Geology, Environmental Impact and Toxicity Concerns.

Steffy, D.A., Johnston, C., Barry, D.A. (Eds.), 1995. A field study of the vertical immiscible displacement of LNAPL associated with a fluctuating water table, IAHS Series of Proceedings and Reports. Presented at the Groundwater Quality: Remediation and Protection, International Association of Hydrological Sciences, IAHS Press, Institute of Hydrology, Wallingford, Oxfordshire, United Kingdom.

Stranden, E., Kolstad, A.K., Lind, B., 1984. The Influence of Moisture and Temperature on Radon Exhalation. Radiat. Prot. Dosimetry 7, 55–58. https://doi.org/10.1093/oxfordjournals.rpd.a082962

Strong, K.P., Levins, D.M., 1982. Effect of moisture content on radon emanation from uranium ore and tailings. Health Phys. 42, 27–32. https://doi.org/10.1097/00004032-198201000-00003

Sukanya, S., Noble, J., Joseph, S., 2022. Application of radon (222Rn) as an environmental tracer in hydrogeological and geological investigations: An overview. Chemosphere 303, 135141. https://doi.org/10.1016/j.chemosphere.2022.135141

Sumesh, C.G., Jha, S.K., Patra, A.C., Aswal, D.K., 2024. Evolution of Analytical Methods for Radon Measurement in India. MAPAN. https://doi.org/10.1007/s12647-023-00700-7

Sweeney, R.E., Ririe, G.T., 2017. Small Purge Method to Sample Vapor from Groundwater Monitoring Wells Screened Across the Water Table. Groundw. Monit. Remediat. 37, 51–59. https://doi.org/10.1111/gwmr.12230

Tanner, A.B., 1980. Radon migration in the ground: a supplementary review. United States.

Tanner, A.B., 1964. Radon migration in the ground : A review. Nat. Radiat. Environ. 161–190.

Teramoto, E.H., Isler, E., Polese, L., Baessa, M.P.M., Chang, H.K., 2019. LNAPL saturation derived from laser induced fluorescence method. Sci. Total Environ. 683, 762–772. https://doi.org/10.1016/j.scitotenv.2019.05.262

Teramoto, E.H., Pede, M.A.Z., Chang, H.K., 2020. Impact of water table fluctuations on the seasonal effectiveness of the pump-and-treat remediation in wet–dry tropical regions. Environ. Earth Sci. 79, 435. https://doi.org/10.1007/s12665-020-09182-1

Thorstenson, D.C., Pollock, D.W., 1989. Gas transport in unsaturated zones: Multicomponent systems and the adequacy of Fick's laws. Water Resour. Res. 25, 477–507. https://doi.org/10.1029/WR025i003p00477

Tsai, Y.-J., Chou, Y.-C., Wu, Y.-S., Lee, C.-H., 2020. Noninvasive survey technology for LNAPL-contaminated site investigation. J. Hydrol. 587, 125002. https://doi.org/10.1016/j.jhydrol.2020.125002

UNSCEAR, 1977. Sources and effects of ionizing radiation.

US EPA, 2015. Technical Guide For Addressing Petroleum Vapor Intrusion At Leaking Underground Storage Tank Sites.

US EPA, 2005. Cost and performance report for LNAPL characterization and remediation partition interwell tracer testing (PITT) and rapid optical screening tool (ROSTTM). Characterization and evaluation of the feasibility of surfactant enhanced aquifer remediation (SEAR) at the Chevron Cincinnati Facility, Hooven, OH.

US EPA, 2004. A decision-making framework for cleanup of sites impacted with light non-aqueous phase liquids (LNAPL).

US EPA, 1995. Ground Water Issue: Light Nonaqueous Phase Liquids.

USDA, 2012. Chapter 11, Cone penetrometer. Part 631 Geology, National Engineering Handbook.

Van Der Spoel, W.H., Van Der Graaf, E.R., De Meijer, R.J., 1997. Diffusive Transport of Radon in a Homogeneous Column of Dry Sand. Health Phys. 72, 766.

Van Genuchten, M.Th., 1981. Analytical solutions for chemical transport with simultaneous adsorption, zero-order production and first-order decay. J. Hydrol. 49, 213–233. https://doi.org/10.1016/0022-1694(81)90214-6

Vandana, Priyadarshanee, M., Mahto, U., Das, S., 2022. Chapter 2 - Mechanism of toxicity and adverse health effects of environmental pollutants, in: Das, S., Dash, H.R. (Eds.), Microbial Biodegradation and Bioremediation (Second Edition). Elsevier, pp. 33–53. https://doi.org/10.1016/B978-0-323-85455-9.00024-2

Verginelli, I., 2024. Petroleum Vapor Intrusion, in: García-Rincón, J., Gatsios, E., Lenhard, R.J., Atekwana, E.A., Naidu, R. (Eds.), Advances in the Characterisation and Remediation of Sites Contaminated with Petroleum Hydrocarbons, Environmental Contamination Remediation and Management. Springer International Publishing, Cham, pp. 139–169. https://doi.org/10.1007/978-3-031-34447-3_6

Verginelli, I., Baciocchi, R., 2021. Refinement of the gradient method for the estimation of natural source zone depletion at petroleum contaminated sites.

J. Contam. Hydrol. 241, 103807. https://doi.org/10.1016/j.jconhyd.2021.103807

Voltaggio, M., Spadoni, M., 2013. Determination of 222Rn in water by absorption in polydimethylsiloxane mixed with activated carbon and gamma-ray spectrometry: An example application in the radon budget of Paterno submerged sinkhole (Central Italy). Appl. Geochem., Special issue dedicated to Giovanni Maria (Gian Maria) Zuppi (1947-2011) 34, 65–74. https://doi.org/10.1016/j.apgeochem.2012.12.012

Wang, X., Li, H., Zhang, Y., Qu, W., Schubert, M., 2019. Submarine groundwater discharge revealed by 222Rn: comparison of two continuous on-site 222Rn-in-water measurement methods. Hydrogeol. J. 27, 1879–1887. https://doi.org/10.1007/s10040-019-01988-z

Werner, D., Höhener, P., 2002. Diffusive Partitioning Tracer Test for Nonaqueous Phase Liquid (NAPL) Detection in the Vadose Zone. Environ. Sci. Technol. 36, 1592–1599. https://doi.org/10.1021/es010098x

WHO, 2008. Guidelines for drinking-water quality, 3rd edition: Volume 1.

Wilhelm, E., Battino, R., Wilcock, R.J., 2002. Low-pressure solubility of gases in liquid water [WWW Document]. ACS Publ. https://doi.org/10.1021/cr60306a003

Winkler, R., Ruckerbauer, F., Bunzl, K., 2001. Radon concentration in soil gas: a comparison of the variability resulting from different methods, spatial heterogeneity and seasonal fluctuations. Sci. Total Environ., Radon in the Living Environment 272, 273–282. https://doi.org/10.1016/S0048-9697(01)00704-5

Wu, M., Zhao, Z., Cai, G., Duan, W., Wang, C., Cheng, G., Wang, X., 2022. In situ evaluation of soil contaminated by total petroleum hydrocarbons using membrane interface probe: a case study from Nanjing, China. Bull. Eng. Geol. Environ. 81, 140. https://doi.org/10.1007/s10064-022-02639-6

Yang, C., Wang, Z., Hollebone, B.P., Brown, C.E., Yang, Z., Landriault, M., 2014. Chromatographic Fingerprinting Analysis of Crude Oils and Petroleum Products, in: Handbook of Oil Spill Science and Technology. John Wiley & Sons, Ltd, pp. 93–163. https://doi.org/10.1002/9781118989982.ch5

Yao, Y., Wu, Y., Wang, Y., Verginelli, I., Zeng, T., Suuberg, E.M., Jiang, L., Wen, Y., Ma, J., 2015. A Petroleum Vapor Intrusion Model Involving Upward Advective Soil Gas Flow Due to Methane Generation. Environ. Sci. Technol. 49, 11577–11585. https://doi.org/10.1021/acs.est.5b01314

Yoon, Y.Y., Koh, D.C., Lee, K.Y., Cho, S.Y., Yang, J.H., Lee, K.K., 2013. Using 222Rn as a naturally occurring tracer to estimate NAPL contamination in an aquifer. Appl. Radiat. Isot., 6th International Conference on Radionuclide Metrology - Low Level Radioactivity Measurement Techniques 81, 233–237. https://doi.org/10.1016/j.apradiso.2013.03.061

Zhuo, W., Chen, B., Li, D., Liu, H., 2008. Reconstruction of Database on Natural Radionuclide Contents in Soil in China. J. Nucl. Sci. Technol. 45, 180–184. https://doi.org/10.1080/00223131.2008.10876003

Zimbron, J.A., Sale, T.C., Lyverse, M., 2014. Gas flux measurement using traps. US8714034B2.

SCIENTIFIC PRODUCTION

International Journal Publications

Cecconi, A., Verginelli, I., Baciocchi, R., 2022. Modeling of soil gas radon as an in situ partitioning tracer for quantifying LNAPL contamination. Sci. Total Environ. 806, 150593. https://doi.org/10.1016/j.scitotenv.2021.150593

Cecconi, A., Verginelli, I., Baciocchi, R., Lanari, C., Villani, F., Bonfedi, G., 2023a. Using groundwater monitoring wells for rapid application of soil gas radon deficit technique to evaluate residual LNAPL. J. Contam. Hydrol. 258, 104241. https://doi.org/10.1016/j.jconhyd.2023.104241

Cecconi, A., Verginelli, I., Barrio-Parra, F., De Miguel, E., Baciocchi, R., 2023b. Influence of advection on the soil gas radon deficit technique for the quantification of LNAPL. Sci. Total Environ. 875, 162619. https://doi.org/10.1016/j.scitotenv.2023.162619

Cecconi, A., Verginelli, I., Baciocchi, R., 2024. Assessing LNAPL in the subsurface using the soil gas Rn deficit technique: a literature overview of field studies. Submitted for publication.

Other publications

Vecchio, A., Calà, S., Calace, N., Pietroletti, M., Pascarella, F. Emiliani, R., Macolo, G., Cacciari, F., Gagni, S., Zaccanti, M., Fuin, F., Formenton, G., De Lorenzo, R., Crivellaro, G., Giacopetti, D., Borrelli, R., Oldani, Al., Selvaggio, M., Pasini, T., Di Finizio, V., Lanari, C., Villani, F., Bonfedi, G., Cristofori, M.C., Verginelli, I., Cecconi, A., 2024. Applicazione di diversi sistemi di campionamento passivo per il monitoraggio dei gas interstiziali nei siti contaminati (Accordo di collaborazione ISPRA-UNEM). ISPRA, Quaderni Ambiente e Società 30/2024. ISBN 978-88-448-1206-5.

Conference papers, presentations, and posters

- Oral presentation “Examining the applicability of the soil gas radon deficit technique for quantifying residual LNAPL contamination”. International Conference and Exhibition Remtech Europe 2022, Ferrara, Italy. Cecconi, A., Verginelli, I., Baciocchi, R., 2022.

- Oral presentation “Valutazione dell'applicabilità della tecnica del deficit di radon nel soil gas per la quantificazione della contaminazione residuale da LNAPL”. Workshop Siti Contaminati. Esperienze negli interventi di risanamento, SiCon 2023, Rome, Italy. Cecconi, A., Verginelli, I., Baciocchi, R., Lanari, C., Villani, F., Bonfedi, G., 2023.

- Oral and Poster Presentation “Assessment of the accuracy of the soil gas radon deficit technique for monitoring and quantifying residual LNAPL contamination” Interpore 2023, Edinburgh, Scotland, United Kingdom. Cecconi, A., Verginelli, I., Baciocchi, R., 2023.

- Oral presentation “Evaluation of the applicability of the radon deficit technique in soil gas for quantifying residual LNAPL contamination”. AquaConSoil 2023. Prague, Czech Republic. Cecconi, A., Verginelli, I., Baciocchi, R., Lanari, C., Villani, F., Bonfedi, G., 2023.

- Oral presentation “Modelling the influence of advection on the soil gas radon deficit technique for the quantification of LNAPL saturation”. International Conference and Exhibition Remtech Europe 2023, Ferrara, Italy. Cecconi, A., Verginelli, I., Barrio-Parra, F., De Miguel, E., Baciocchi, R., 2023.

- Oral presentation “Utilizzo di analizzatori portatili di radon nello spazio di testa dei piezometri per la valutazione della fase residuale di LNAPL in siti contaminati da idrocarburi”. 2023, Ferrara, Italy. Cecconi, A., Verginelli, I., Baciocchi, R., Lanari, C., Villani, F., Bonfedi, G., 2023.